Particle Detectors - Principles and Techniques

C. D'Ambrosio, T. Gys, C. Joram, M. Moll and L. Ropelewski

CERN – PH/DT2

The lecture series presents an overview of the physical principles and basic techniques of particle detection, applied to current and future high energy physics experiments. Illustrating examples, chosen mainly from the field of collider experiments, demonstrate the performance and limitations of the various techniques.

Main topics of the series are: interaction of particles and photons with matter; particle tracking with gaseous and solid state devices, including a discussion of radiation damage and strategies for improved radiation hardness; scintillation and photon detection; electromagnetic and hadronic calorimetry; particle identification using specific energy loss dE/dx, time of flight, Cherenkov light and transition radiation.

Outline

- **Lecture 1 - Introduction** — C. Joram, L. Ropelewski
  - What to measure ?
  - Detector concepts
  - Interaction of charged particles
  - Momentum measurement
  - Multiple scattering
  - Specific energy loss
  - Ionisation of gases
  - Gas amplification
  - Single Wire Proportional Counter

cern.ch/ph-dep-dt2/lectures_PD_2005.htm

- **Lecture 2 - Tracking Detectors** — L. Ropelewski, M. Moll
- **Lecture 3 - Scintillation and Photodetection** — C. D'Ambrosio, T. Gys
- **Lecture 4 - Calorimetry, Particle ID** — C. Joram
- **Lecture 5 - Particle ID, Detector Systems** — C. Joram, C. D'Ambrosio

Literature

- **Text books** (a selection)
  - C. Grupen, Particle Detectors, Cambridge University Press, 1996
  - G. Knoll, Radiation Detection and Measurement, 3rd ed. Wiley, 2000
  - W. R. Leo, Techniques for Nuclear and Particle Physics Experiments, Springer, 1994
  - R.S. Gilmore, Single particle detection and measurement, Taylor&Francis, 1992
  - K. Kleinknecht, Detectors for particle radiation , 2nd edition, Cambridge Univ. Press, 1998
  - W. Blum, L. Rolandi, Particle Detection with Drift Chambers, Springer, 1994
  - R. Wigmans, Calorimetry, Oxford Science Publications, 2000
  - G. Lutz, Semiconductor Radiation Detectors, Springer, 1999
- **Review Articles**
  - Experimental techniques in high energy physics, T. Ferbel (editor), World Scientific, 1991.
  - Instrumentation in High Energy Physics, F. Sauli (editor), World Scientific, 1992.
  - Many excellent articles can be found in Ann. Rev. Nucl. Part. Sci.
- **Other sources**
  - Particle Data Book Phys. Lett. B**592**, 1 (2004) http://pdg.lbl.gov/pdg.html
  - R. Bock, A. Vasilescu, Particle Data Briefbook http://www.cern.ch/Physics/ParticleDetector/BriefBook/
  - Proceedings of detector conferences (Vienna CI, Elba, IEEE, Como)
  - Nucl. Instr. Meth. A

Introduction

A W^+W^- decay in ALEPH

e^+e^- ($\sqrt{s}$=181 GeV)
$\rightarrow W^+W^- \rightarrow qq\mu\nu_\mu$
$\rightarrow$ 2 hadronic jets
+ μ + missing momentum

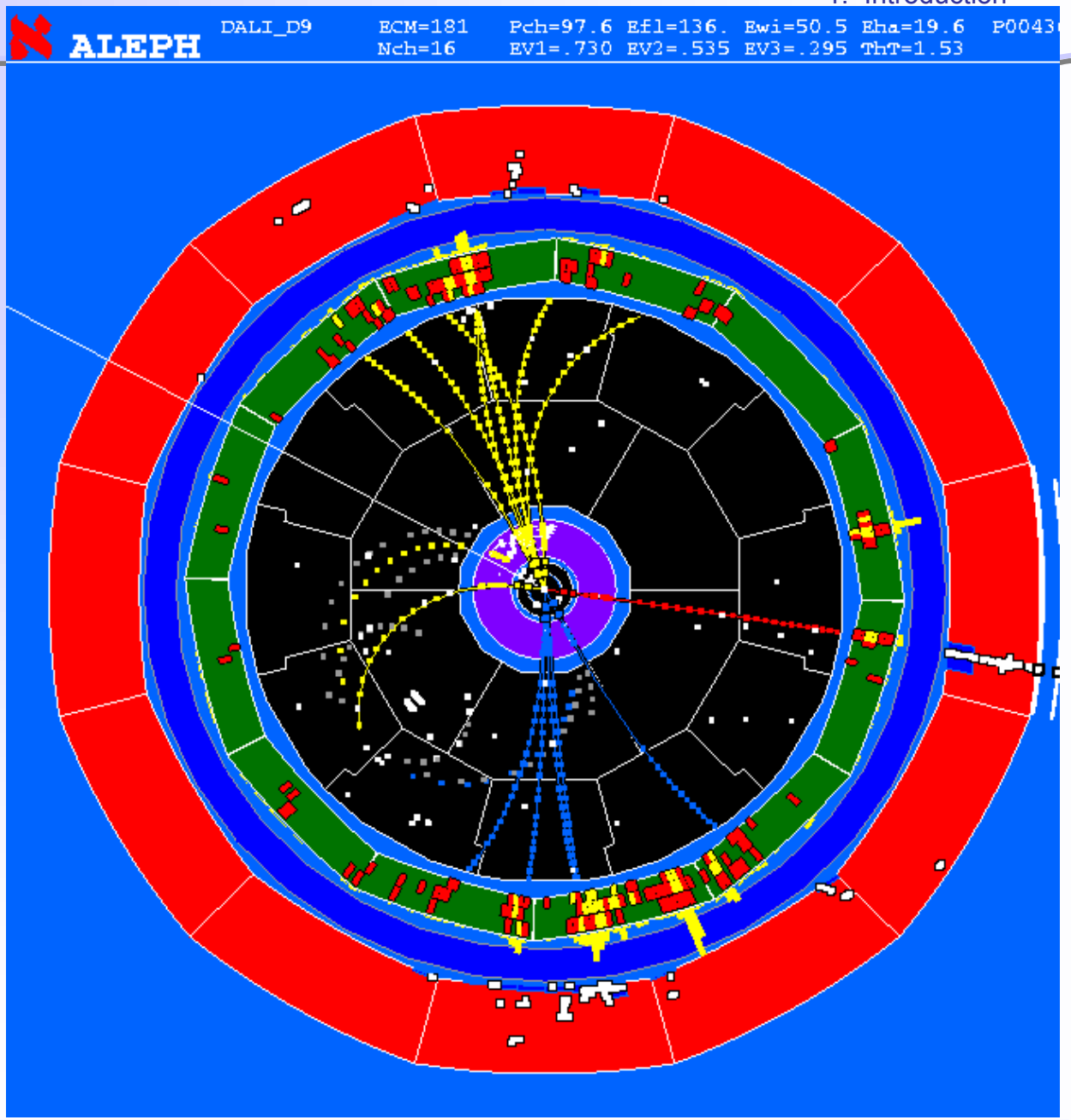

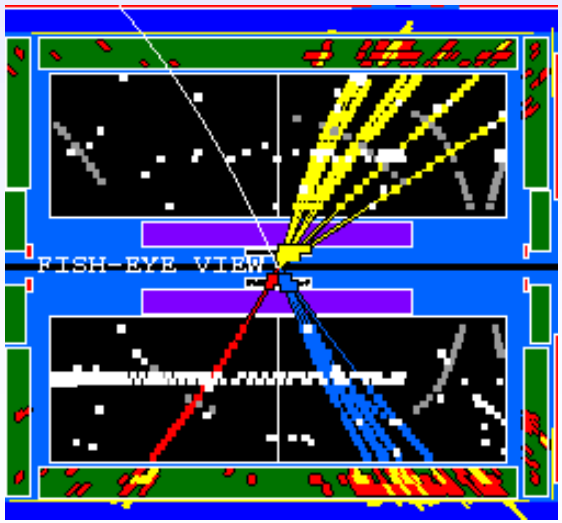

Introduction

Reconstructed

B-mesons in the DELPHI micro vertex detector

$\tau_B \approx 1.6$ ps $l = c\tau\gamma \approx \gamma \cdot 500$ μm

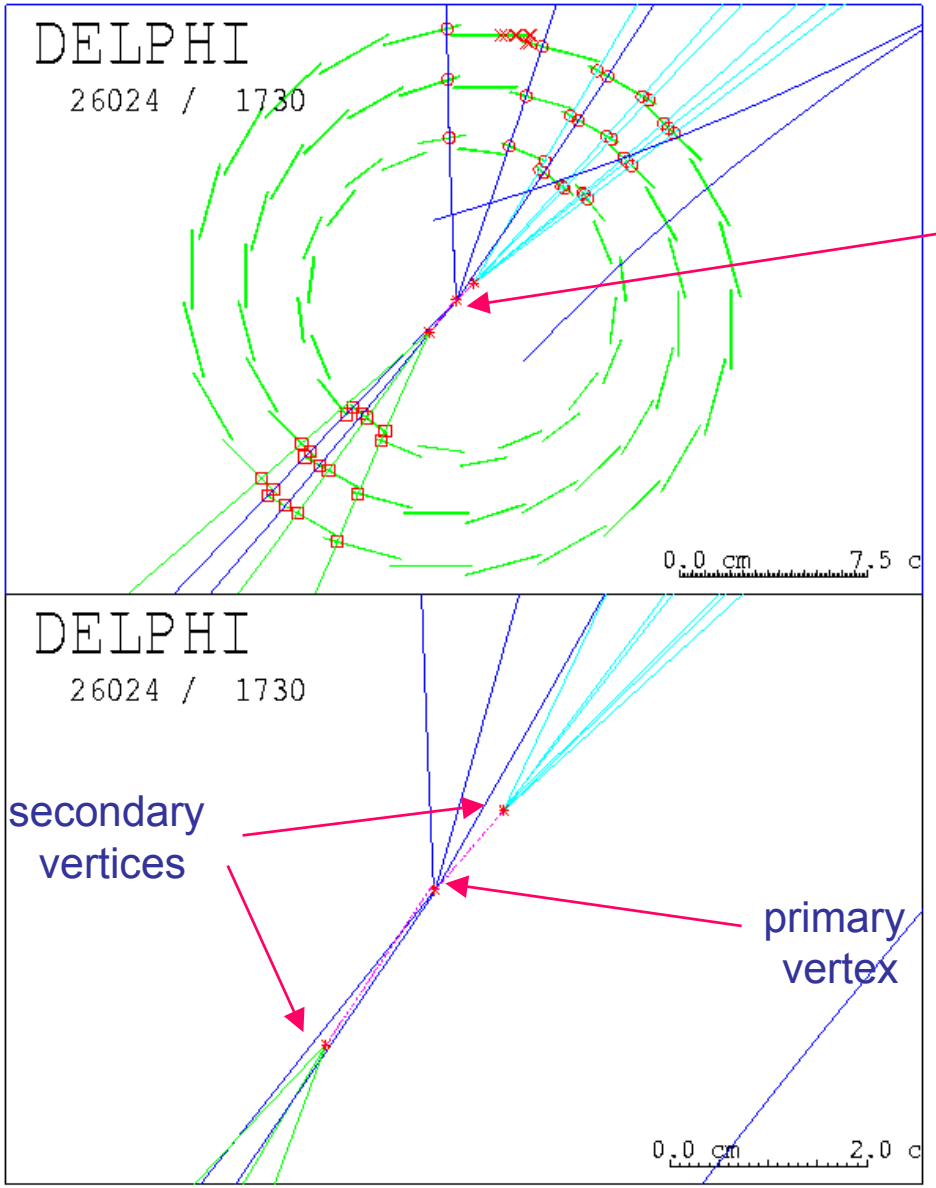

Introduction

$$e^+ + e^- \rightarrow Z^0 \rightarrow q\bar{q}$$

$$(+\text{hadronization})$$

Idealistic views of an elementary particle reaction

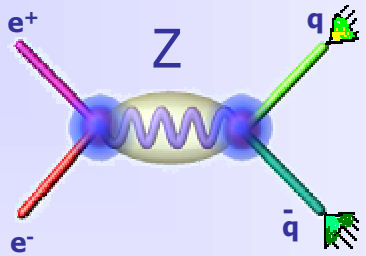

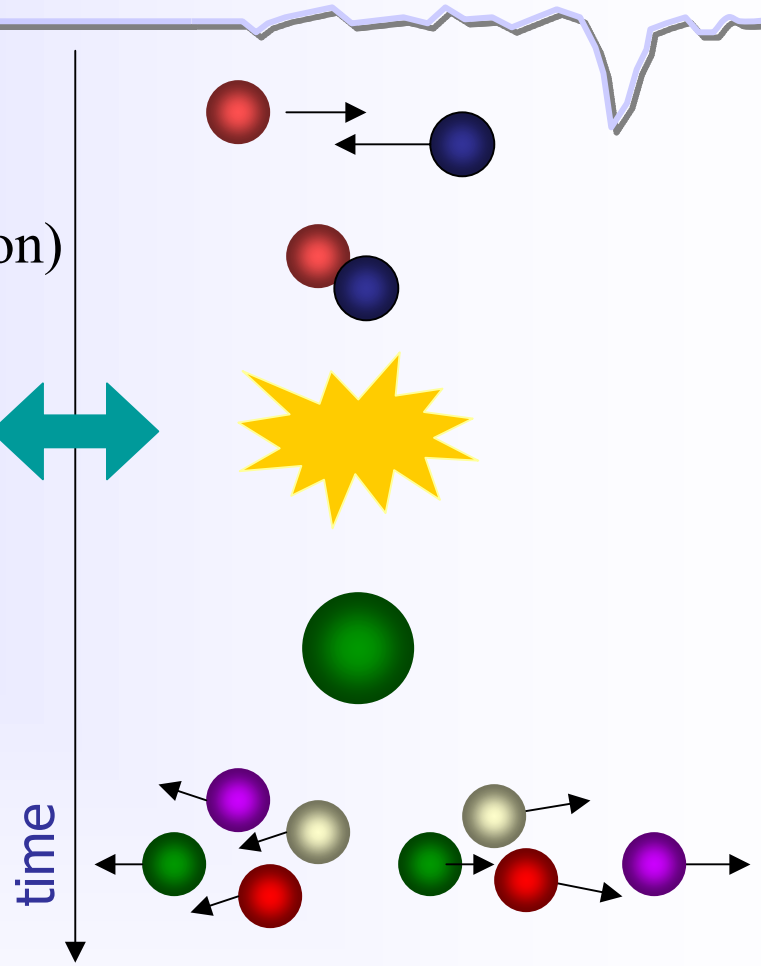

- Usually we can not 'see' the reaction itself, but only the end products of the reaction.
- In order to reconstruct the reaction mechanism and the properties of the involved particles, we want the maximum information about the end products !

Introduction

A simulated event in ATLAS (CMS) $H \rightarrow ZZ \rightarrow 4\mu$

pp collision at $\sqrt{s}$ = 14 TeV, $\sigma_{inel.} \approx 70$ mb

$\times 10^{-12}$

We are interested in processes with $\sigma \approx 10\text{–}100$ fb

$L = 10^{34}$ cm^{-2} s^{-1},
bunch spacing 25 ns

≈ 23 overlapping minimum bias events / BC
≈ 1900 charged + 1600 neutral particles / BC

Brave people have started to think about a Super LHC upgrade to $L = 10^{35}$ cm^{-2} s^{-1} !!!

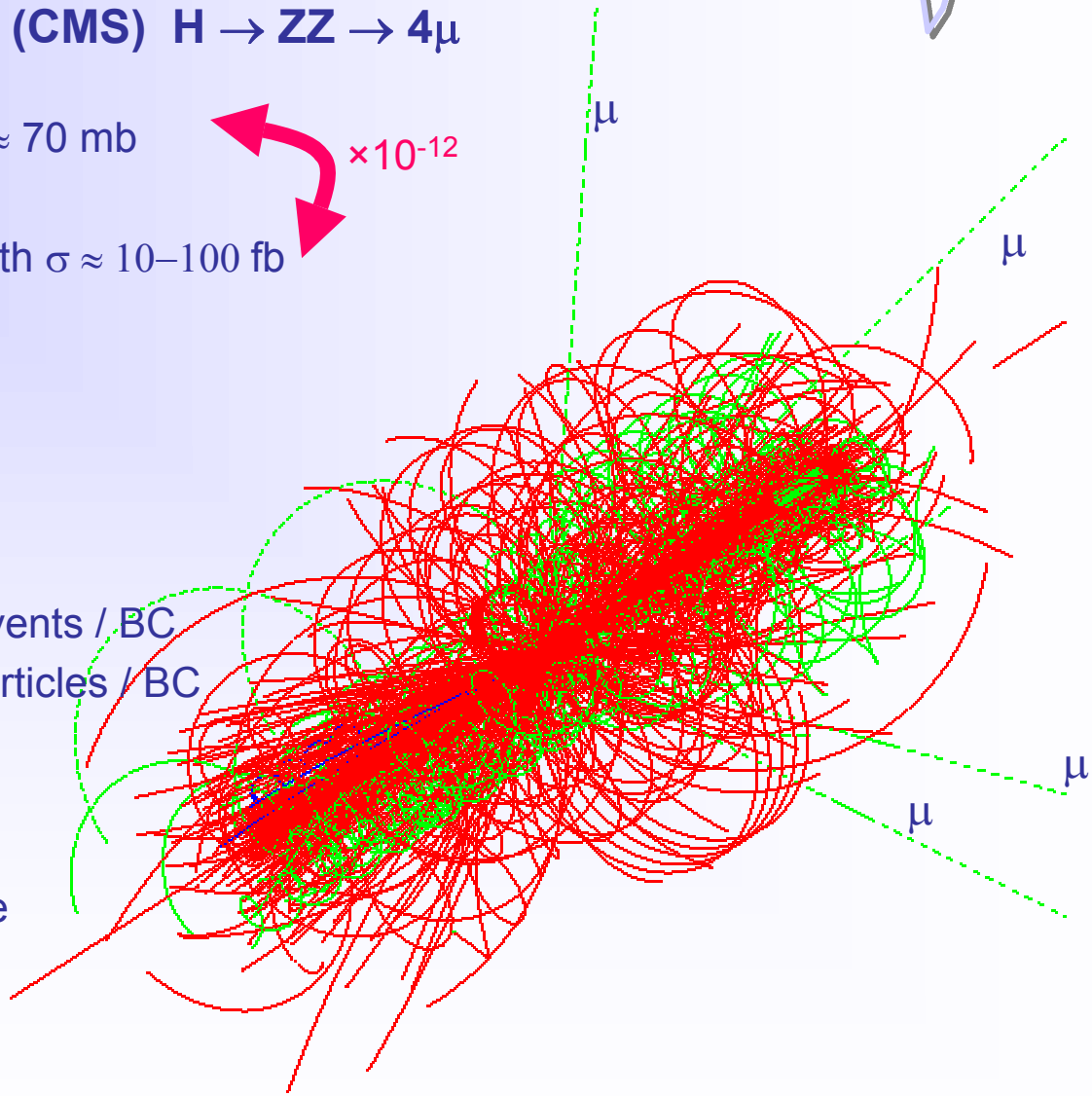

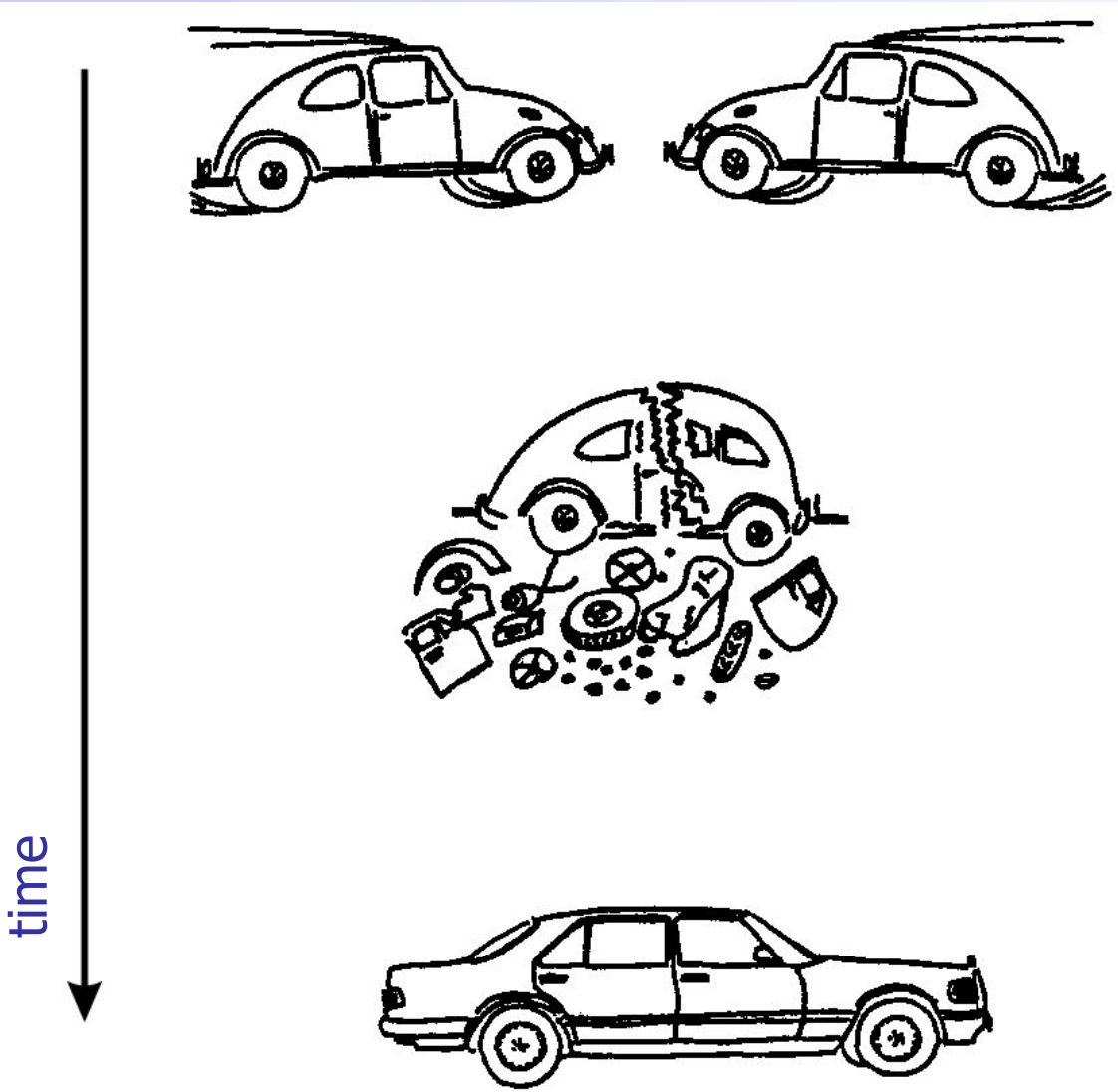

Cartoon by Claus Grupen, University of Siegen

Higgs production:
a rather rare event!

Introduction

The 'ideal' particle detector should provide…

- coverage of full solid angle (no cracks, fine segmentation)
- measurement of momentum and/or energy
- detect, track and identify all particles (mass, charge)
- fast response, no dead time

- practical limitations (technology, space, budget) !

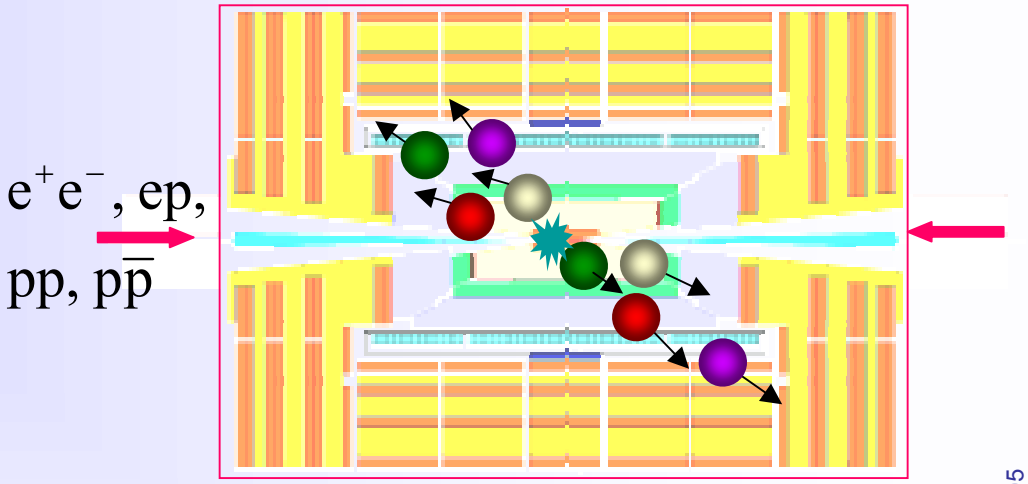

end products
- charged particles
- neutral particles
- photons

- **Particles are detected via their interaction with matter.**
- **Many different physical principles are involved (mainly of electromagnetic nature). Finally we will always observe ionization and excitation of matter.**

Detector Systems

- number of particles
- event topology
- momentum / energy
- particle identity

Can't be achieved with a single detector !

→ integrate detectors to detector systems

Geometrical concepts

Fixed target geometry

"Magnet spectrometer"

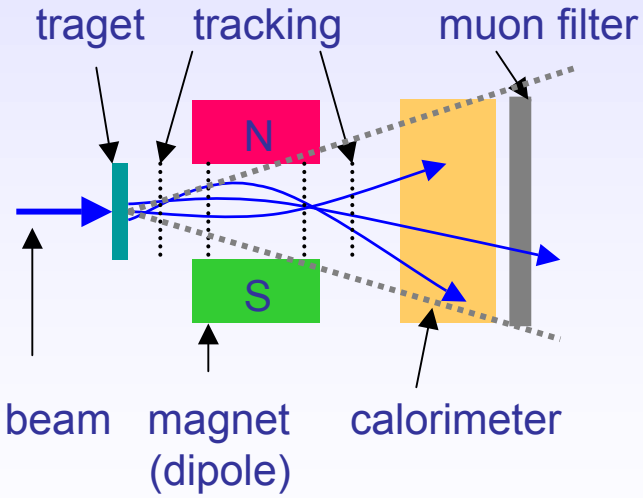

- Limited solid angle dΩ coverage
- rel. easy access (cables, maintenance)

Collider Geometry

"4π multi purpose detector"

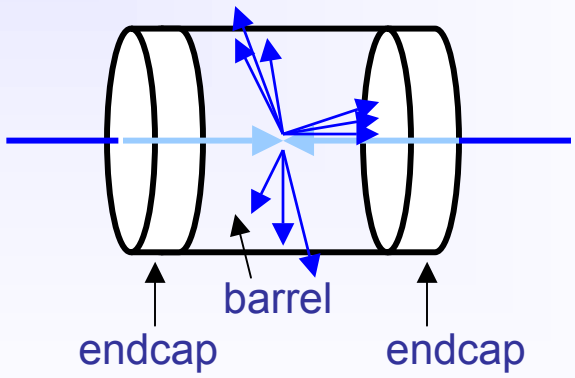

- "full" dΩ coverage
- very restricted access

Magnet concepts for 4π detectors

solenoid

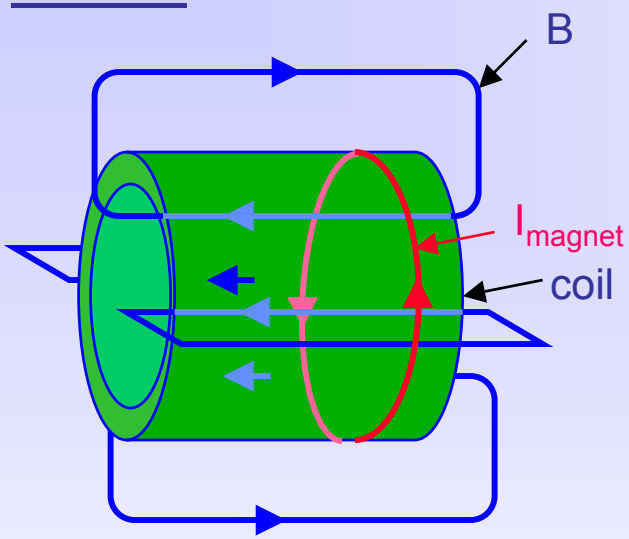

+ Large homogenous field inside coil
- weak opposite field in return yoke
- Size limited (cost)
- rel. high material budget

Examples:
- DELPHI: SC, 1.2T, Ø5.2m, L 7.4m
- L3: NC, 0.5T, Ø11.9m, L 11.9m
- CMS: SC, 4.0T, Ø5.9m, L 12.5m

toroid

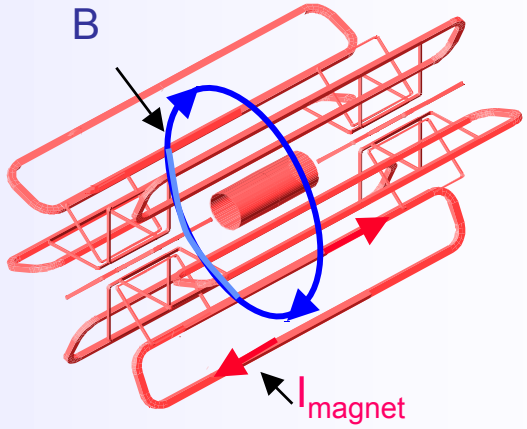

+ Field always perpendicular to $\vec{p}$
+ Rel. large fields over large volume
+ Rel. low material budget
- non-uniform field
- complex structure

Example:
- ATLAS: Barrel air toroid, SC, ~1T, Ø9.4, L 24.3m

2 ATLAS toroid coils

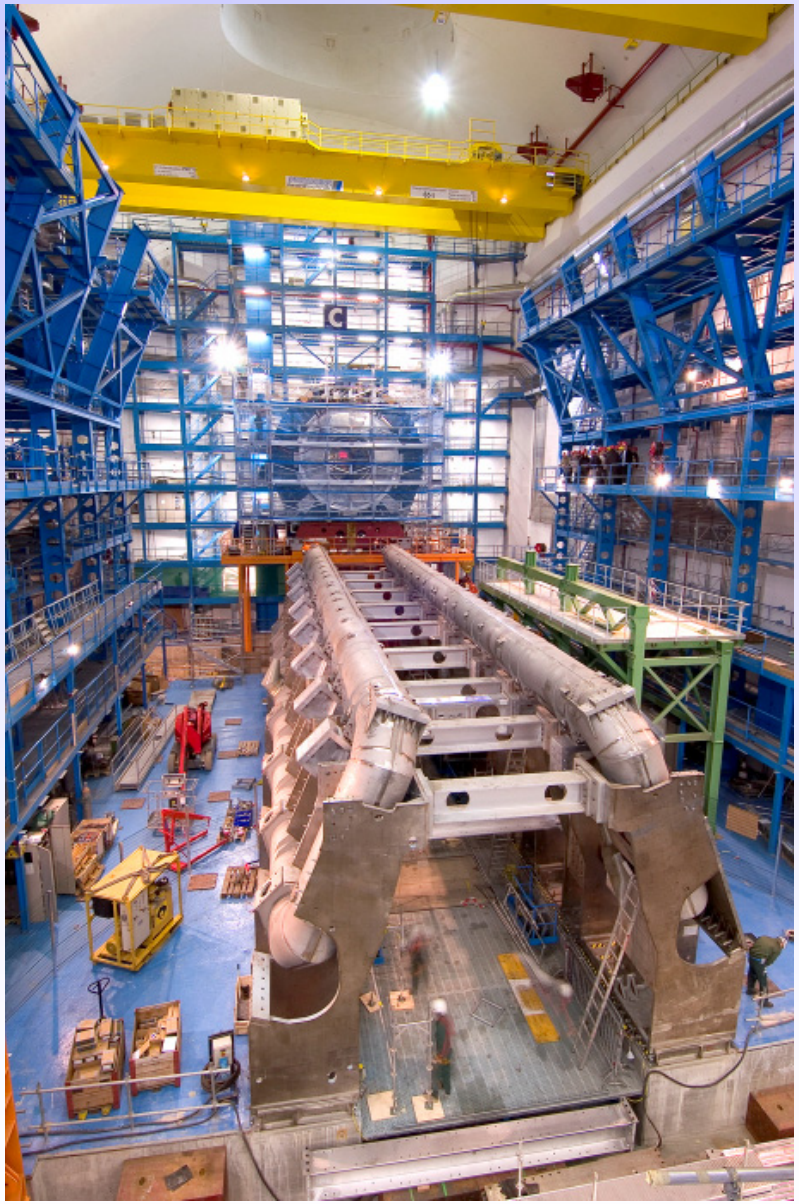

Artistic view of CMS coil

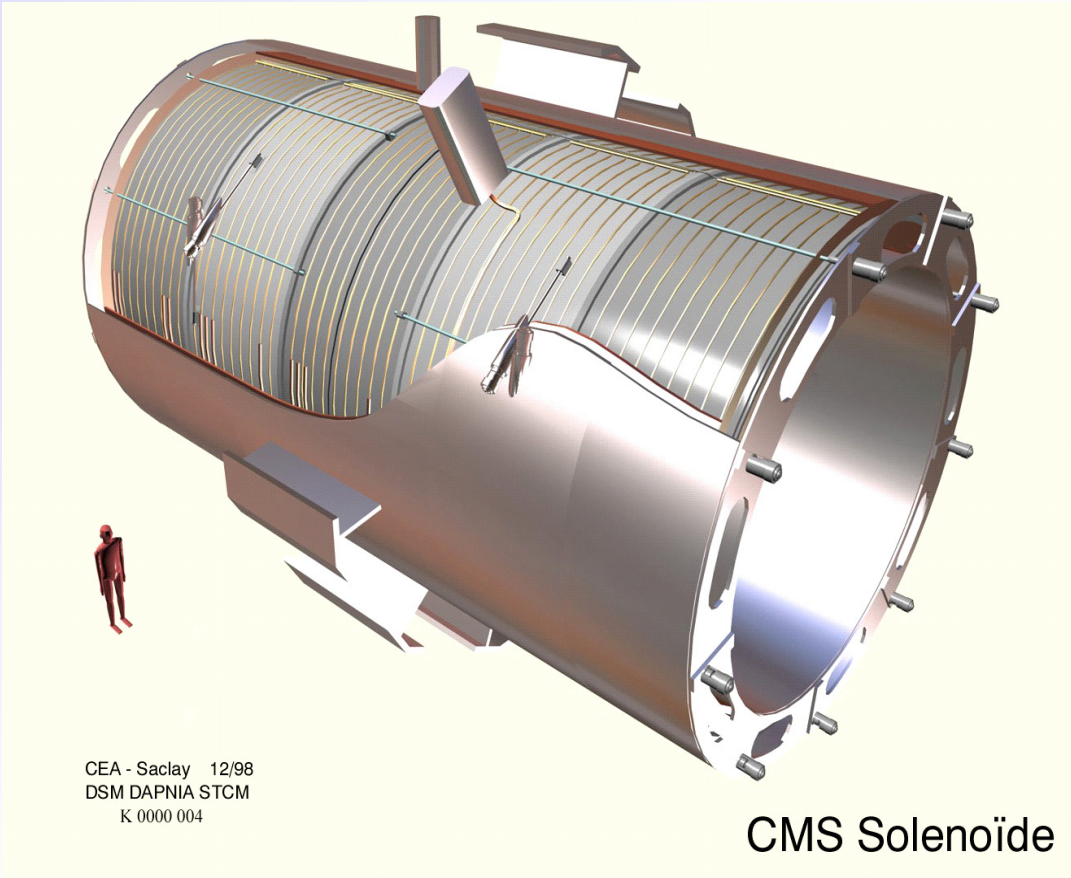

CMS Solenoïde

CERN A

Momentum measurement

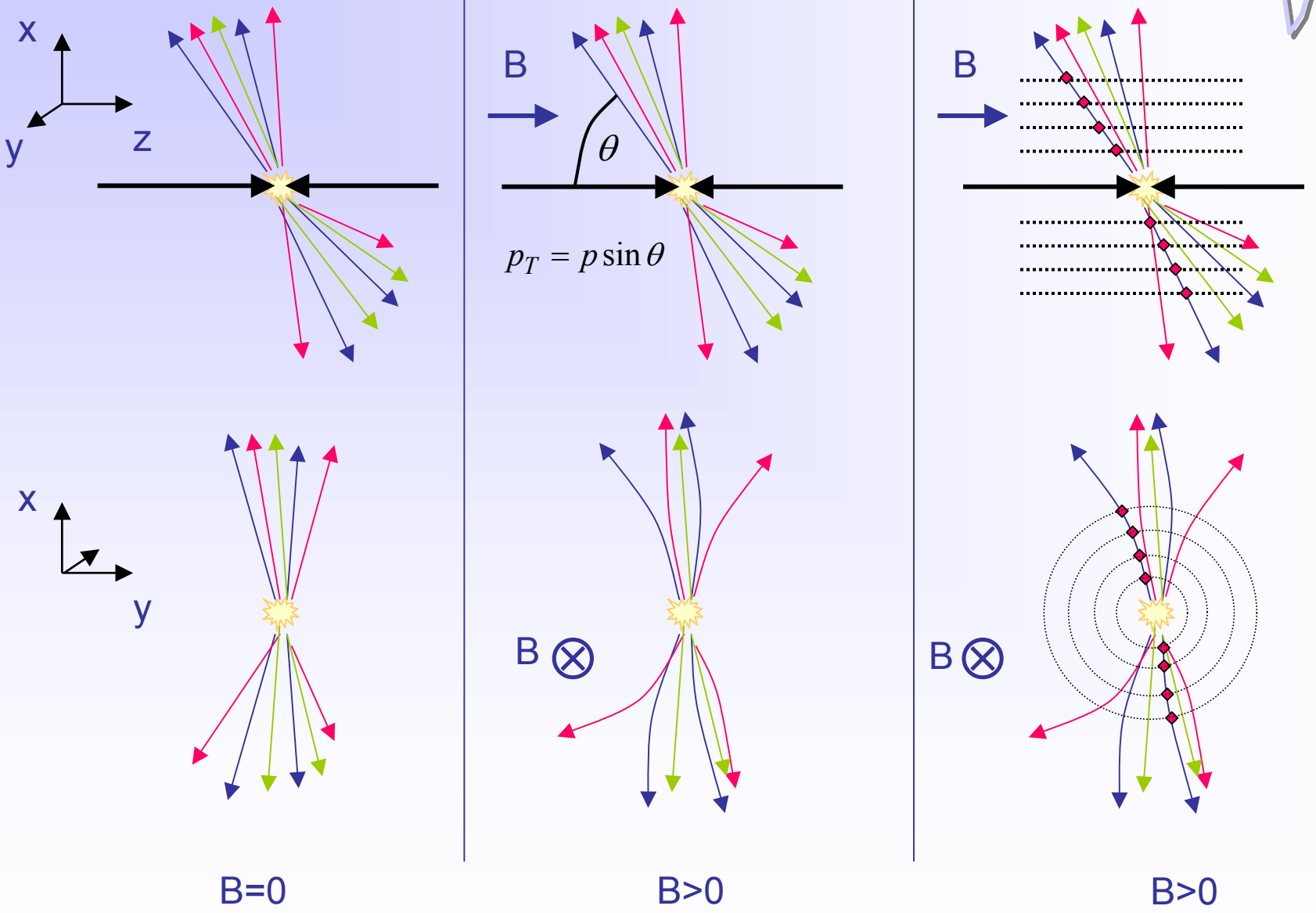

Momentum measurement

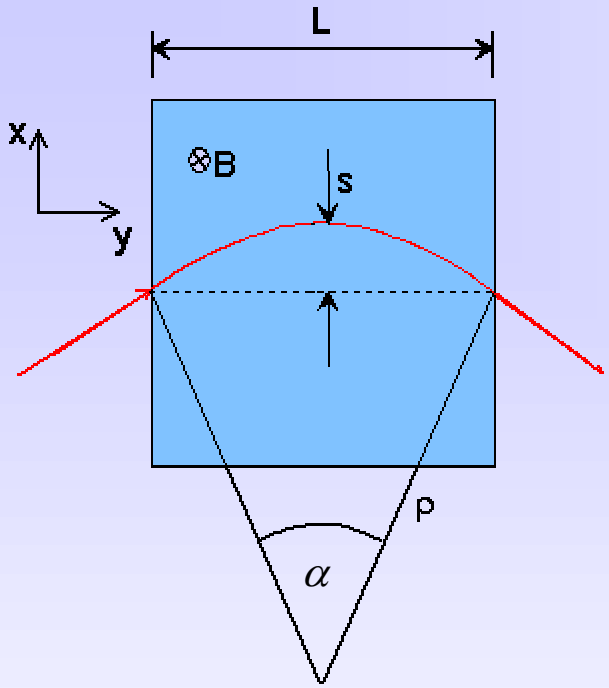

We measure only p-component transverse to B field !

$$p_T = qB\rho \quad \rightarrow \quad p_T\,(\mathrm{GeV/c}) = 0.3B\rho \quad (\mathrm{T\cdot m})$$

$$\frac{L}{2\rho} = \sin\alpha/2 \approx \alpha/2 \quad \rightarrow \quad \alpha \approx \frac{0.3L\cdot B}{p_T}$$

$$s = \rho\left(1-\cos\alpha/2\right) \approx \rho\frac{\alpha^2}{8} \approx \frac{0.3}{8}\frac{L^2B}{p_T}$$

the sagitta s is determined by 3 measurements with error *s(x):*

$$s = x_2 - \frac{x_1+x_3}{2} \qquad \left.\frac{\sigma(p_T)}{p_T}\right|^{meas.} = \frac{\sigma(s)}{s} = \frac{\sqrt{\frac{3}{2}}\sigma(x)}{s} = \frac{\sqrt{\frac{3}{2}}\sigma(x)\cdot 8p_T}{0.3\cdot BL^2}$$

$$\left.\frac{\sigma(p_T)}{p_T}\right|^{meas.} \propto \frac{\sigma(x)\cdot p_T}{BL^2}$$

for N equidistant measurements, one obtains (R.L. Gluckstern, NIM 24 (1963) 381)

$$\left.\frac{\sigma(p_T)}{p_T}\right|^{meas.} = \frac{\sigma(x)\cdot p_T}{0.3\cdot BL^2}\sqrt{720/(N+4)} \qquad \text{(for N ≥ ~10)}$$

Interaction of charged particles

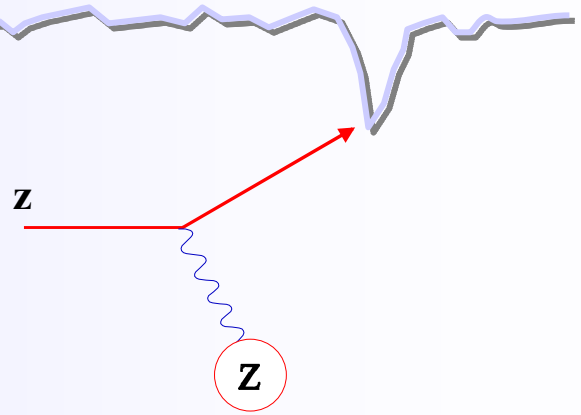

Scattering

An incoming particle with charge z interacts elastically with a target of nuclear charge Z.
The cross-section for this e.m. process is

$$\frac{d\sigma}{d\Omega} = 4zZr_e^2\left(\frac{m_e c}{\beta p}\right)^2 \frac{1}{\sin^4\theta/2}$$

Rutherford formula

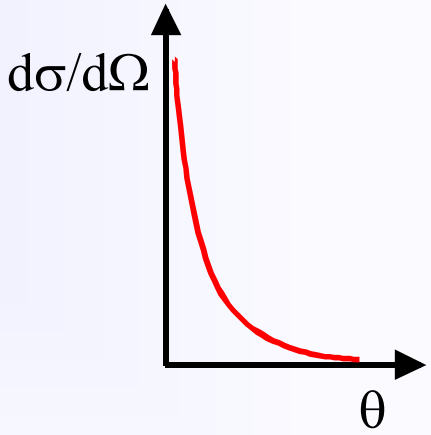

- Approximation
  - Non-relativistic
  - No spins

- Average scattering angle $\langle\theta\rangle = 0$
- Cross-section for $\theta \to 0$ infinite !

- Scattering does not lead to significant energy loss

Interaction of charged particles

In a sufficiently thick material layer a particle will undergo …

- **Multiple Scattering**

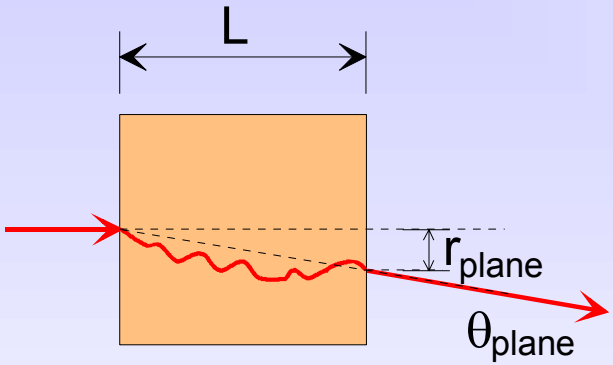

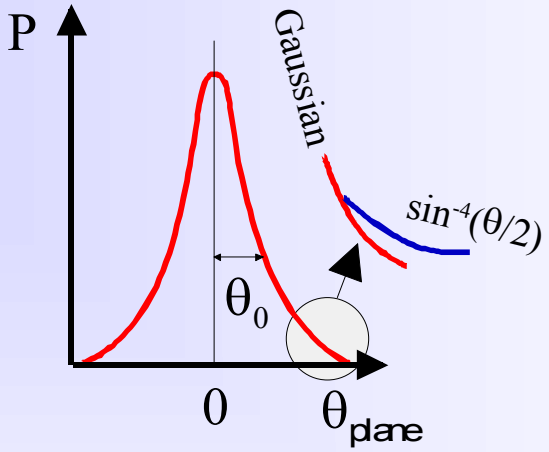

$$\theta_0 = \theta_{plane}^{RMS} = \sqrt{\left\langle \theta_{plane}^{\ 2} \right\rangle}$$

$$= \frac{1}{\sqrt{2}} \theta_{space}^{RMS}$$

Approximation $\theta_0 \propto \frac{1}{p}\sqrt{\frac{L}{X_0}}$ X_0 is radiation length of the medium (discuss later)

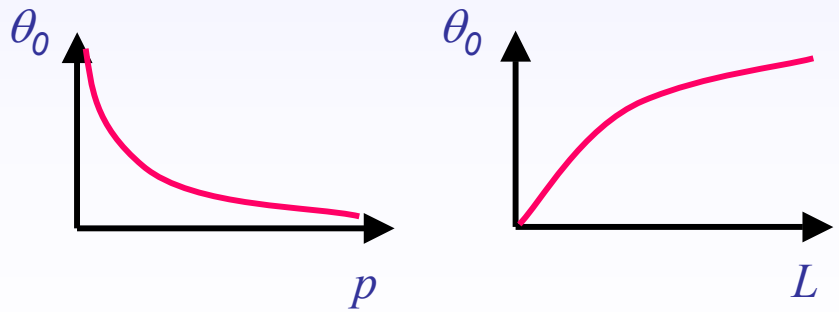

Interaction of charged particles

Back to momentum measurements:

What is the contribution of multiple scattering to $\frac{\sigma(p)}{p_T}$?

remember $\frac{\sigma(p)}{p_T} \propto \sigma(x) \cdot p_T$

$\sigma(x)\Big|^{MS} \propto \theta_0 \propto \frac{1}{p}$

$\Big\} \quad \frac{\sigma(p)}{p_T}\Big|^{MS} = \text{constant}$, i.e. independent of p !

More precisely: $\frac{\sigma(p)}{p_T}\Big|^{MS} = 0.045 \frac{1}{B\sqrt{LX_0}}$

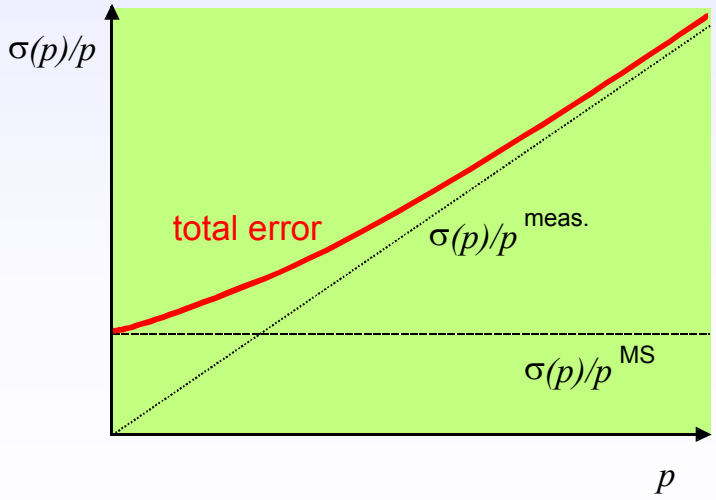

Example:

$p_t = 1$ GeV/c, $L = 1$m, $B = 1$ T, $N = 10$

$\sigma(x) = 200$ μm: $\frac{\sigma(p_T)}{p_T}\Big|^{meas.} \approx 0.5\%$

Assume detector (L = 1m) to be filled with 1 atm. Argon gas (X_0 = 110m),

$\frac{\sigma(p)}{p_T}\Big|^{MS} \approx 0.5\%$

Interaction of charged particles

Detection of charged particles

Particles can only be detected if they deposit energy in matter.
How do they lose energy in matter ?

Discrete collisions with the atomic electrons of the absorber material.

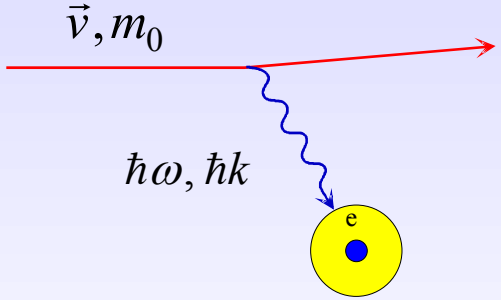

$$\left\langle \frac{dE}{dx} \right\rangle = -\int_0^\infty NE \frac{d\sigma}{dE} \hbar \, d\omega$$

N : electron density

Collisions with nuclei not important ($m_e << m_N$) for energy loss.

If $\hbar\omega, \hbar k$ are in the right range ⇨ ionization.

Interaction of charged particles

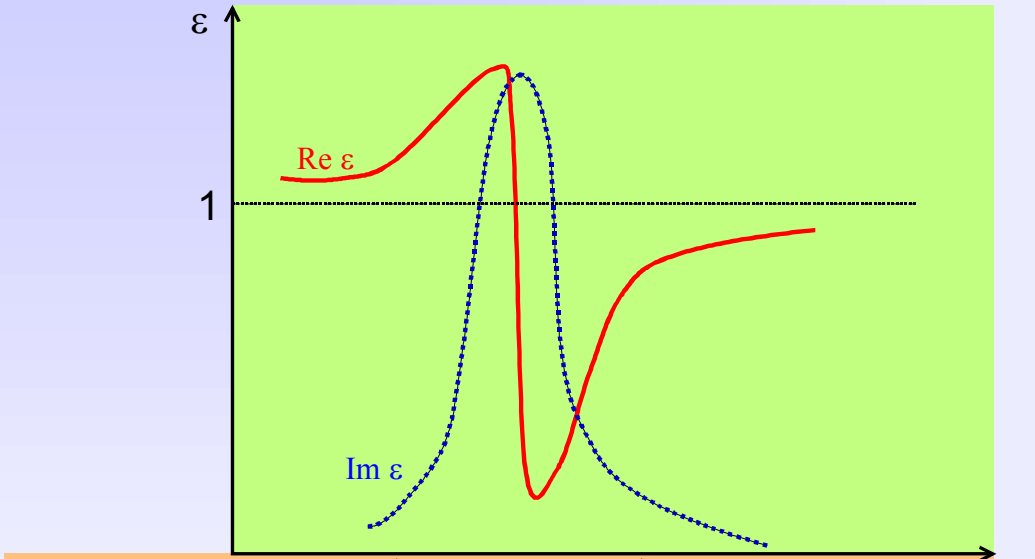

regime:	optical	absorptive	X-ray
effect:	Cherenkov radiation	ionisation	transition radiation

Optical behaviour of medium is characterized by the complex dielectric constant ε

$\mathrm{Re}\sqrt{\varepsilon} = n$ Refractive index

$\mathrm{Im}\,\varepsilon = k$ Absorption parameter

Instead of ionizing an atom or exciting the matter, under certain conditions the photon can also escape from the medium.

⇨ Emission of **Cherenkov** and **Transition** radiation. (See later). This emission of real photons contributes also to the energy loss.

Interaction of charged particles

- **Average differential energy loss** $\left\langle \frac{dE}{dx} \right\rangle$

… making Bethe-Bloch plausible.

Energy loss at a single encounter with an electron

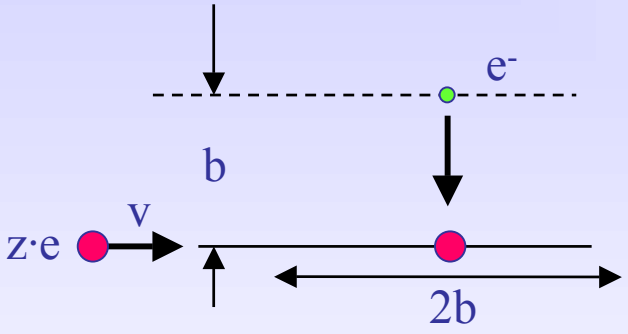

$$F_c = \frac{ze^2}{b^2} \quad \Delta t = \frac{2b}{v} \quad \Delta p_e = F_c \Delta t$$

$$\Delta E_e = \frac{(\Delta p_e)^2}{2m_e} = \frac{2z^2e^4}{b^2v^2m_e} = \frac{2r_e^2 m_e c^2 z^2}{b^2} \cdot \frac{1}{\beta^2}$$

Introduced classical electron radius $r_e = \frac{e^2}{m_e c^2}$

How many encounters are there ?

Should be proportional to electron density in medium $N_e \propto \frac{Z}{A} N_A \cdot \rho$

The real Bethe-Bloch formula.

$$\left\langle \frac{dE}{dx} \right\rangle = -4\pi N_A r_e^2 m_e c^2 z^2 \frac{Z}{A} \frac{1}{\beta^2} \left[\frac{1}{2} \ln \frac{2m_e c^2 \gamma^2 \beta^2 T^{\max}}{I^2} - \beta^2 - \frac{\delta}{2} \right]$$

Interaction of charged particles

Energy loss by Ionisation only → Bethe - Bloch formula

$$\left\langle \frac{dE}{dx} \right\rangle = -4\pi N_A r_e^2 m_e c^2 z^2 \frac{Z}{A}\frac{1}{\beta^2}\left[\frac{1}{2}\ln\frac{2m_e c^2\gamma^2\beta^2 T^{\max}}{I^2} - \beta^2 - \frac{\delta}{2}\right]$$

- dE/dx in [MeV g^{-1} cm^2]
- valid for "heavy" particles ($m \geq m_\mu$).
- dE/dx depends only on β, independent of m !
- First approximation: medium simply characterized by Z/A ~ electron density

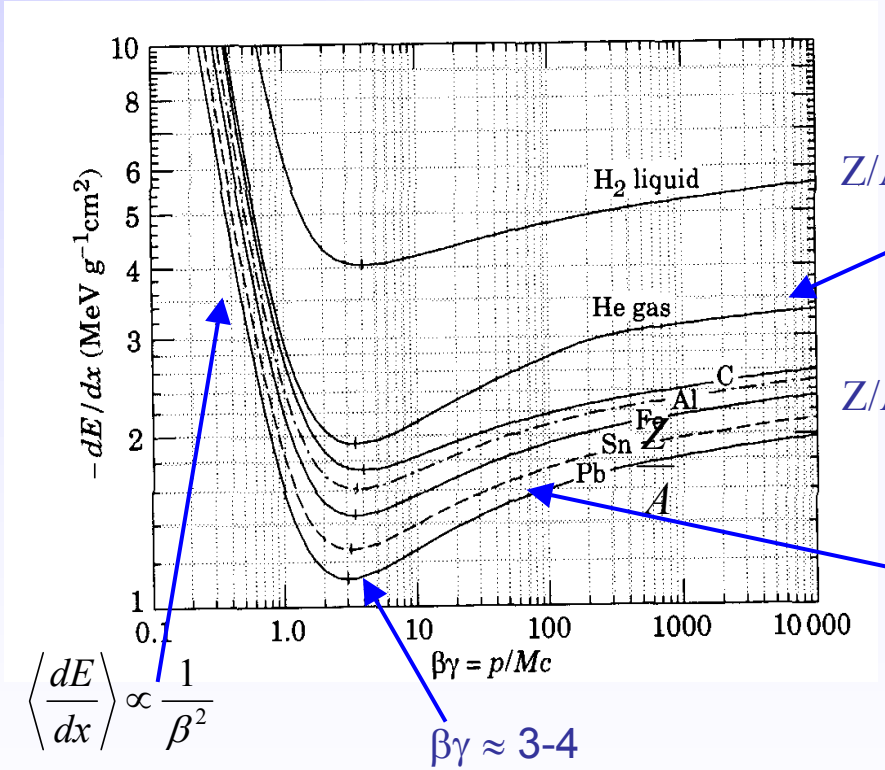

Z/A = 1

"Fermi plateau"

Z/A~0.5

$\left\langle \frac{dE}{dx} \right\rangle \propto \ln \beta^2\gamma^2$

"relativistic rise"

$\left\langle \frac{dE}{dx} \right\rangle \propto \frac{1}{\beta^2}$

"kinematical term"

$\beta\gamma \approx 3\text{-}4$

minimum ionizing particles, MIPs

Interaction of charged particles

Bethe - Bloch formula cont'd $$\left\langle \frac{dE}{dx} \right\rangle = -4\pi N_A r_e^2 m_e c^2 z^2 \frac{Z}{A}\frac{1}{\beta^2}\left[\frac{1}{2}\ln\frac{2m_e c^2\gamma^2\beta^2 T^{\max}}{I^2} - \beta^2 - \frac{\delta}{2}\right]$$

- Formula takes into account energy transfers

  $I \le dE \le T^{\max}$ I : mean excitation potential $I \approx I_0 Z$ with $I_0 = 10$ eV (approx., I fitted for each element)

- relativistic rise - ln γ^2 term - attributed to relativistic expansion of transverse E-field → contributions from more distant collisions.

- relativistic rise cancelled at high γ by "density effect", polarization of medium screens more distant atoms. Parameterized by δ (material dependent) → Fermi plateau

- many other small corrections

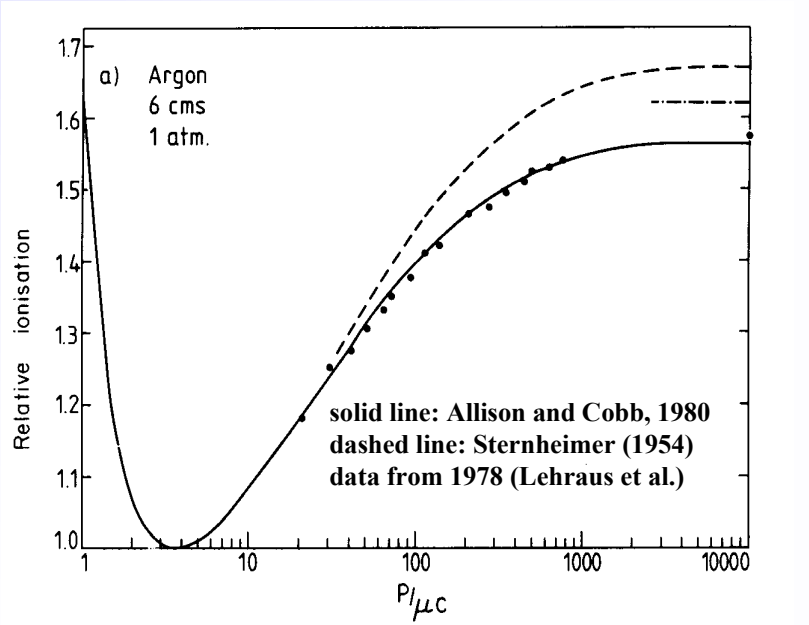

Measured and calculated dE/dx

Interaction of charged particles

Real detector (limited granularity) can not measure <*dE/dx*> !

It measures the energy ΔE deposited in a layer of finite thickness δx.

For thin layers or low density materials:

→ Few collisions, some with high energy transfer.

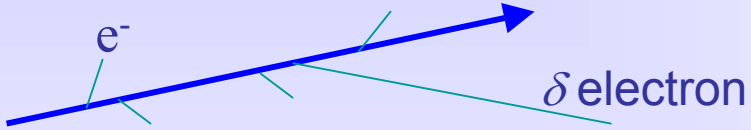

→ Energy loss distributions show large fluctuations towards high losses: "Landau tails"

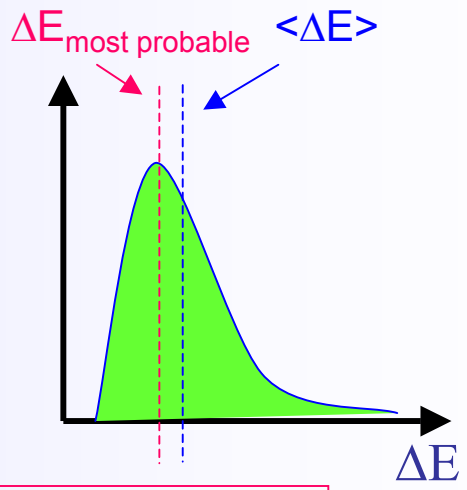

Example: Si sensor: 300 μm thick. $\Delta E_{m.p} \sim 82$ keV $\quad <\Delta E> \sim 115$ keV

For thick layers and high density materials:

→ Many collisions.

→ Central Limit Theorem → Gaussian shaped distributions.

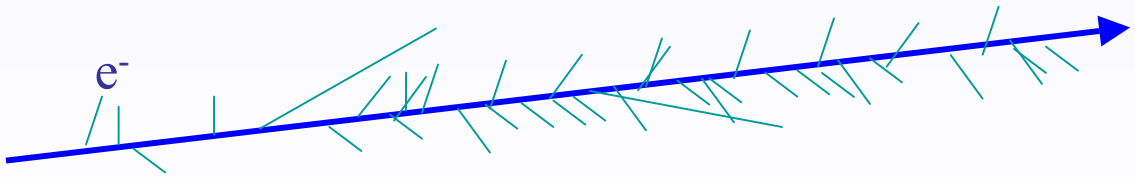

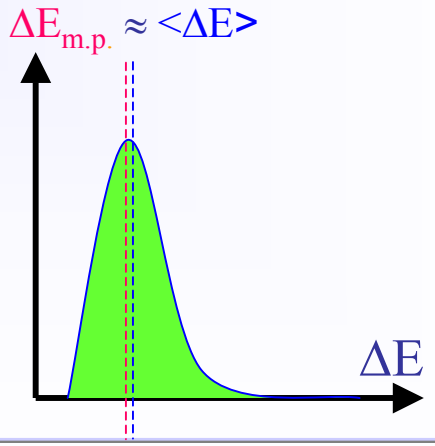

Interaction of charged particles

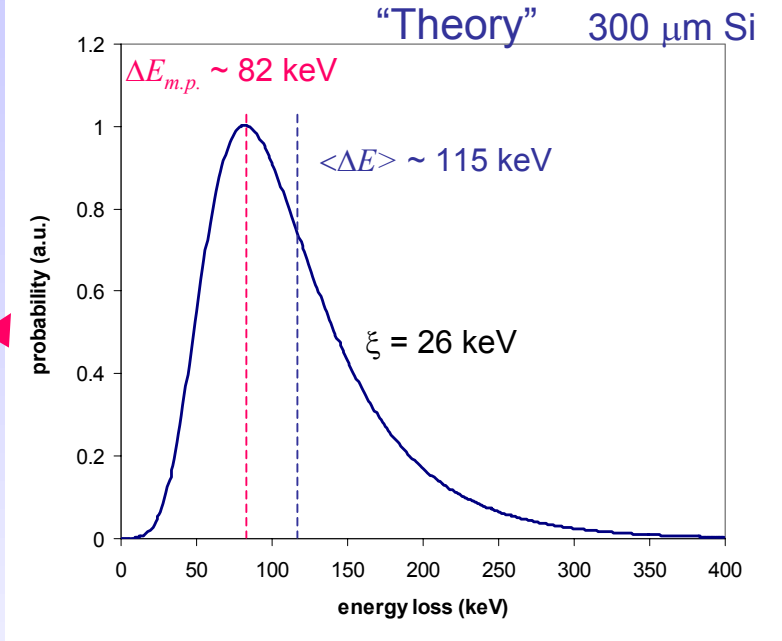

charge collection is not 100%

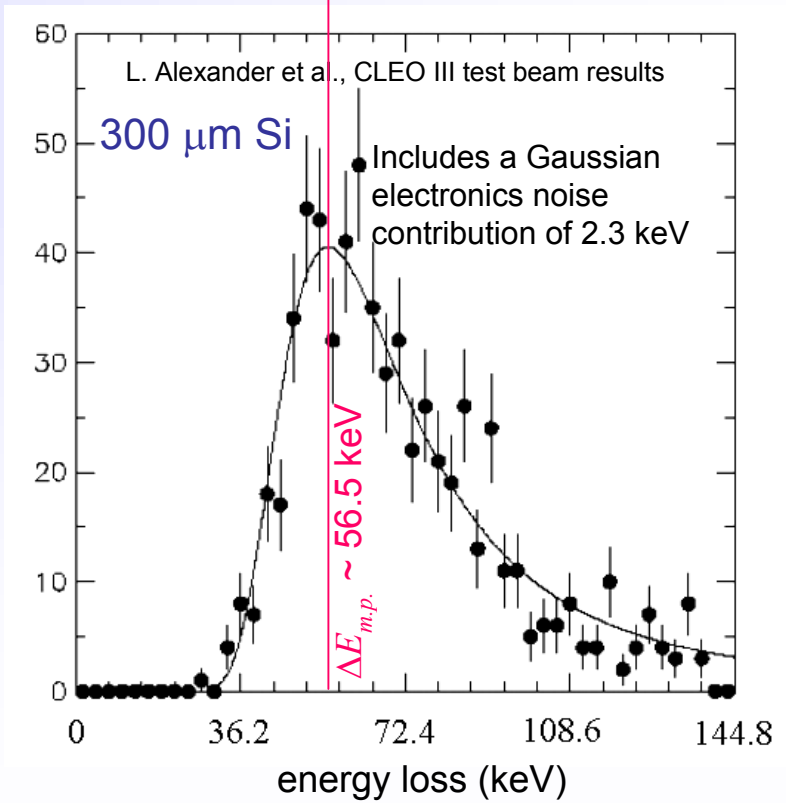

Landau's theory J. Phys (USSR) 8, 201 (1944)

$$f(x,\Delta E) = \frac{1}{\xi}\Omega(\lambda) \qquad \Omega(\lambda) \approx \frac{1}{\sqrt{2\pi}}\exp\left\{-\tfrac{1}{2}(\lambda + e^{-\lambda})\right\}$$

$$\lambda = \frac{\Delta E - \Delta E_{m.p.}}{\xi}$$

$$\xi = \frac{2\pi N e^4}{m_e v^2}\frac{Z}{A}x$$

x (300 μm Si) = 69 mg/cm^2

Outline

- **Lecture 1 - Introduction** — C. Joram, L. Ropelewski
- **Lecture 2a - Gas Detectors** — L. Ropelewski
  - Ionization of Gases
  - Gas Amplification
  - Single Wire Proportional Chamber
  - Drift Chamber
  - Drift and Diffusion of Charge Carriers in Gases
  - Examples of Detectors (CSC, RPC, TPC)
  - New Technologies – Micropattern Detectors
  - Limitations of Gas Detectors
  - Gas Detectors Simulations
  - Applications
- **Lecture 2b – Silicon Detectors** — M. Moll
- **Lecture 3 - Scintillation and Photodetection** — C. D'Ambrosio, T. Gys
- **Lecture 4 - Calorimetry, Particle ID** — C. Joram
- **Lecture 5 - Particle ID, Detector Systems** — C. Joram, C. D'Ambrosio

Ionization of Gases

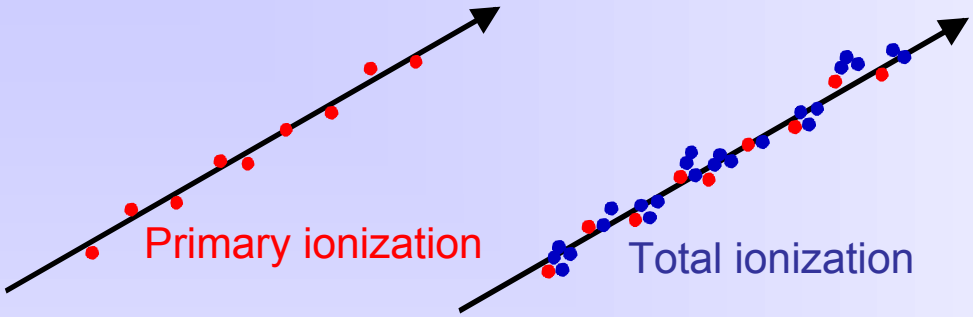

Lohse and Witzeling, Instrumentation In High Energy Physics, World Scientific,1992

Fast charged particles ionize atoms of gas. Often resulting primary electron will have enough kinetic energy to ionize other atoms.

$$n_{total} = \frac{\Delta E}{W_i} = \frac{\frac{dE}{dx}\Delta x}{W_i}$$

$$n_{total} \approx 3\ldots4 \cdot n_{primary}$$

n_{total} - number of created electron-ion pairs

Δ_E = total energy loss

W_i = effective <energy loss>/pair

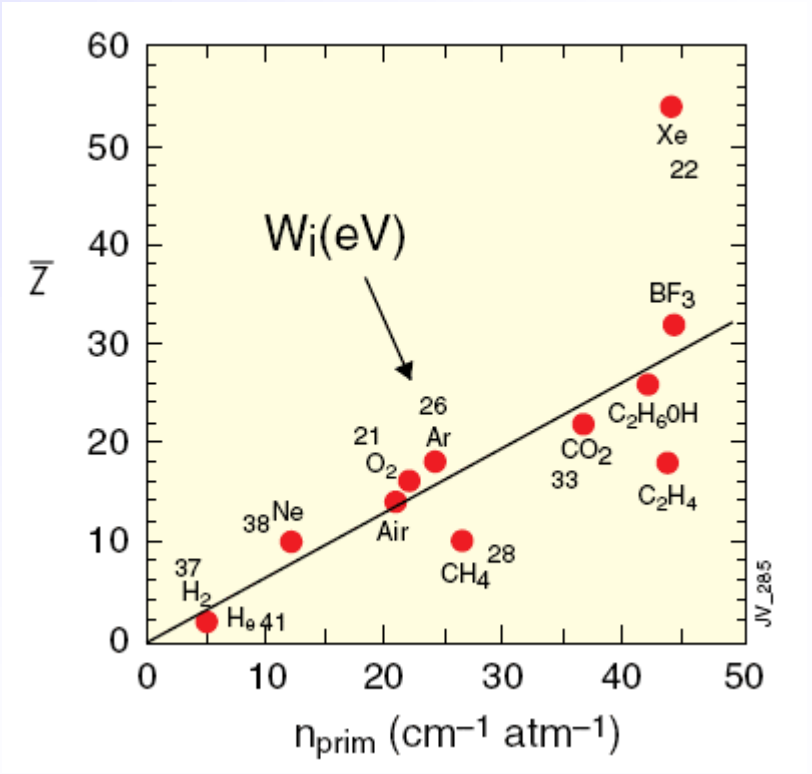

Number of primary electron/ion pairs in frequently used gases.

Ionization of Gases

- The actual number of primary electron/ion pairs is Poisson distributed.

$$P(m) = \frac{\bar{n}^m e^{-\bar{n}}}{m!} \qquad \bar{n} = \frac{L}{\lambda} = LN\sigma_i$$

The detection efficiency is therefore limited to :

$$\varepsilon_{\text{det}} = 1 - P(0) = 1 - e^{-\bar{n}}$$

For thin layers ε_{det} can be significantly lower than 1.

For example for 1 mm layer of Ar $n_{primary} = 2.5 \rightarrow \varepsilon_{det} = 0.92$.

- 100 electron/ion pairs created during ionization process is not easy to detect.
  Typical noise of the amplifier ≈ 1000 e^- (ENC) → gas amplification .

Single Wire Proportional Chamber

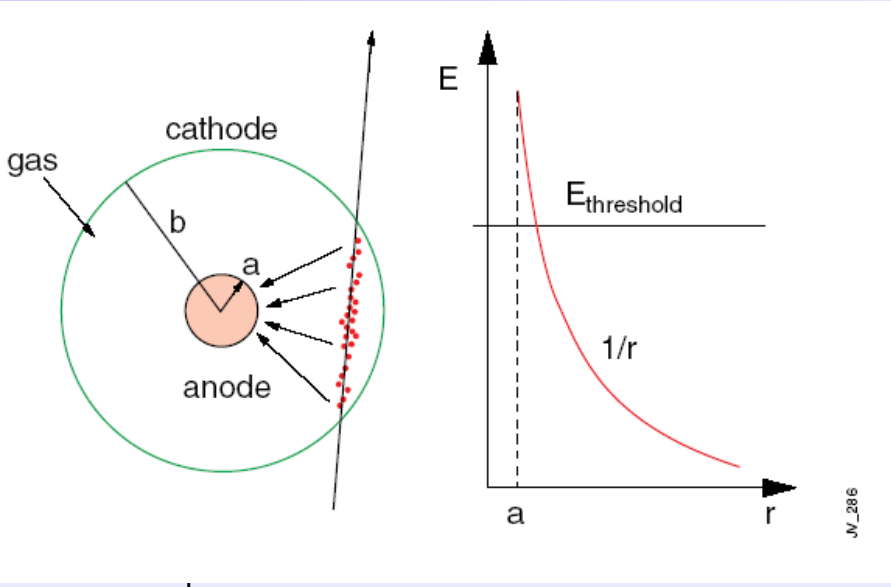

Electrons liberated by ionization drift towards the anode wire.

Electrical field close to the wire (typical wire Ø ~few tens of μm) is sufficiently high for electrons (above 10 kV/cm) to gain enough energy to ionize further → avalanche – exponential increase of number of electron ion pairs.

$$E(r) = \frac{CV_0}{2\pi\varepsilon_0} \cdot \frac{1}{r}$$

$$V(r) = \frac{CV_0}{2\pi\varepsilon_0} \cdot \ln\frac{r}{a}$$

C – capacitance/unit length

Cylindrical geometry is not the only one able to generate strong electric field:

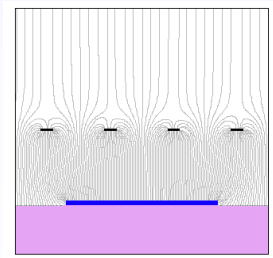
parallel plate

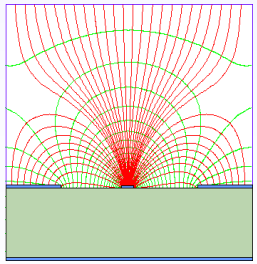
strip

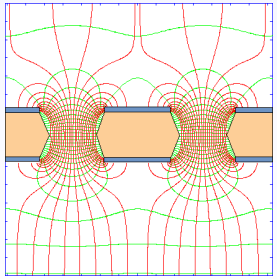
hole

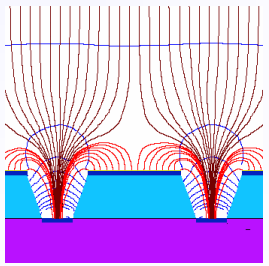
groove

Single Wire Proportional Chamber

Multiplication of ionization is described by the first Townsend coefficient $\alpha(E)$

$$dn = n\alpha dx \qquad \alpha = \frac{1}{\lambda}$$

λ – mean free path

$$n = n_0 e^{\alpha(E)x} \quad \text{or} \quad n = n_0 e^{\alpha(r)x}$$

$\alpha(E)$ is determined by the excitation and ionization cross sections of the electrons in the gas.

It depends also on various and complex energy transfer mechanisms between gas molecules.

There is no fundamental expression for $\alpha(E)$ → it has to be measured for every gas mixture.

$$M = \frac{n}{n_0} = \exp\left[\int_a^{r_C} \alpha(r)dr\right]$$

Amplification factor or Gain

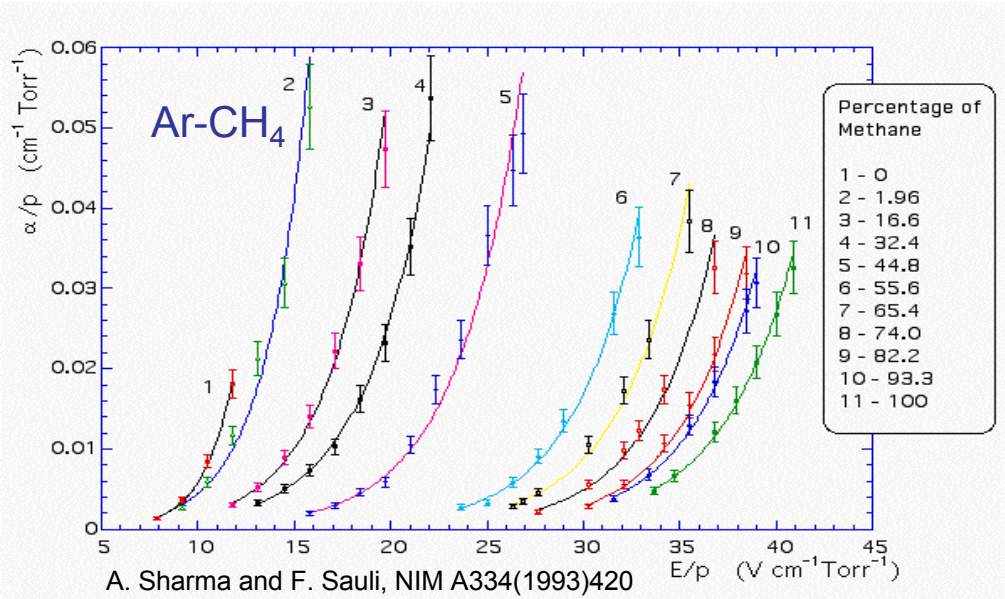

A. Sharma and F. Sauli, NIM A334(1993)420

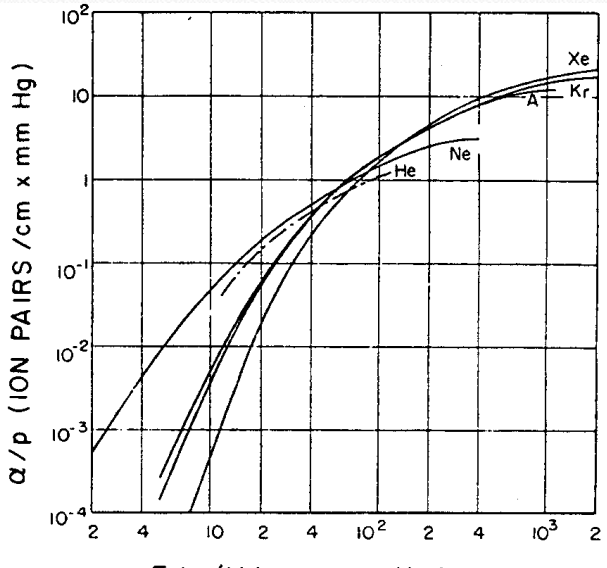

S.C. Brown, Basic data of plasma physics (MIT Press, 1959)

SWPC – Choice of Gas

In the avalanche process molecules of the gas can be brought to excited states.

S. Biagi, NIM A421 (1999) 234

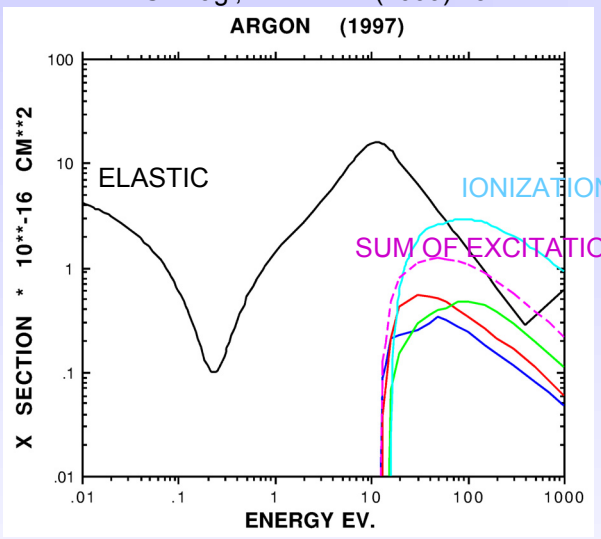

De-excitation of noble gases only via emission of photons;
e.g. 11.6 eV for Ar.
This is above ionization threshold of metals;
e.g. Cu 7.7 eV.

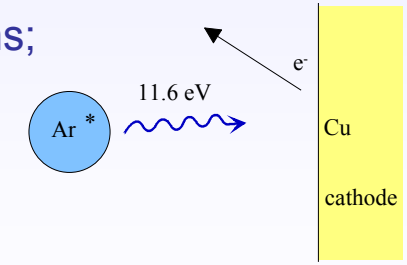

new avalanches → permanent discharges

Solution: addition of polyatomic gas as a quencher

Absorption of photons in a large energy range (many vibrational and rotational energy levels).

Energy dissipation by collisions or dissociation into smaller molecules.

S. Biagi, NIM A421 (1999) 234

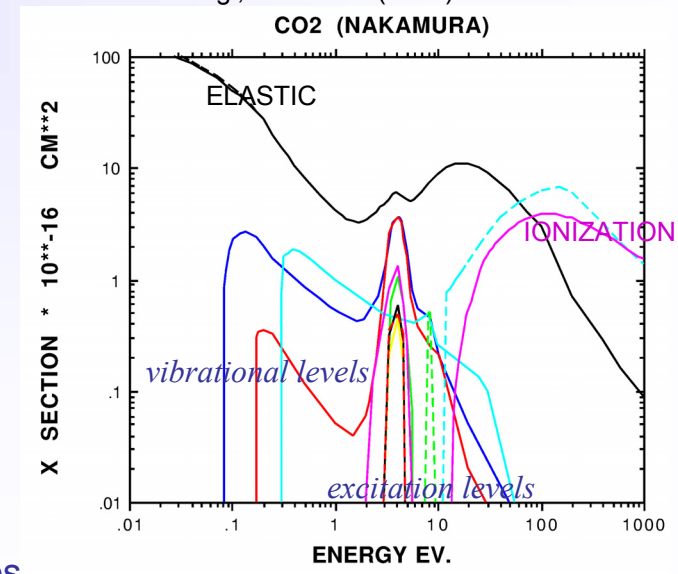

SWPC – Operation Modes

- ionization mode – full charge collection, but no charge multiplication;
  gain ~ 1
- proportional mode – multiplication of ionization starts; detected signal proportional to original ionization → possible energy measurement (dE/dx); secondary avalanches have to be quenched;
  gain ~ 10^4 – 10^5
- limited proportional mode (saturated, streamer) – strong photoemission; secondary avalanches merging with original avalanche; requires strong quenchers or pulsed HV; large signals → simple electronics;
  gain ~ 10^{10}
- Geiger mode – massive photoemission; full length of the anode wire affected; discharge stopped by HV cut; strong quenchers needed as well

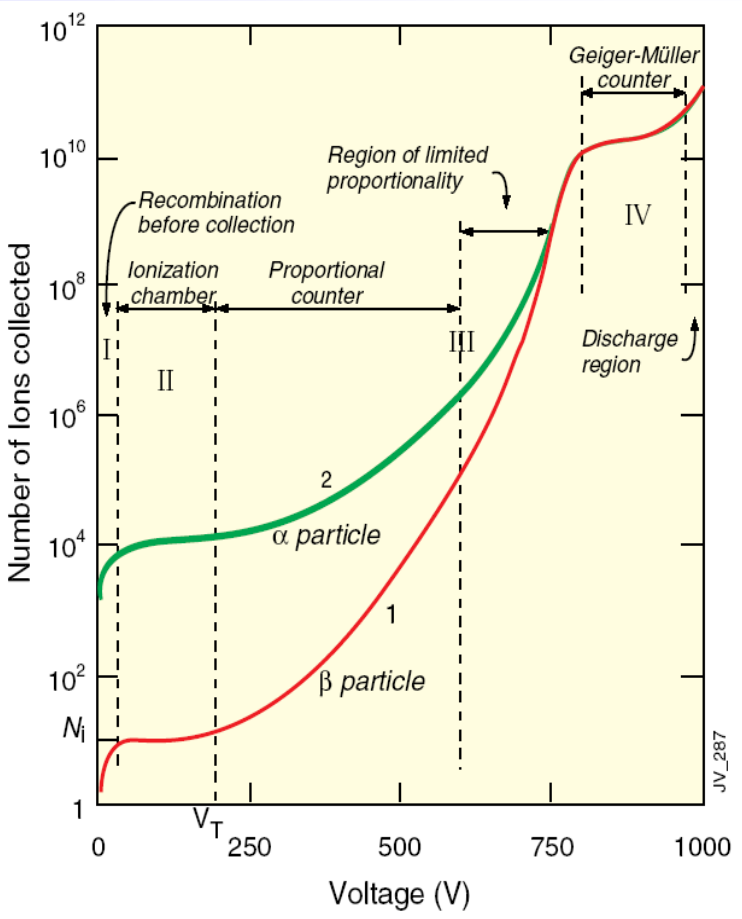

SWPC – Signal Formation

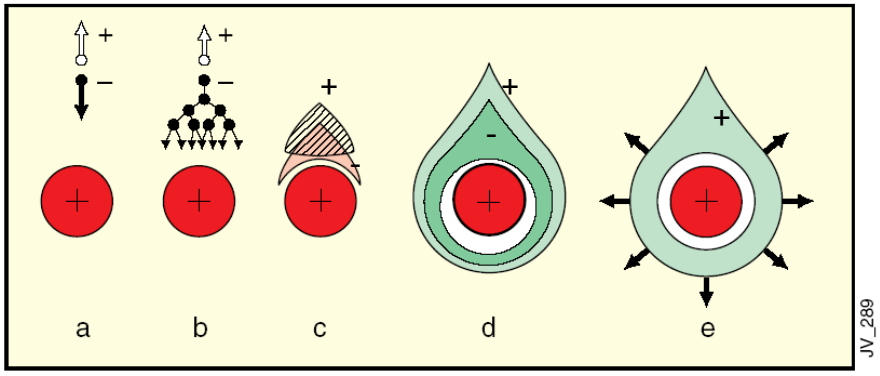

Avalanche formation within a few wire radii and within t < 1 ns.
Signal induction both on anode and cathode due to moving charges (both electrons and ions).

$$dv = \frac{Q}{lCV_0}\frac{dV}{dr}dr$$

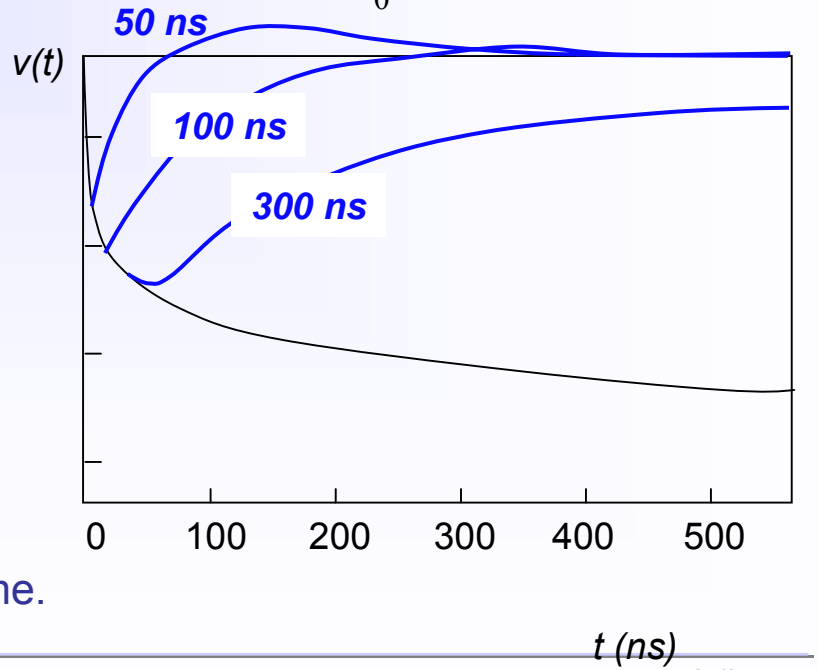

Electrons collected by the anode wire i.e. dr is very small (few μm). Electrons contribute only very little to detected signal (few %).
Ions have to drift back to cathode i.e. dr is large (few mm). Signal duration limited by total ion drift time.

Need electronic signal differentiation to limit dead time.

Multiwire Proportional Chamber

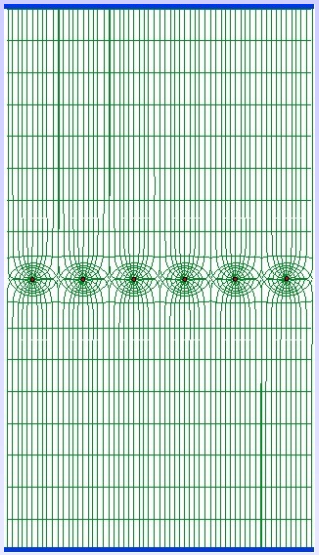

Simple idea to multiply SWPC cell : Nobel Prize 1992

First electronic device allowing high statistics experiments !!

Typical geometry

5mm, 1mm, 20 μm

Normally digital readout :

spatial resolution limited to

$$\sigma_x \approx \frac{d}{\sqrt{12}}$$

for d = 1 mm σ_x = 300 μm

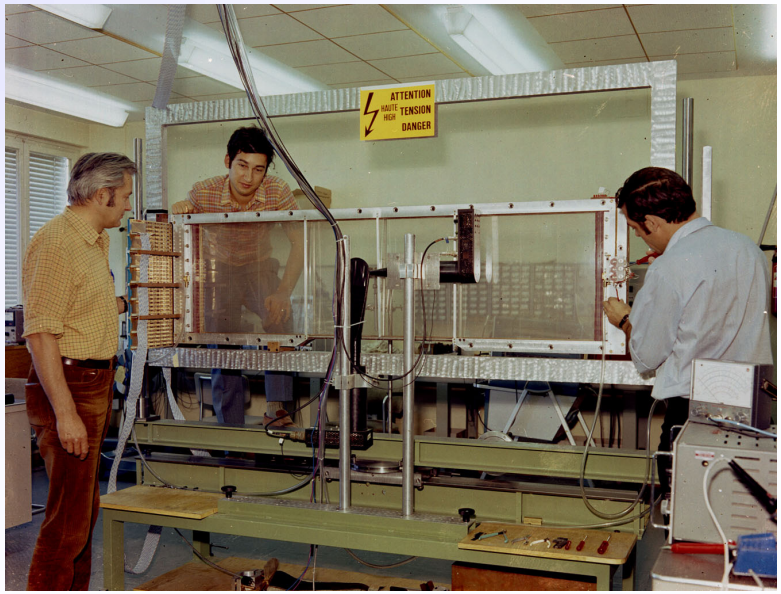

G. Charpak, F. Sauli and J.C. Santiard

CSC – Cathode Strip Chamber

Precise measurement of the second coordinate by interpolation of the signal induced on pads.
Closely spaced wires makes CSC fast detector.

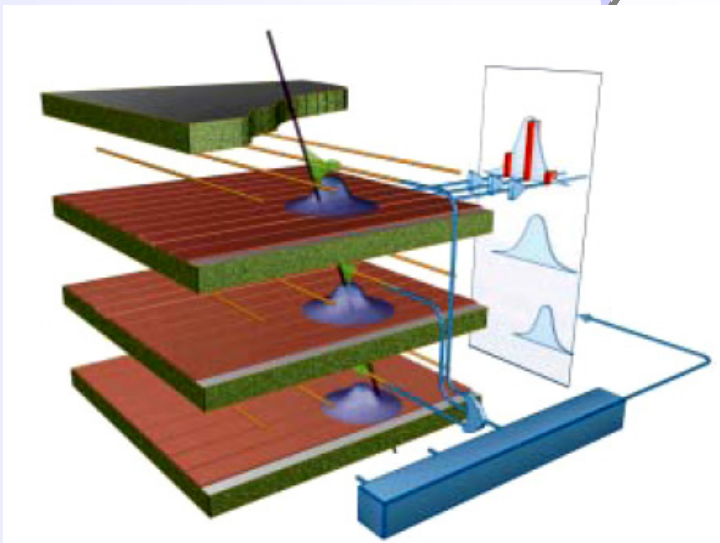

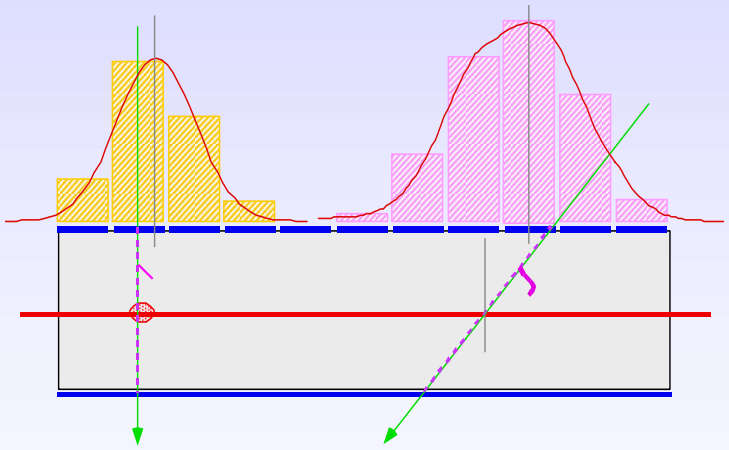

Center of gravity of induced signal method.

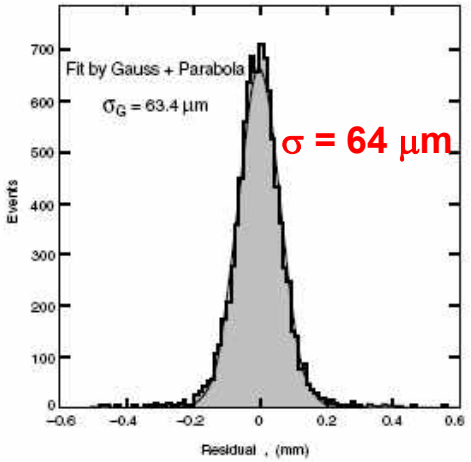

Space resolution

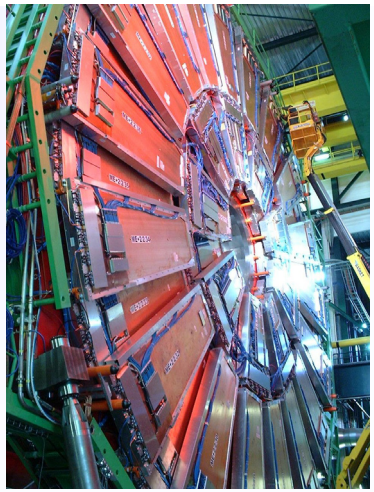

CMS

RPC – Resistive Plate Chamber

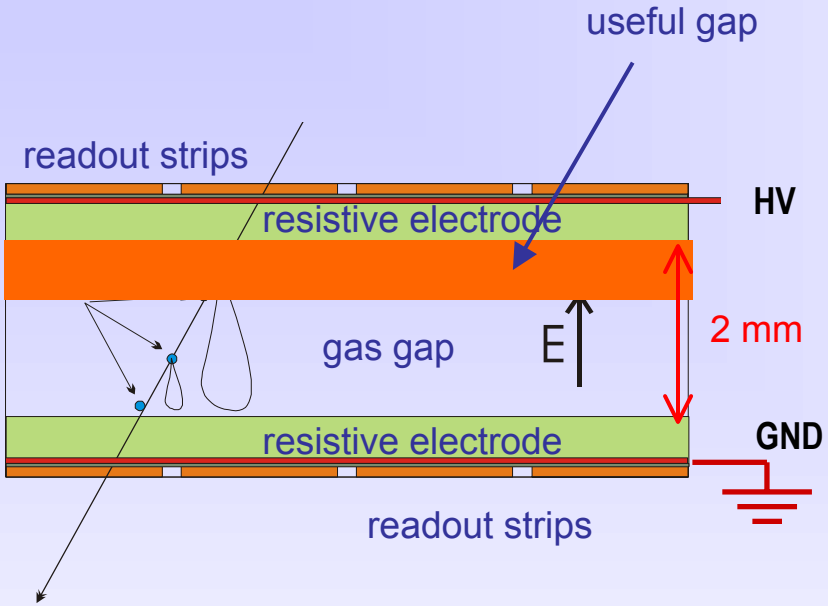

MRPC

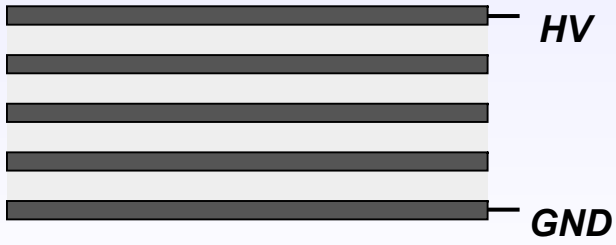

Multigap RPC - exceptional time resolution suited for the trigger applications

Rate capability strong function of the resistivity of electrodes in streamer mode.

A. Akindinov et al., NIM A456(2000)16

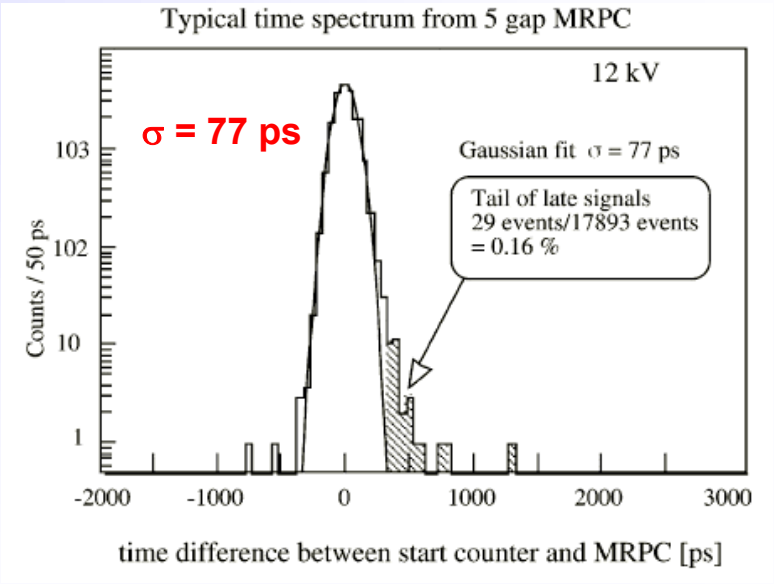

Time resolution

Drift Chambers

Spatial information obtained by measuring time of drift of electrons

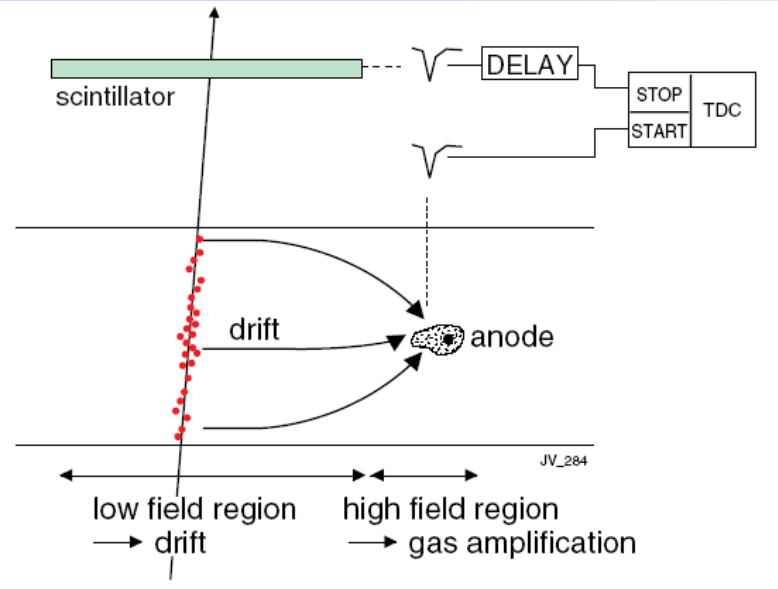

Measure arrival time of electrons at sense wire relative to a time t_0.

Need a trigger (bunch crossing or scintillator).

Drift velocity independent from E.

F. Sauli, NIM 156(1978)147

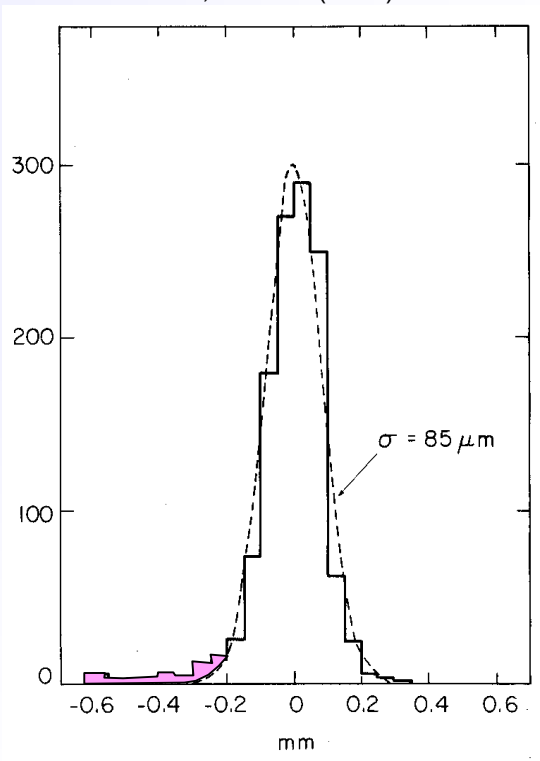

Advantages: smaller number of electronics channels.

Resolution determined by diffusion, primary ionization statistics, path fluctuations and electronics.

Drift Chambers

Planar drift chamber designs

Essential: linear space-time relation; constant E-field; little dpendence of v_D on E.

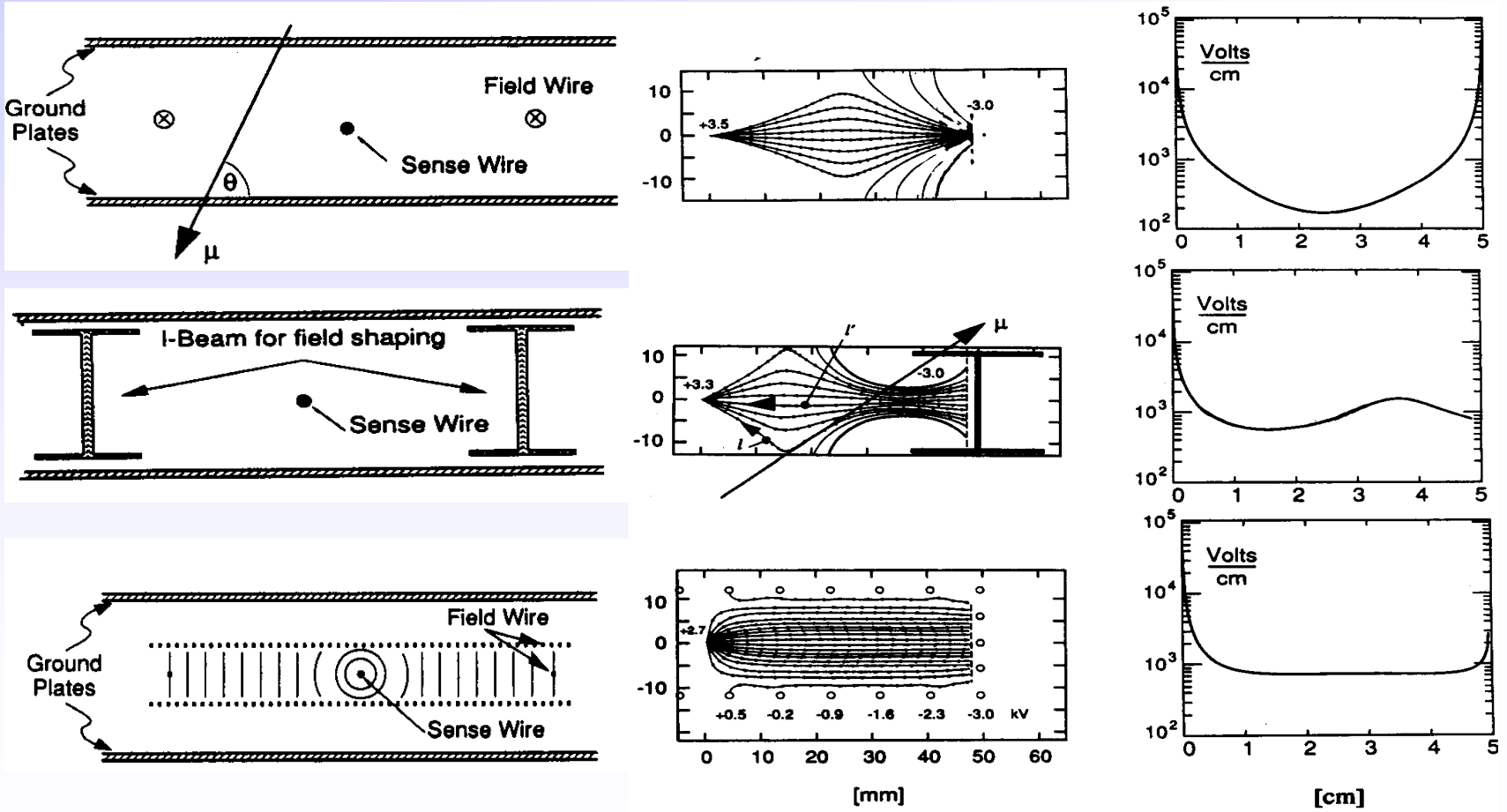

U. Becker in Instrumentation in High Energy Physics, World Scientific

Diffusion of Free Charges

F. Sauli, IEEE Short Course on Radiation Detection and Measurement, Norfolk (Virginia) November 10-11, 2002

Free ionization charges lose energy in collisions with gas atoms and molecules (thermalization).

Maxwell - Boltzmann energy distribution:

$$F(\varepsilon) = const\sqrt{\varepsilon}e^{-\frac{\varepsilon}{kT}}$$

Average (thermal) energy:

$$\varepsilon_T = \frac{3}{2}kT \approx 0.040eV$$

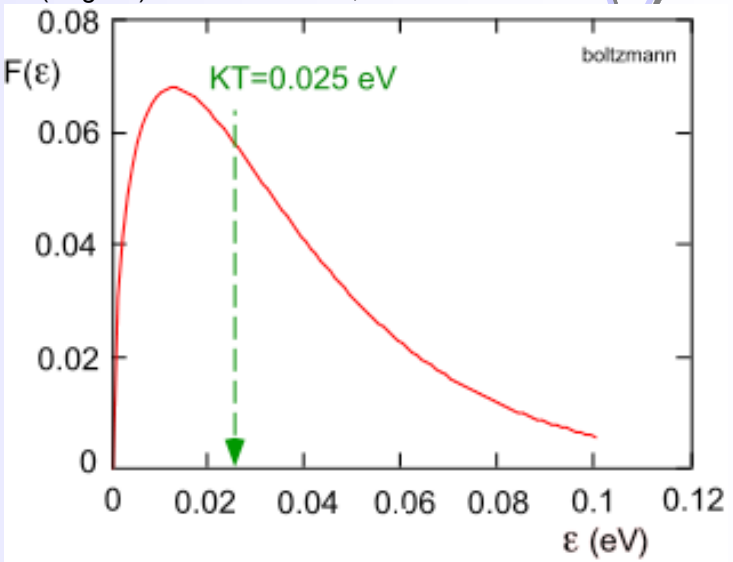

Diffusion equation:

Fraction of free charges at distance x after time t.

$$\frac{dN}{N} = \frac{1}{\sqrt{4\pi Dt}}e^{-\frac{x^2}{4Dt}}dt$$

D: diffusion coefficient

RMS of linear diffusion:

$$\sigma_x = \sqrt{2Dt}$$

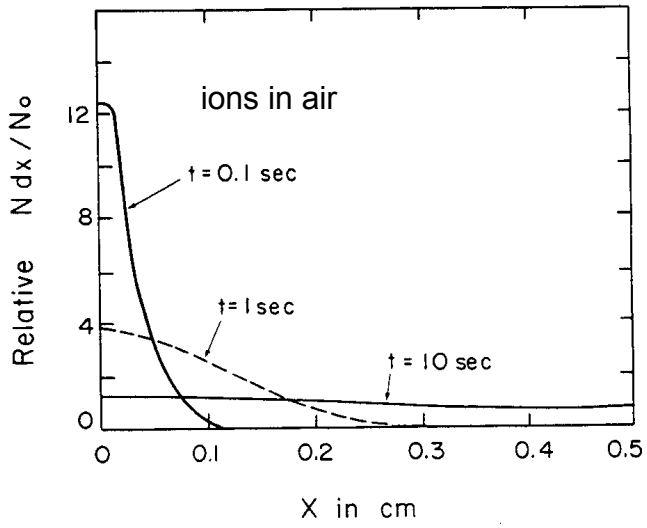

L.B. Loeb, Basic processes of gaseous electronics
Univ. of California Press, Berkeley, 1961

Drift and Diffusion in Presence of E field

E=0 thermal diffusion $\langle v \rangle_t = 0$

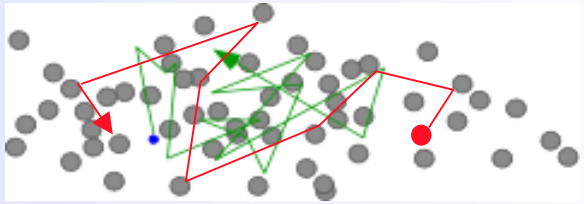

E>0 charge transport and diffusion $\langle v \rangle_t = v_D$

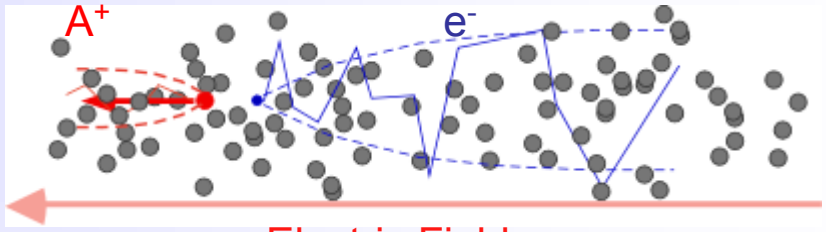

Electron swarm drift

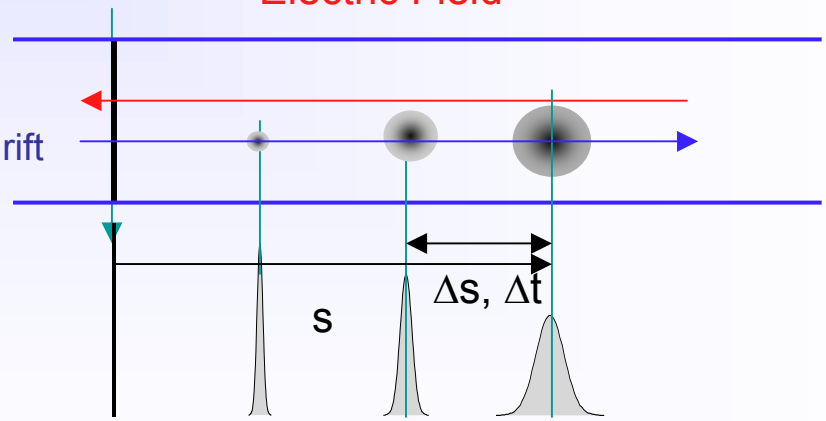

$$v_D = \frac{\Delta s}{\Delta t}$$

Drift velocity

$$\sigma_x = \sqrt{2Dt} = \sqrt{2D\frac{s}{v_D}}$$

Diffusion

Drift and Diffusion of Ions in Presence of E Field

Drift velocity of ions

is almost linear function of E $v_D^{ion} = \mu^{ion} E$

Mobility: $\mu^{ion} = \frac{e\tau}{m}$ is

constant for given gas at fixed P and T,

direct consequence of the fact that

average energy of ion is unchanged

up to very high E fields.

Diffusion of ions

from microscopic picture can be shown:

$$\varepsilon = \frac{3}{2}\frac{De}{\mu}$$

$$\frac{D}{\mu^{ion}} = \frac{kT}{e} \quad \rightarrow \quad \sigma_x^{ion} = \sqrt{\frac{2kT}{e}\frac{x}{E}}$$

thermal limit

the same for all gases !!

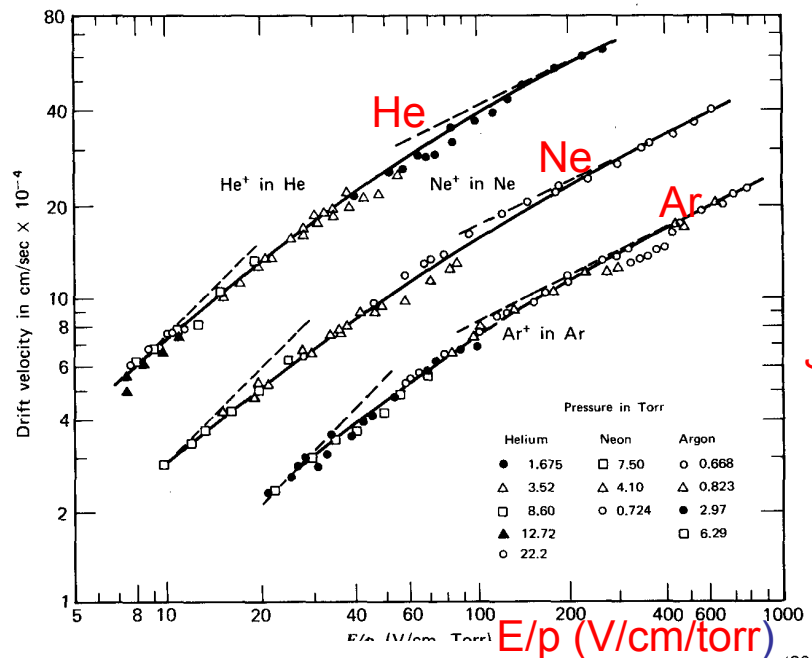

E. McDaniel and E. Mason
The mobility and diffusion of ions in gases, Wiley 1973

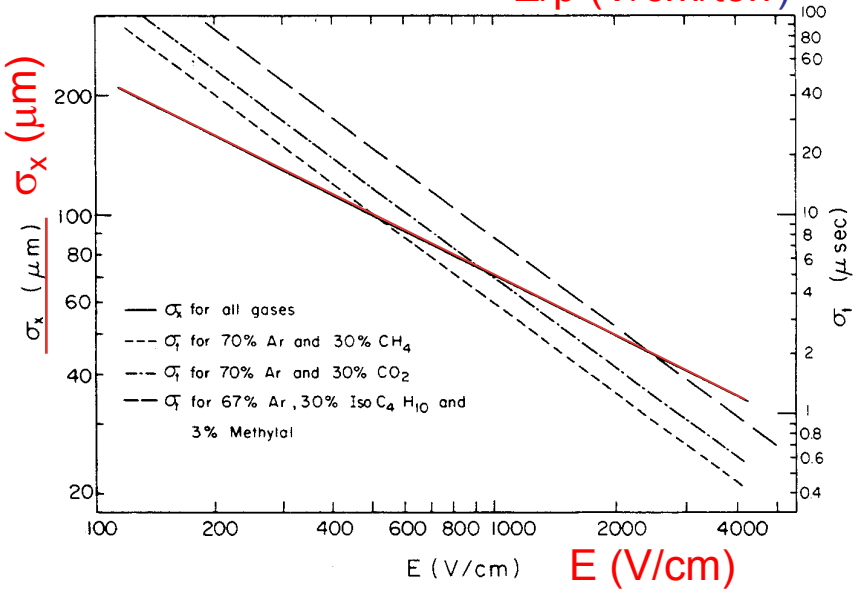

Simplified Electron Transport Theory

$$v_D = \mu E = \frac{eE}{m}\tau$$

Townsend expression; acceleration in the field times time between collisions

$$\frac{x}{v_D\tau}\lambda(\varepsilon)\varepsilon_E = eEx$$

balance between energy acquired from the field and collision losses

$\frac{x}{v_D\tau}$ number of collisions; $\lambda(\varepsilon)$ fractional energy loss per collision

ε_E part of equilibrium energy not containing thermal motion

$$\tau = \frac{1}{N\sigma(\varepsilon)v}$$

time between collisions; v instantaneous velocity

$$\varepsilon_E + \frac{3}{2}kT$$

total energy

$$v_D^2 = \frac{eE}{mN\sigma(\varepsilon)}\sqrt{\frac{\lambda(\varepsilon)}{2}}$$

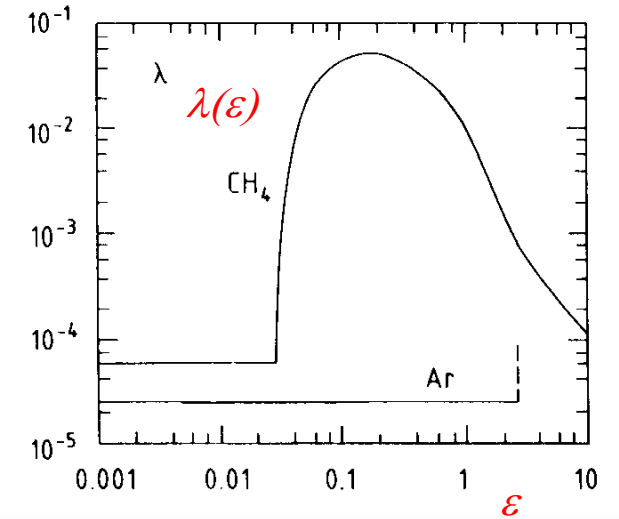

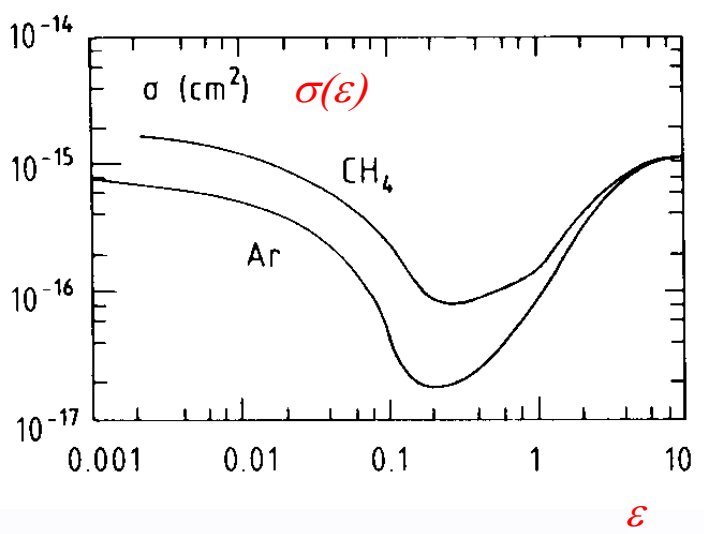

B. Schmidt, thesis, unpublished, 1986

Drift and Diffusion of Electrons in Gases

Large range of drift velocity and diffusion:

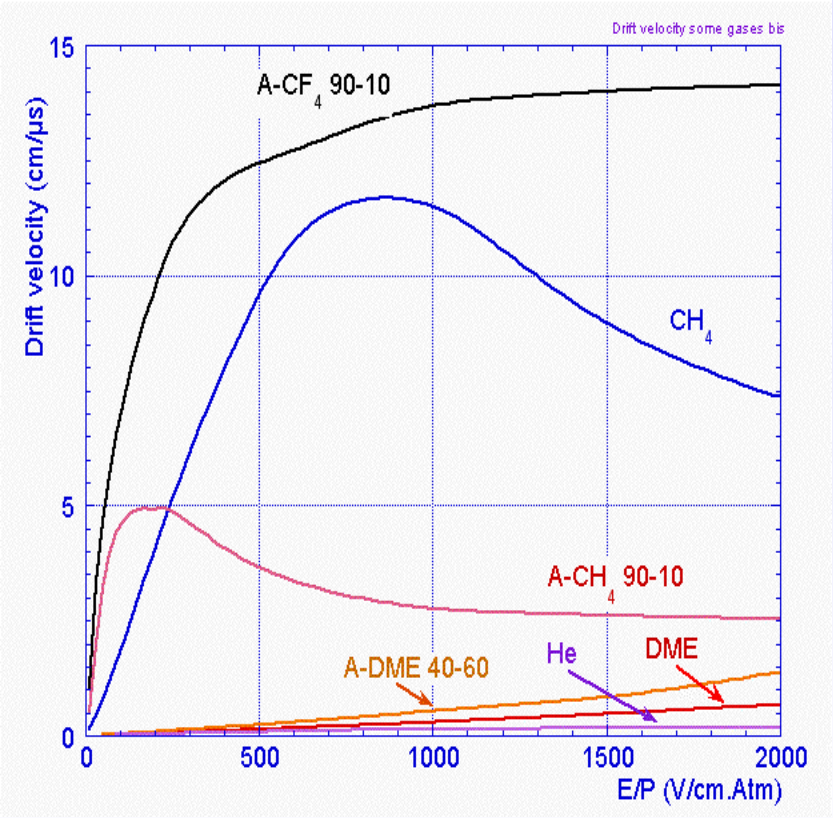

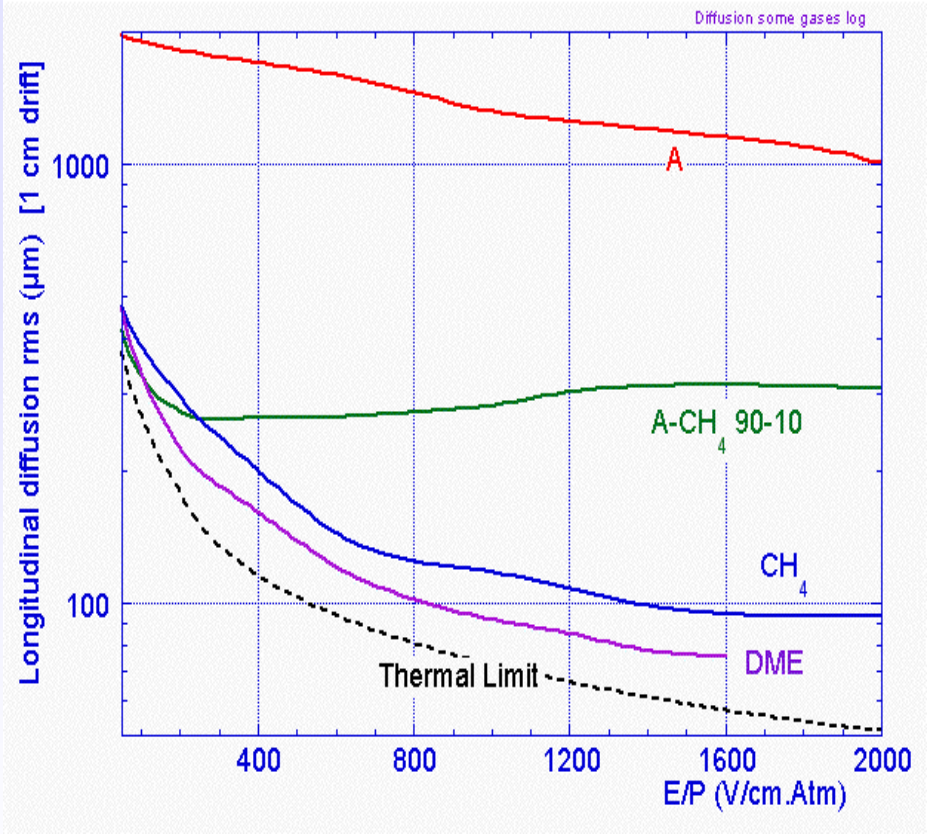

F. Sauli, IEEE Short Course on Radiation Detection and Measurement, Norfolk (Virginia) November 10-11, 2002

Diffusion Electric Anisotropy

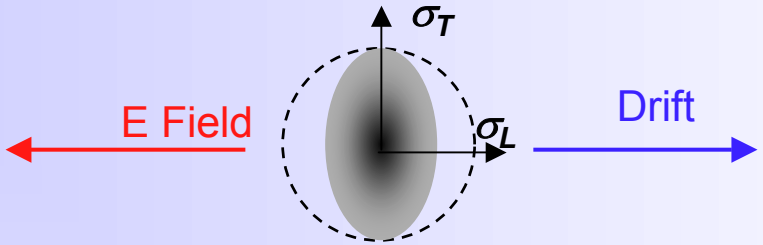

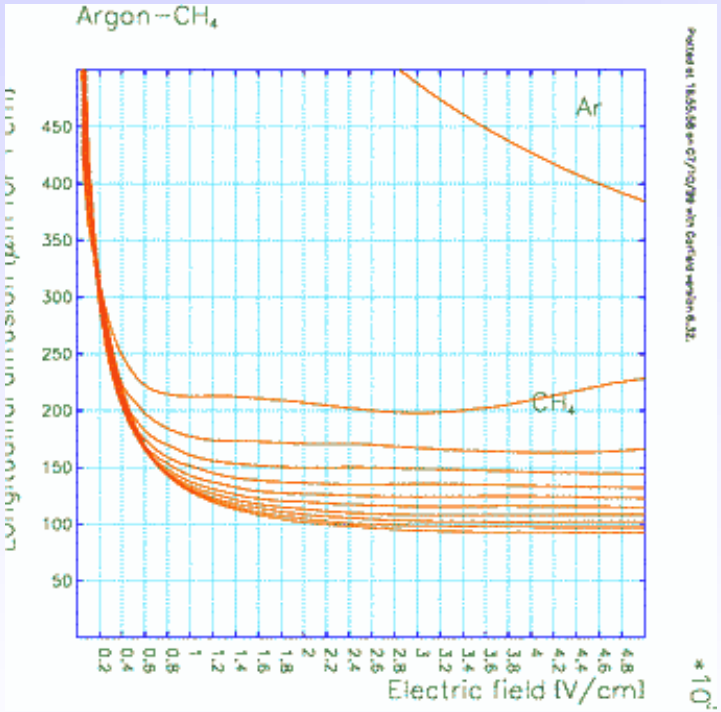

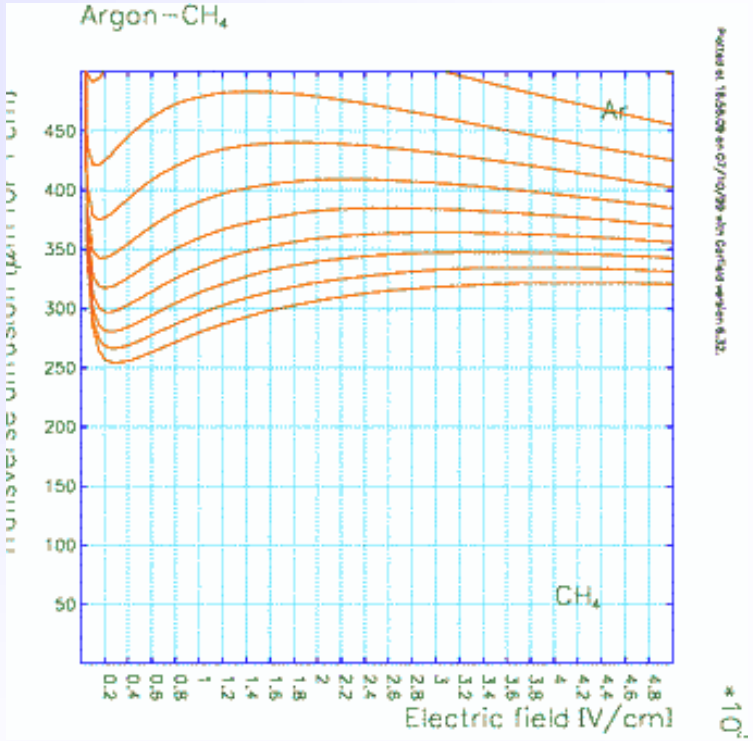

S. Biagi http://consult.cern.ch/writeup/magboltz/

Drift in Presence of E and B Fields

Equation of motion of free charge carriers in presence of E and B fields:

$$m\frac{d\vec{v}}{dt} = e\vec{E} + e(\vec{v}\times\vec{B}) + \vec{Q}(t)$$ where $\vec{Q}(t)$ stochastic force resulting from collisions

Time averaged solutions with assumptions: $\vec{v}_D = \langle\vec{v}\rangle = const.$; $< \vec{Q}(t) >= \frac{m}{\tau}\vec{v}_D$ friction force

$$\left\langle\frac{d\vec{v}}{dt}\right\rangle = 0 = e\vec{E} + e(\vec{v}_D\times\vec{B}) - \frac{m}{\tau}\vec{v}_D$$ τ mean time between collisions

$$\vec{v}_D = \frac{\mu|\vec{E}|}{1+\omega^2\tau^2}\left[\hat{E} + \omega\tau(\hat{E}\times\hat{B}) + \omega^2\tau^2(\hat{E}\cdot\hat{B})\hat{B}\right]$$

$\mu = \frac{e\tau}{m}$ mobility $\omega = \frac{eB}{m}$ cyclotron frequency

$B=0 \rightarrow \vec{v}_D^{\,B} = \vec{v}_D^{\,0} = \mu\vec{E}$

$\vec{E} \parallel \vec{B} \rightarrow v_D^B = v_D^0$

$\vec{E} \perp \vec{B} \rightarrow v_D^B = \frac{E}{B}\frac{\omega\tau}{\sqrt{1+\omega^2\tau^2}}$

In general drift velocity has 3 components: $\parallel \vec{E}; \parallel \vec{B}; \parallel \vec{E}\times\vec{B}$

$\omega\tau << 1$ particles follow E-field

$\omega\tau >> 1$ particles follow B-field

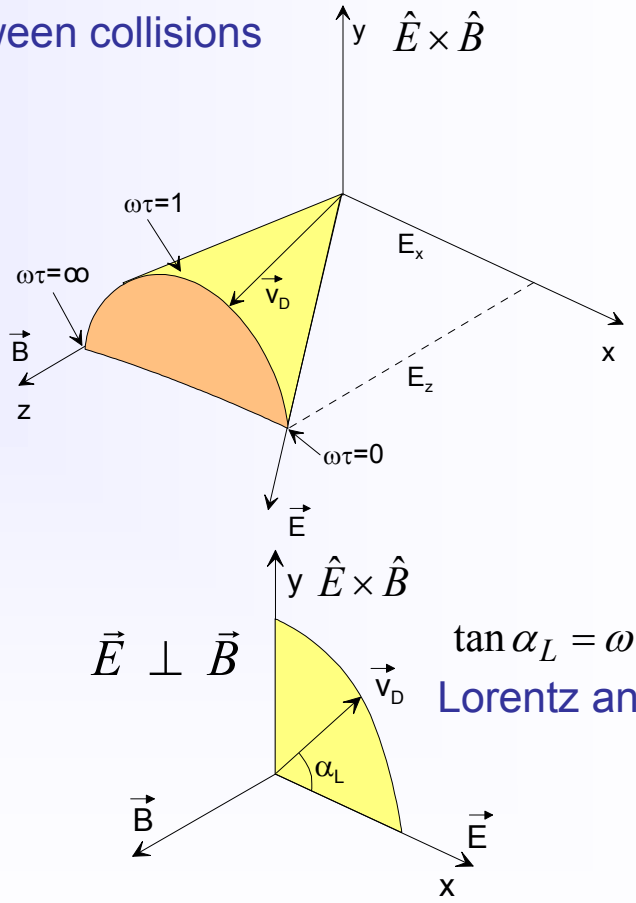

$\tan\alpha_L = \omega\tau$ Lorentz angle

Diffusion Magnetic Anisotropy

$\vec{E} \parallel \vec{B}$

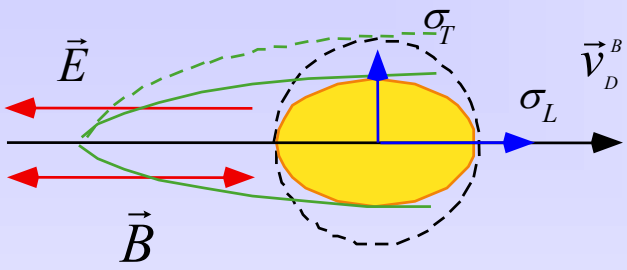

$$\sigma_L = \sigma_0$$

$$\sigma_T = \frac{\sigma_0}{\sqrt{1+\omega^2\tau^2}}$$

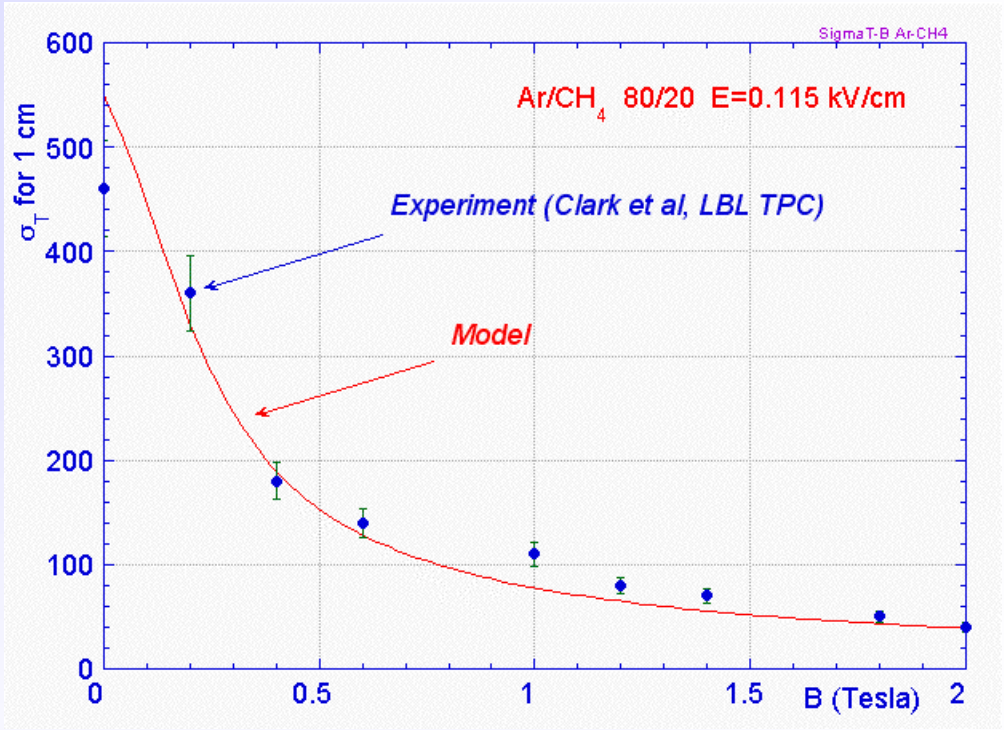

F. Sauli, IEEE Short Course on Radiation Detection and Measurement, Norfolk (Virginia) November 10-11, 2002

TPC – Time Projection Chamber

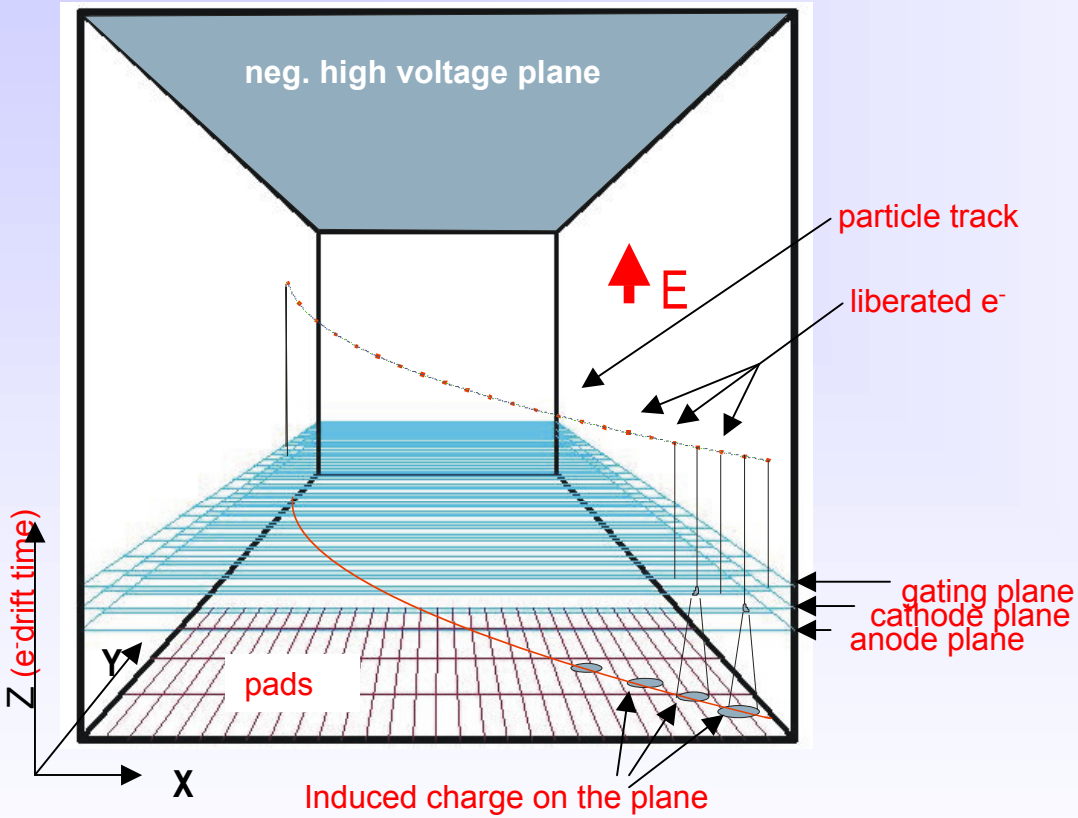

Time Projection Chamber

full 3D track reconstruction:

x-y from wires and segmented cathode of MWPC (or GEM)

z from drift time

- momentum resolution
  space resolution + B field
  (multiple scattering)
- energy resolution
  measure of primary ionization

TPC – Time Projection Chamber

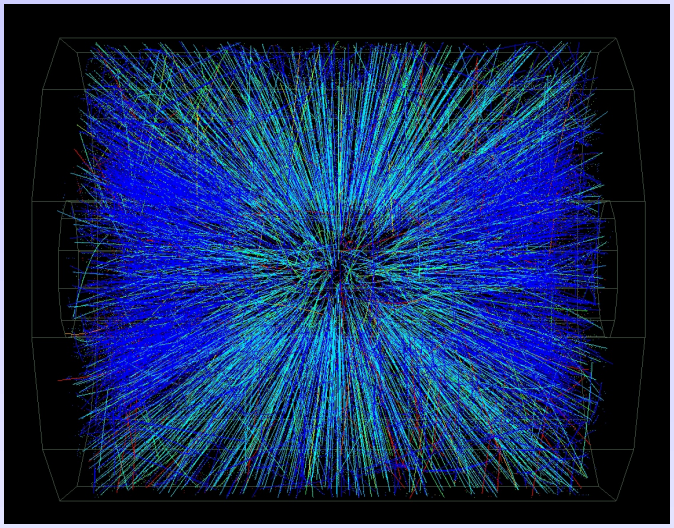

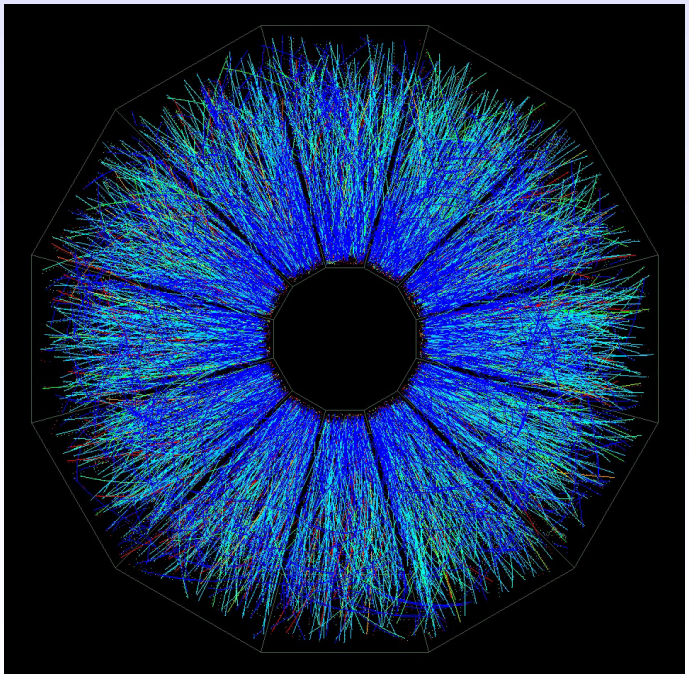

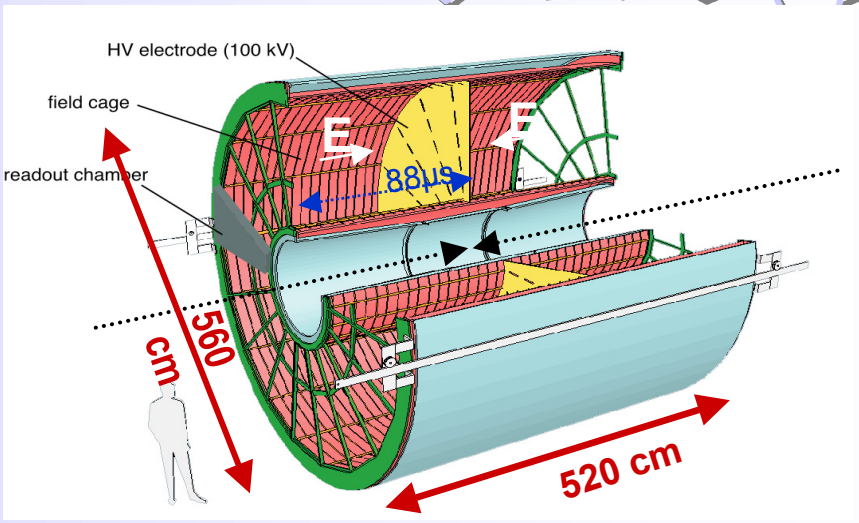

Alice TPC

HV central electrode at –100 kV

Drift lenght 250 cm at E=400 V/cm

Gas Ne-CO_2 90-10

Space point resolution ~500 µm

dp/p 2%@1GeV; 10%@10GeV

Events from STAR TPC at RHIC

Au-Au collisions at CM energy of 130 GeV/n

Typically ~2000 tracks/event

TPC – Time Projection Chamber

Positive ion backflow modifies electric field resulting in track distortion.

Solution : gating

Prevents electrons to enter amplification region in case of uninteresting event;

Prevents ions created in avalanches to flow back to drift region.

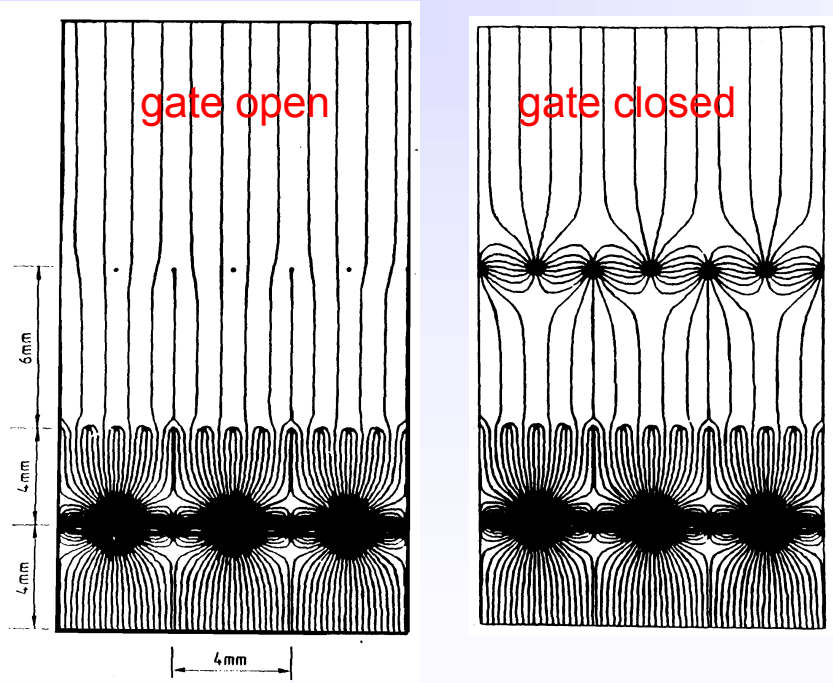

ALEPH coll., NIM A294(1990)121

Micropattern Gas Detectors

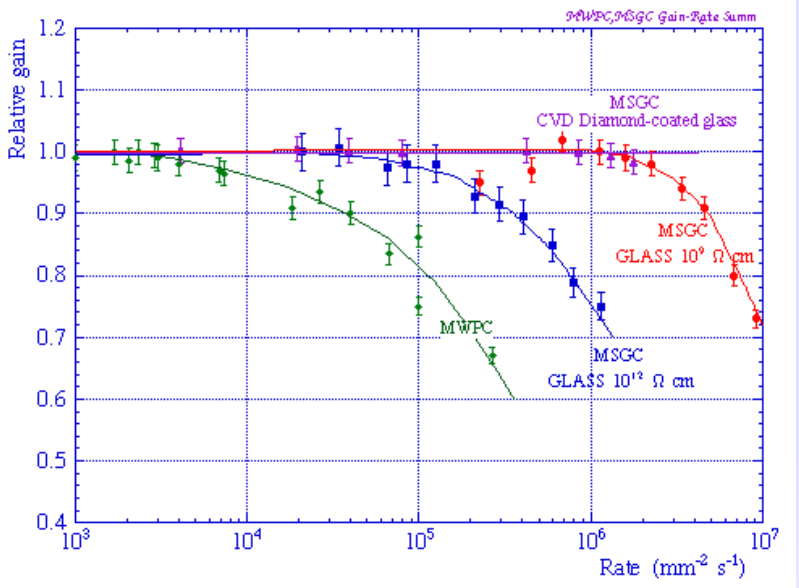

Advantages of gas detectors:

- low radiation length
- large areas at low price
- flexible geometry
- spatial, energy resolution …

Problem:

- rate capability limited by space charge defined by the time of evacuation of positive ions

scale factor

1

5

10

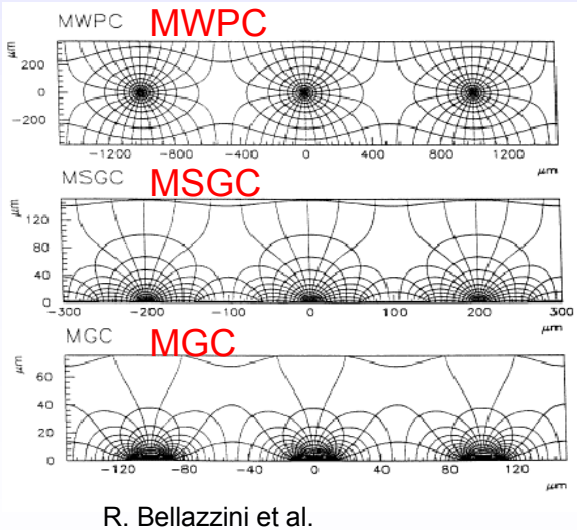

R. Bellazzini et al.

Solution:

- reduction of the size of the detecting cell (limitation of the length of the ion path) using chemical etching techniques developed for microelectronics and keeping at same time similar field shape.

MSGC – Microstrip Gas Chamber

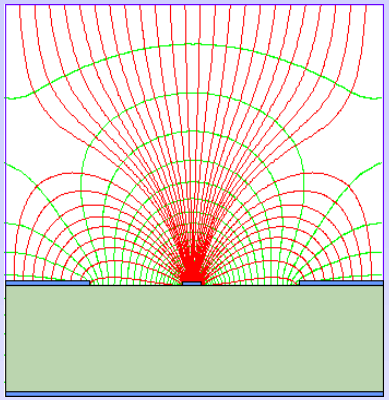

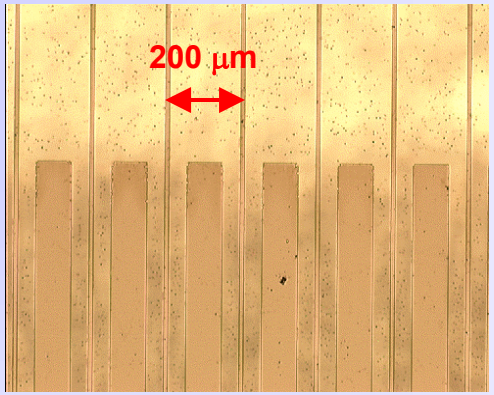

Thin metal anodes and cathodes on insulating support (glass, flexible polyimide ..)

Problems:

High discharge probability under exposure to highly ionizing particles caused by the regions of very high E field on the border between conductor and insulator.

Charging up of the insulator and modification of the E field → time evolution of the gain.

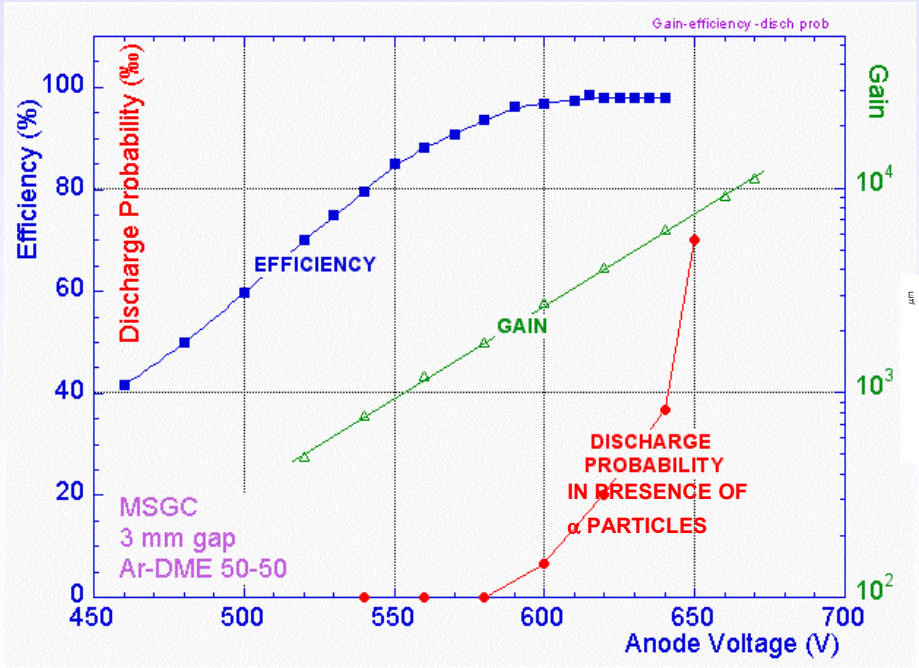

insulating support

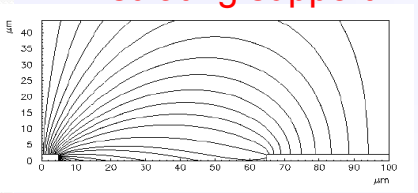

slightly conductive support

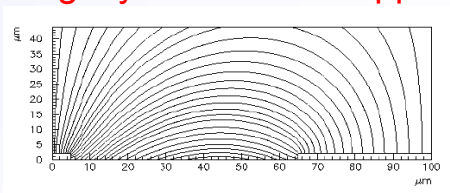

R. Bellazzini et al.

Solutions:

slightly conductive support

multistage amplification

Micromegas – Micromesh Gaseous Structure

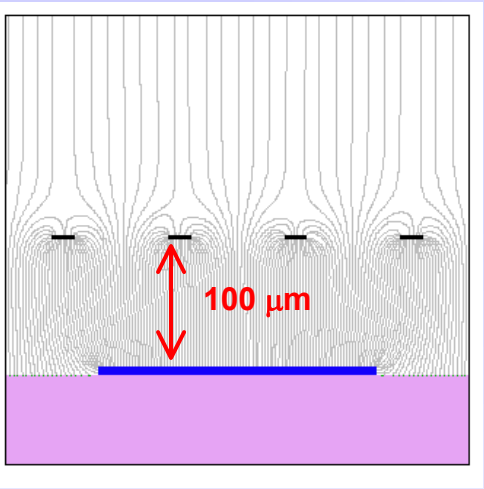

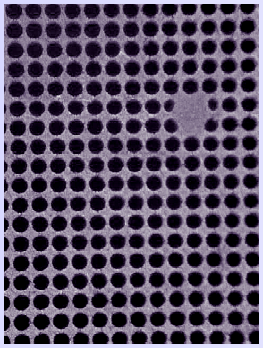

micromesh

Micromesh mounted above readout structure (typically strips).

E field similar to parallel plate detector.

E_a/E_i ~ 50 to secure electron transparency and positive ion flowback supression.

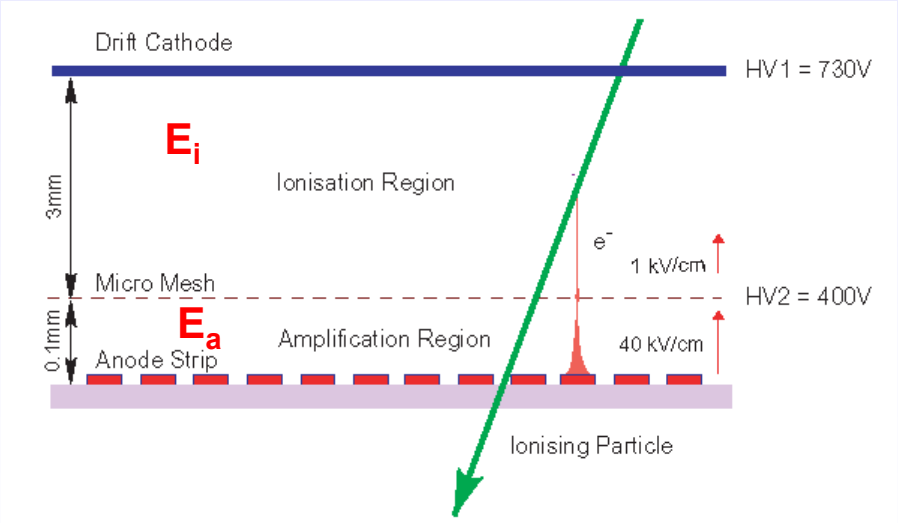

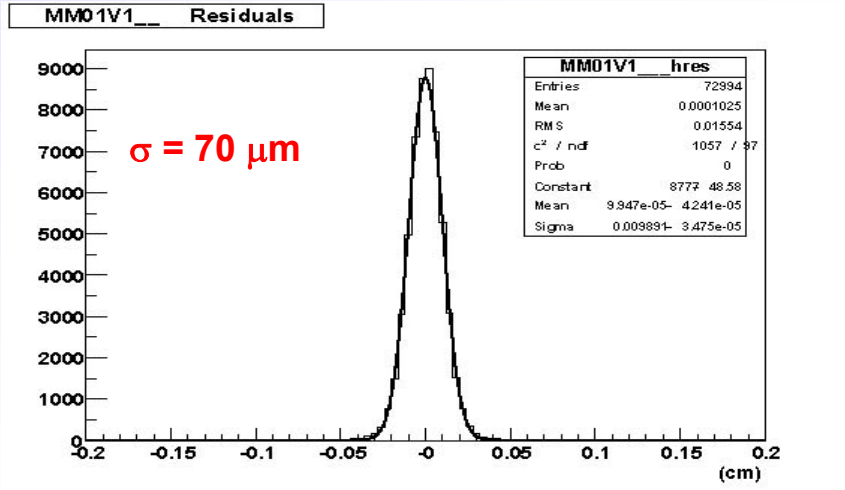

Space resolution

GEM – Gas Electron Multiplier

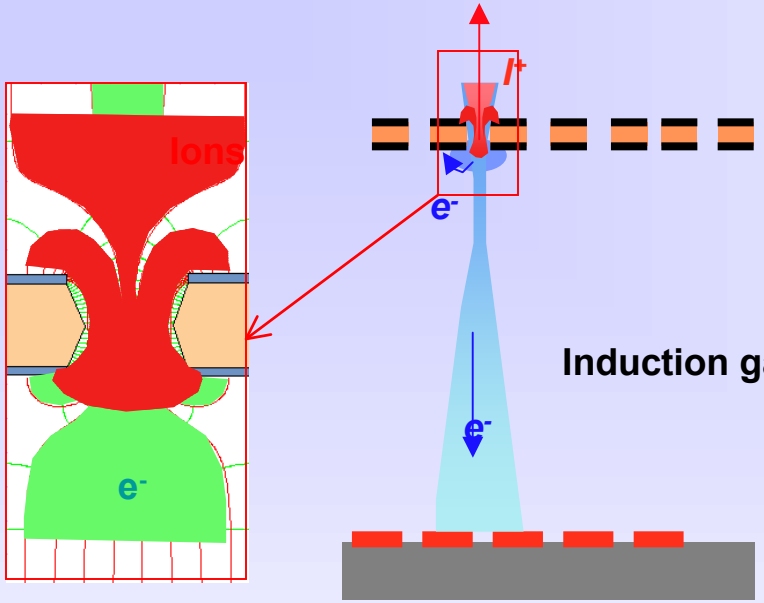

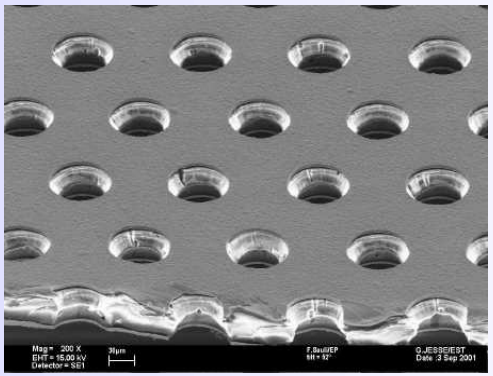

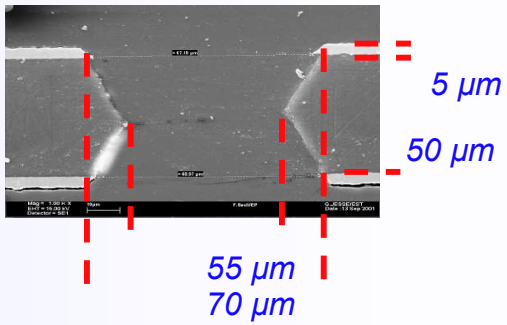

Thin, metal coated polyimide foil perforated with high density holes.

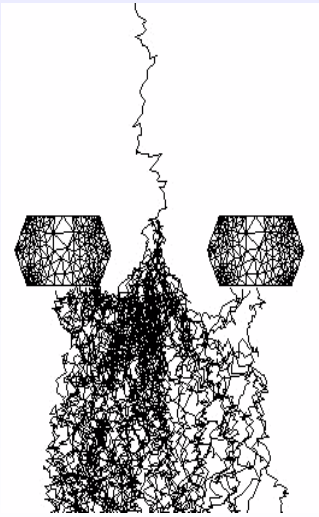

Electrons are collected on patterned readout board.
A fast signal can be detected on the lower GEM electrode for triggering or energy discrimination.
All readout electrodes are at ground potential.
Positive ions partially collected on the GEM electrodes.

GEM – Gas Electron Multiplier

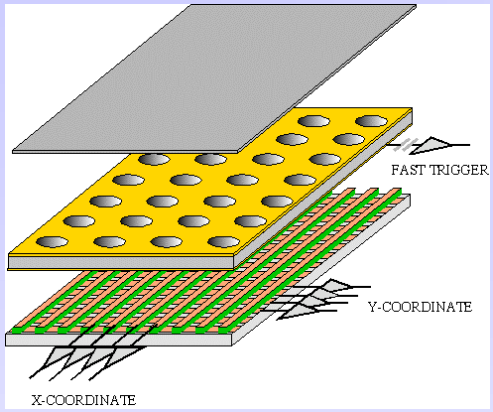

Full decupling of the charge ampification structure from the charge collection and readout structure.

Both structures can be optimized independently !

A. Bressan et al, Nucl. Instr. and Meth. A425(1999)254

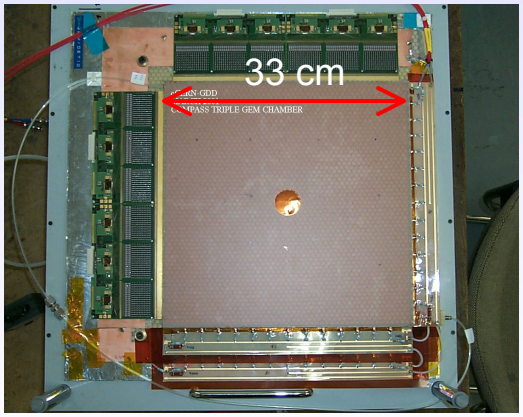

Compass

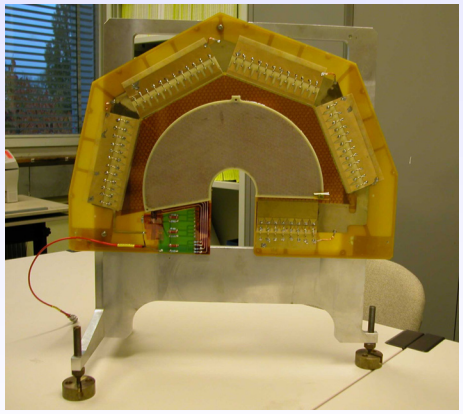

Totem

Both detectors use three GEM foils in cascade for amplification to reduce discharge probability by reducing field strenght.

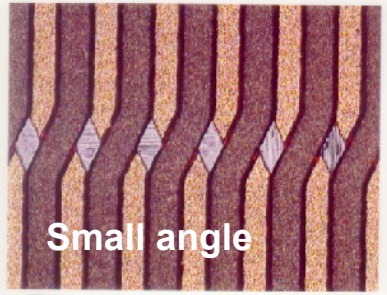

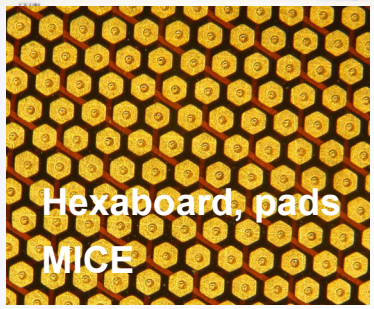

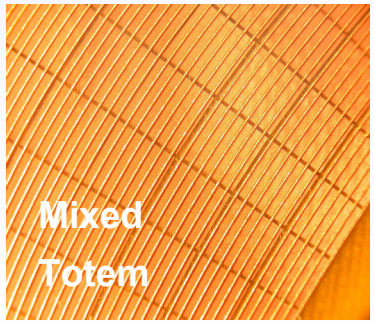

GEM – Gas Electron Multiplier

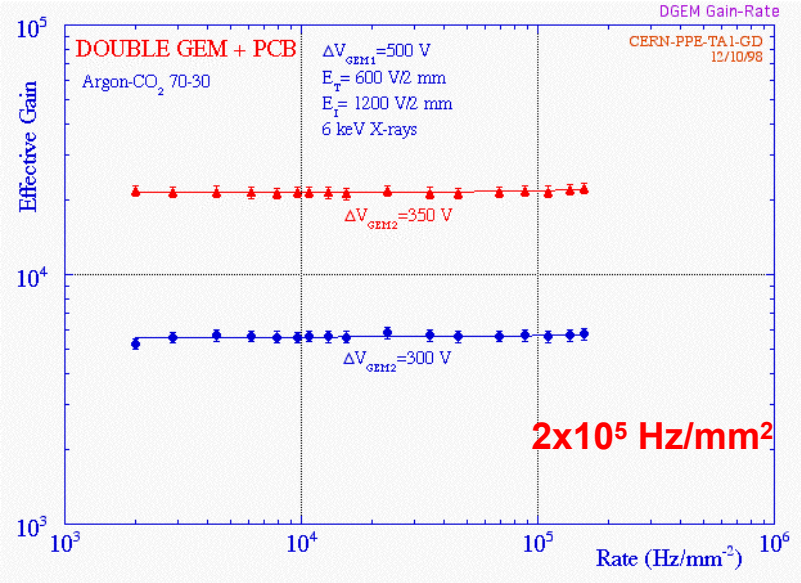

Rate capability

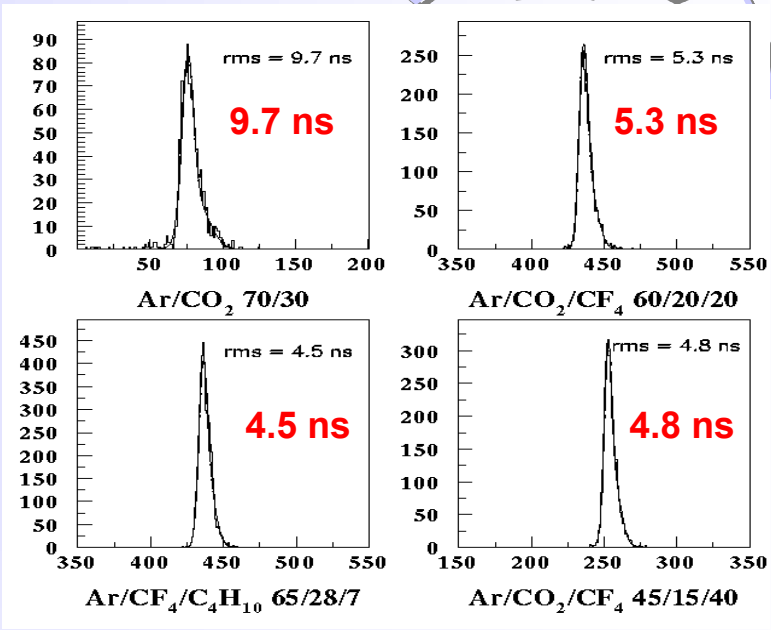

Time resolution

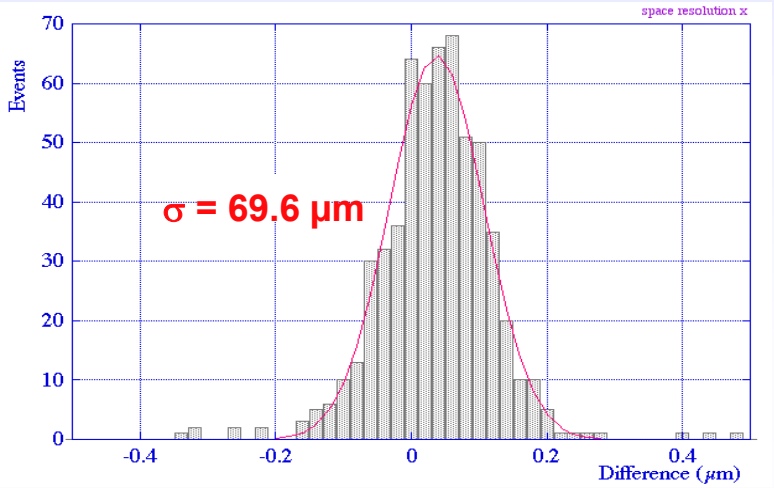

Space resolution

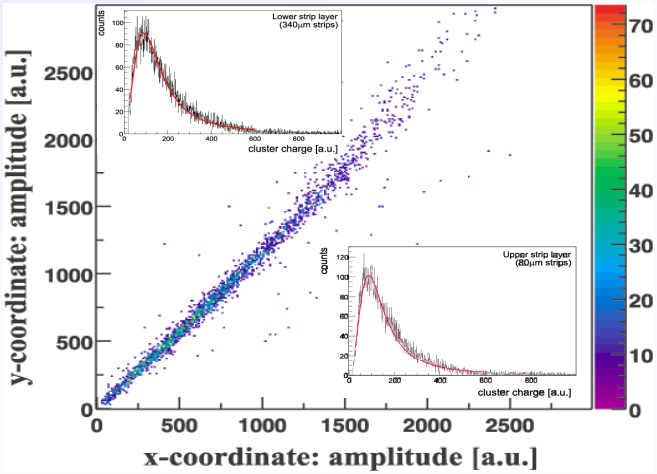

Charge corellation (cartesian readout)

Limitations of Gas Detectors

Classical ageing

Avalanche region → plasma formation
(complicated plasma chemistry)

- Dissociation of detector gas and pollutants
- Highly active radicals formation
- Polymerization (organic quenchers)
- Insulating deposits on anodes and cathodes

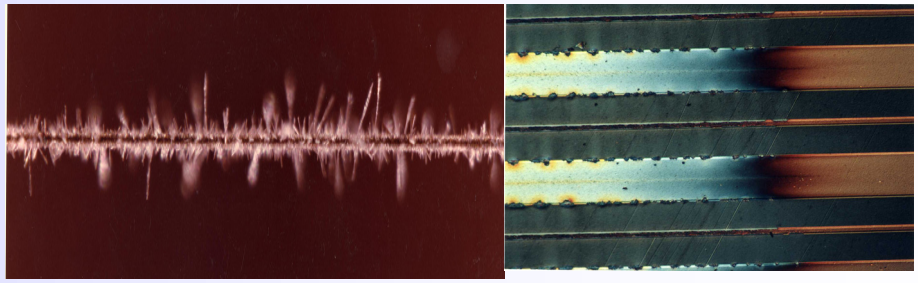

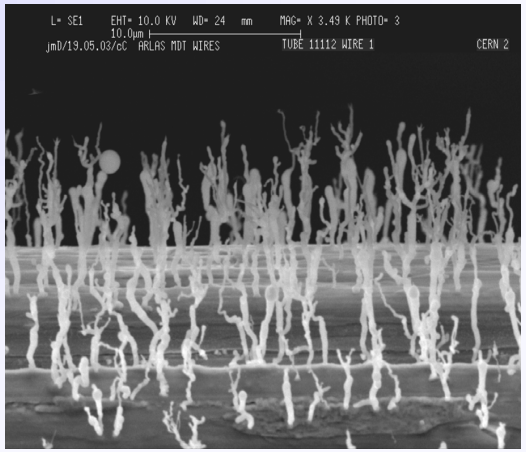

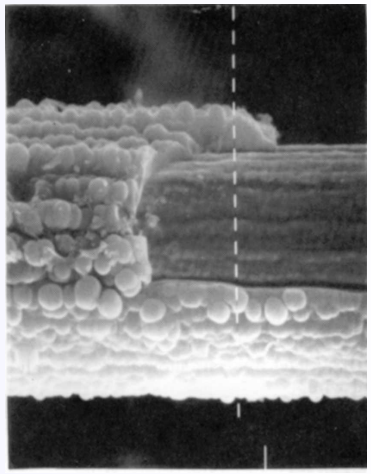

Anode: increase of the wire diameter, reduced and variable field, variable gain and energy resolution.

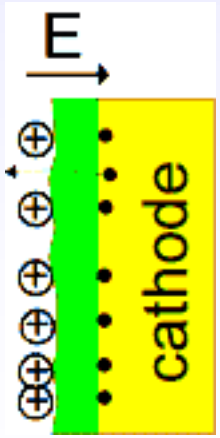

Cathode: formation of strong dipoles, field emmision and microdischarges (Malter effect).

Limitations of Gas Detectors

Solutions: carefull material selection for the detector construction and gas system, detector type (GEM is resitant to classical ageing), working point, non-polymerizing gases, additives supressing polymerization (alkohols, methylal), additives increasing surface conductivity (H_2O vapour), clening additives (CF_4).

Discharges

Field and charge density dependent effect.

Solution: multistep amplification

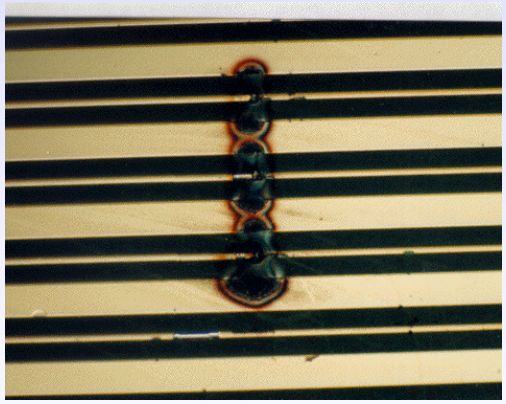

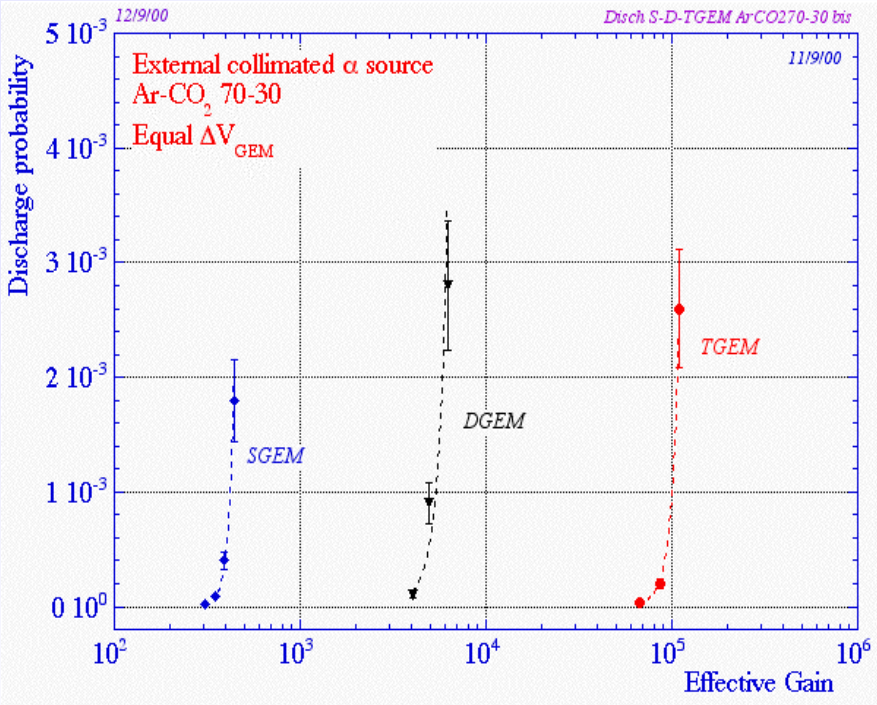

Space charge limiting rate capability

Solution: reduction of the lenght of the positive ion path

Insulator charging up resulting in gain variable with time and rate

Solution: slightly conductive materials

Computer Simulations

MAXWELL *(Ansoft)*

electrical field maps in 2D& 3D, finite element calculation for arbitrary electrodes & dielectrics

HEED *(I.Smirnov)*

energy loss, ionization

MAGBOLTZ *(S.Biagi)*

electron transport properties: drift, diffusion, multiplication, attachment

Garfield *(R.Veenhof)*

fields, drift properties, signals (interfaced to programs above)

PSpice *(Cadence D.S.)* electronic signal

Computer Simulations

Input: detector geometry, materials and elctrodes potentials, gas cross sections.

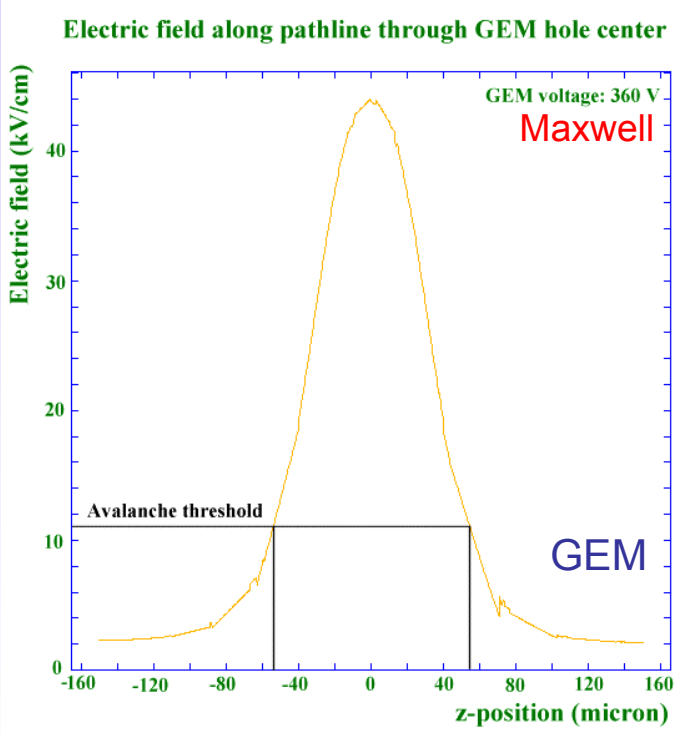

Field Strenght

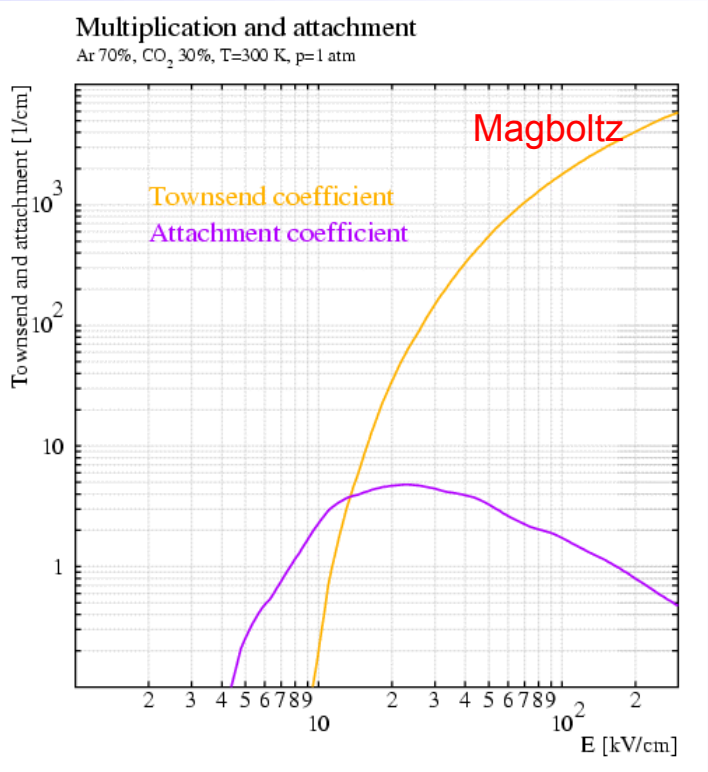

Townsend coefficient

P. Cwetanski, http://pcwetans.home.cern.ch/pcwetans/

Computer Simulations

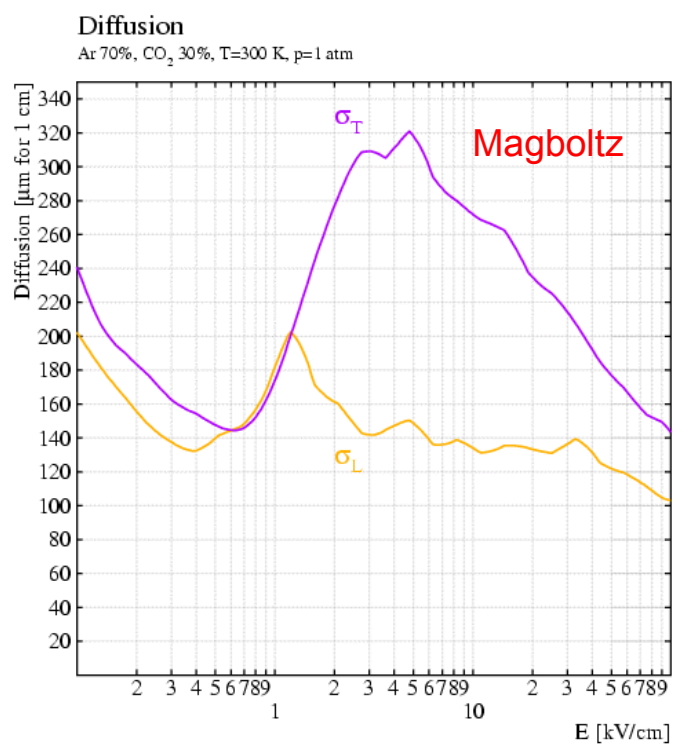

Longitudinal, transverse diffusion

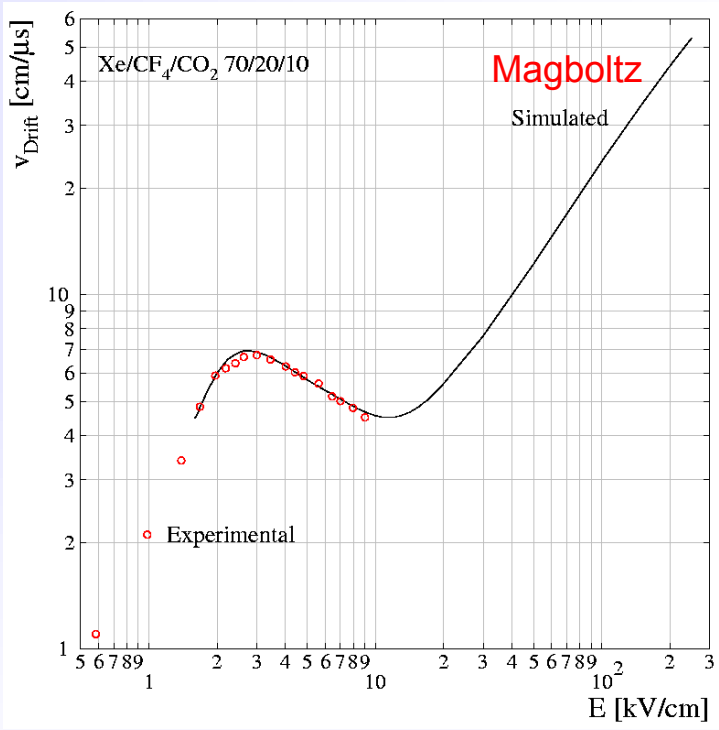

Drift velocity

P. Cwetanski, http://pcwetans.home.cern.ch/pcwetans/

Computer Simulations

P. Cwetanski, http://pcwetans.home.cern.ch/pcwetans/

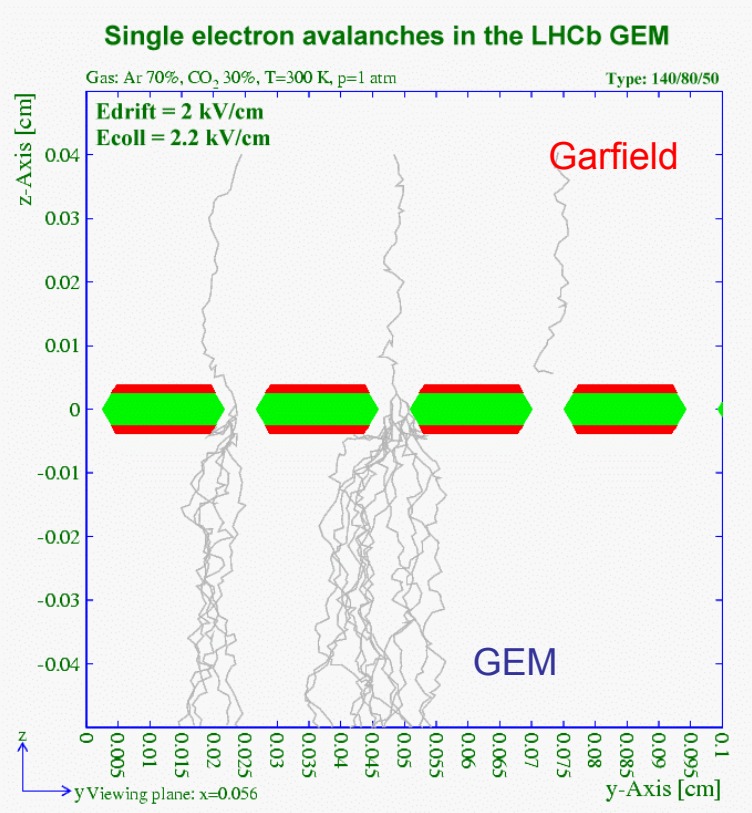

Electrons paths and multiplication

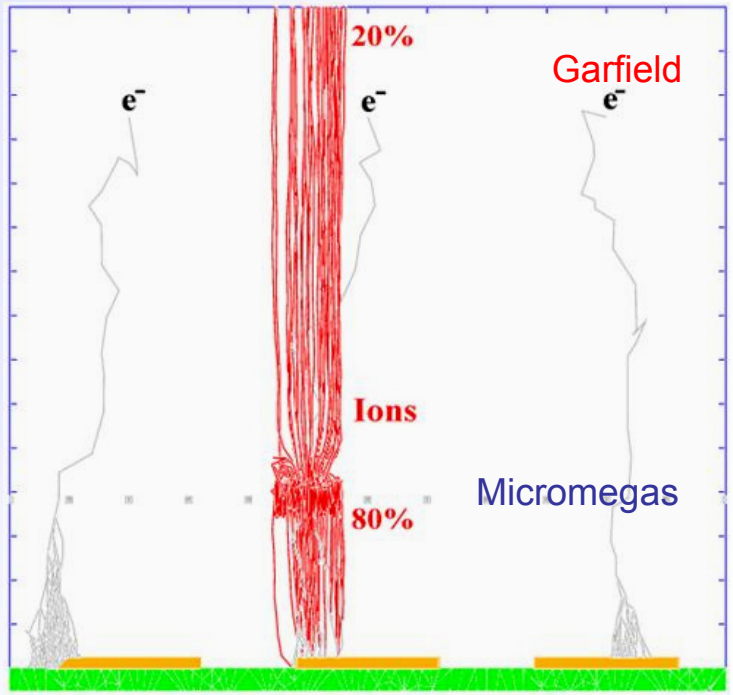

Positive ion backflow

Conclusion: we don't need to built detector to know its performance

Other (than tracking) Applications

Radiography with GEM (X-rays)

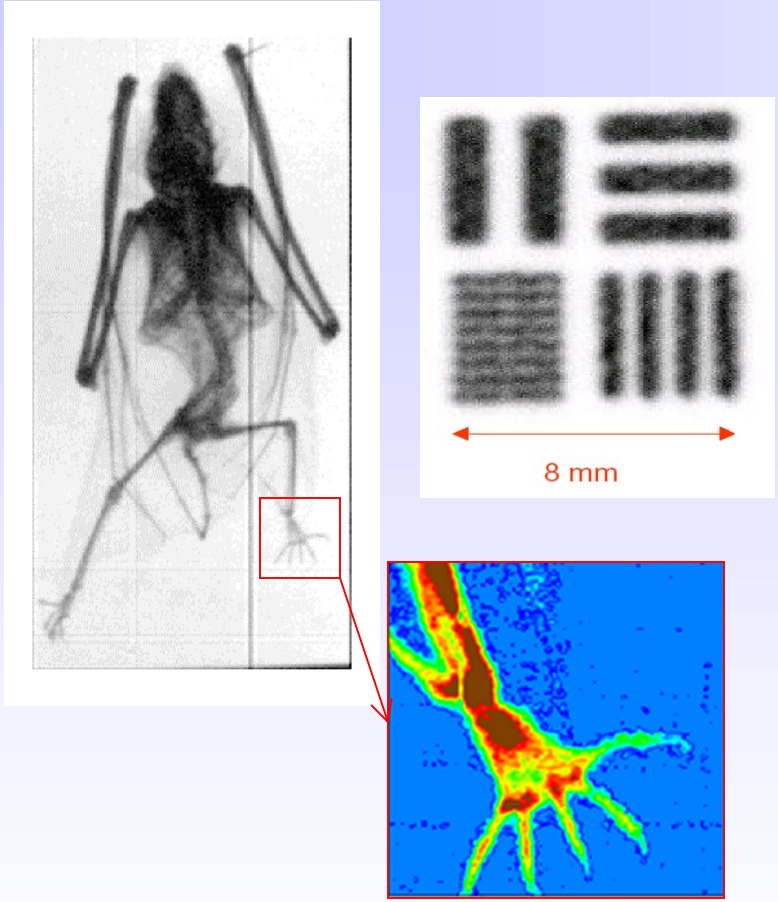

Trigger from the bottom electrode of GEM.

UV light detection with GEM

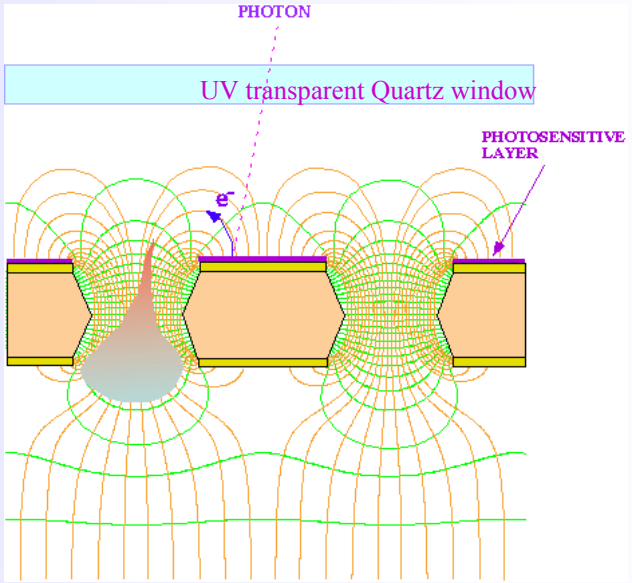

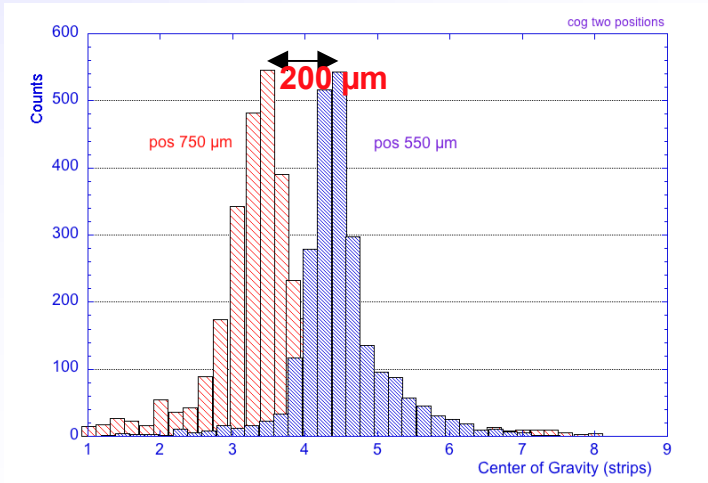

Gas Detectors in LHC Experiments

ALICE: TPC (tracker), TRD (transition rad.), TOF (MRPC), HMPID (RICH-pad chamber), Muon tracking (pad chamber), Muon trigger (RPC)

ATLAS: TRD (straw tubes), MDT (muon drift tubes), Muon trigger (RPC, thin gap chambers)

CMS: Muon detector (drift tubes, CSC), RPC (muon trigger)

LHCb: Tracker (straw tubes), Muon detector (MWPC, GEM)

TOTEM: Tracker & trigger (CSC , GEM)

Acknowledgments

F. Sauli, IEEE Short Course on Radiation Detection and Measurement, Norfolk (Virginia) November 10-11, 2002

C. Joram, CERN Academic Training, Particle Detectors 1998

P. Cwetanski , http://pcwetans.home.cern.ch/pcwetans/

M. Hoch, Trends and new developments in gaseous detectors, NIM A535(2004)1-15

Literature:

F. Sauli, Principles of operation of multiwire proportional and drift chambers, CERN 77-09

W. Blum and L. Rolandi, Particle Detection with Drift Chambers, Springer 1994

C. Grupen, Particle Detectors, Cambridge University Press, 1996

F. Sauli and A. Sharma, Micropattern Gaseous Detectors, Annu. Rev. Nucl. Part. Sci. 1999.49:341-88

http://gdd.web.cern.ch/GDD/

Lecture 2b

Tracking with Solid State Detectors

Michael Moll
CERN – PH – DT2

IIb Tracking with Solid State Detectors

- **Lecture 1 - Introduction** — C. Joram, L. Ropelewski
- **Lecture 2 - Tracking Detectors** — L. Ropelewski, M. Moll
  - **2a) Tracking with Gas detectors**
  - **2b) Tracking with Solid State Detectors** — **Michael Moll (CERN - PH/DT2)**
    - Why use Semiconductor Detectors ?
    - How are Silicon Detectors made and how do they work ?
    - Detector types: Microstrip and Pixel Detectors, CCDs
    - Examples: Detectors at LHC
    - Radiation Damage in Silicon Detectors
    - Outlook: Radiation tolerant detectors
    - References
- **Lecture 3 - Scintillation and Photodetection** — C. D'Ambrosio, T. Gys
- **Lecture 4 - Calorimetry, Particle ID** — C. Joram
- **Lecture 5 - Particle ID, Detector Systems** — C. Joram, C. D'Ambrosio

Transparencies: **http://cern.ch/ph-dep-dt2/lectures_PD_2005.htm**

Solid State Detectors – Why silicon?

Some characteristics of Silicon crystals

- Small band gap E_g = 1.12 eV $\Rightarrow$ E(e-h pair) = 3.6 eV ($\approx$ 30 eV for gas detectors)
- High specific density 2.33 g/cm^3 ; dE/dx (M.I.P.) $\approx$ 3.8 MeV/cm $\approx$ 106 e-h/μm (average)
- High carrier mobility μ_e =1450 cm^2/Vs, μ_h = 450 cm^2/Vs $\Rightarrow$ fast charge collection (<10 ns)
- Very pure < 1ppm impurities and < 0.1ppb electrical active impurities
- Rigidity of silicon allows thin self supporting structures
- Detector production by microelectronic techniques

  $\Rightarrow$ well known industrial technology, relatively low price, small structures easily possible

Alternative semiconductors

- Diamond
- GaAs
- Silicon Carbide
- Germanium

	Diamond	SiC (4H)	GaAs	Si	Ge
Atomic number Z	6	14/6	31/33	14	32
Bandgap E_g [eV]	5.5	3.3	1.42	1.12	0.66
E(e-h pair) [eV]	13	7.6-8.4	4.3	3.6	2.9
density [g/cm^3]	3.515	3.22	5.32	2.33	5.32
e-mobility μ_e [cm^2/Vs]	1800	800	8500	1450	3900
h-mobility μ_h [cm^2/Vs]	1200	115	400	450	1900

How to obtain a signal ?

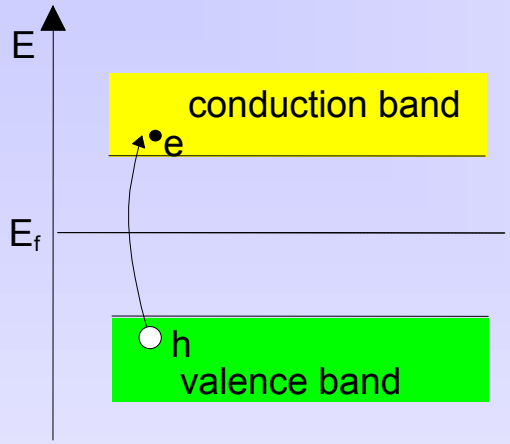

In a pure intrinsic (undoped) semiconductor the electron density *n* and hole density *p* are equal.

$n = p = n_i$ For Silicon: $n_i \approx 1.45 \cdot 10^{10}$ cm^{-3}

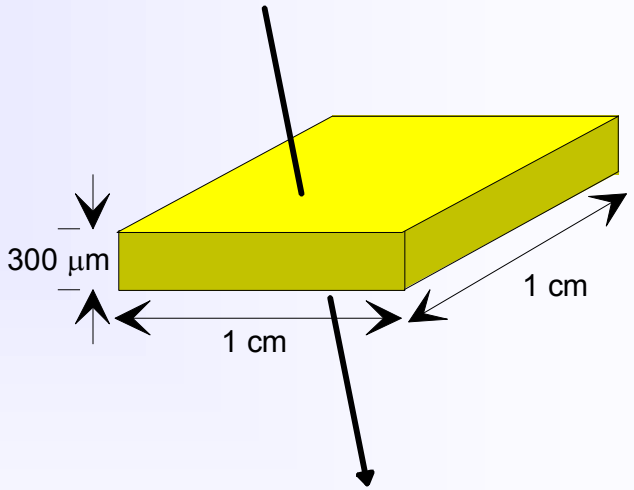

4.5 $\cdot 10^8$ free charge carriers in this volume,
but only 3.2 $\cdot 10^4$ e-h pairs produced by a M.I.P.

$\Rightarrow$ Reduce number of free charge carriers, i.e. deplete the detector

$\Rightarrow$ **Most detectors make use of reverse biased p-n junctions**

Doping, resistivity and p-n junction

Doping: n-type Silicon

- add elements from Vth group
  ⇒ **donors** (P, As,..)
- electrons are majority carriers

e.g. Phosphorus

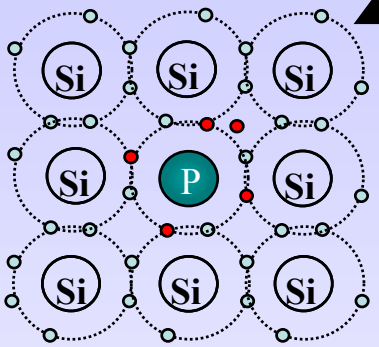

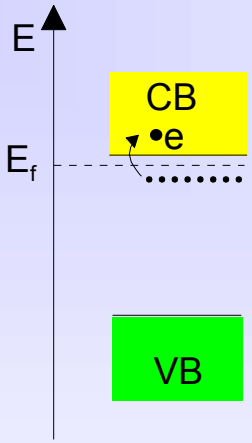

Doping: p-type Silicon

- add elements from IIIrd group
  ⇒ **acceptors** (B,..)
- holes are the majority carriers

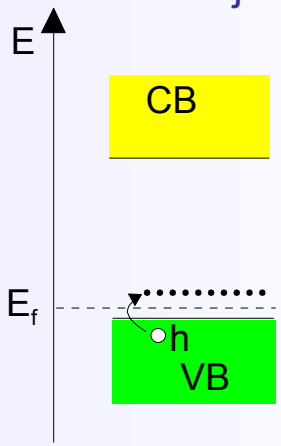

Resistivity

- carrier concentrations *n*, *p*
- carrier mobility μ_n, μ_p

$$\rho = 1 / q_0 (\mu_n n + \mu_p p)$$

	detector grade	electronics grade
doping	≈ 10^{12} cm^{-3}	≈ 10^{17} cm^{-3}
resistivity ρ	≈ 5 kΩ·cm	≈1 Ω·cm

p-n junction

There must be a single
Fermi level !
⇒ band structure deformation
⇒ potential difference
⇒ depleted zone

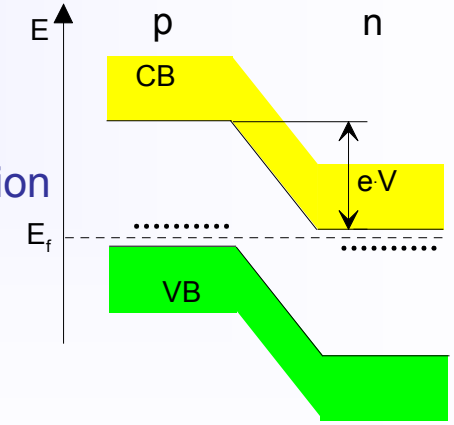

Reverse biased abrupt p⁺ n junction

Poisson's equation

$$-\frac{d^2}{dx^2}\phi(x)=\frac{q_0}{\varepsilon\varepsilon_0}\cdot N_{eff}$$

Positive space charge, N_{eff} =[P]
(ionized Phosphorus atoms)

neutral bulk
(no electric field)

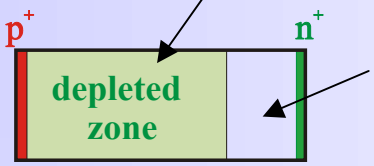

Electrical
charge density

Electrical
field strength

Electron
potential energy

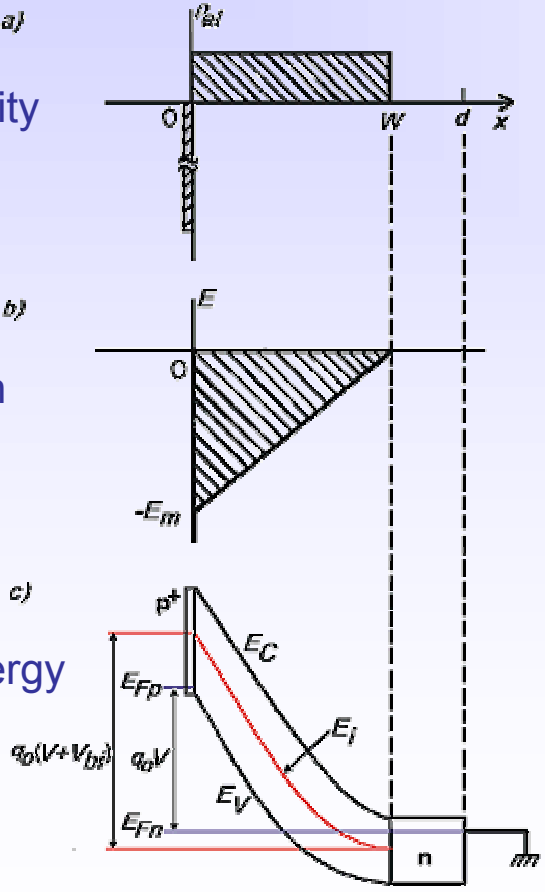

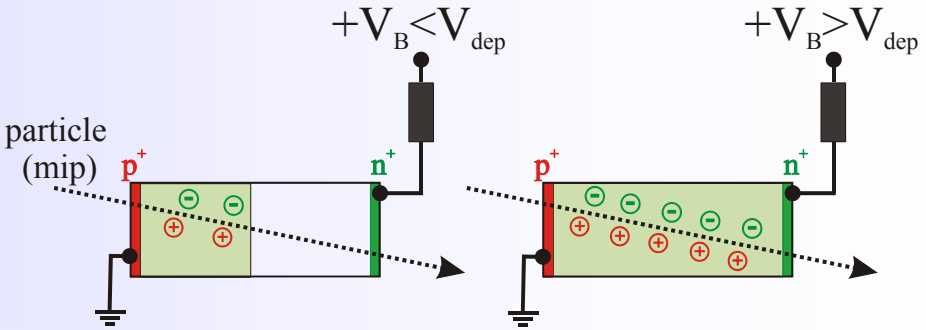

Full charge collection only for $V_B > V_{dep}$!

depletion voltage

$$V_{dep}=\frac{q_0}{\varepsilon\varepsilon_0}\cdot\left|N_{eff}\right|\cdot d^2$$

effective space charge density

Calculation of depletion voltage (diode)

extra slide not shown

Poisson's equation

$$-\frac{d^2}{dx^2}\phi(x)=\frac{q_0}{\varepsilon\varepsilon_0}\cdot N_{eff}$$

w = depletion depth
d = detector thickness
U = voltage

N_{eff} = effective doping concentration

with

$$\frac{d}{dx}\phi(x=w)=0$$
$$\phi(x=w)=0$$

$$-\frac{d}{dx}\phi(x)=\frac{q_0}{\varepsilon\varepsilon_0}\cdot N_{eff}\cdot(x-w)$$

$$\phi(x)=\frac{1}{2}\cdot\frac{q_0}{\varepsilon\varepsilon_0}\cdot N_{eff}\cdot(x-w)^2$$

$$C=\frac{dQ}{dU}=\frac{dQ\cdot dw}{dw\cdot dU}$$

$$dQ=q_0\cdot|N_{eff}|\cdot A\cdot dw$$

$$dw=\sqrt{\frac{\varepsilon\varepsilon_0}{q_0|N_{eff}|2U}}\cdot dU$$

$$w(V)=\sqrt{\frac{2\varepsilon\varepsilon_0}{q_0|N_{eff}|}\cdot V}$$

depletion voltage

$$V_{dep}=\frac{q_0}{2\varepsilon\varepsilon_0}\cdot|N_{eff}|\cdot d^2$$

effective space charge density

$$C(U)=A\cdot\sqrt{\frac{\varepsilon\varepsilon_0 q_0|N_{eff}|}{2U}}$$

$$C(w)=\frac{\varepsilon\varepsilon_0 A}{w}$$

How to make a Float Zone Silicon wafer?

extra slide not shown

Produce a polysilicon rod

- Melt very pure sand (SiO_2) together with coke (~1800°C)

$$SiO_2 + 2C \rightarrow Si + 2CO$$

- Grind the "metallurgical grade silicon" (98% Si) and expose it to hydrochloric gas

$$Si + 3HCl\ (gas) \rightarrow SiHCl_3 + H_2$$

- Trichlorsilane boils at 31.7°C and can thus be distilled and purified
- Deposit silicon in a Chemical Vapour Deposition process

$$SiHCl_3 + H_2 \rightarrow Si + 3HCl$$

- Cast silicon into a polycrystalline silicon rod

Float Zone process

- Using a single Si crystal seed, melt the vertically oriented rod onto the seed using RF power and "pull" the monocrystalline ingot

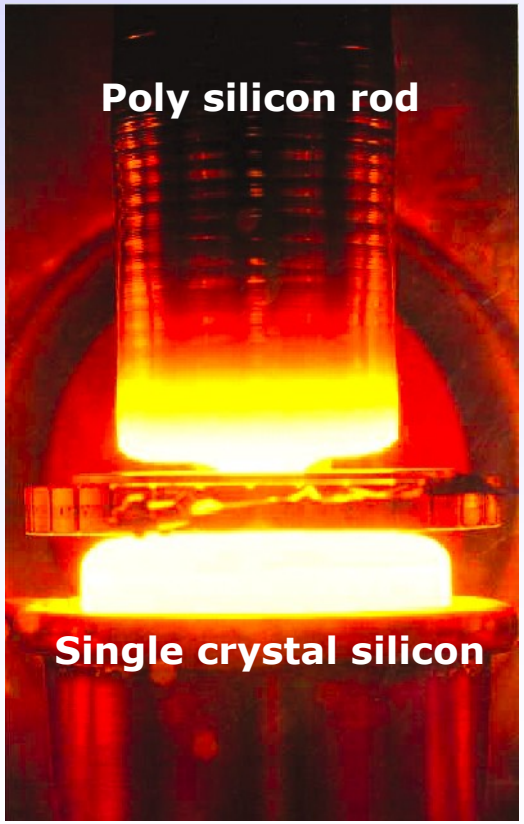

Monocrystalline Ingot

- grind into round shape
- make the flat or a notch

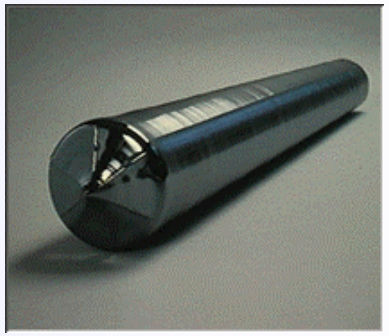

Wafer production

- Slice the ingot into wafers of 300-500 μm (diamond saw)
- lapping of wafers
- etching of wafers
- polishing of wafers

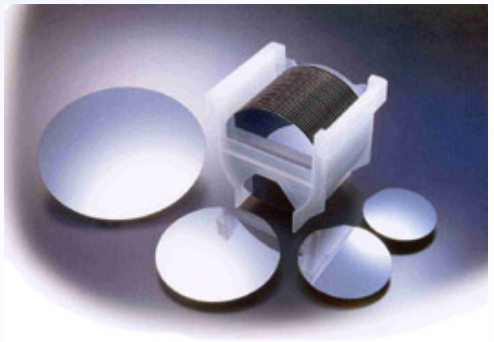

Silicon Sensor Production

A "simple“ production sequence (schematic)

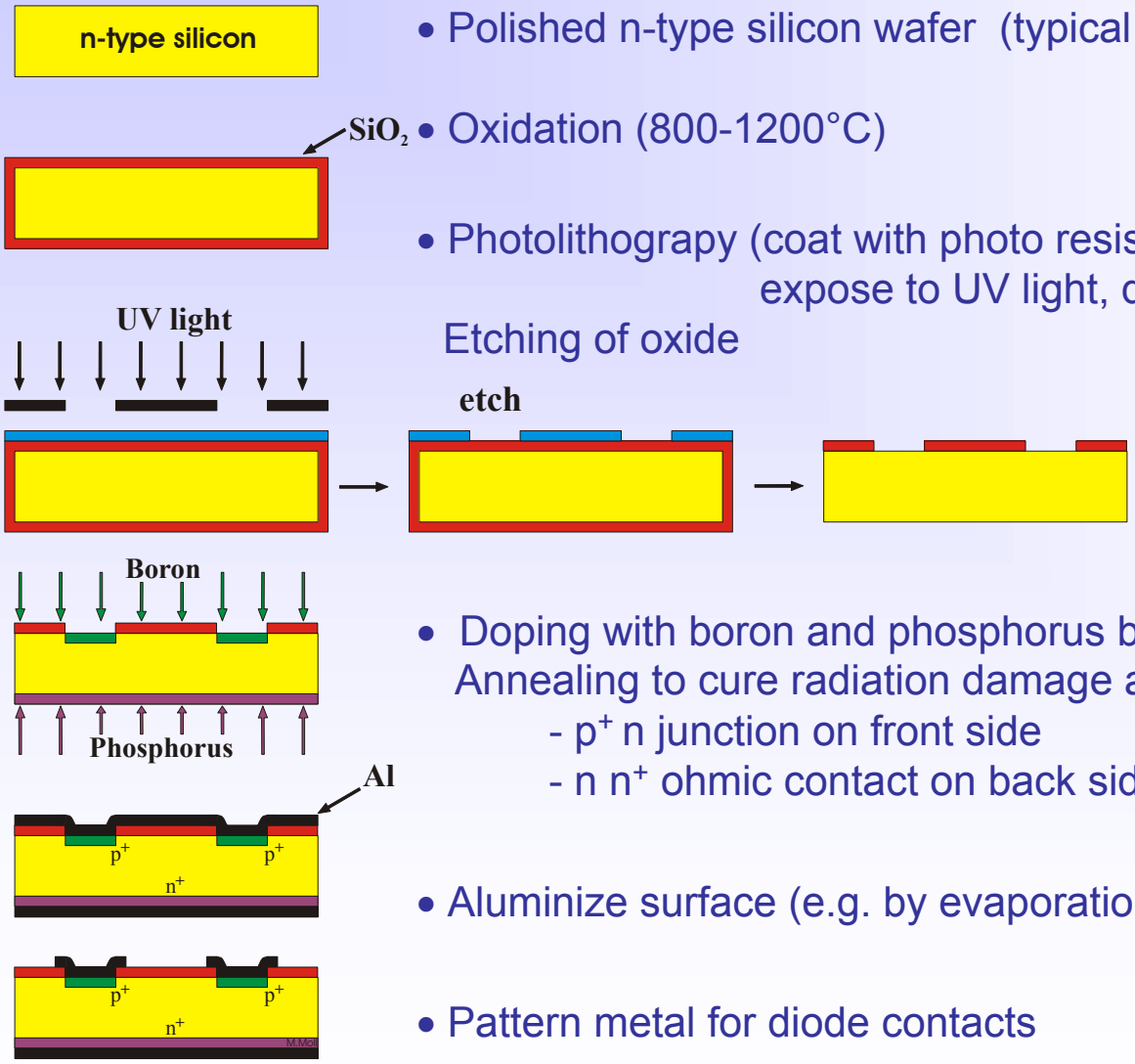

- Polished n-type silicon wafer (typical ρ ~ 1-10 KΩcm)
- Oxidation (800-1200°C)
- Photolithograpy (coat with photo resist; align mask, expose to UV light, develop photoresist);
  Etching of oxide
- Doping with boron and phosphorus by implantation (or by diffusion)
  Annealing to cure radiation damage and activate dopants
  - p^+ n junction on front side
  - n n^+ ohmic contact on back side
- Aluminize surface (e.g. by evaporation)
- Pattern metal for diode contacts

Single Sided Strip Detector

- Segmentation of the p^+ layer into strips (Diode Strip Detector) and connection of strips to individual read-out channels gives spatial information

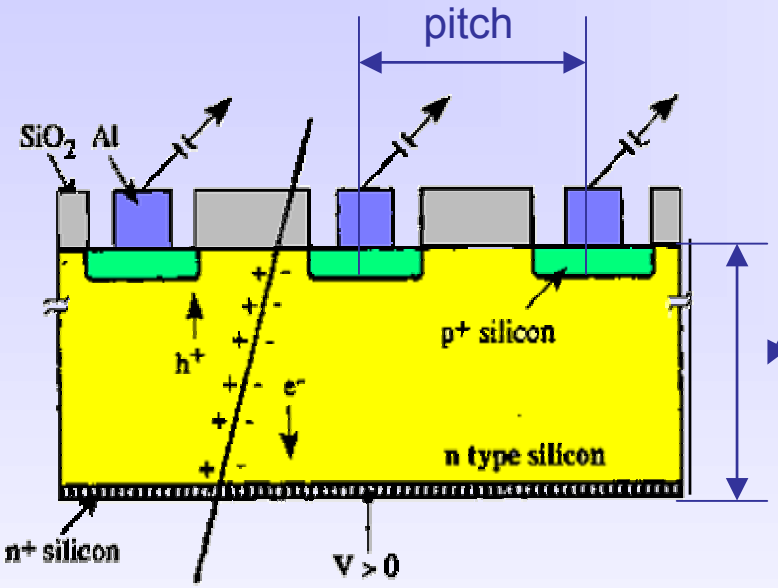

typical thickness: 300μm (150μm - 500μm used)

- using n-type silicon with a resistivity of
  ρ = 2 KΩcm (N_D ~$2.2 \cdot 10^{12}$cm^{-3})
  results in a depletion voltage ~ 150 V

- Resolution σ depends on the pitch p (distance from strip to strip)

  - e.g. detection of charge in binary way (threshold discrimination) and using center of strip as measured coordinate results in

$$\sigma = \frac{p}{\sqrt{12}}$$

typical pitch values are 20 μm– 150 μm ⇒ 50 μm pitch results in 14.4 μm resolution

Capacitive charge division

extra slide not shown

- Analog readout (measurement of signal height) of every strip leads to substantial improvement of position resolution, however not every strip has to be read:

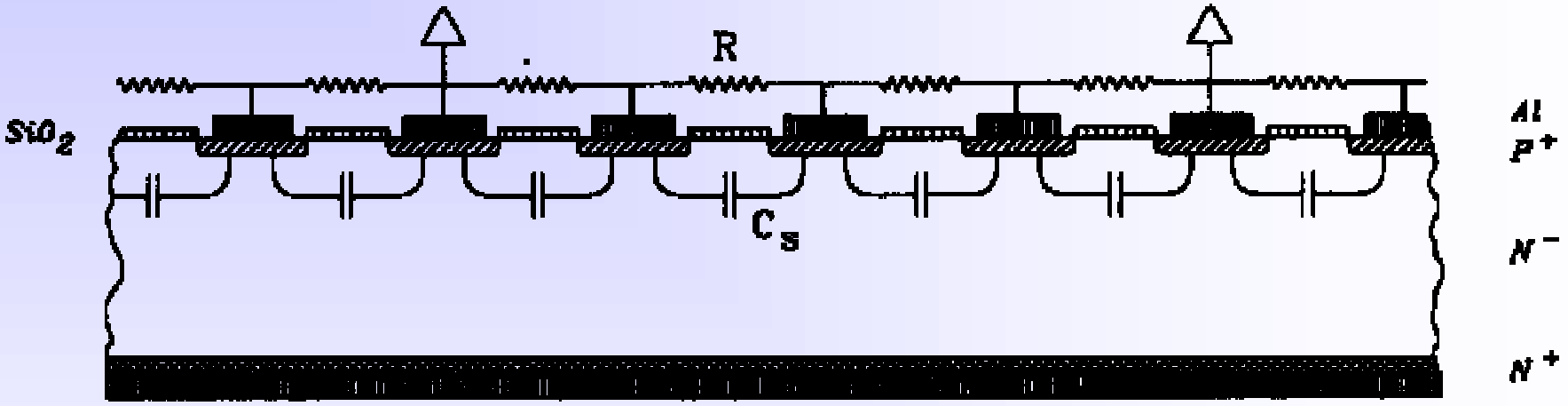

- Charge division readout reduces the number of readout channels as only a fraction of the strips is connected to readout amplifier.

- Charge collected at the interpolation strips is divided between the two neighboring readout channels according to the relative position.

Bias resistor and AC Coupling

extra slide not shown

Bias resistor

- Need to isolate strips from each other to collect/measure charge on each strip
  ⇒ high impedance bias connection (≈ 1MΩ resistor)

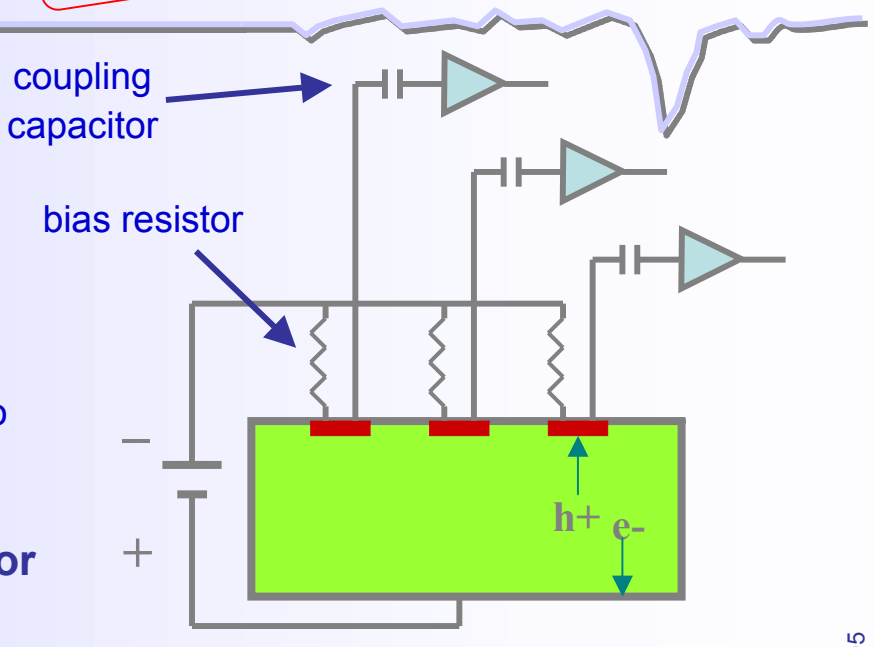

Coupling capacitor

- Couple input amplifier through a capacitor (AC coupling) to avoid large DC input from leakage current

Integration of capacitors and resistors on sensor

- Bias resistors via deposition of doped polysilicon
- Capacitors via metal readout lines over the implants but separated by an insulating dielectric layer (SiO_2,Si_3N_4).

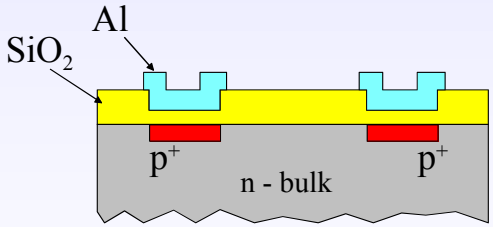

⇒ nice integration
⇒ more masks, processing steps
⇒ pin holes

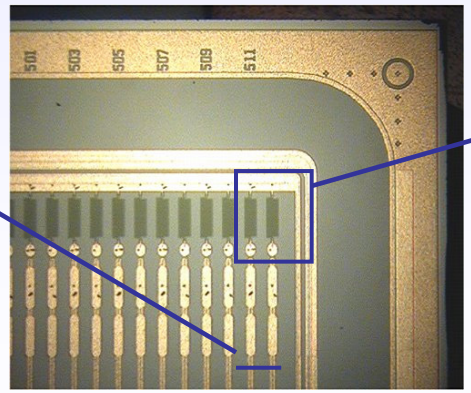

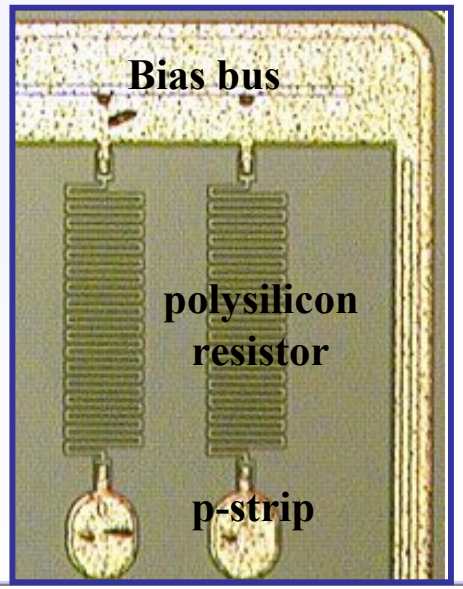

The Charge Signal

extra slide not shown

Collected Charge for a Minimum Ionizing Particle (MIP)

- **Mean energy loss**
  dE/dx (Si) = 3.88 MeV/cm
  $\Rightarrow$ 116 keV for 300μm thickness

- **Most probable energy loss**
  $\approx$ 0.7 $\times$mean
  $\Rightarrow$ 81 keV

- **3.6 eV to create an e-h pair**
  $\Rightarrow$ 72 e-h / μm (mean)
  $\Rightarrow$ 108 e-h / μm (most probable)

- **Most probable charge** (300 μm)

  $\approx$ 22500 e $\approx$ 3.6 fC

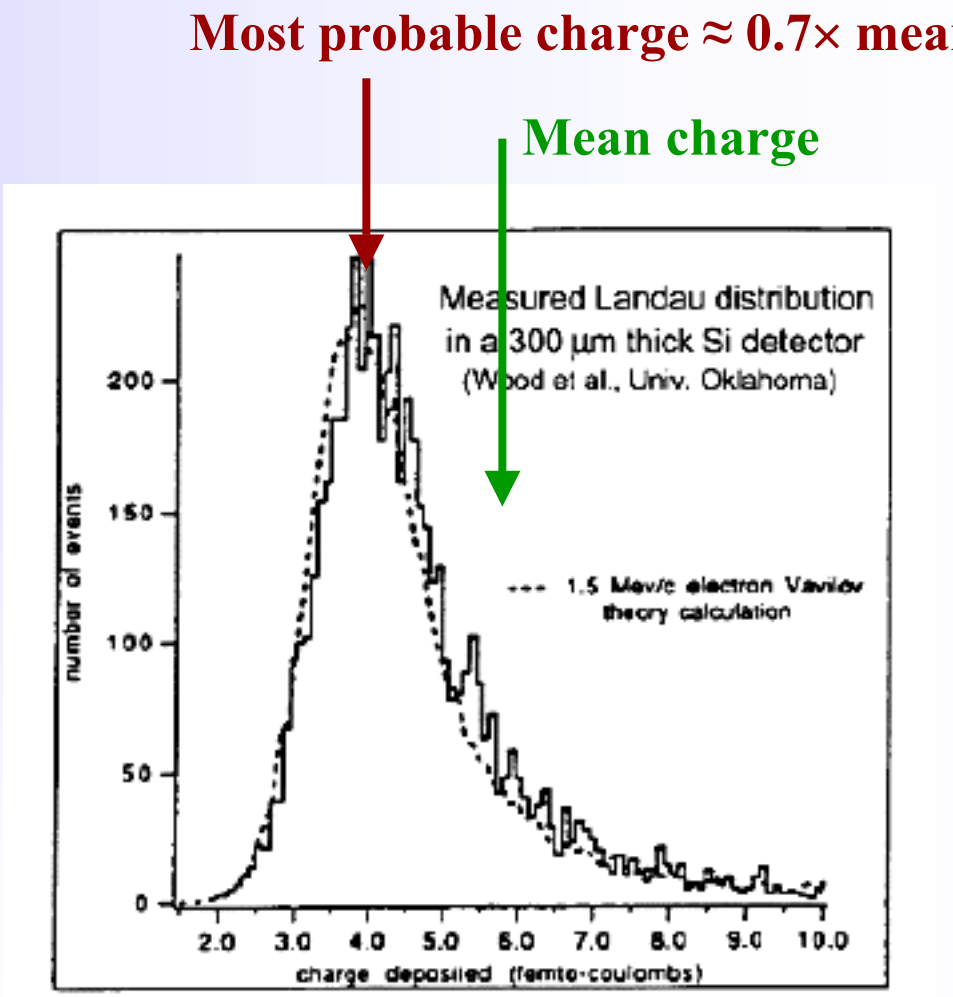

Signal to noise ratio (S/N)

- **Landau distribution** has a low energy tail
  - becomes even lower by noise broadening

Noise sources: (ENC = Equivalent Noise Charge)

- Capacitance $ENC \propto C_d$
- Leakage Current $ENC \propto \sqrt{I}$
- Thermal Noise (bias resistor) $ENC \propto \sqrt{k_B T / R}$

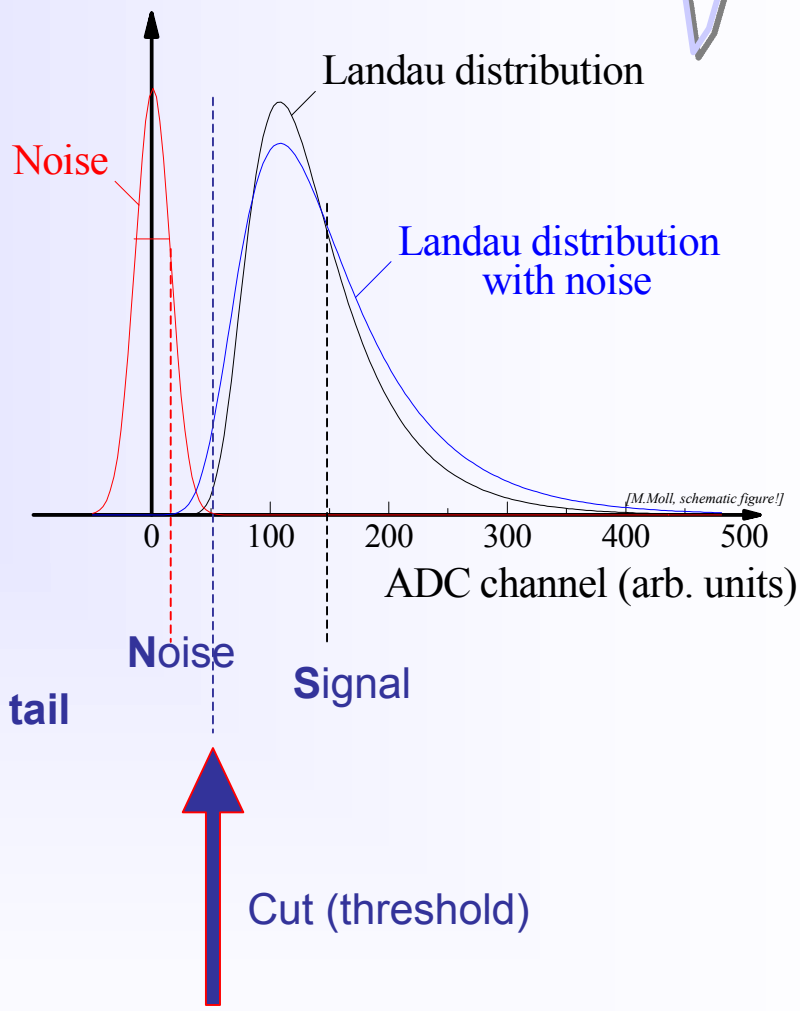

- **Good hits selected by requiring N_{ADC} > noise tail**
  If cut too high ⇒ efficiency loss
  If cut too low ⇒ noise occupancy
- **Figure of Merit: Signal-to-Noise Ratio S/N**
- **Typical values >10-15, people get nervous below 10.**
  Radiation damage severely degrades the S/N.

Charge Collection time and diffusion

extra slide not shown

Charge Collection time

- Drift velocity of charge carriers $v \approx \mu E$, so drift time, $t_d = d/v = d/\mu E$

Typical values: d=300 μm, E= 2.5 kV/cm,
with μ_e= 1350 cm² / V·s and μ_h= 450 cm² / V·s

$\Rightarrow$ $t_d(e)$= 9ns , $t_d(h)$= 27ns

Diffusion

- Diffusion of charge "cloud" caused by scattering of drifting charge carriers, radius of distribution after time td:

$\sigma = \sqrt{2Dt_d}$ with diffusion constant $D = \mu kT/q$

- Same radius for e and h since $t_d \propto 1/\mu$

Typical charge radius: $\sigma \approx 6\mu$m, could exploit this to get better position resolution due to charge sharing between adjacent strips (using centroid finding), but need to keep drift times long (low field).

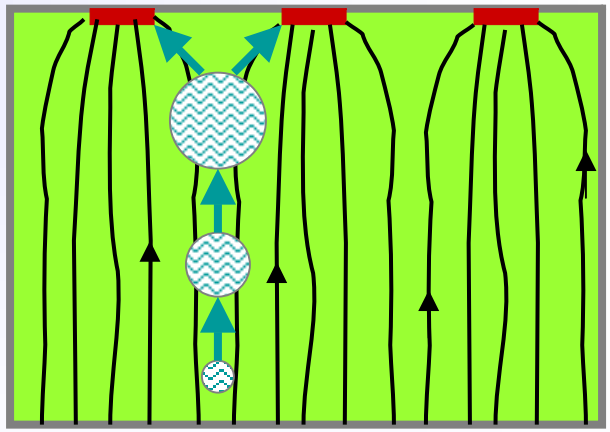

Double sided silicon detectors

extra slide not shown

- **Get a 2nd coordinate**
  Put n^+ and p^+ strips on opposite sides and read them both

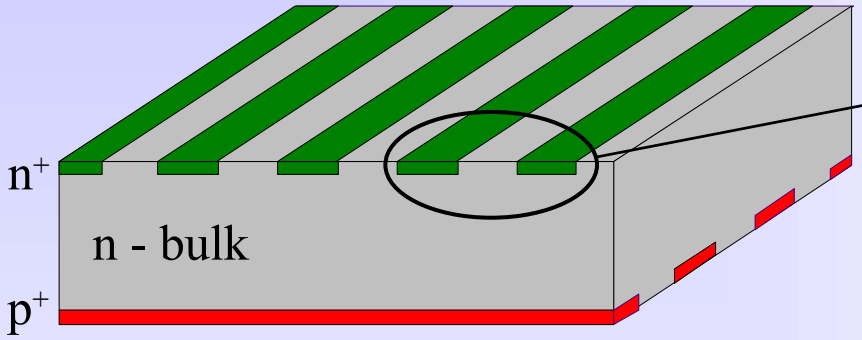

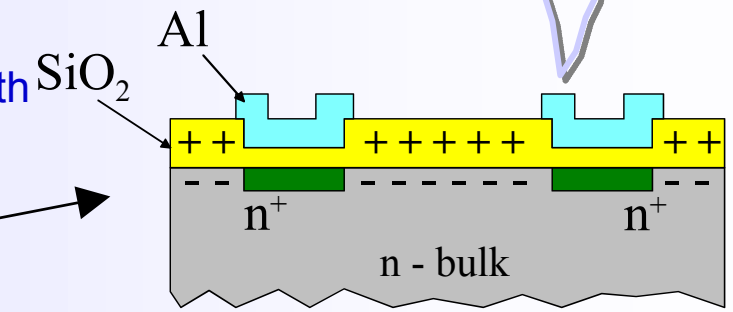

"p-stop"

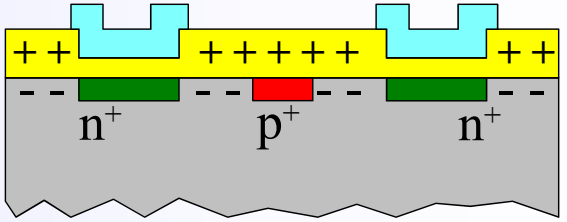

- **Problem: Electron accumulation layer**
  n^+-strips are not isolated because of an electron accumulation layer at the Si-SiO_2 interface. This effect is due to the presence of positive charge in SiO_2 layer which attracts electrons.

"p-spray"

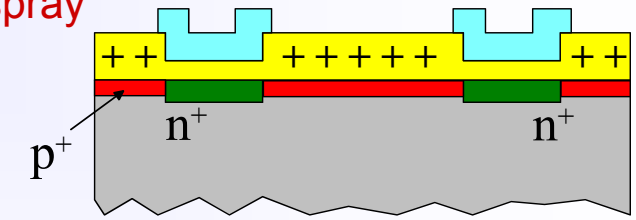

- **Solution:** "Break" accumulation layer
  - p-strips in between the n-strips ("**p-stop**")
  - moderate p^+-implantation over all surface ("**p-spray**")
  - "**field plates**" (metal over oxide) over the n^+-strips and apply negative potential with respect to n^+-strips to repel electrons.

"field plates"

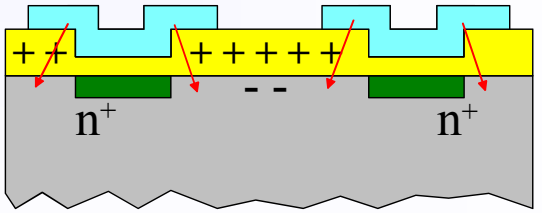

Detector Module

- **Detector Modules** - "Basic building block of tracking detectors"
  - Silicon Sensors
  - Mechanical support (cooling)
  - Front end electronics and signal routing (connectivity)

SCT = SemiConductor Tracker
ASICS = Application Specific Integrated CircuitS
TPG = Thermal Pyrolytic Graphite

- **Example: ATLAS SCT Barrel Module**

128 mm

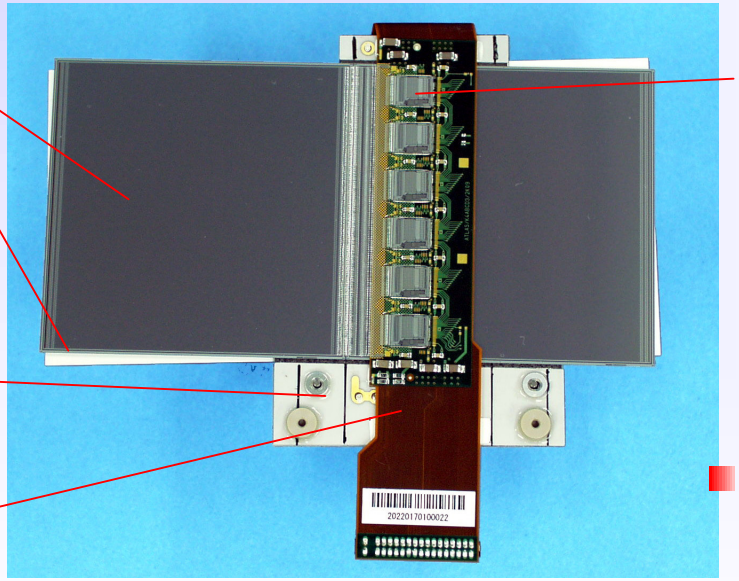

- **Silicon sensors (x4)**
  - 64 x 64 mm^2
  - p-in-n, single sided
  - AC-coupled
  - 768 strips
  - 80μm pitch/12μm width
- **ASICS (x12)**
  - ABCD chip (binary readout)
  - DMILL technology
  - 128 channels
- **Wire bonds** (~3500)
  - 25 μm Al wires
- **Mechanical support**
  - TPG baseboard
  - BeO facings
- **Hybrid (x1)**
  - flexible 4 layer copper/kapton hybrid
  - mounted directly over two of the four silicon sensors
  - carrying front end electronics, pitch adapter, signal routing, connector

$\sigma(r\phi) \sim 16\ \mu m$, $\sigma(z) \sim 850\mu m$ [NIMA538 (2005) 384]

- **ATLAS – SCT**
  - 15.552 microstrip sensors
  - 2.112 barrel modules
  - 1.976 forward modules
  - 61 m^2 silicon, 6.3·10^{6}strips

Wire bonding

extra slide not shown

- Uses ultrasonic power to vibrate needle-like tool on top of wire. Friction welds wire to metallized substrate underneath.
- Can easily handle 80μm pitch in a single row and 40μm in two staggered rows (typical FE chip input pitch is 44μm).
- Generally use 25μm diameter aluminum wire and bond to aluminum pads (chips) or gold pads (hybrid substrates).
- Heavily used in industry (PC processors) but not with such thin wire or small pitch.

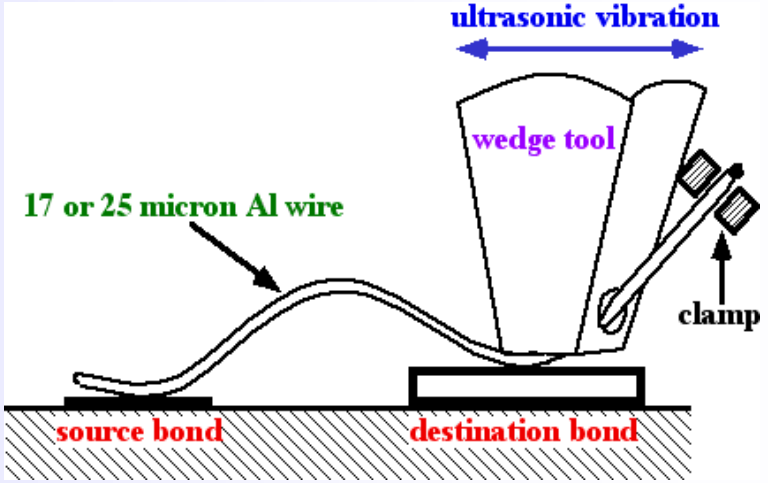

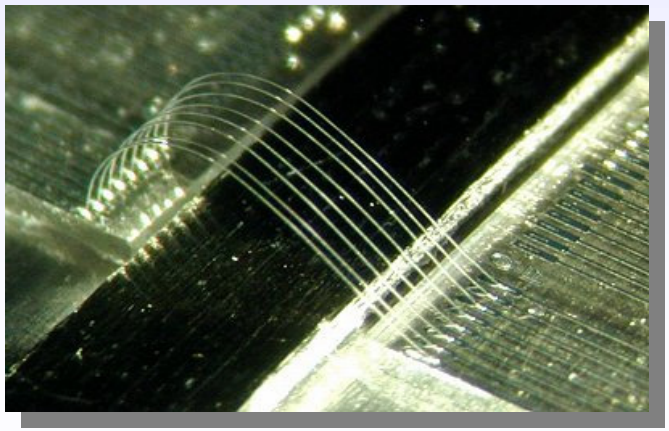

Microscope: connect sensor to fan-out circuit

Electron microscope: bond "foot"

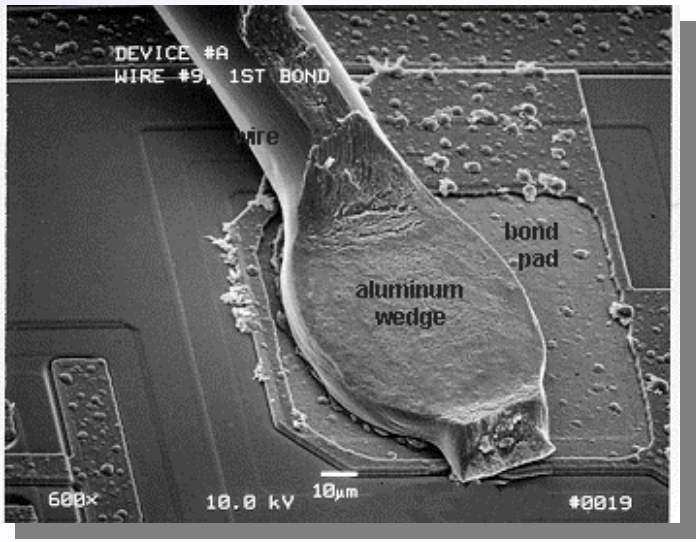

Silicon Drift Detectors

extra slide not shown

- Principle of sideways depletion (as for DEPFET sensors)
- p^+ segmentation on both sides of sensor
- complete depletion of wafer from segmented n^+ anodes located at one side of sensor
- electrons drift parallel to substrate surface to n^+ anodes
- voltage divider network (resistors) for p-strips to provide uniform drift field

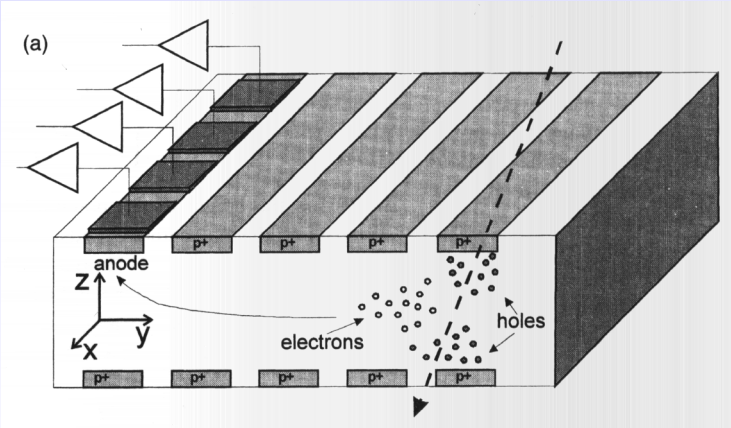

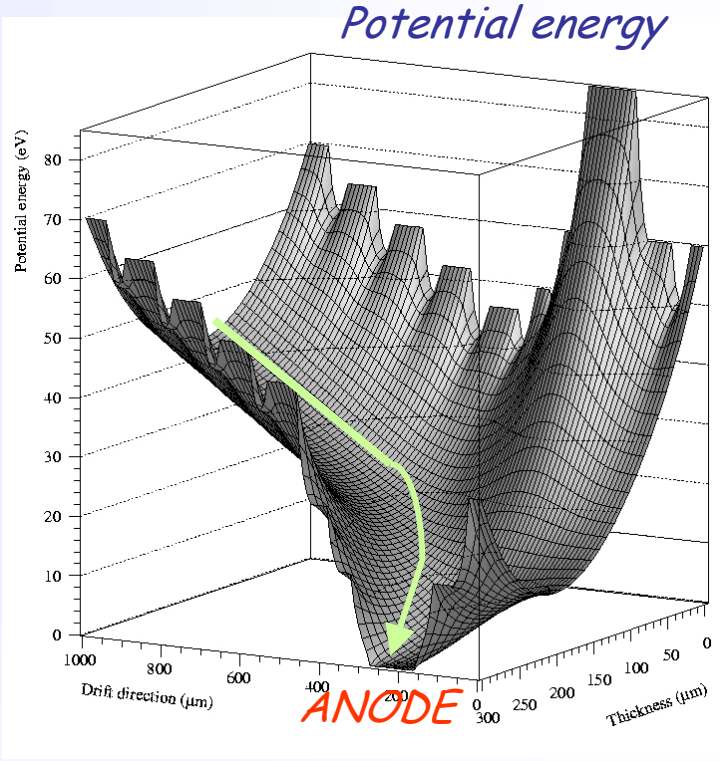

- Need to ensure good material uniformity, low defect rates, good drift field homogeneity, precise voltage dividing on p-strips and good temperature control.
- HEP: Implemented for STAR at RHIC and for ALICE at LHC

Hybrid Pixel Detectors

CERN Globe is a 3 million times bigger bump!

HAPS – Hybrid Active Pixel Sensors

- segment silicon to diode matrix with high granularity (⇒ true 2D, no reconstruction ambiguity)
- readout electronic with same geometry (every cell connected to its own processing electronics)
- connection by "bump bonding"
- requires sophisticated readout architecture
- Hybrid pixel detectors will be used in LHC experiments: ATLAS, ALICE, CMS and LHCb

Solder Bump: Pb-Sn

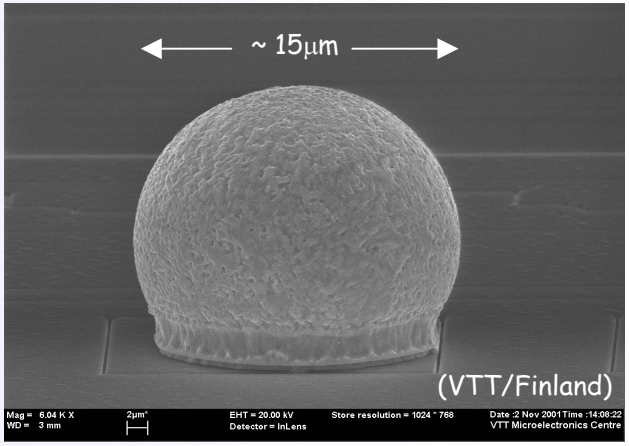

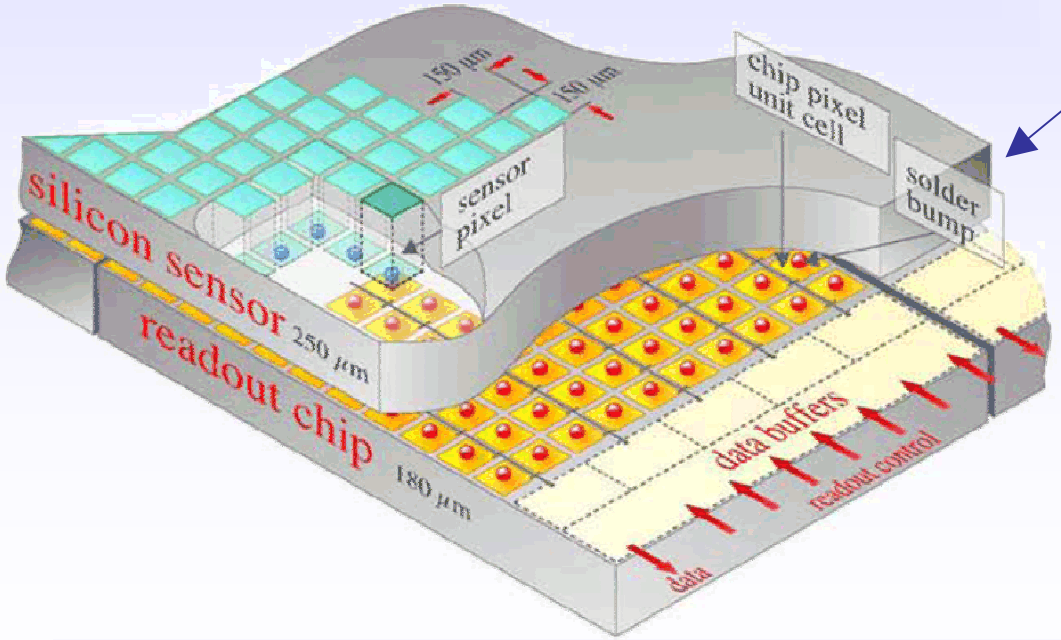

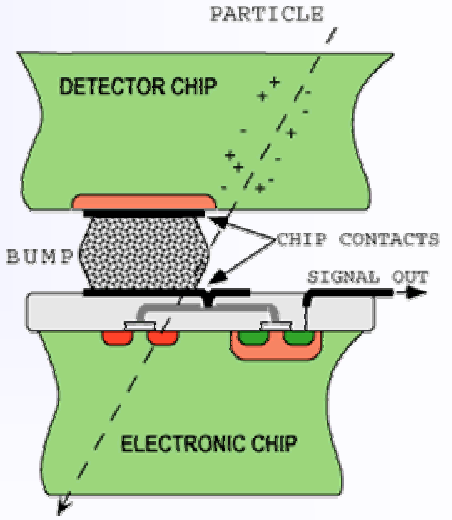

Flip-chip technique

CCD – Charged Coupled Devices

(1) MOS structure with segmented metal layer;
Charge is captured in a potential well.

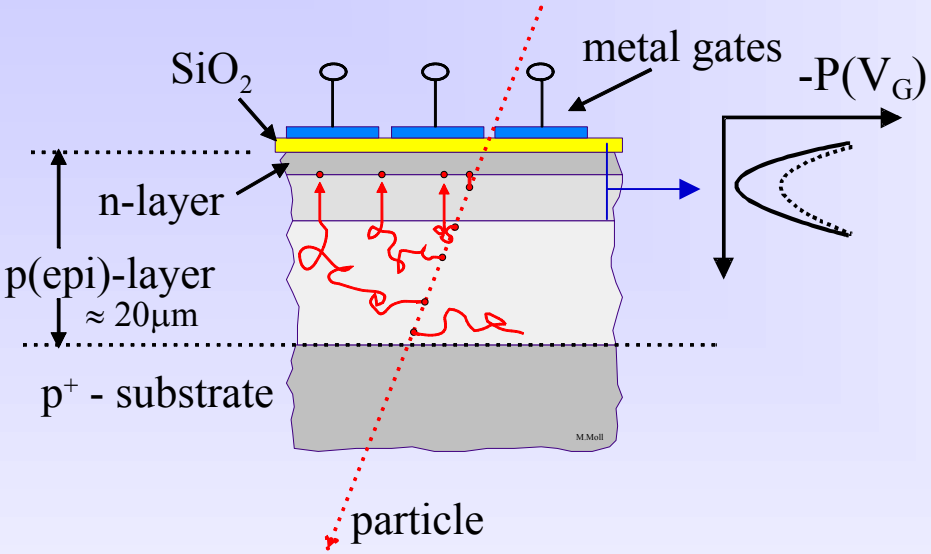

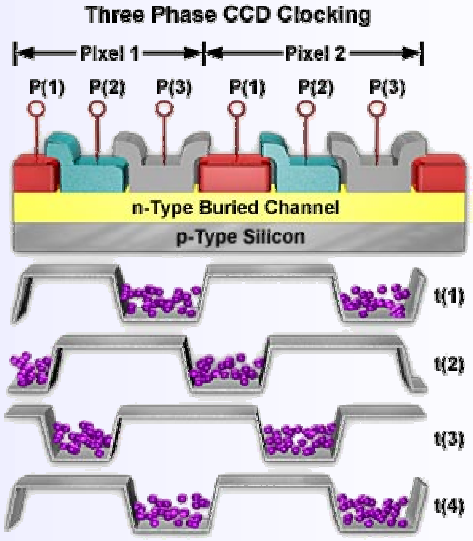

(2) Readout: Shift electrons towards anode
by periodic variation of 3 potentials

(3) Create an array of pixel for
a 2D detector

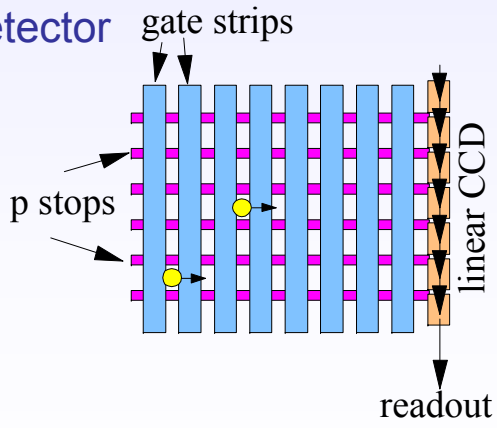

Pixel CCD

- needs only few readout channels
- small charge (≈2000 e) ⇒ needs cooling
- long readout time, active during readout
- sensitive to radiation damage

⇒ applicable for low rate experiment
without high intensity radiation field

MAPS – Monolithic Active Pixel Sensors

extra slide not shown

Monolithic detectors

- readout electronics directly within sensor material (same epi layer)

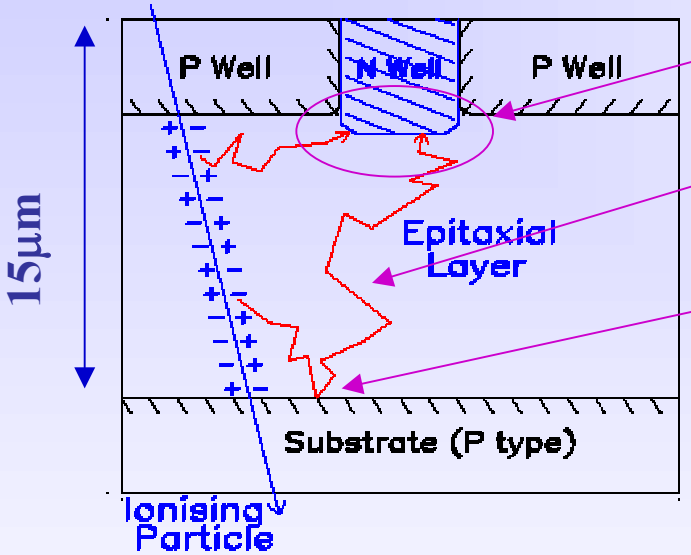

- charge collected at n-well / p-epi diode
- thermal diffusion of free charge
- reflection at potential barriers between areas with different doping concentration
- no depletion voltage applied
  ⇒ potential formed by different doping concentrations only

- no connections needed to electronics (e.g. no bumps)
- very small sizes achievable

DEPFET - DEP(leted)F(ield)E(ffect)T(ransistor)

extra slide not shown

- FET integrated on high resistivity bulk, bulk sideward depleted
- electrons collected in potential minimum at internal gate
  - transistor current modulated by collected charge
  - charge removed by reset mechanism (clear)
- switch on/off by (external) top gate to read out

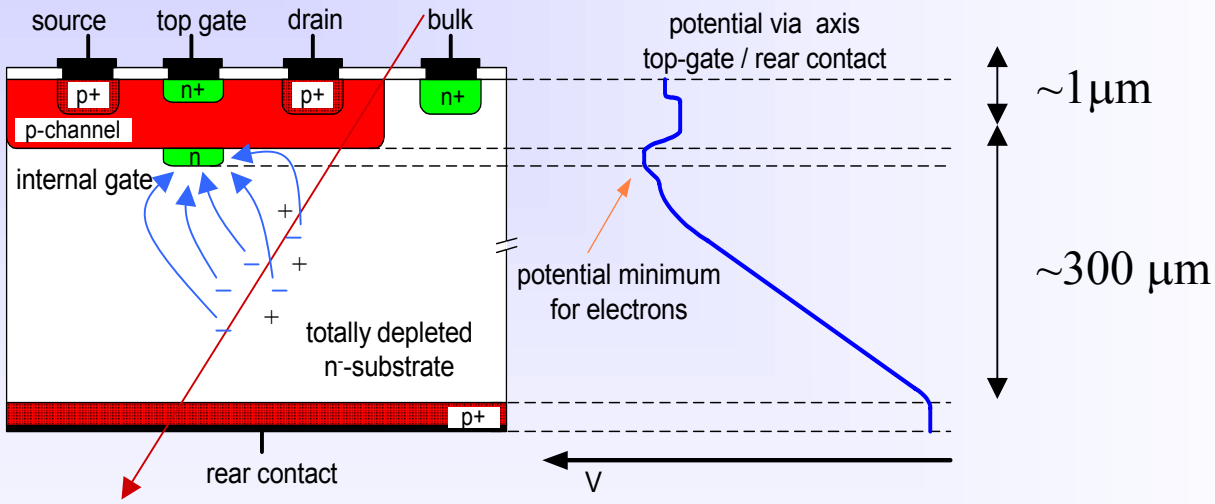

- amplification of charge at the position of collection ⇒ no transfer loss
- full bulk sensitivity, bulk can be thinned down to 50 μm if needed
- non structured entrance window (backside)
- very low imput capacitance ⇒ very low noise

Example from LHC: The CMS tracker

CMS

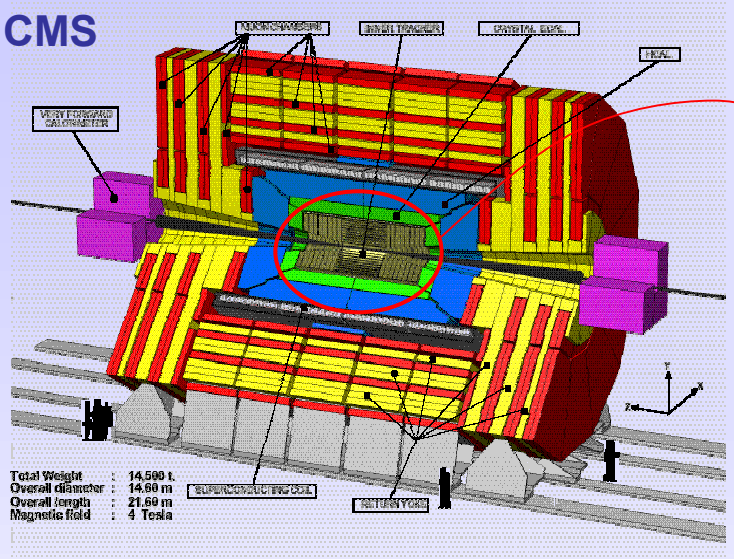

Inner Tracker

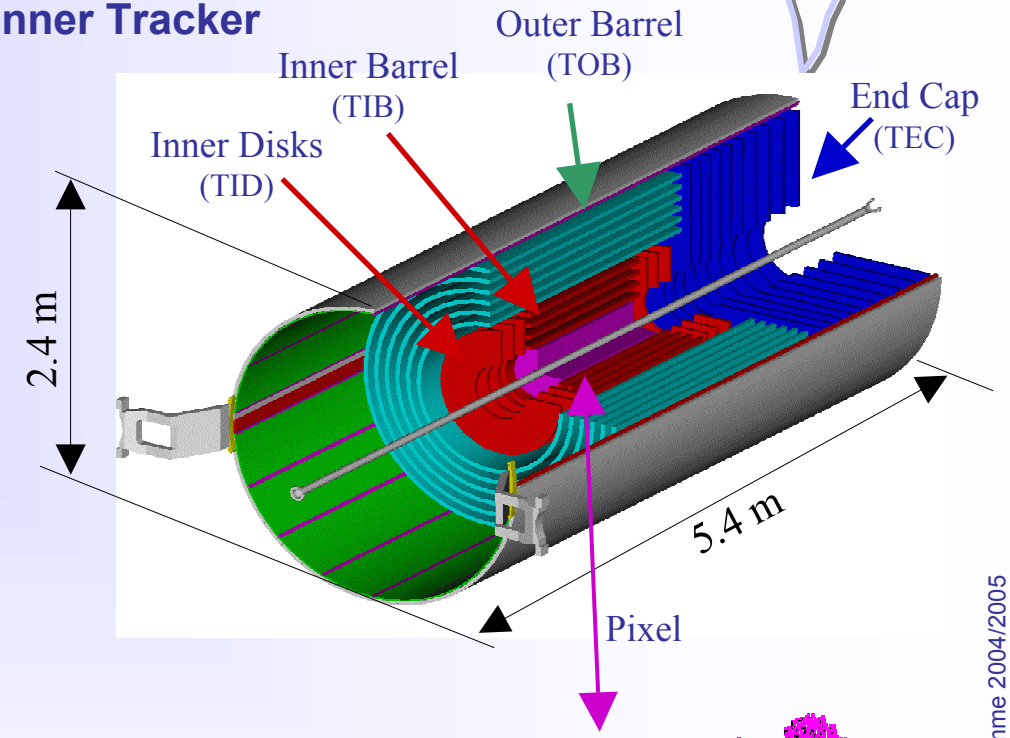

CMS - Currently the Most Silicon

Micro Strip:

- ~ 214 m^2 of silicon strip sensors
- 11.4 million strips

Pixel:

- Inner 3 layers: silicon pixels (~ $1m^2$)
- 66 million pixels (100x150μm)
- Precision: σ(rφ) ~ σ(z) ~ 15μm
- Most challenging operating environments (LHC)

Pixel Detector

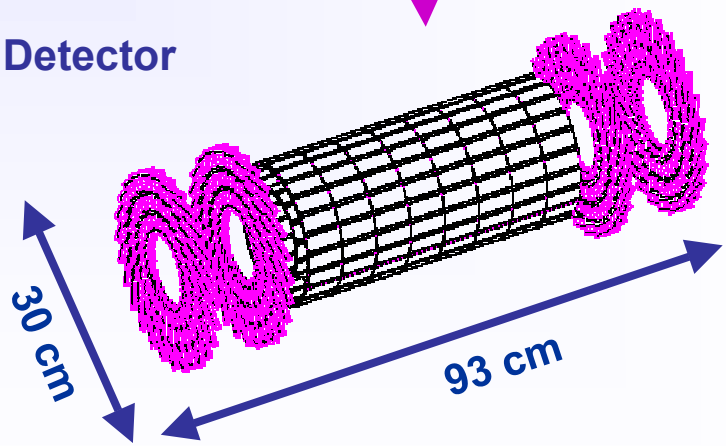

Radiation Levels at LHC and SLHC

Example: ATLAS

- Fluences per year at full Luminosity

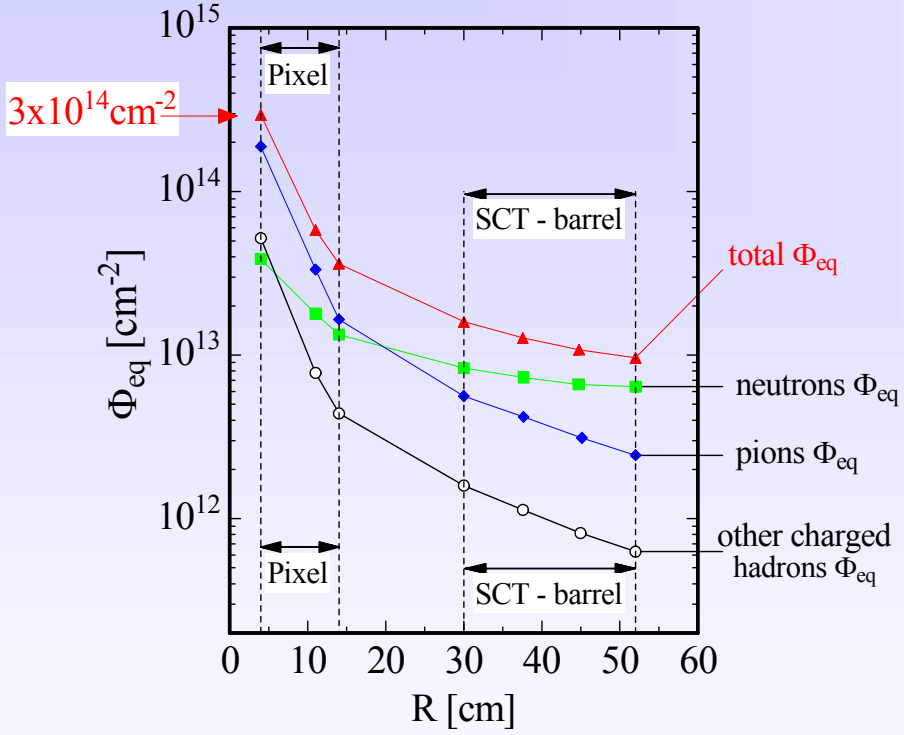

- Pixel detector: up to $\Phi_{eq} \approx 3.5 \cdot 10^{14}$ cm^{-2} /year
- Dominating type of particle is different for pixel (pions) and strip detectors (neutrons)

LHC silicon detectors:

- All detectors have been extensively tested and developed for radiation tolerance and are expected to survive the LHC radiation environment.

- Some experiments have already foreseen upgrades (e.g. LHCb Velo after 3 years).

Super LHC

- upgrade of LHC to 10 x higher Luminosity

  $\Rightarrow$ 10 x higher radiation levels

  $\Rightarrow$ Radiation damage will become a critical issue!

$\Rightarrow$ New, radiation tolerant detectors needed!

- What is radiation damage ?
- How to cope with it ?

Radiation Damage: Microscopic defects

- **Damage to the silicon crystal:** Displacement of lattice atoms

particle → Si_S → E_K>25 eV → V + I

Vacancy + Interstitial ⟺ **"point defects", mobile in silicon, can react with impurities (O,C,..)**

E_K > 5 keV → **point defects and clusters of defects**

80 nm

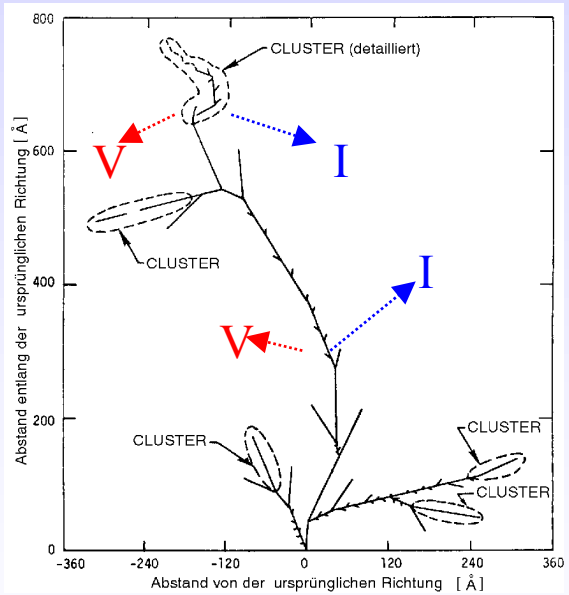

Distribution of vacancies created by a 50 keV Si-ion in silicon (typical recoil energy for 1 MeV neutrons):

← **Schematic** [Van Lint 1980]

Simulation → [M.Huhtinen 2001]

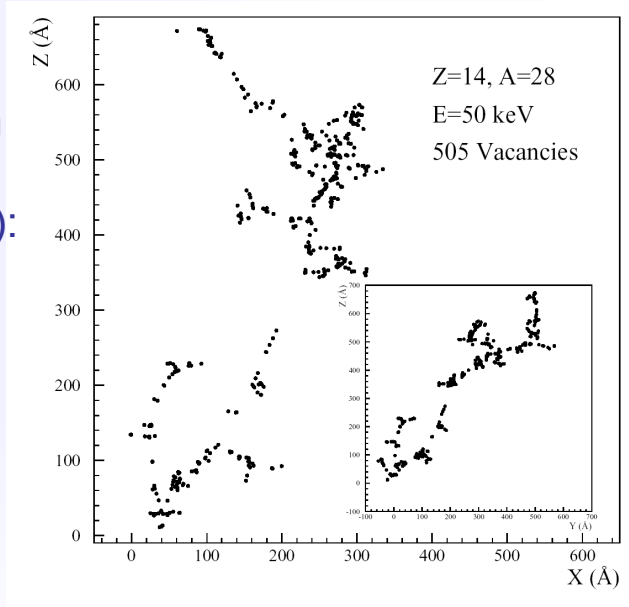

- **Defects can be electrically active (levels in the band gap)**
  - capture and release electrons and holes from conduction and valence band
  - ⇒ can be charged - can be generation/recombination centers - can be trapping centers

Radiation Damage: Particle dependence

extra slide not shown

particle → Si_S → E_K>25 eV → Vacancy + Interstitial → point defects (V-O, C-O, ..)

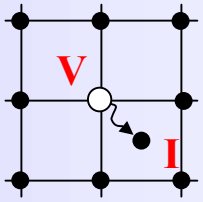

E_K > 5 keV point defects and clusters of defects

^{60}Co-gammas	Electrons	Neutrons (elastic scattering)
Compton Electrons with max. $E_\gamma \approx$ MeV (no cluster production)	E_e > 255 keV for displacement E_e > 8 MeV for cluster	E_n > 185 eV for displacement E_n > 35 keV for cluster

only point defects ⟷ point defects & clusters ⟷ mainly clusters

Simulation:

Initial distribution of vacancies in $(1\mu m)^3$ after 10^{14} particles/cm^2

[Mika Huhtinen NIMA 491(2002) 194]

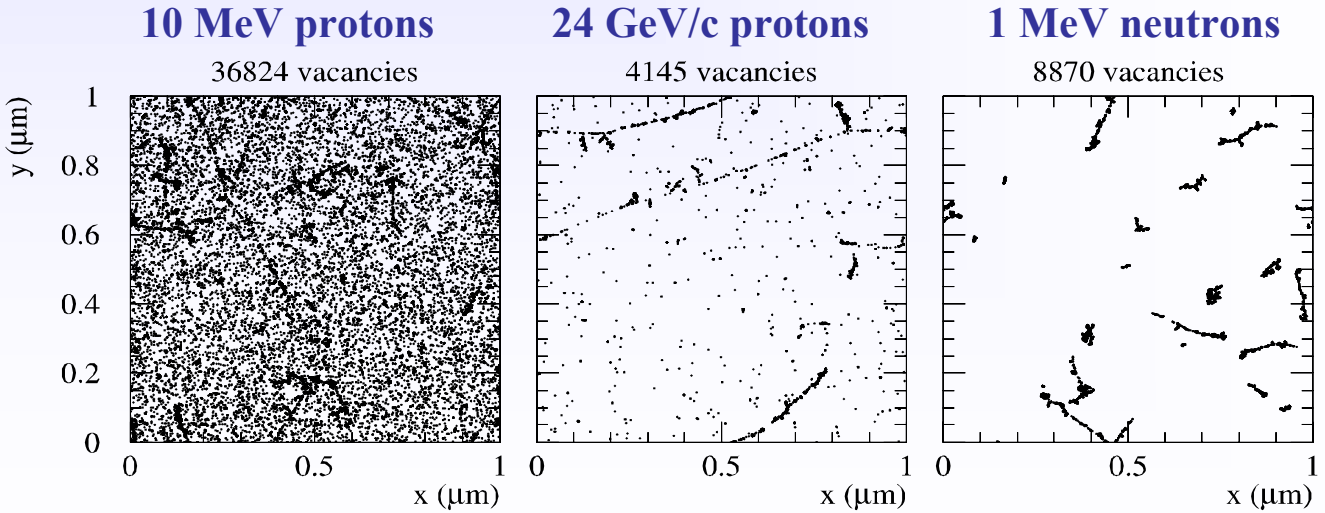

Impact of defects on detector properties

extra slide not shown

Shockley-Read-Hall statistics
(standard textbook theory)

Inter-center charge transfer model
(inside clusters only)

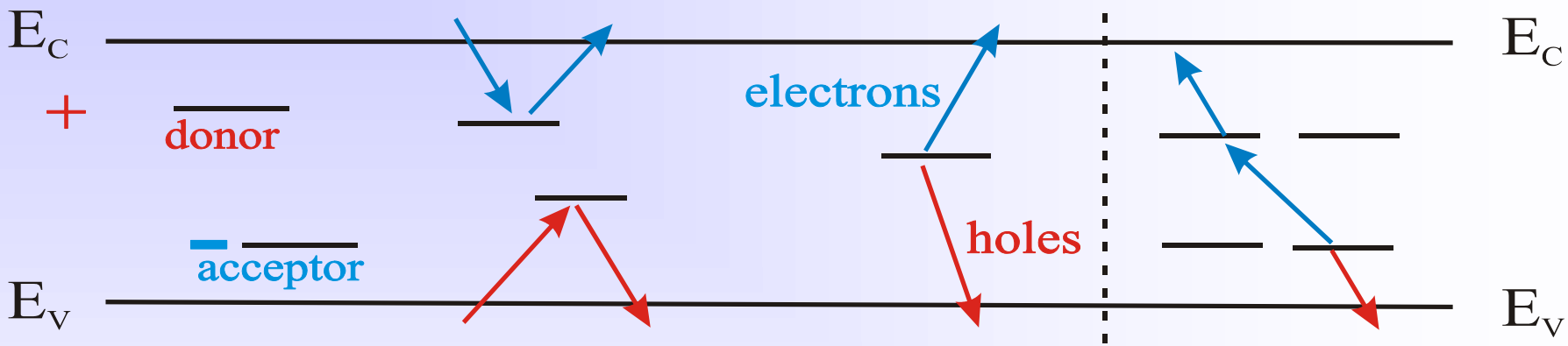

charged defects
⇒ N_{eff} , V_{dep}
e.g. donors in upper and acceptors in lower half of band gap

trapping (e and h)
⇒ **CCE**
shallow defects do not contribute at room temperature due to fast detrapping

generation
⇒ **leakage current**
Levels close to midgap are most effective

enhanced generation
⇒ **leakage current**
⇒ **space charge**

- **Impact on detector properties can be calculated if all defect parameters are known:**

$\sigma_{n,p}$: **cross sections** ΔE : **ionization energy** N_t : **concentration**

Radiation Damage in Silicon Sensors

- **Two general types of radiation damage:**

  - **Bulk (Crystal) damage** due to **Non Ionizing Energy Loss (NIEL)**
    - Displacement Damage –

    I. Change of **depletion voltage** (higher operation voltage, underdepletion)
    ⇒ constant cooling needed to avoid reverse annealing

    II. Increase of **leakage current** (increase of shot noise, thermal runaway)
    ⇒ needs cooling of sensors during operation

    III. Decrease of **charge collection efficiency**
    due to underdepletion and increased trapping

  - **Surface damage** due to **Ionizing Energy Loss (IEL)**
    - accumulation of positive in the oxide (SiO_2) and the Si/SiO_2 interface –

    affects: interstrip capacitance (noise factor), breakdown behavior
    and other structures depending on near-surface effects

- **Signal/noise ratio is the quantity to watch**

  ⇒ **Sensors can fail from radiation damage !**

Radiation Damage – I. Depletion Voltage

Change of Depletion Voltage V_{dep} (N_{eff})

…. with particle fluence:

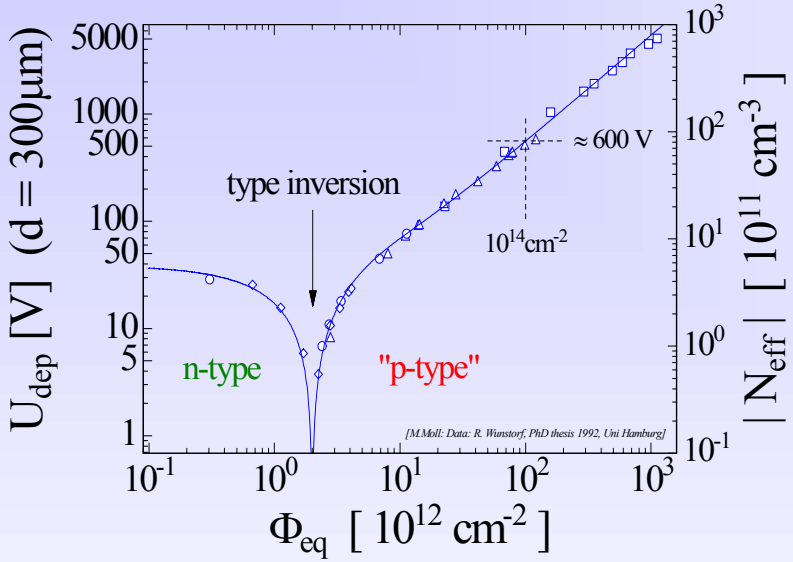

…. with time (annealing):

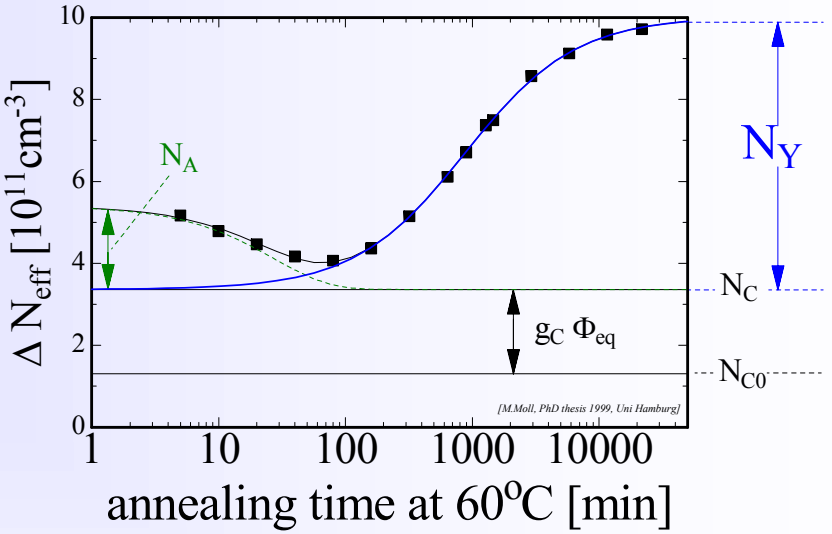

- "Type inversion": N_{eff} changes from positive to negative (Space Charge Sign Inversion)

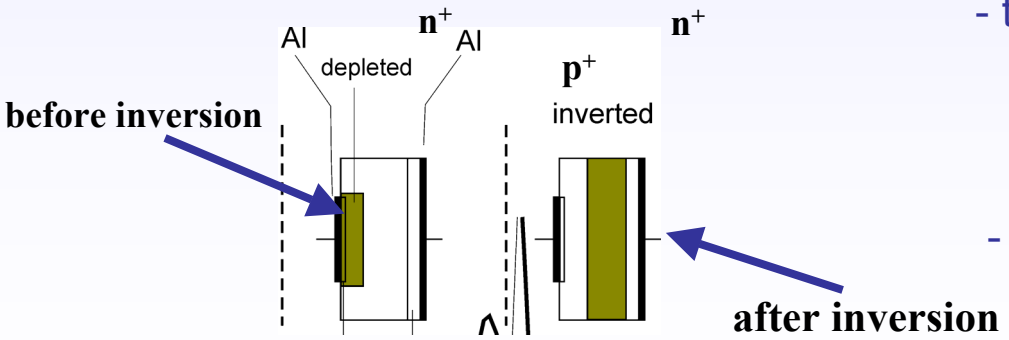

- **Short term:** "Beneficial annealing"
- **Long term:** "Reverse annealing"
  - time constant depends on temperature:
    - ~ 500 years (-10°C)
    - ~ 500 days (20°C)
    - ~ 21 hours (60°C)
  - **Consequence:** Detectors must be cooled even when the experiment is not running!

Radiation Damage – II. Leakage Current

extra slide not shown

Change of Leakage Current (after hadron irradiation)

…. with particle fluence:

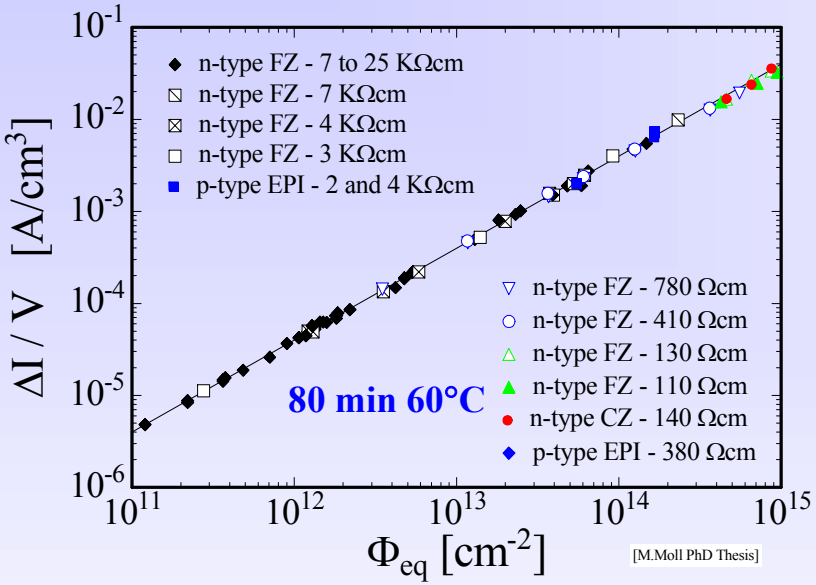

- Damage parameter α (slope in figure)

$$\alpha = \frac{\Delta I}{V \cdot \Phi_{eq}}$$

Leakage current per unit volume and particle fluence

- α is constant over several orders of fluence and independent of impurity concentration in Si
  ⇨ can be used for fluence measurement

…. with time (annealing):

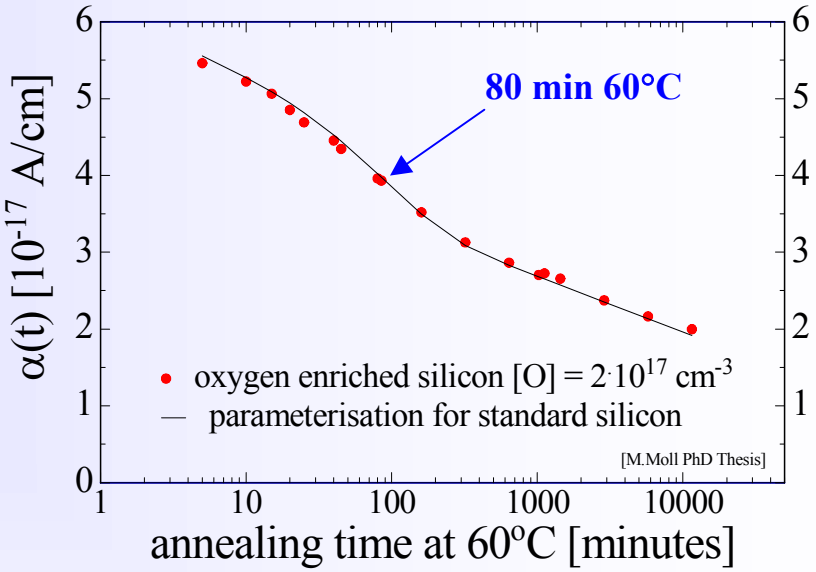

- Leakage current decreasing in time (depending on temperature)
- Strong temperature dependence

$$I \propto \exp\left(-\frac{E_g}{2k_BT}\right)$$

Consequence:
Cool detectors during operation!
Example: *I*(-10°C) ~1/16 *I*(20°C)

Radiation Damage – III. CCE

extra slide not shown

Deterioration of Charge Collection Efficiency (CCE)

2 mechanisms: - Trapping of electrons and holes
- Underdepletion (loss of active detector volume due to increase of V_{dep})

Trapping is characterized by an effective trapping time τ_{eff} for electrons and holes:

$$Q_{e,h}(t) = Q_{0e,h} \exp\left(-\frac{1}{\tau_{eff\ e,h}} \cdot t\right) \qquad \text{where} \qquad \frac{1}{\tau_{eff\ e,h}} \propto N_{defects}$$

Increase of inverse trapping time ($1/\tau$) with fluence ….. and change with time (annealing):

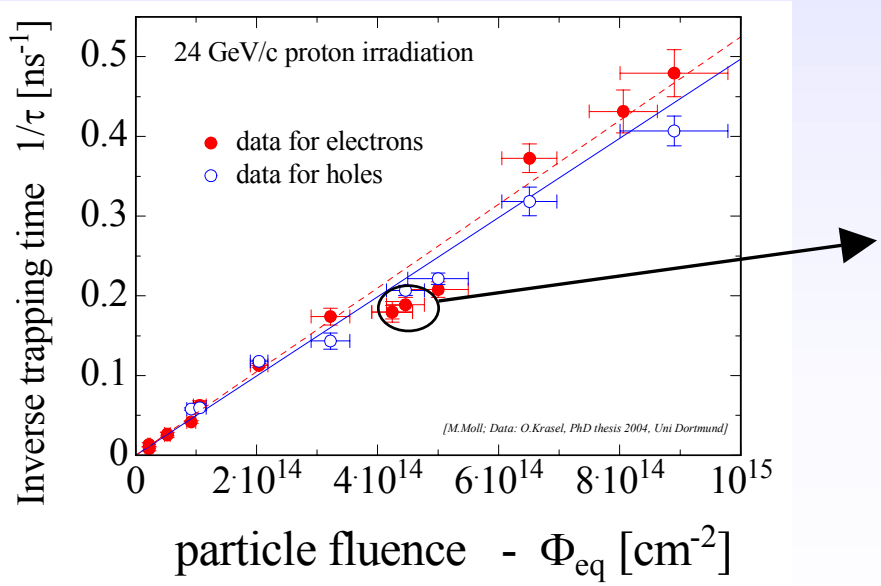

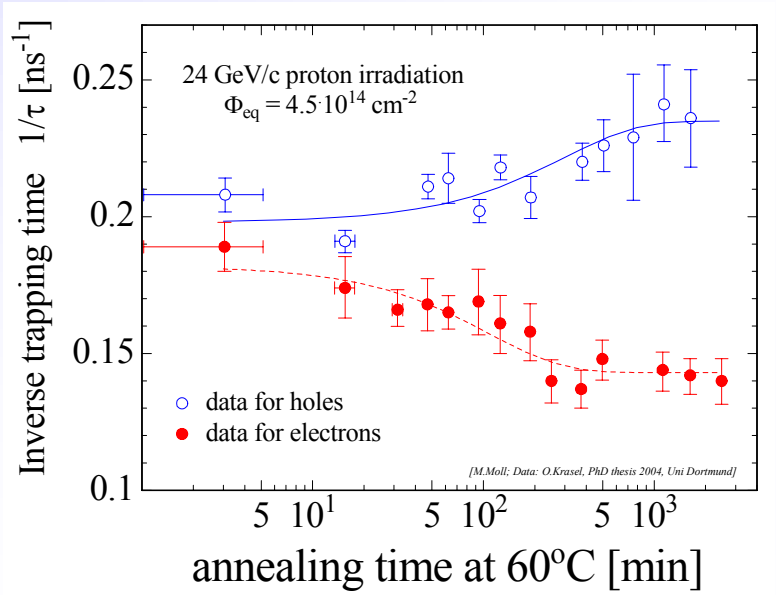

R&D : Radiation tolerant tracking detectors

extra slide not shown

Scientific Strategies:

I. **Material engineering**

II. **Device engineering**

III. **Variation of detector operational conditions**

Defect Engineering of Silicon

Deliberate incorporation of impurities or defects into the silicon bulk to improve radiation tolerance of detectors

- **Needs:** profound understanding of radiation damage
  (microscopic defects, macroscopic parameters, dependence on particles type and energy, defect formation kinetics and annealing processes)
- **Examples:** - Oxygen enriched silicon
  - Hydrogen enriched silicon
  - Pre-irradiated silicon

New Materials (other semiconductors than Si)

- Diamond, Silicon Carbide (SiC), …

New detector designs

- **Examples:** - p-type silicon detectors (n-in-p)
  - thin detectors, epitaxial detectors
  - 3D and Semi 3D detectors

Cryogenic operation of detectors

Operate detectors at 100-200K to reduce the charge loss ("Lazarus effect")

Active CERN R&D collaborations:

- *RD50 "Radiation hard semiconductor devices for very high luminosity colliders"*
- *RD42 "CVD Diamond Radiation Detectors"*
- *RD39 "Cryogenic Tracking Detectors"*

New Material: Oxygen enriched silicon – DOFZ

DOFZ (Diffusion Oxygenated Float Zone Silicon)

- 1982 First oxygen diffusion tests on FZ [Brotherton et al. J.Appl.Phys.,Vol.53, No.8.,5720]
- 1995 First tests on detector grade silicon [Z.Li et al. IEEE TNS Vol.42,No.4,219]
- 1999 Introduced to the HEP community by CERN - RD48 (ROSE-Collaboration)

Very long oxidation (e.g. 48h at 1150°C) increases the oxygen content in silicon

Strong improvement after charged hadron irradiation observed

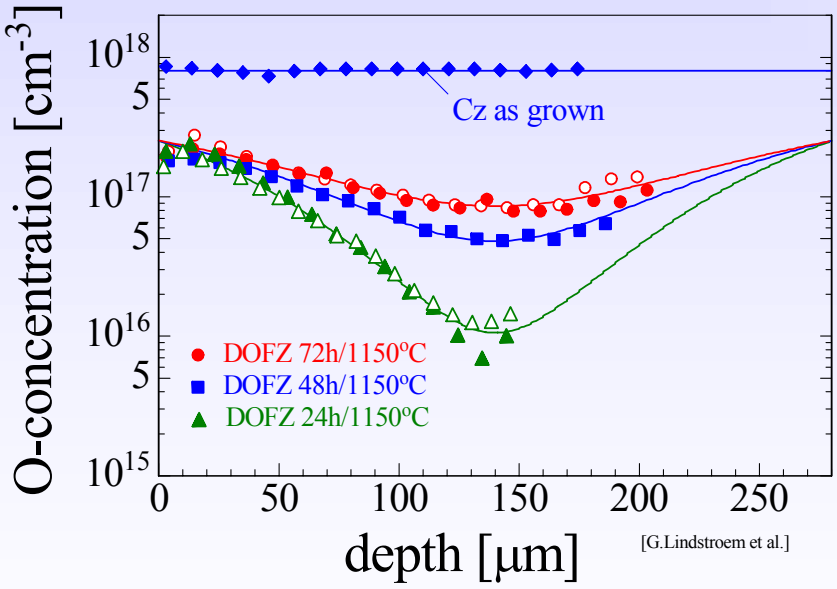

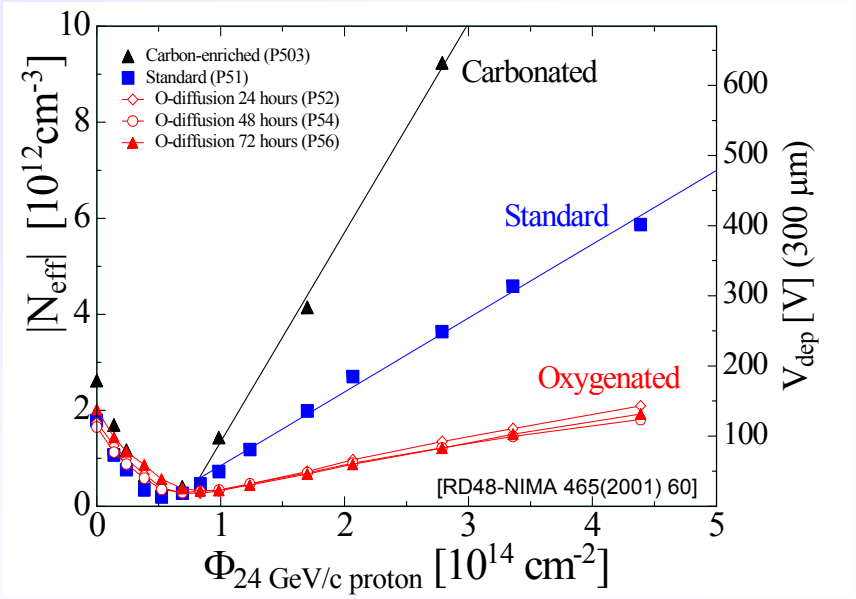

- 2005: DOFZ silicon used for the ATLAS and CMS Pixel detectors
- 2005: Other types of oxygen rich silicon under investigation: Czochralski Si, epitaxial Si

n-in-n vs p-in-n

extra slide not shown

n-type silicon after type inversion:

p⁺on-n

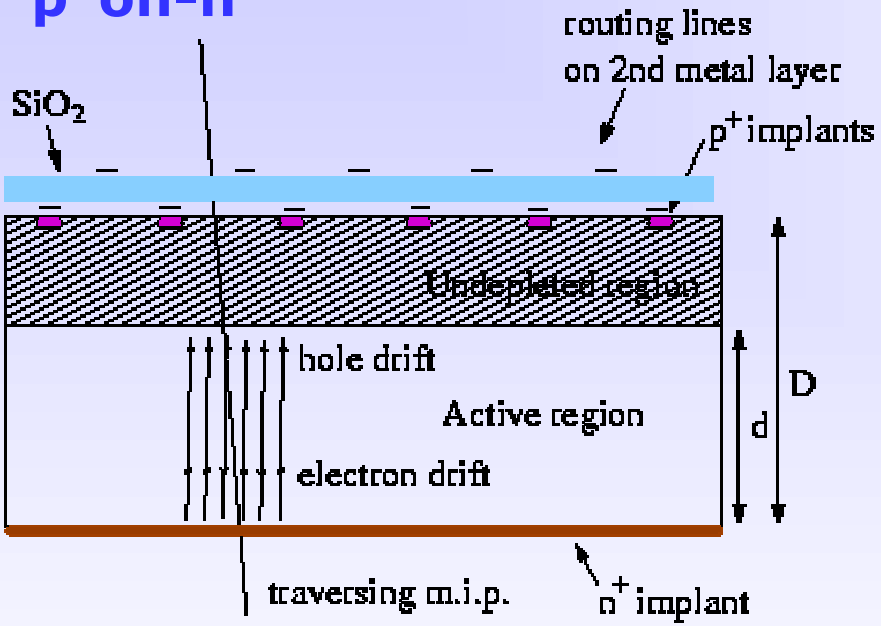

n⁺on-n

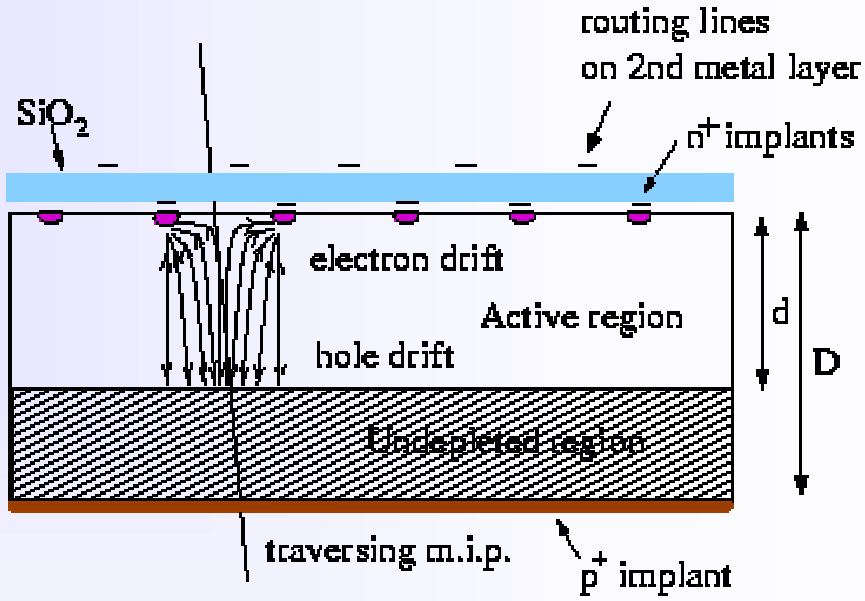

p-on-n silicon, under-depleted:

- Charge spread – degraded resolution
- Charge loss – reduced CCE

n-on-n silicon, under-depleted:

- Limited loss in CCE
- Less degradation with under-depletion
- Collect electrons (fast)

New detector concepts: 3D detectors

extra slide not shown

- **Electrodes:**
  - narrow columns along detector thickness-"3D"
  - diameter: ≈10μm; distance: 50 - 100μm

- **Lateral depletion:**
  - lower depletion voltage needed ($V_{dep} \sim d^2$)
  - radiation tolerant or thick detectors possible
  - fast signal (≈ 3.5 ns measured)

- **Processing of detectors:**
  - complex fabrication: Holes have to be made and filled with electrodes (DRIE etching, Laser drilling, Photo Electro Chemical etching); present aspect ratio (depth to diameter) ≈ 30:1
  - possibility to implement narrow dead regions at edges "edgeless detectors"

- **Application:**
  - detectors still under development!
  - option for LHC experiments upgrade ?

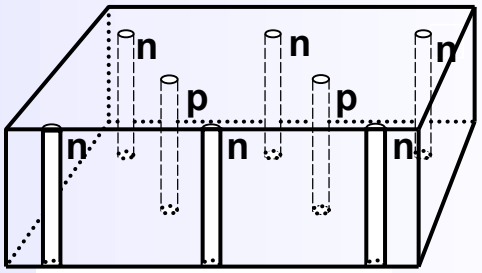

[Proposed: S.I. Parker et al., NIMA 395 (1997) 328]

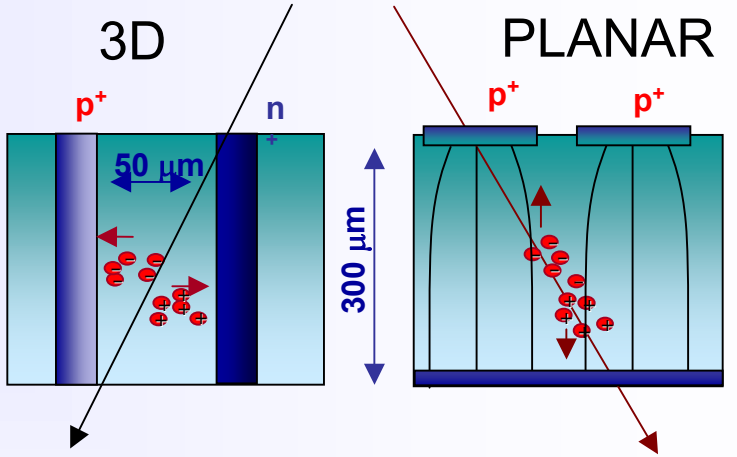

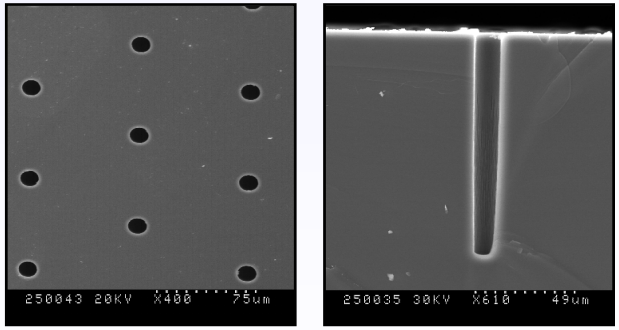

References and Acknowledgements

Besides references given on the transparencies, the following sources have been used:

Books

- **Gerhard Lutz, "Semiconductor Radiation Detectors", Springer, ISBN 3-540-64859-3**
- S.M.Sze, "Physics of Semiconductor Devices", John Wiley & Sons, ISBN 0-471-05661-8

Articles

- Anna Peisert, "Silicon microstrip detectors", Instrumentation in High Energy Physics, World Scientific, 1992
- Michael Moll, "Radiation Damage in Silicon Particle Detectors", PhD thesis, DESY, December 1999
- Geoffrey Hall, "Semiconductor particle tracking detectors", Rep.Prog.Phys. 57 (1994) 481-531

Lectures and Presentations

- **Alan Honma, "Silicon Detectors", Nato Advanced Study Institute, Virgin Islands, 06/2002,** http://cern.ch/honma/
- **Christian Joram, "Particle Detectors", CERN, Summer Student Lectures June 2003**
- Paula Collins, "Recent Detector R&D and operational experience", IWORID07, Riga, September 2003
- Gerhard Lutz, "Semiconductor Radiation Detectors", Louvain, Seminar, June 2002
- Marcello Mannelli, "Tracking at the LHC: The CMS example", CERN Academic Training, March 2005
- Pierre Jarron, "Microelectronics, Nanoelectronics, Monolithic Pixel Detectors" CERN Academic Training, Jan. 2004
- Hans Dijkstra, "Overview of Silicon Detectors", Vienna conference, VCI 2001
- Volker Adler, "The TESLA Vertex Detector" ZEUS Student Seminar, Jan.2004
- Daniela Bortoletto, "An introduction to semiconductor detectors", Vienna conference, VCI 2004
- A list of conferences about Solid State Detectors and Radiation Damage: http://cern.ch/mmoll/links/conferences.htm
- Vertex 2004 conference: http://sucimaweb.dipscfm.uninsubria.it/vertex04/

A short Overview on Scintillators

By C. D'Ambrosio (CERN)

Geneva, 13 April 2005

Outline

Lecture 1 - Introduction C. Joram, L. Ropelewski

Lecture 2 - Tracking Detectors L. Ropelewski, M. Moll

Lecture 3 - Scintillation and Photodetection C. D'Ambrosio, T. Gys

3a A short overview on scintillators (a personal cut)

- **What are scintillators**
- **Inorganic scintillators**
  - **Main properties**
  - **Applications**
- **Organic scintillators**
  - **Scintillation mechanisms**
  - **Plastic scintillators and their readout**
  - **Scintillating plastic fibres**

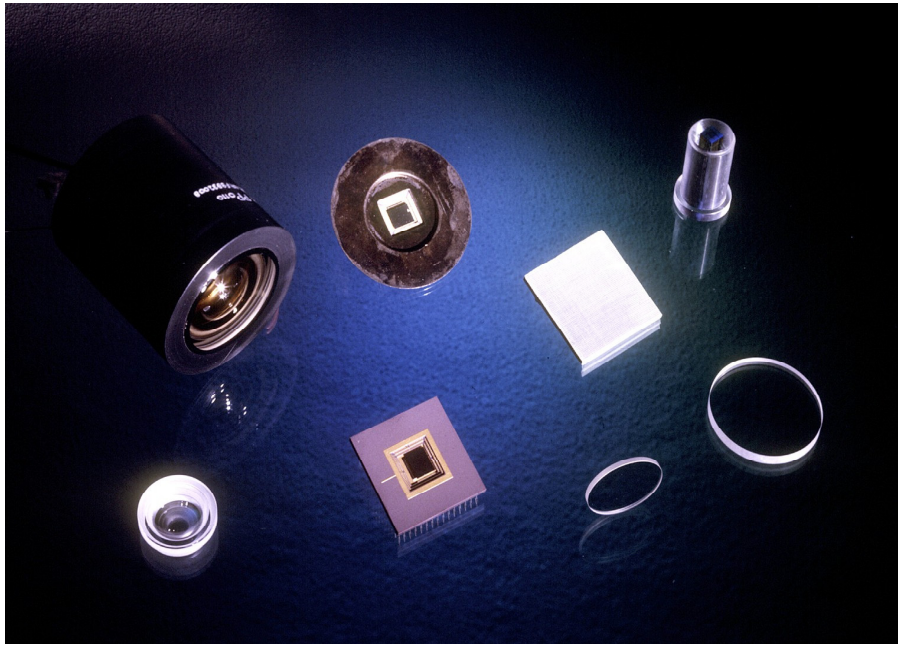

3b Photodetectors

Lecture 4 - Calorimetry, Particle ID C. Joram

Lecture 5 - Particle ID, Detector Systems C. Joram, C. D'Ambrosio

Introduction to Scintillators

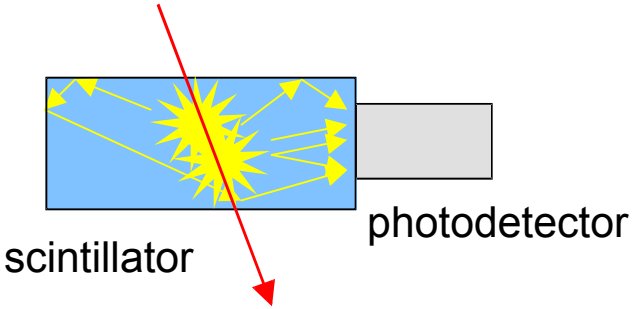

Energy deposition by a ionizing particle

→generation
→transmission
→detection
} of scintillation light

Two categories: Inorganic and organic scintillators

Inorganic
(crystalline structure)

Up to 40000 photons per MeV
High Z
Large variety of Z and ρ
Undoped and doped
ns to μs decay times
Expensive

E.m. calorimetry (e, γ)
Medical imaging
Fairly Rad. Hard (100 kGy/year)

Organic
(plastics or liquid solutions)

Up to 10000 photons per MeV
Low Z
ρ~1gr/cm^3
Doped, large choice of emission wavelength
ns decay times
Relatively inexpensive

Tracking, TOF, trigger, veto counters,
sampling calorimeters.
Medium Rad. Hard (10 kGy/year)

Inorganic Scintillators

- Basic scintillation mechanisms in crystals and liquefied noble gases
- Temperature dependence of scintillation yield
- Photon absorption processes in crystals
- Table of common scintillators properties
- Applications:
  - X-ray and Gamma Spectroscopy
  - Imaging

Basic crystal scintillation mechanism

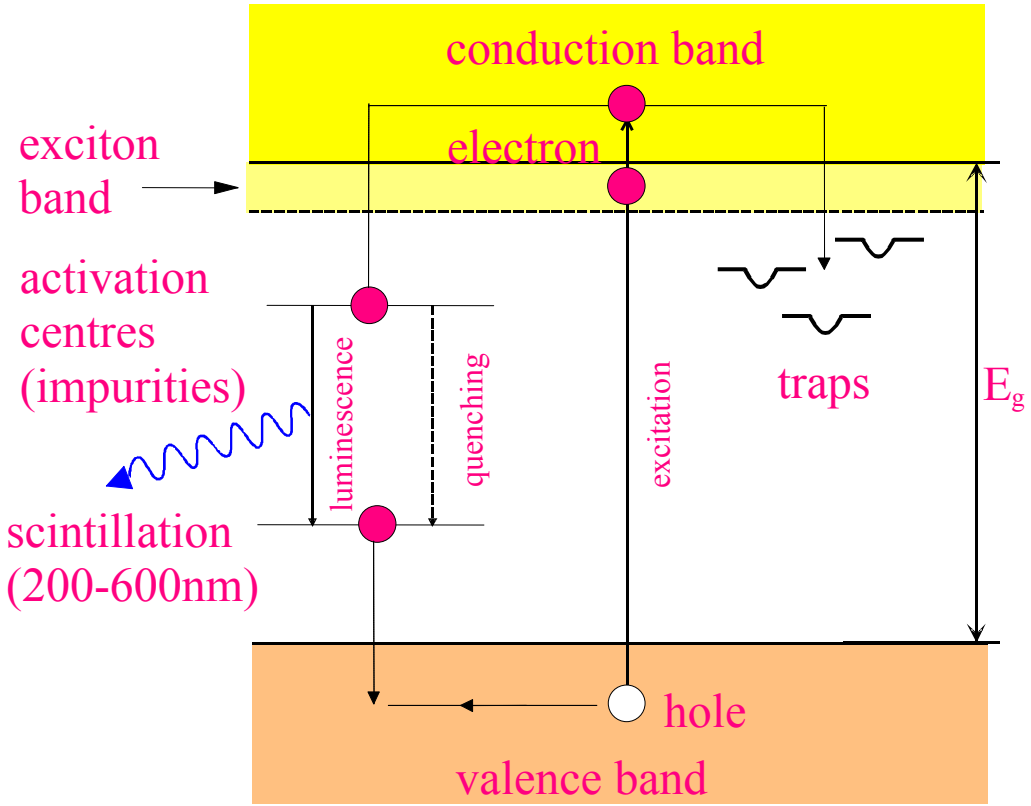

Warning, sometimes ≥ 2 time constants:

- fast recombination (ns-μs) from activation centers
- delayed recombination due to trapping (μs-ms)

•full control of growth, doping and impurities is imperative to optimize light yield, transmission and decay time

Liquefied noble gases

Liquefied noble gases: LAr, LXe, LKr

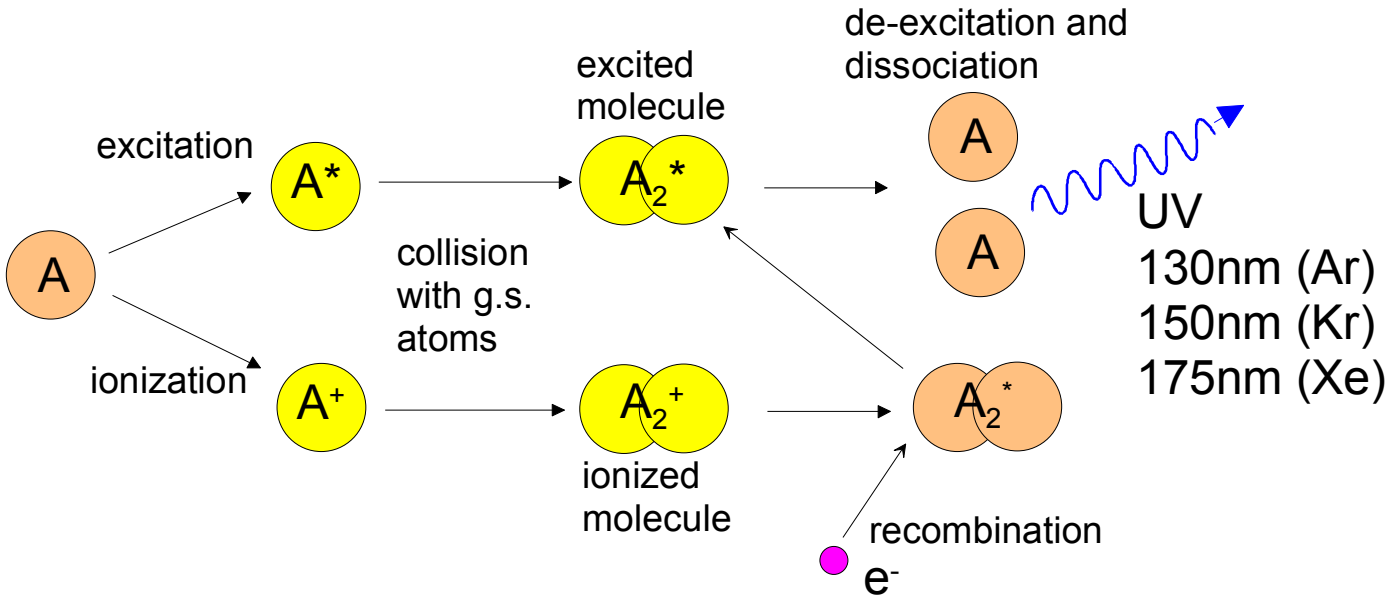

Also here one finds 2 time constants: from a few ns to 1 μs.

Crystals

Light output of crystals depends on temperature

(From Bicron catalogue)

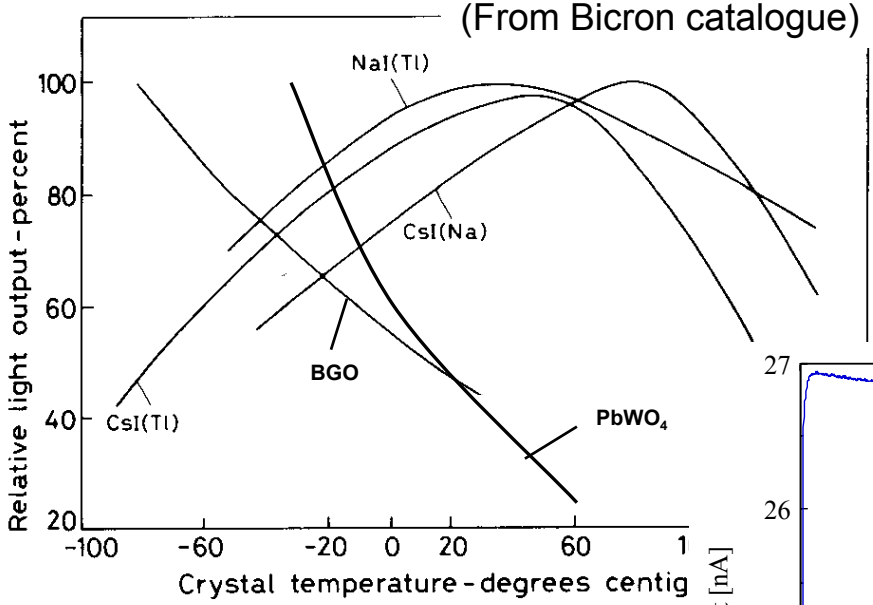

Low dose irradiation of an old $PbWO_4$ crystal and check of the temperature dependence of its light yield (1996). The blue curve is the photocurrent generated by the irradiation and the red curve is the temperature of the sample.

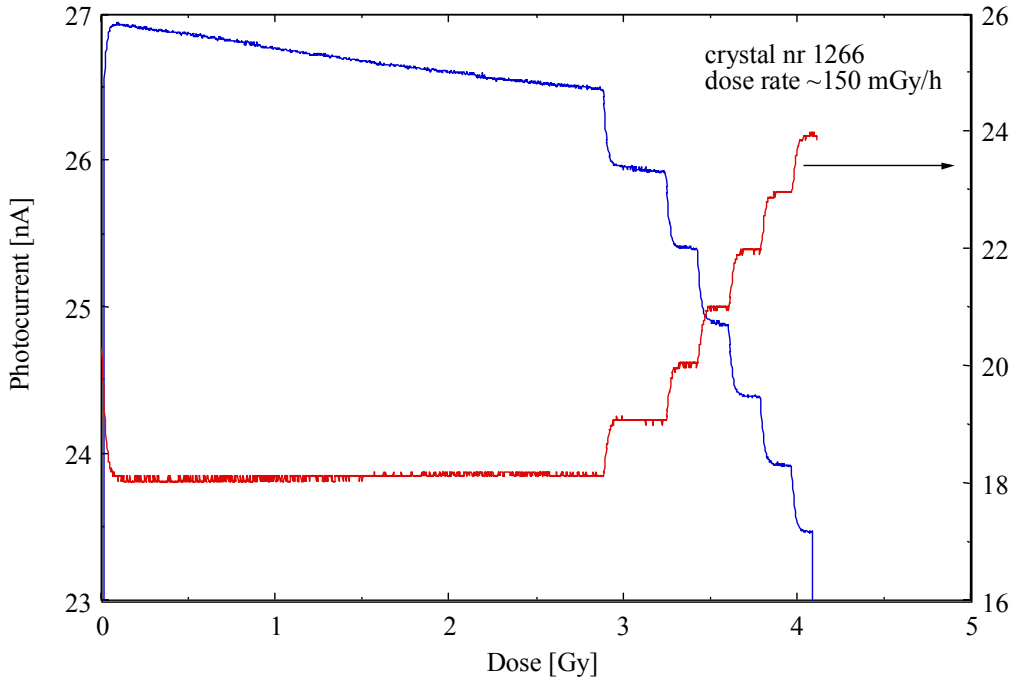

The $PbWO_4$ crystal is used in CMS ECAL and its ~2% light yield decrease per °C asks for temp. control and monitoring

Photon absorption in crystals

The intensity I of a gamma beam traversing a target of thickness d is

$$I = I_0 e^{-\mu d}$$

Where μ is the sum of three processes taking place in the material:

Photoel. Abs. → Z^4 to Z^5 → $E^{-3.5}$ to E^{-1}

Compton scatt. → Z → E^{-1}

Pair production → Z^2 → ln E

(curve will extend to higher energies, see Christian's talk)

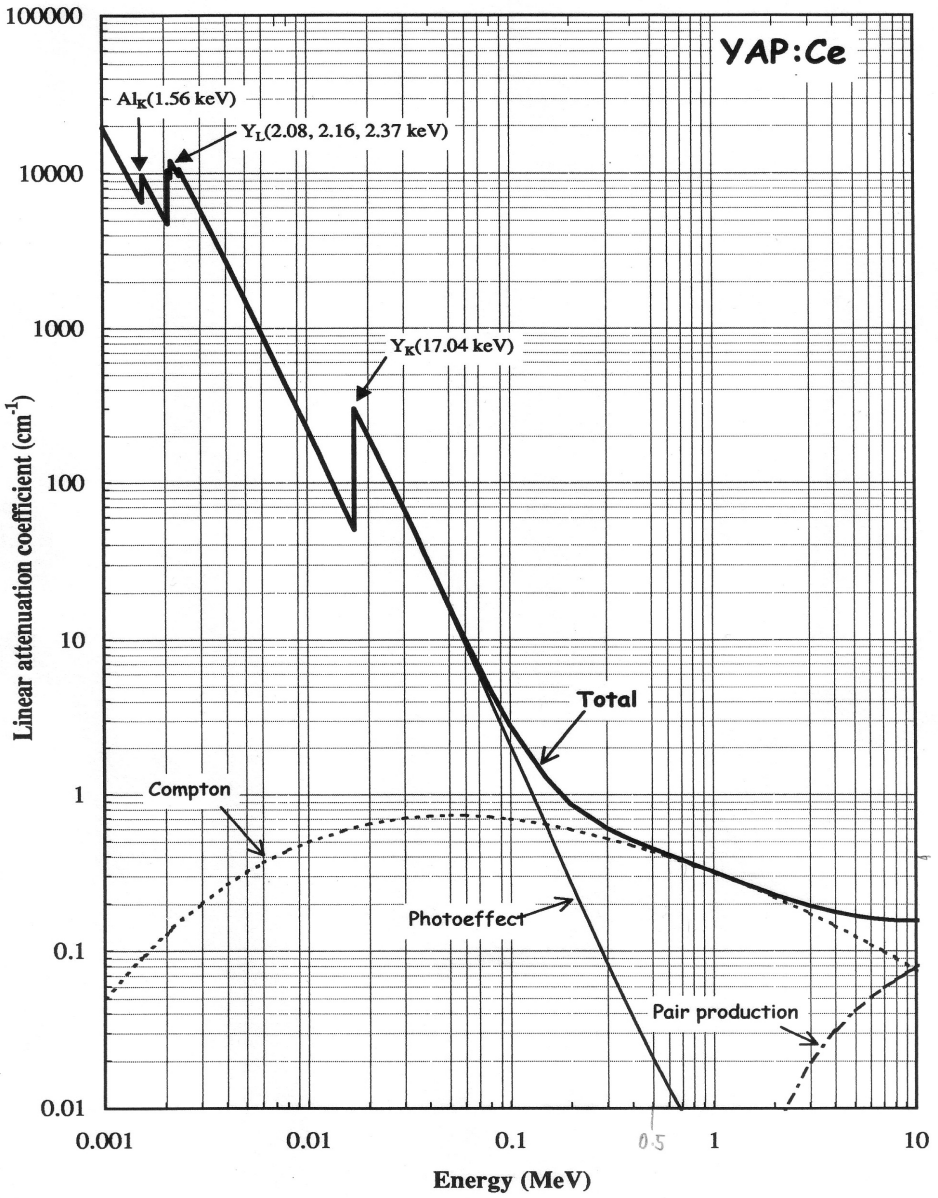

Properties of some crystal scintillators

Scintillator composition	Density (g/cm^3)	Index of refraction	Wavelength of max.Em. (nm)	Decay time Constant (μs)	Scinti Pulse height[1)]	Notes
NaI(Tl)	3.67	1.9	410	0.25	100	2)
CsI	4.51	1.8	310	0.01	6	3)
CsI(Tl)	4.51	1.8	565	1.0	45	3)
CaF_2(Eu)	3.19	1.4	435	0.9	50	
BaF_2	4.88	1.5	190/220 310	0,0006 0.63	5 15	
BGO	7.13	2.2	480	0.30	10	
$CdW0_4$	7.90	2.3	540	5.0	40	
$PbWO_4$	8.28	2.1	440	0.020	0.1	
CeF_3	6.16	1.7	300 340	0.005 0.020	5	
GSO	6.71	1.9	430	0.060	40	
LSO	7	1.8	420	0.040	75	
YAP	5.50	1.9	370	0.030	70	

1) Relative to NaI(Tl) in %; 2) Hygroscopic; 3) Water soluble

Most common applications of inorganic scintillators

- Calorimetry (for HEP, see Christian's lecture)
- X-ray and gamma spectroscopy
- Imaging
  - Positron Emission Tomography (PET) in medical imaging
  - Gamma Imaging (Anger camera) (see Thierry's talk)
- Monitoring in nuclear plants
- Oil wells, Mining, etc.

X-ray and gamma spectroscopy

The simple set-up:

each detected gamma provides an amplitude signal, which fills a pulse-height spectrum.

We can monitor radiation, study atomic or nuclear spectra, research and characterize new crystals, test new photo-detectors, produce special probes, etc..

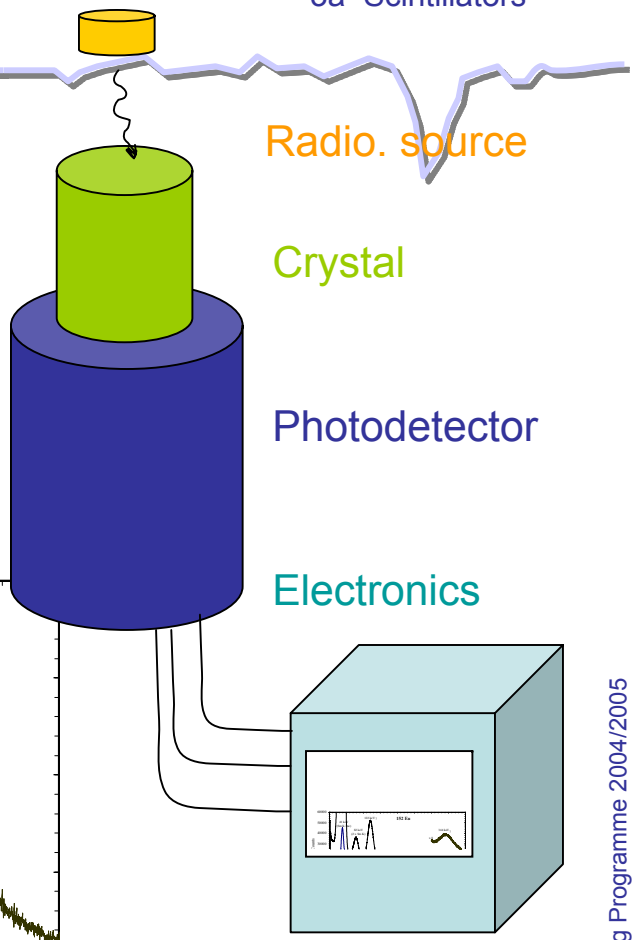

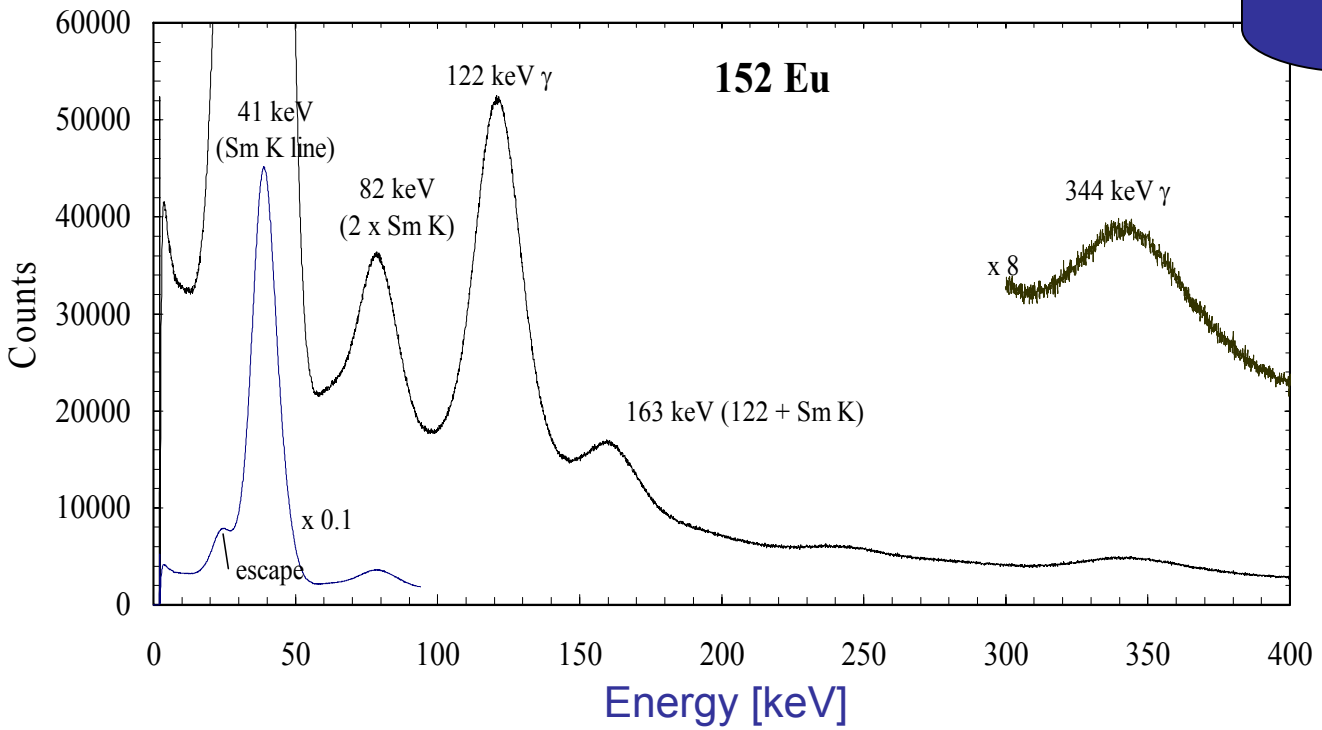

Irradiation of a YAP(Ce) crystal by ^{152}Eu on a HPD

Positron Emission Tomography (PET)

http://www.medical.philips.com/main/products/pet/products/gemini/clinicalimages/10/index.asp

http://www.triumf.ca/welcome/petscan.html

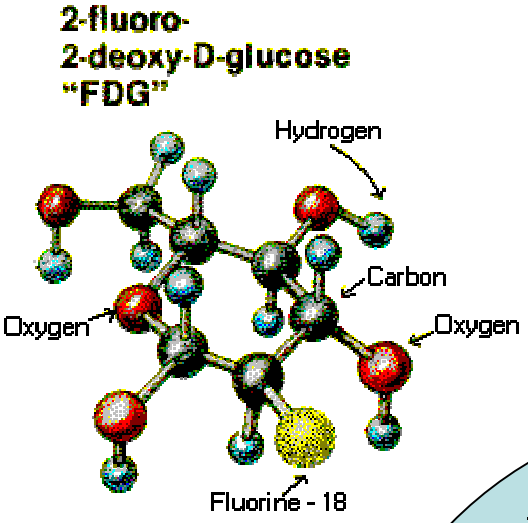

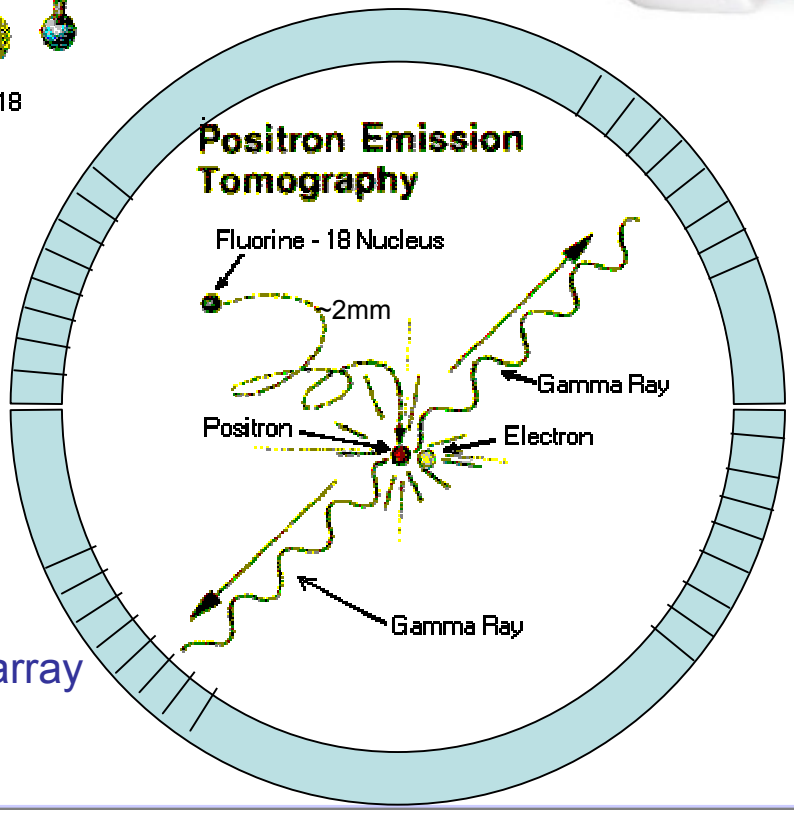

NOT TO SCALE!!

Crystals array

2 x 511 keV energy

γ-γ co-linearity

time coincidence

reconstruct functional image

CERN Academic Training Programme 2004/2005

PET images to be found on the web

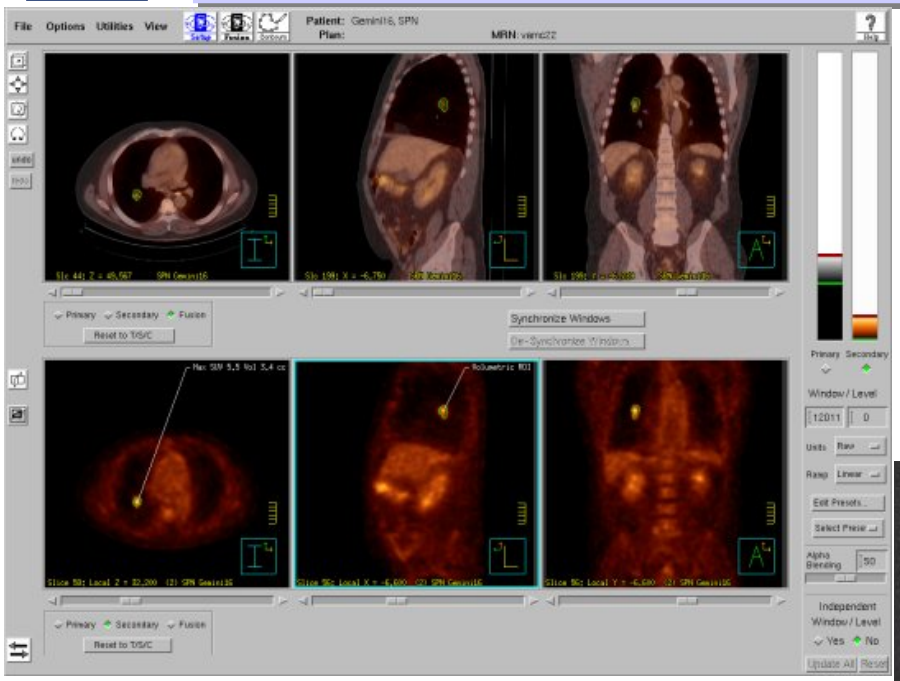

http://www.medical.philips.com/main/products/pet/products/gemini/clinicalimages

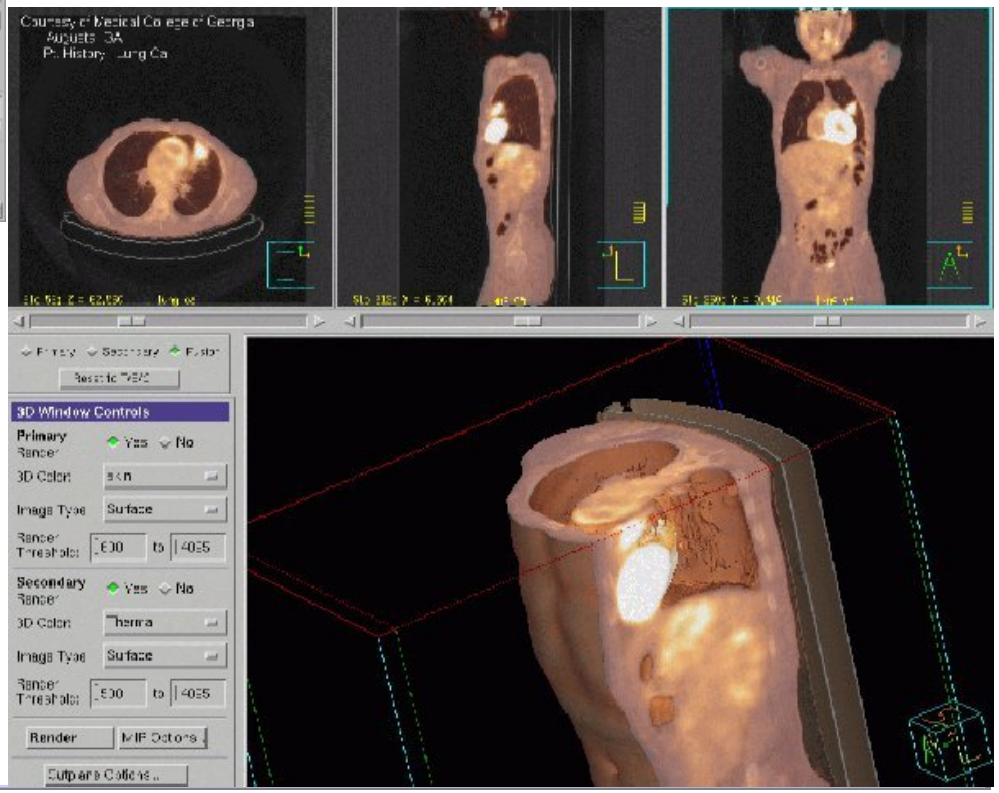

Main R&D on inorganic scintillators

- Higher densities for higher Z (improve photoabsorption)
- High light yield (NaI(Tl) light yield still unchallenged)
- Short decay time (improve time resolution)
- Improve light coupling with photon detector
- More radiation hard
- Inexpensive, “easy” to manufacture, reproducible
- Large size, easy handling and “machinable”

Organic Scintillators

- Basic scintillation mechanisms in organic scintillators
- Förster energy transfer and self absorption
- One dopant and two dopants scintillators
- Readout of scintillators
- Applications of organic scintillators
- Example: small diameter scintillating fibres and their readout

Liquid and plastic scintillators

They usually consist of a solvent + scintillator and a secondary fluor as wavelength shifters.

A traversing ionizing particle releases energy in the solvent. Then, energy flows radiationless* to the scintillator. Finally, light emitted by the scintillator is absorbed (radiative transfer**) and re-emitted at longer wavelength by the secondary fluor.

Ex. energy states in the solvent

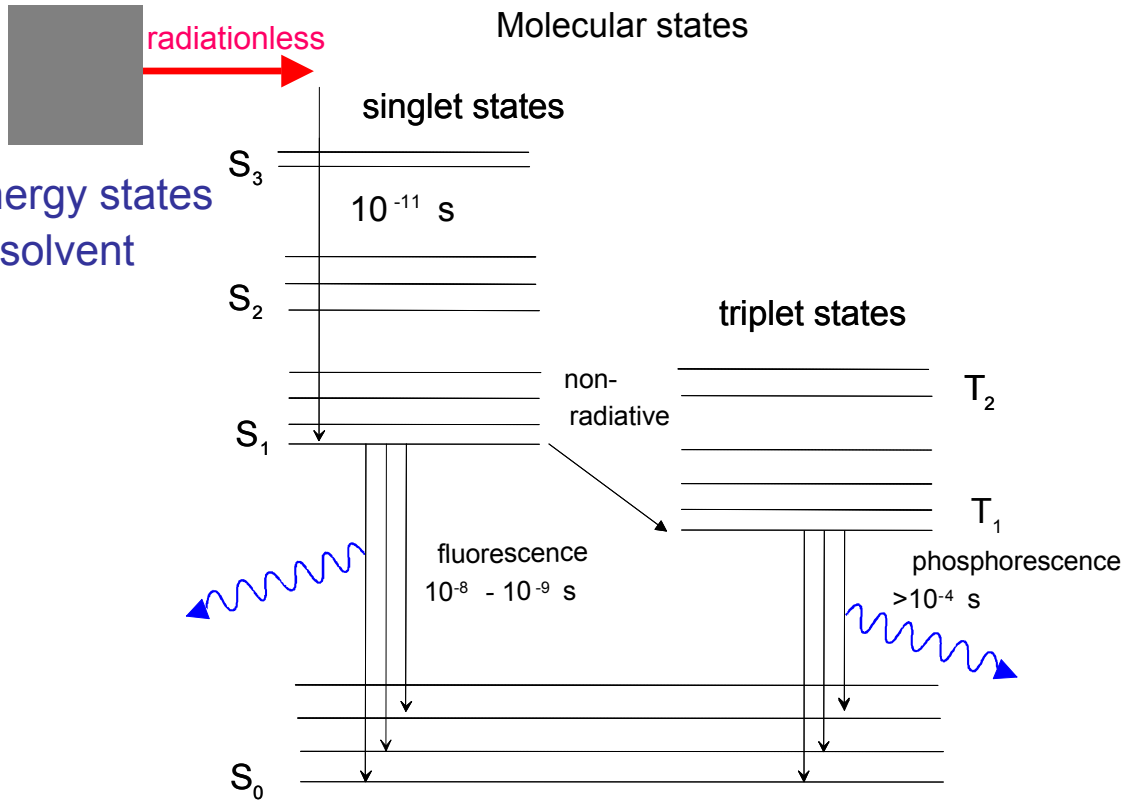

A fluor has its absorption and emission spectra shifted. The two peaks difference is called Stokes shift

*fast and local energy transfer via non-radiative dipole-dipole interactions (Förster transfer).

**~$1/R^2$ light attenuation

The Förster transfer

Efficient Förster transfer asks for high concentrations of scintillator:

$$k_{D\to A} \propto \frac{1}{\tau_D R_{DA}^6} \int \frac{f_D(\nu)\varepsilon_A(\nu)}{\nu^4} d\nu$$

where the integral is the overlap between Acceptor abs. and Donor emission spectra and R is the D-A distance

But…

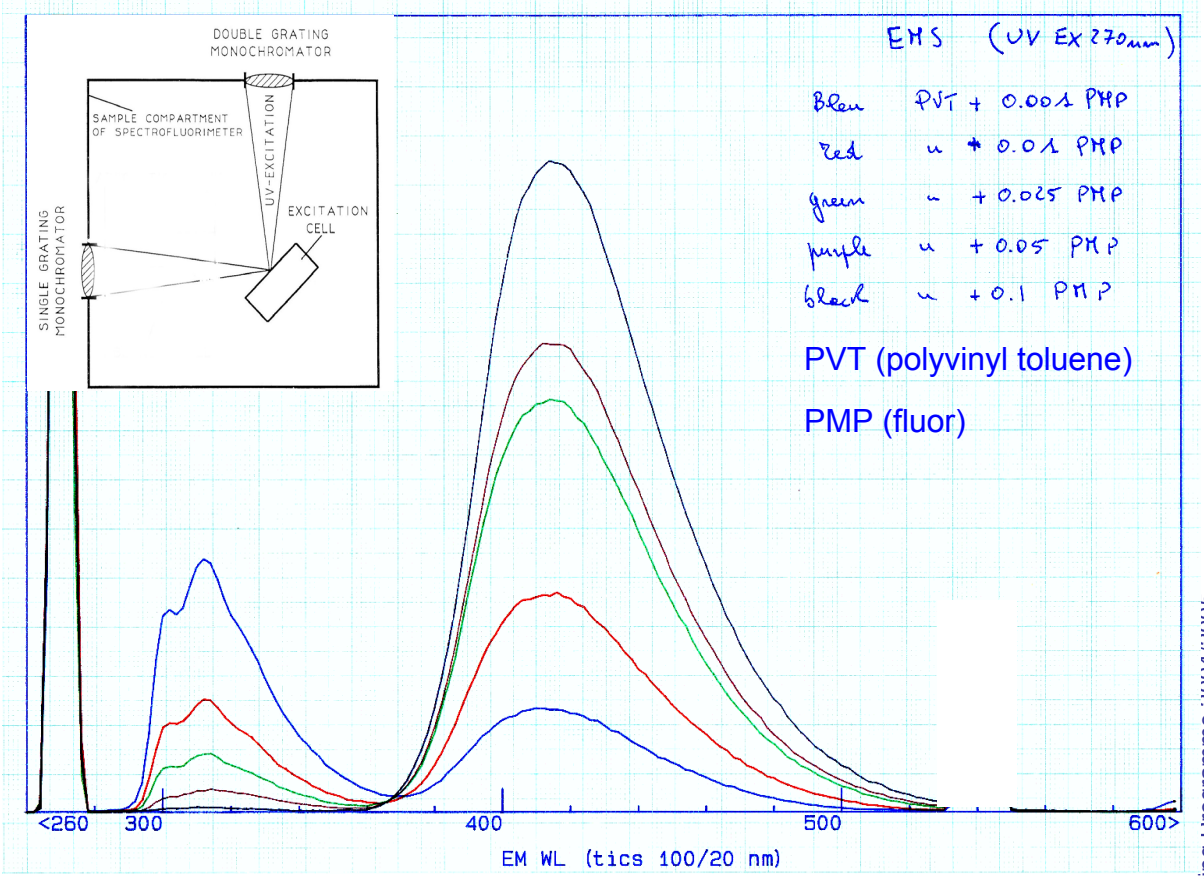

Self-absorption increases with doping concentration, that is smaller light yields and shorter attenuation lengths:

Therefore, add a low concentration wavelenght shifter (2 dop. Scheme) **or**

Find large Stokes shift dopants (1 dop. Scheme, ex. 3hf, pmp)

Two / One Dopant scheme

Abs. and emission spectra

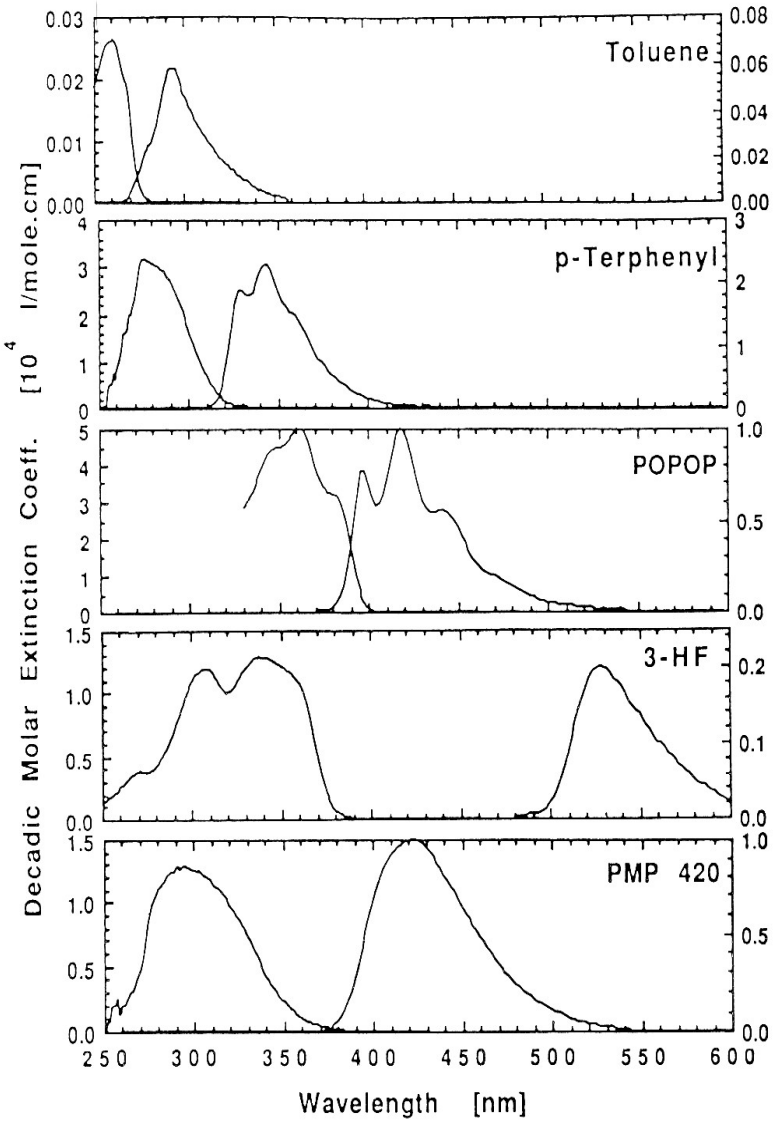

solvent + scintillator + wave shifter

Förster Radiative

Förster

solvent + large stokes shift scintillator

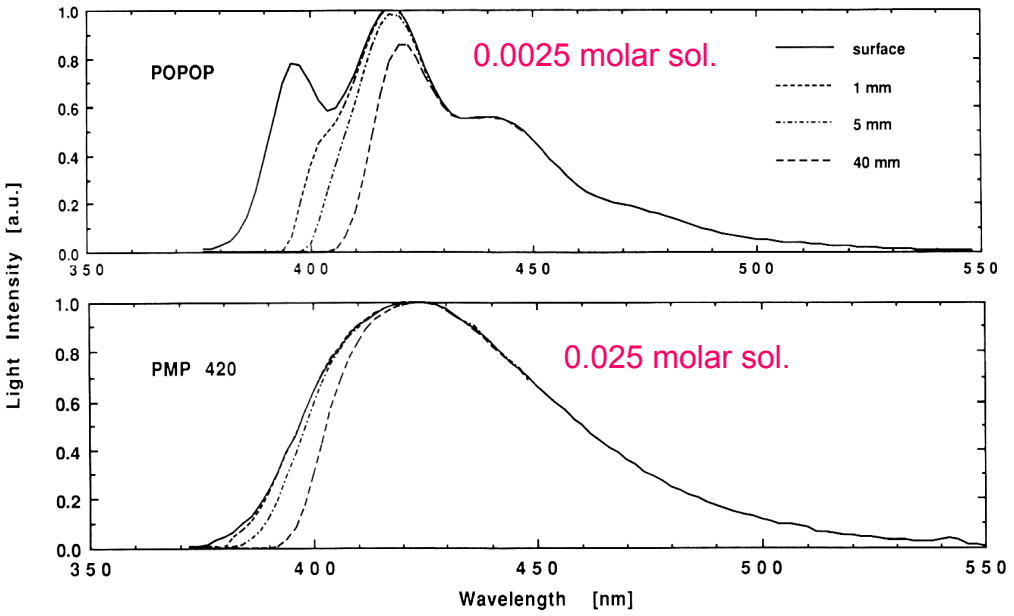

Dopants in toluene: large Stokes shift dopants feature a much smaller self-absorption

Application of the two types of doping

The two dopants scheme is the most common: it is applied to all plastic scintillators, down to ~1mm fibres.

The one dopant scheme is needed to keep the light emission local (only Förster transfer) as it is the case for small diameter fibres

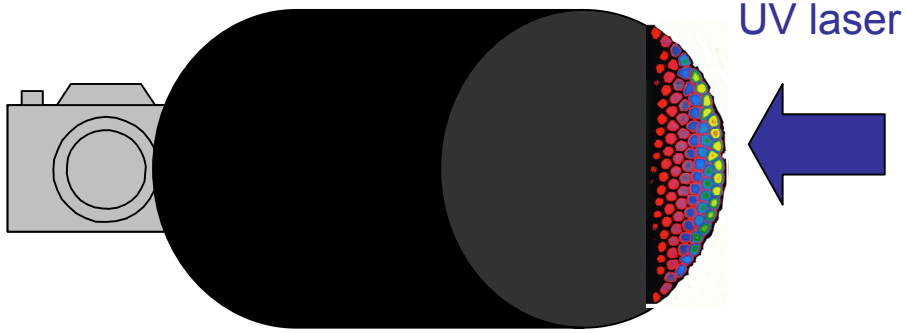

Plastic microfibres bundle
(30 μm dia.)

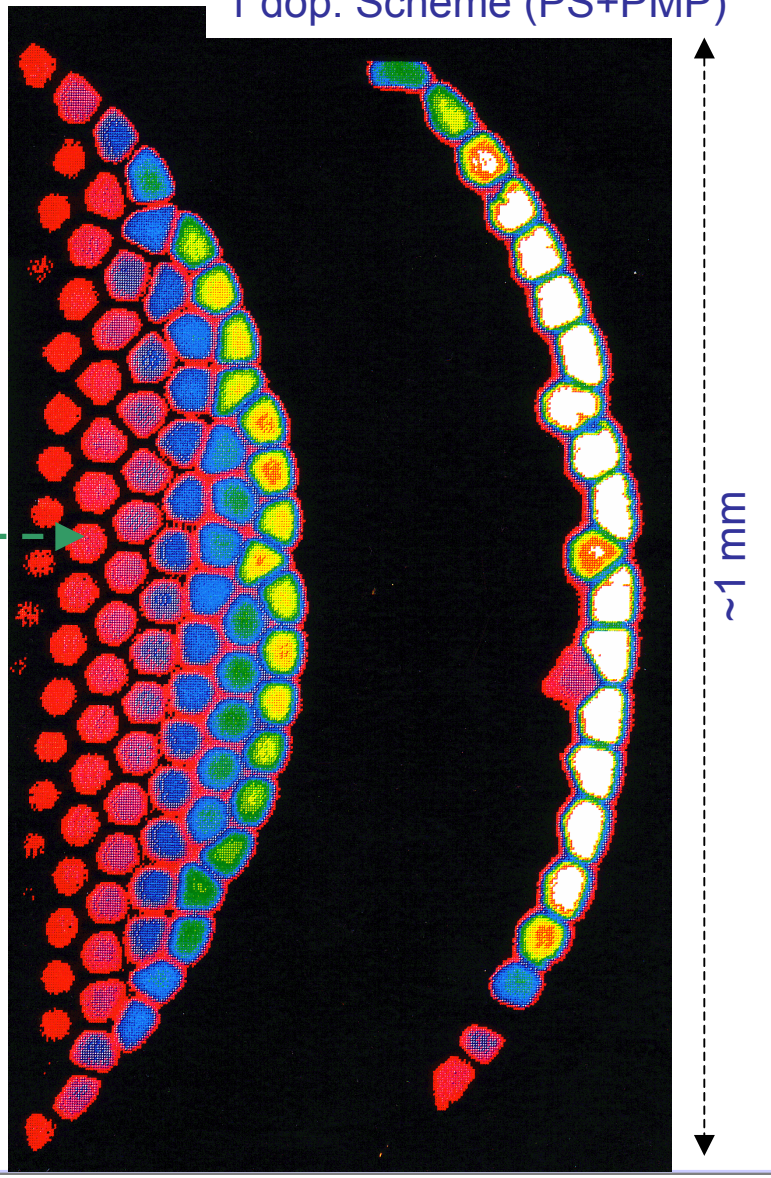

Scintillators readout

Readout has to be adapted to geometry, granularity and emission spectrum of scintillator.

Geometrical adaptation:

- Light guides: transfer by total internal reflection (+outer reflector)

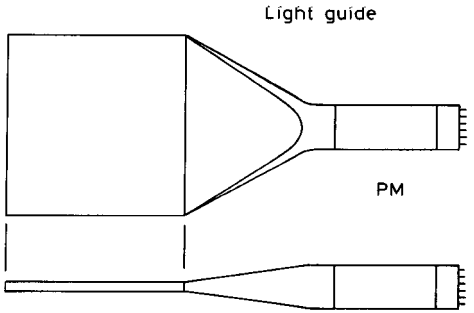

"fish tail"

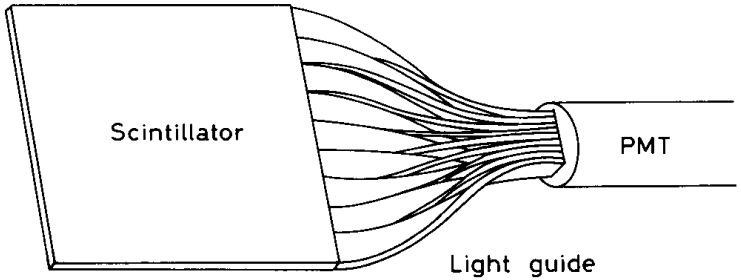

adiabatic

- wavelength shifter (WLS) bars

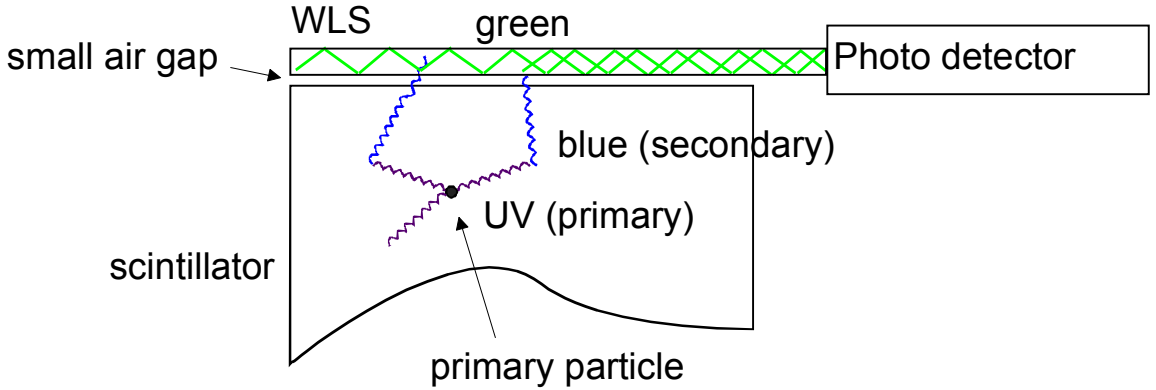

ATLAS Hadron Calorimeter

Scintillating tile readout via fibers and photomultipliers

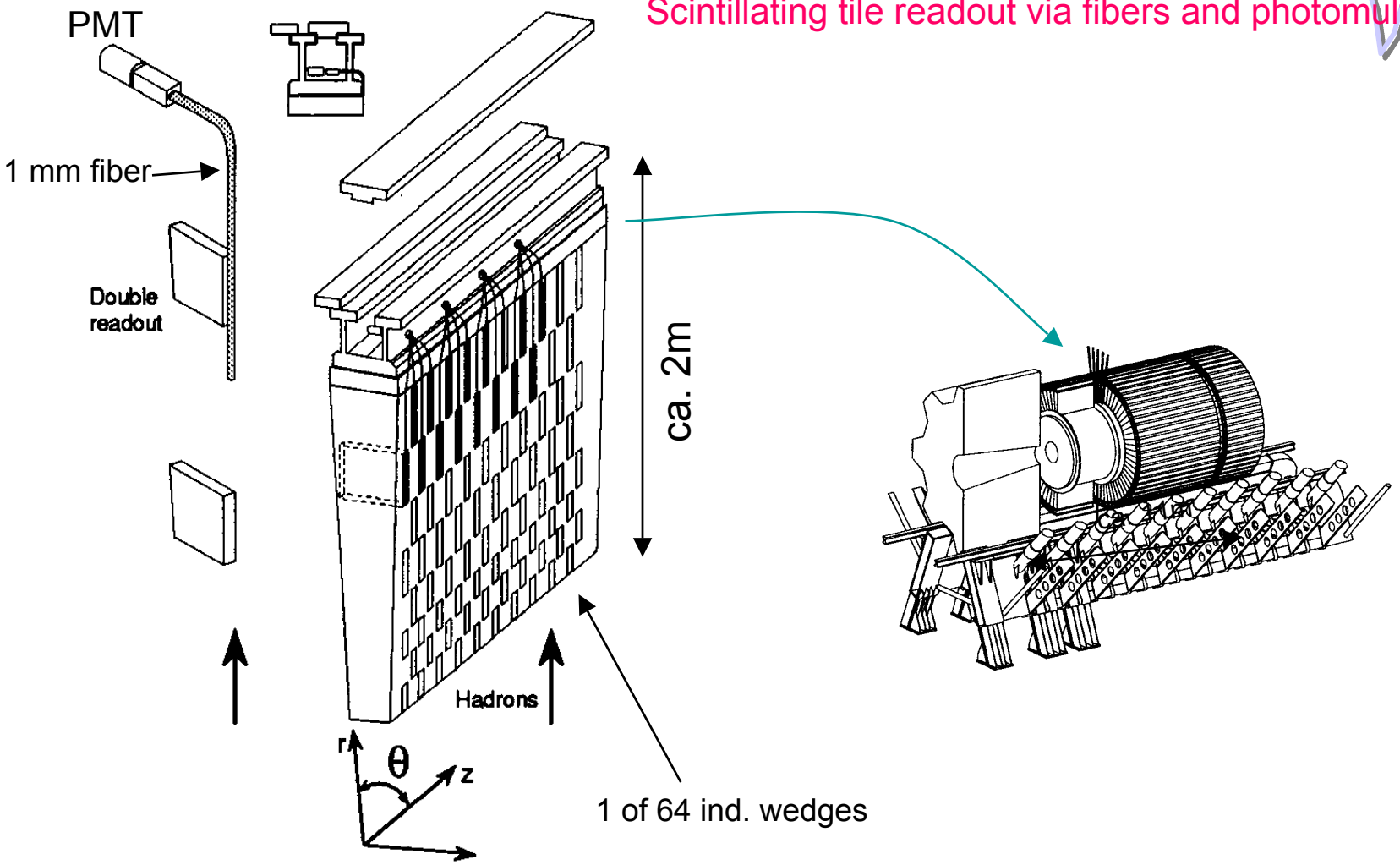

Periodical arrangement of scintillator tiles (3 mm thick) in a steel absorber structure

(ATLAS TDR)

Most common applications of organic scintillators

Large volume liquid or solid detectors (in form of tiles): underground experiments, sampling calorimeters (HCAL in CMS or ATLAS, etc.), counters, light guides.

High precision, small volume active targets and fibre tracking (UA2, D0, CHORUS).

As an example, a scintillating plastic fibre working principle:

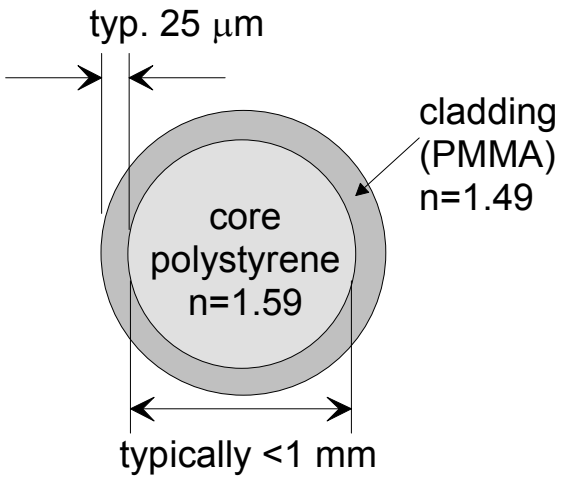

light transport by total internal reflection

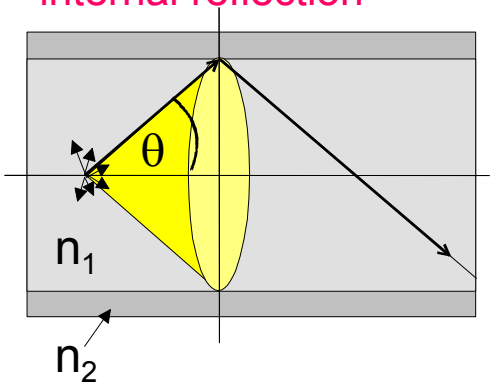

Double cladding system
(developed by RD7)

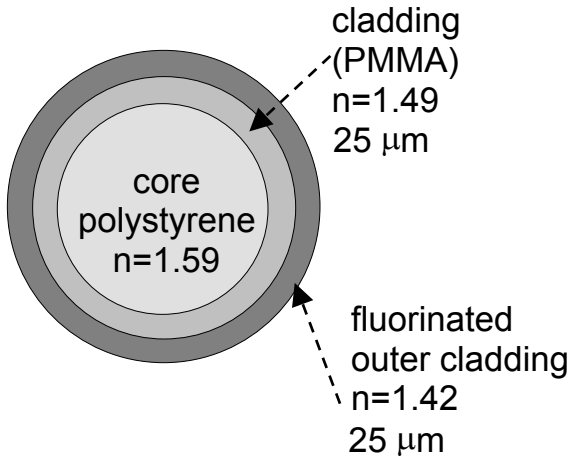

$$\frac{d\Omega}{4\pi} = 0.5\,(1-\cos^2\theta) = 3\%$$

$$\theta \le \arccos\frac{n_2}{n_1} \approx 69.6^\circ$$

$$\frac{d\Omega}{4\pi} = 0.5\,(1-\cos^2\theta) \approx 5.3\%$$

Small diameter scintillating fibres

Developed in RD7, they consist of bundles of hexagonal fibres (typ. 60 μm dia., 2.5 mm bundle size)

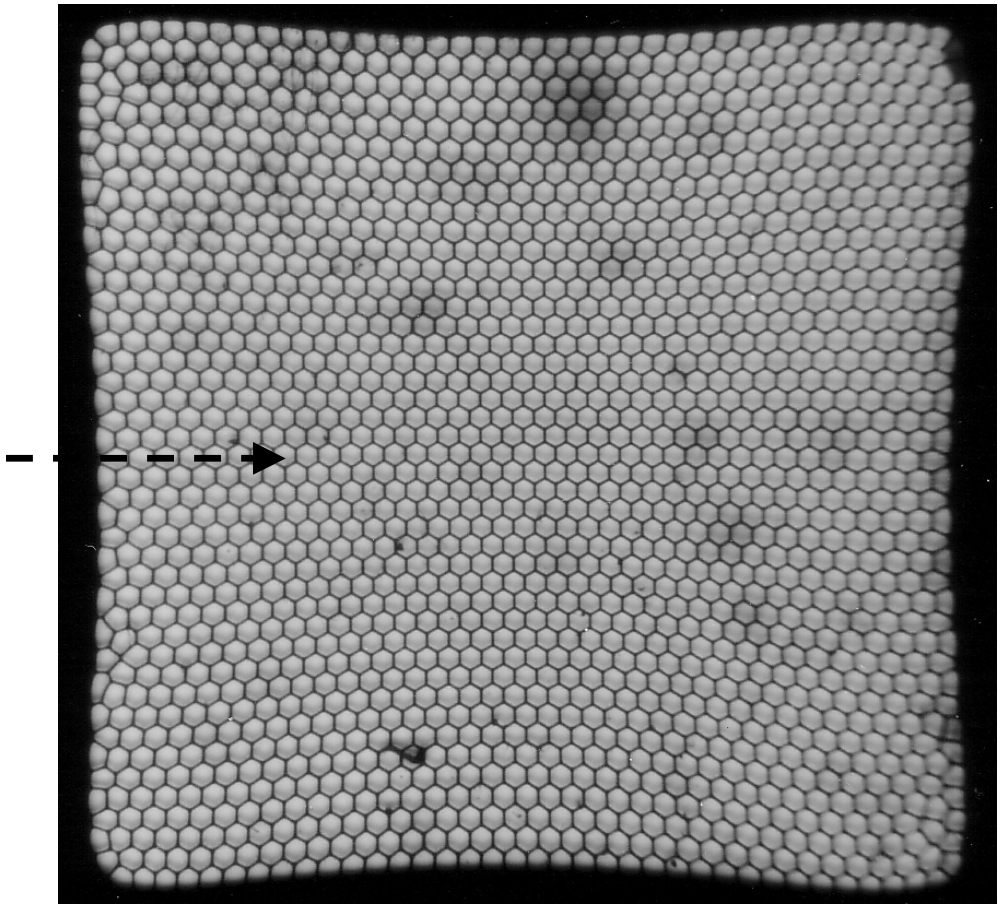

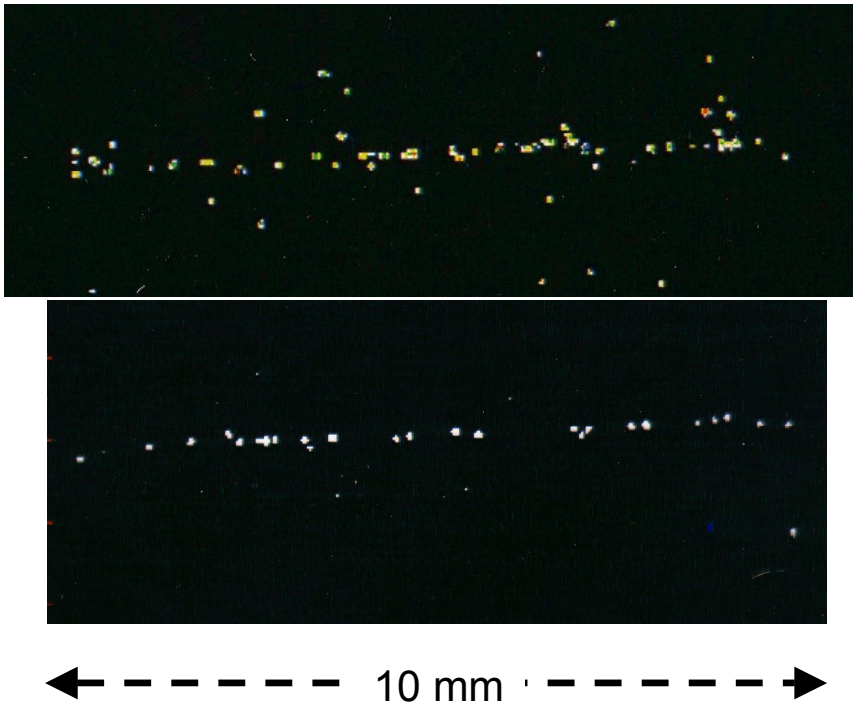

Images of tracks from 5 GeV/c pions (1989)

Beautiful tracks with only **2.2% of X_0 and >20 hits**, but…

Small diameter scintillating fibres readout

The readout of fibres is a key point for the whole system

Active target in WA84 (1989)

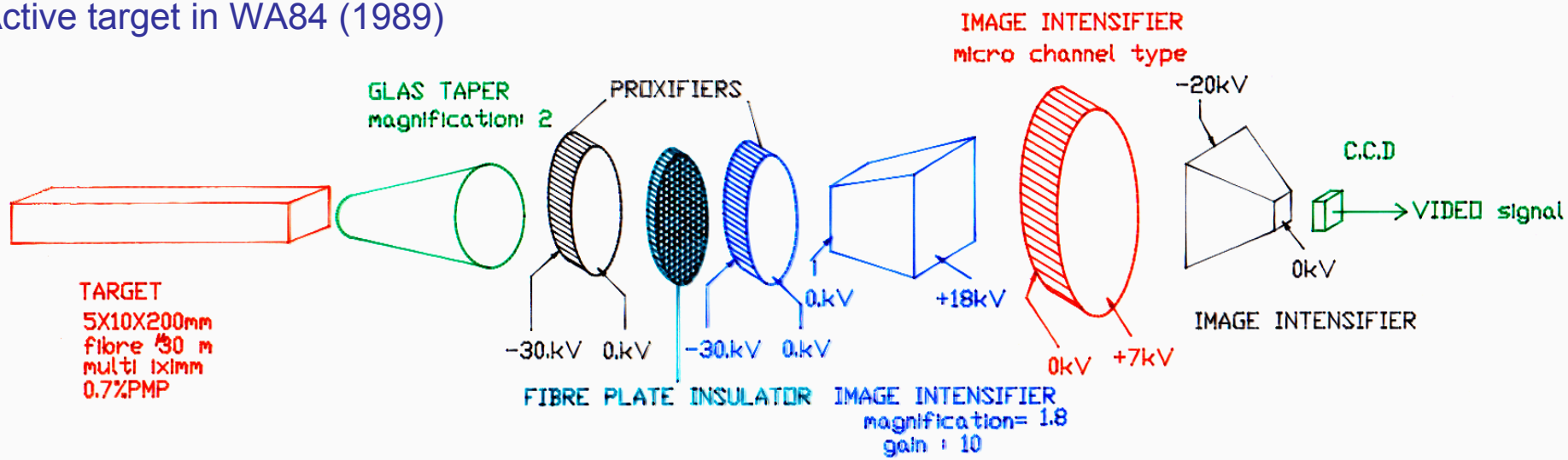

For a tracker, the readout has to match the high granularity of the fibres and bunch crossing time, but stay in the experiment's budget, size, etc.**: a real challenge.**

The ISPA tube was especially developed for this (see Thierry's talk)

Radiation Hardness in Plastic

500 kGy irradiation of SCSN81T and SCSN38 from Kuraray

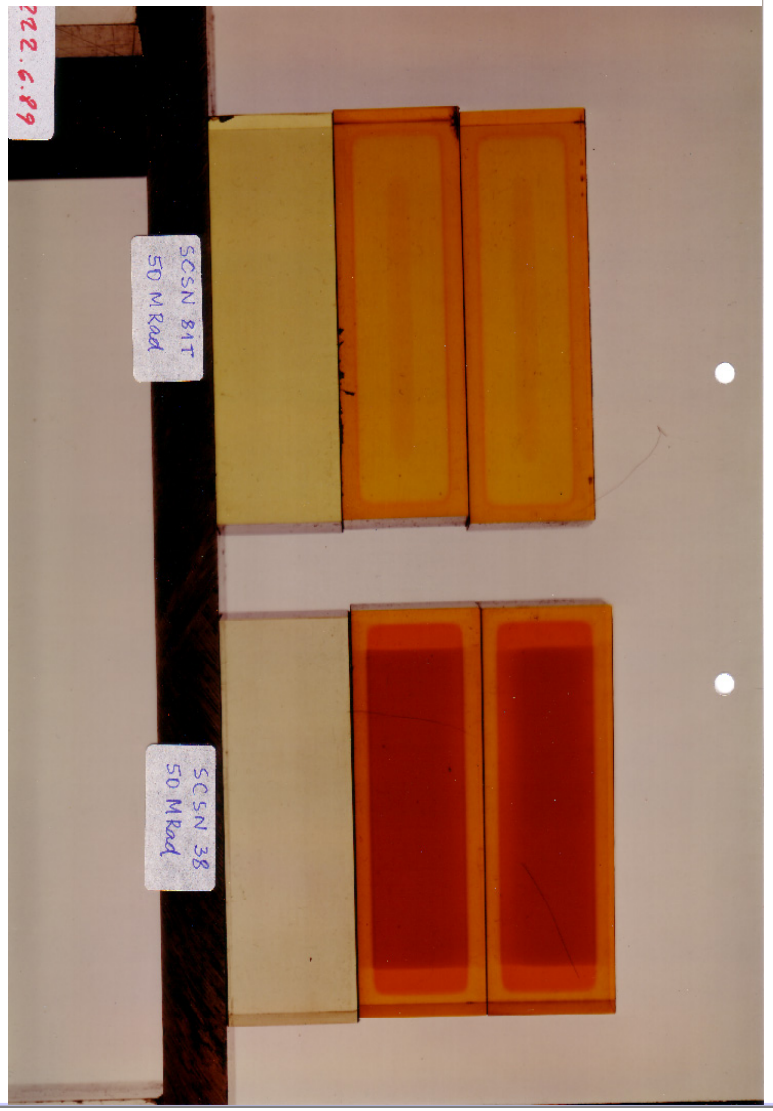

and after 3 weeks recovery in an oxygen-rich atmosphere

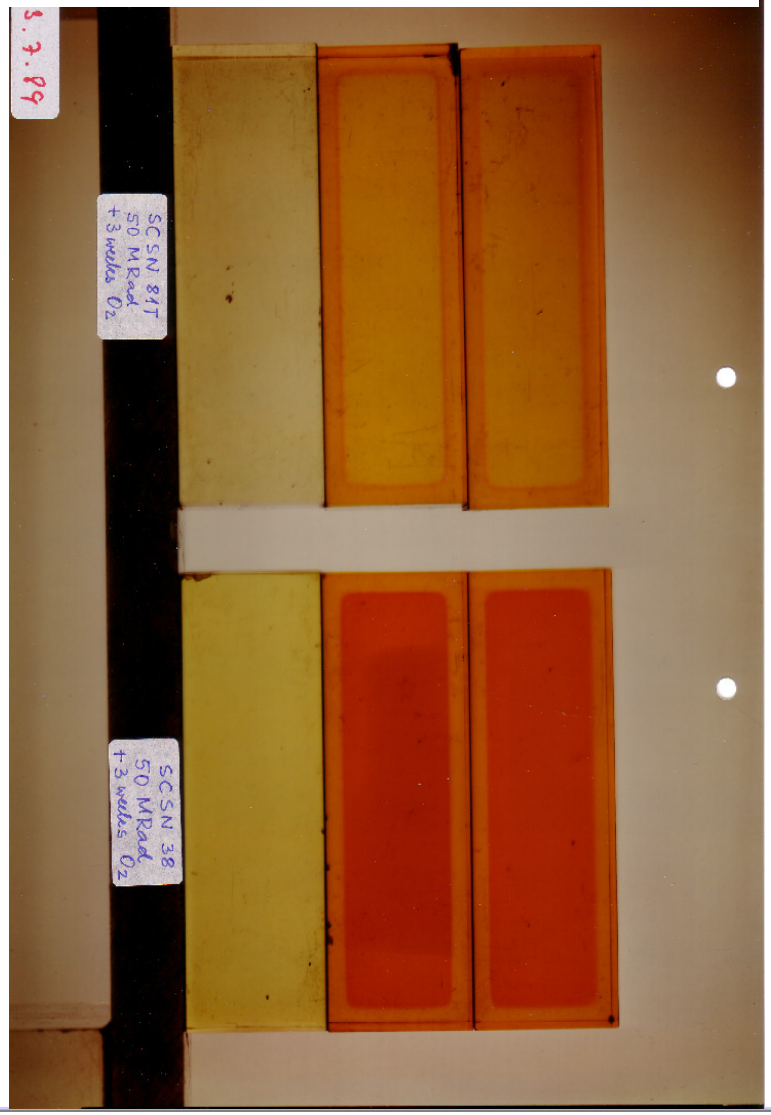

R&D on organic scintillators

- New dopants with better light yield and larger Stokes shift
- High granularity readout of fibres
- Larger attenuation lengths in plastic fibres
- New radiation hard plastics to stand 100 kGy/year dose

References

- Crismatec, "*Catalogue of Scintillation Detectors*", Saint-Gobain (1992);
- G. F. Knoll, "*Radiation detection and measurement*" ; 3rd ed., New York, Wiley, 2000;
- C. D'Ambrosio et al., "Low dose-rate irradiation set-up for scintillating crystals", NIM A, V. 388,1-2, (1997);
- C. D'Ambrosio et al., "A HPMT based set-up to characterize scintillating crystals",NIM A, V. 434, 2-3, (1999);
- M. Moszynski, "Inorganic scintillation detectors in γ-ray spectrometry", NIM A, V.505, 1-2, (2003);

- J. B. Birks, "*Scintillation counters*", Pergamon Press, (1954) London;
- I. B. Berlmann, "*Handbook of fluorescence spectra of aromatic molecules*" ; 2nd ed., Academic Press, (1971) New York
- H. Leutz,"Scintillating Fibres", NIM A, V. 364, (1995) 422;
- RD7, DRDC Status Reports, CERN, Geneva;
- ATLAS Technical Design Report, CERN, (1999);
- C. D'Ambrosio and H. Leutz, "Hybrid photon detectors" NIM A, V.501, 2-3, (2003);

Particle Detectors – Principles and Techniques (3/5)

Lecture 3b – Photo-detection

Speaker: Thierry GYS (CERN–PH/DT2)

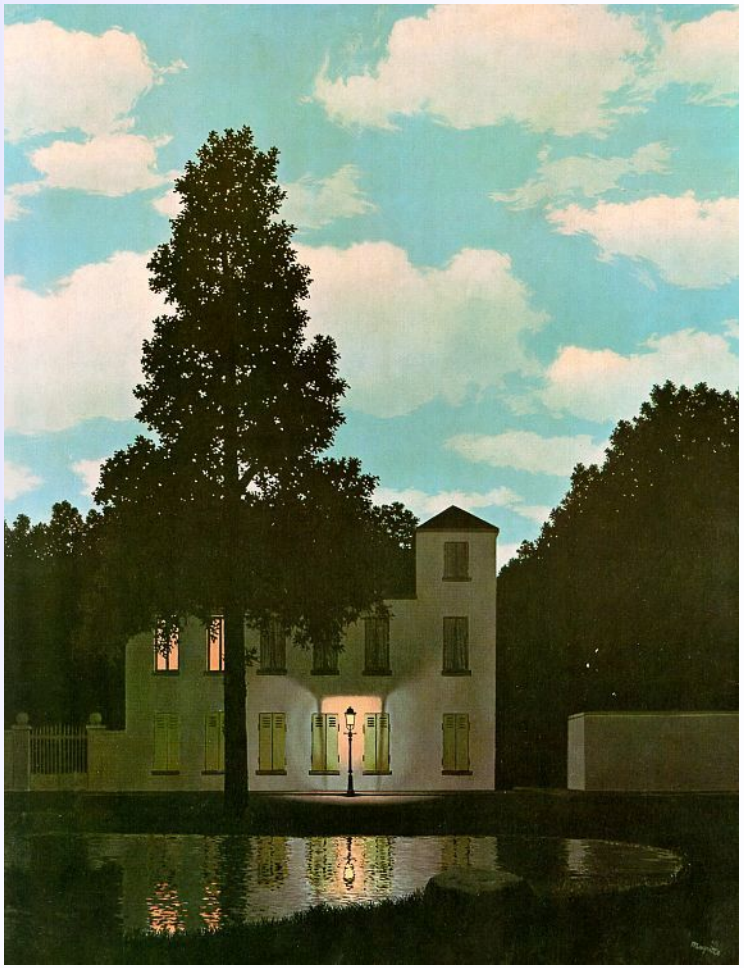

The Empire of Lights (René Magritte, Lessines 1898 – Brussels 1967)

(1954, Canvas, 146 x 114 cm, Brussels, Royal Museums of Fine Arts of Belgium, © SABAM 2001)

General outline

- **Lecture 1 - Introduction** C. Joram, L. Ropelewski
- **Lecture 2 - Tracking Detectors** L. Ropelewski, M. Moll
- **Lecture 3 - Scintillation and Photo-detection** C. D'Ambrosio, T. Gys
  - **3a) Scintillation**
  - **3b) Photo-detection** **Thierry Gys (CERN - PH/DT2)**
    - Photon detectors: purpose, basic principle and general requirements
    - Vacuum photon detectors
    - Solid-state photon detectors
    - Hybrid photon detectors
    - Literature
- **Lecture 4 - Calorimetry, Particle ID** C. Joram
- **Lecture 5 - Particle ID, Detector Systems** C. Joram, C. D'Ambrosio

Detailed outline

extra slide not shown

- **Photon detectors**
  - Purpose, basic principle and general requirements
- **Vacuum photon detectors**
  - The photoelectric effect, photo-cathodes and optical windows
  - Photomultipliers:
    - Basic principle and gain fluctuations
    - Dynode configurations: traditional and position-sensitive
  - Image intensifiers: principles, generations and Micro Channel Plates
- **Solid-state photon detectors**
  - Basic principle, PIN and avalanche diodes, light absorption
  - A detailed example of CCD optimization for astronomy
- **Hybrid photon detectors**
  - Basic principle and gain fluctuations
  - Description of various HPD types
- **Literature**

Photon detectors

Purpose:

- Convert light into detectable (electronic) signal

Principle:

- Use photoelectric effect to convert photons (γ) to photoelectrons (pe)

Standard requirements:

- High sensitivity, usually expressed as:
  - quantum efficiency: $$QE(\%) = \frac{N_{pe}}{N_{\gamma}}$$
  - radiant sensitivity S(mA/W) with: $$QE(\%) \approx 124 \cdot \frac{S(mA/W)}{\lambda(nm)}$$
- Low intrinsic noise
- Low gain fluctuations
- High active area

Photon detectors

Main types of photon detectors:

- gas-based (not covered in this lecture, see lecture 2a)
- vacuum-based
- solid-state (see also lecture 2b)
- hybrid

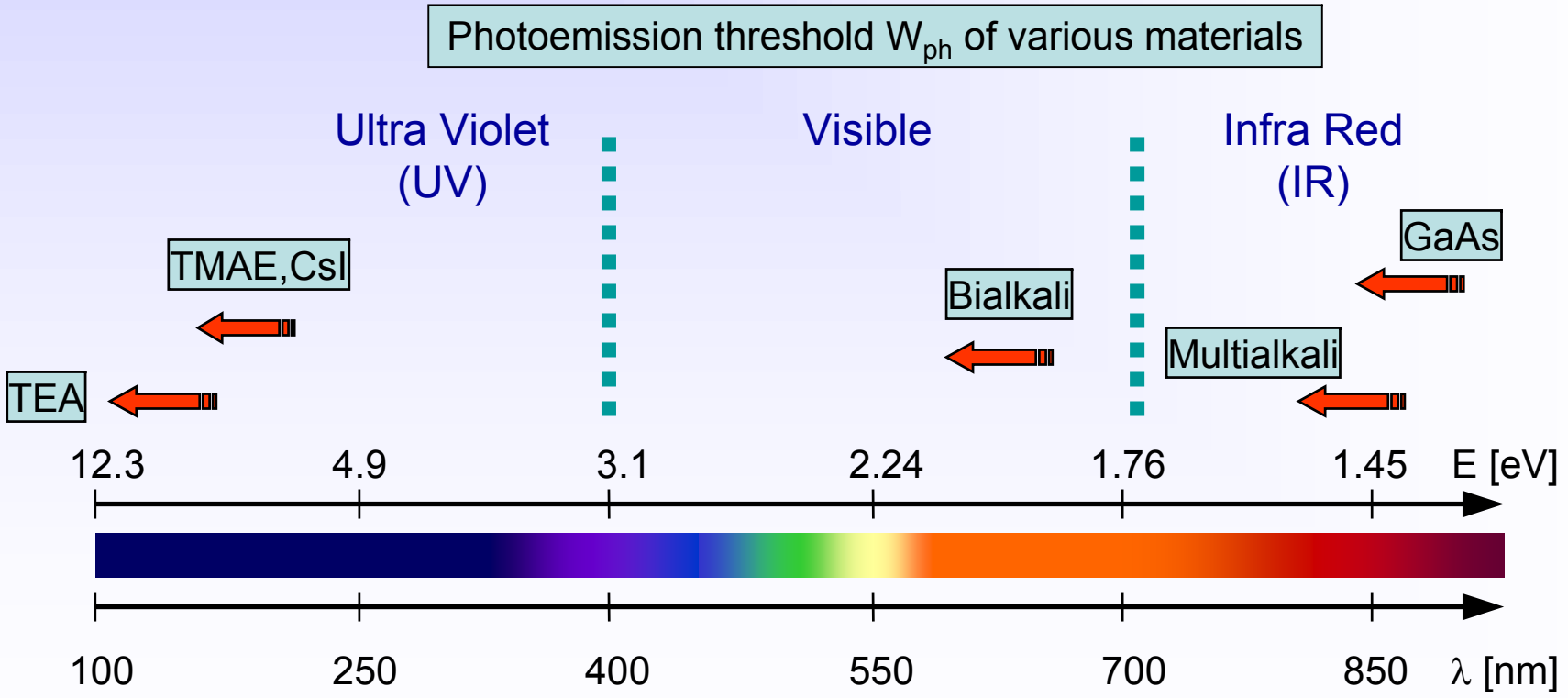

The photoelectric effect

3-step process:

- absorbed γ's impart energy to electrons (e) in the material;
- energized e's diffuse through the material, losing part of their energy;
- e's reaching the surface with sufficient excess energy escape from it;

⇒ ideal photo-cathode (PC) must absorb all γ's and emit all created e's

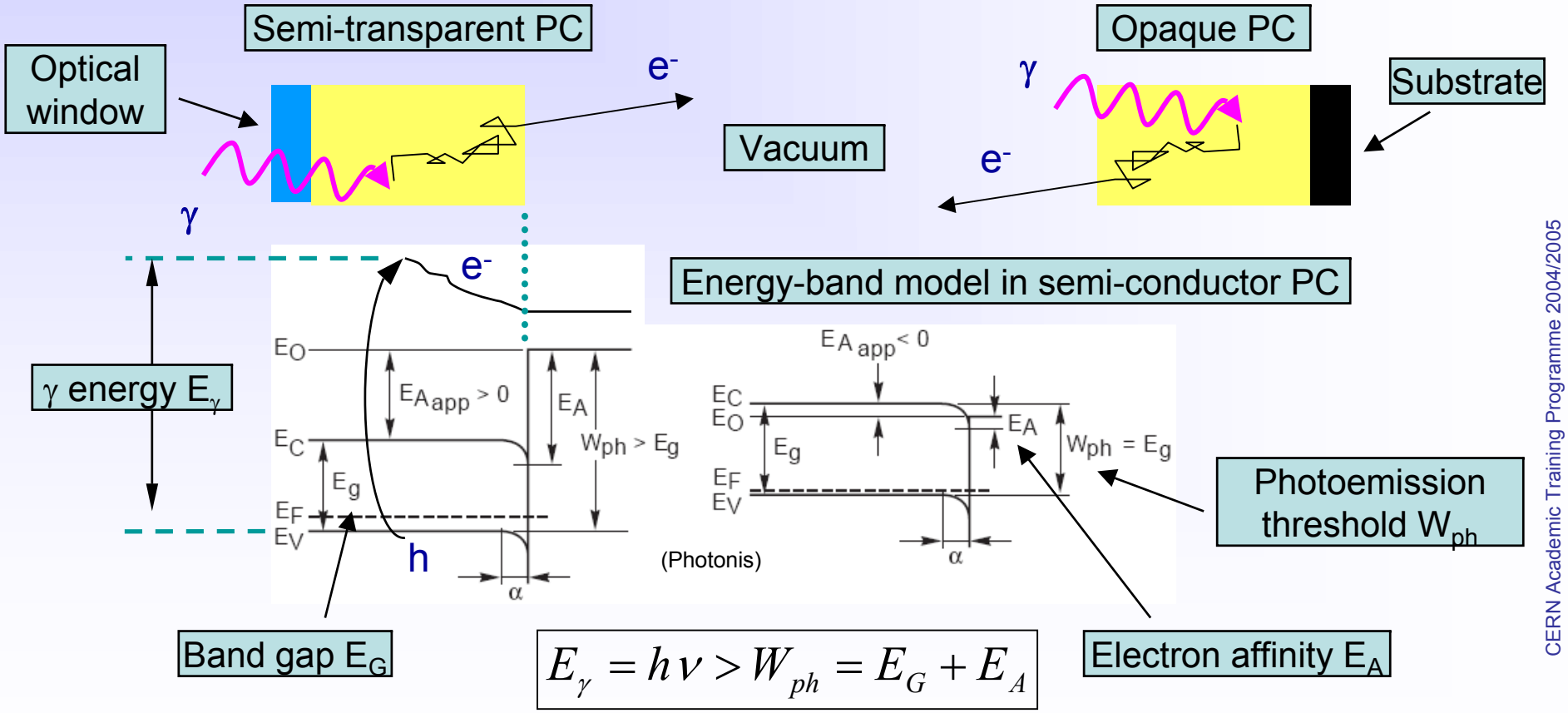

$$E_\gamma = h\nu > W_{ph} = E_G + E_A$$

QE's of typical photo-cathodes

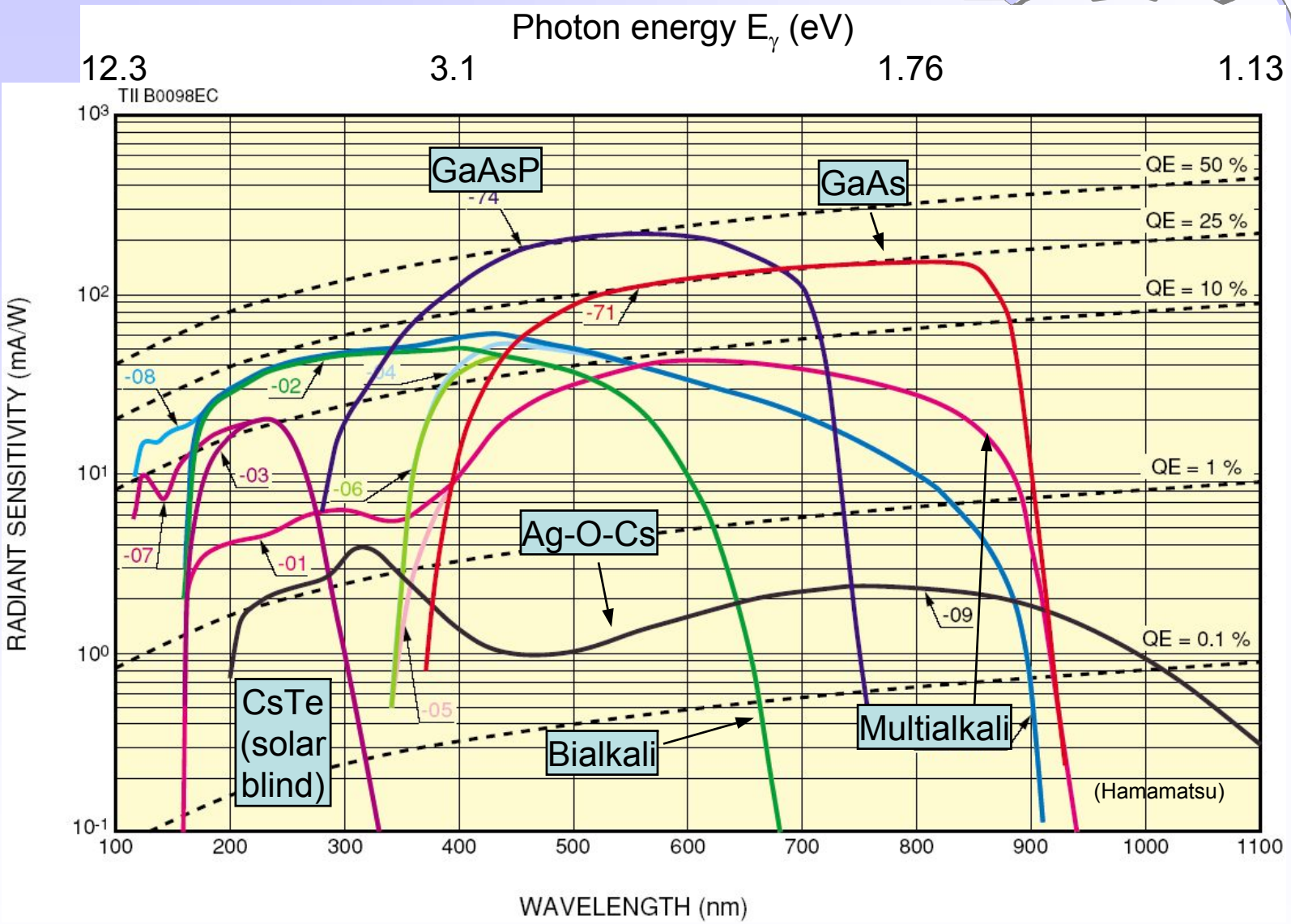

Bialkali: SbKCs, SbRbCs Multialkali: $SbNa_2KCs$ (alkali metals have low work function)

Transmission of optical windows

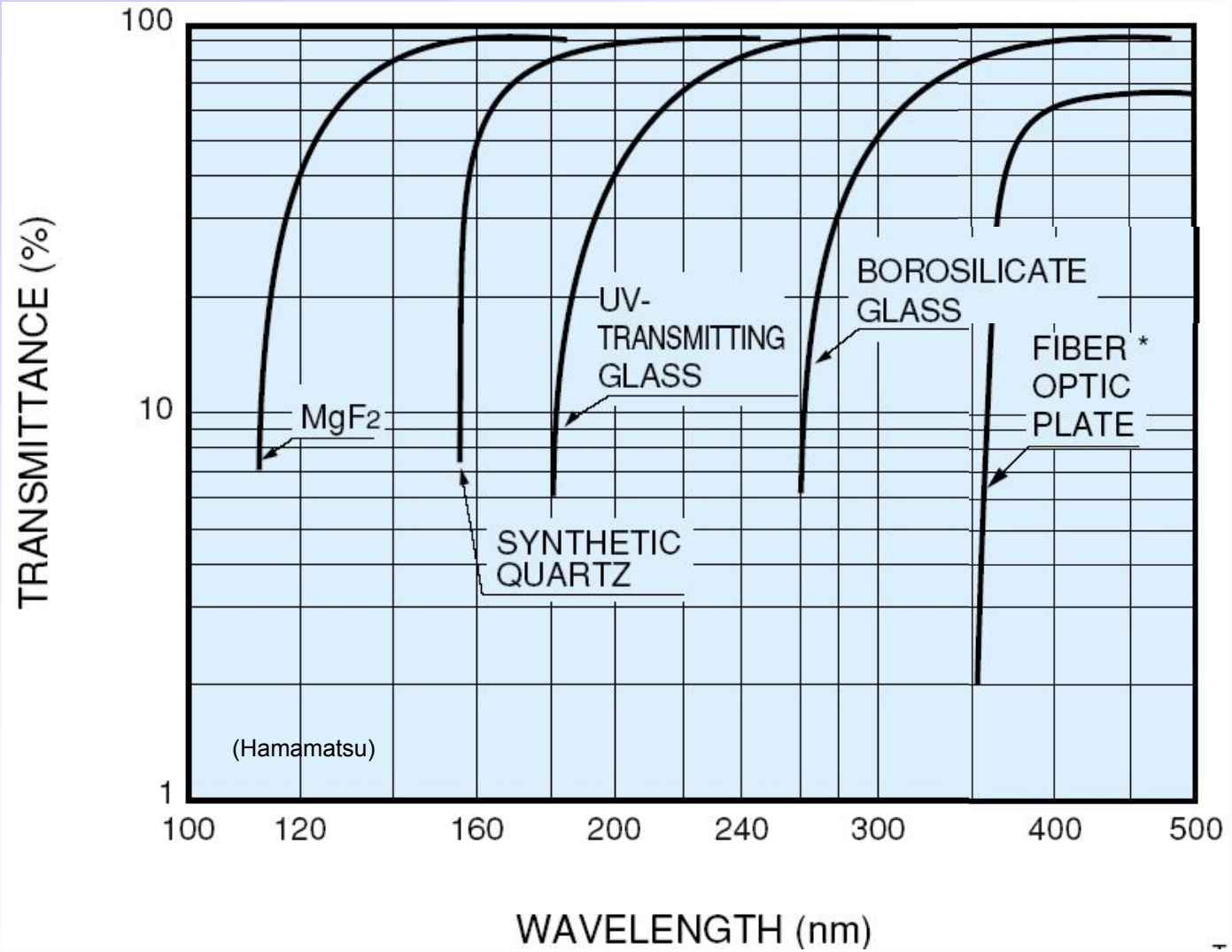

Photo-multiplier tubes (PMT's)

Basic principle:

- Photo-emission from photo-cathode
- Secondary emission (SE) from N dynodes:
  - dynode gain g≈3-50 (function of incoming electron energy E);
  - total gain *M*:

$$M = \prod_{i=1}^{N} g_i$$

- Example:
  - 10 dynodes with g=4
  - $M = 4^{10} \approx 10^6$


(Hamamatsu)

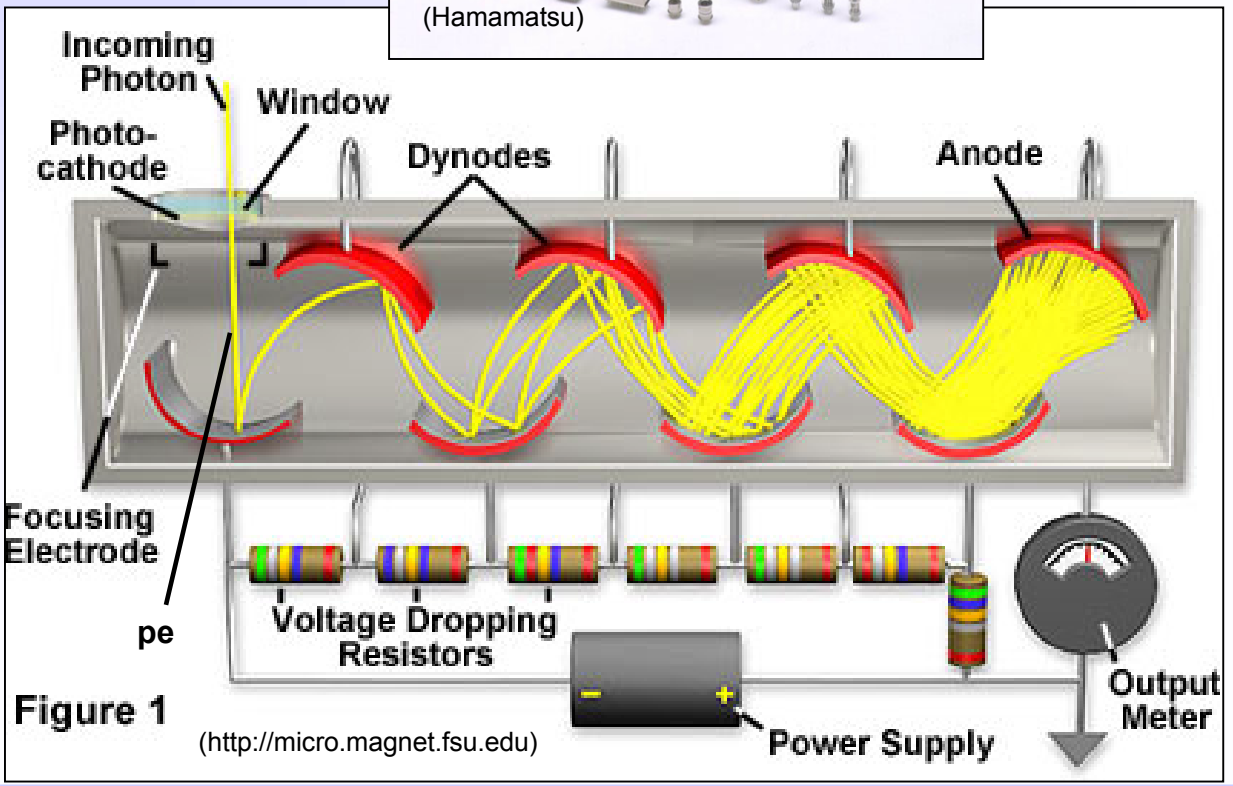

Figure 1

Gain fluctuations of PMT's

- Mainly determined by the fluctuations of the number m(δ) of secondary e's emitted from the dynodes;
- Poisson distribution: $$P_\delta(m) = \frac{\delta^m e^{-\delta}}{m!}$$
- Standard deviation: $$\frac{\sigma_m}{\delta} = \frac{\sqrt{\delta}}{\delta} = \frac{1}{\sqrt{\delta}}$$

$\Rightarrow$ fluctuations dominated by 1st dynode gain;

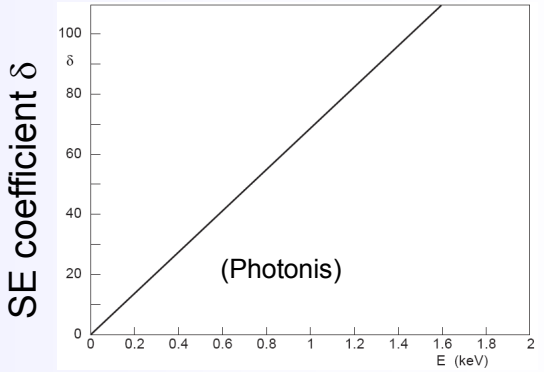

e energy

GaP(Cs) dynodes E_A<0

CuBe dynodes E_A>0

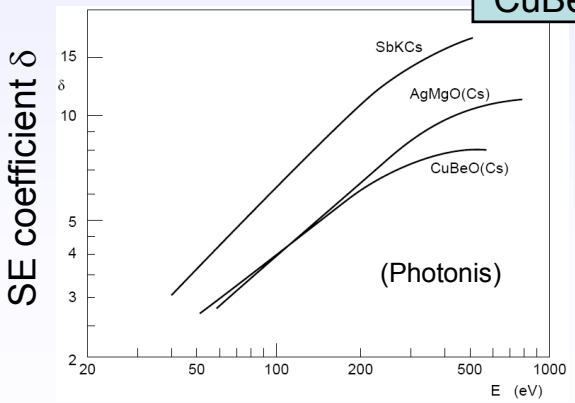

e energy

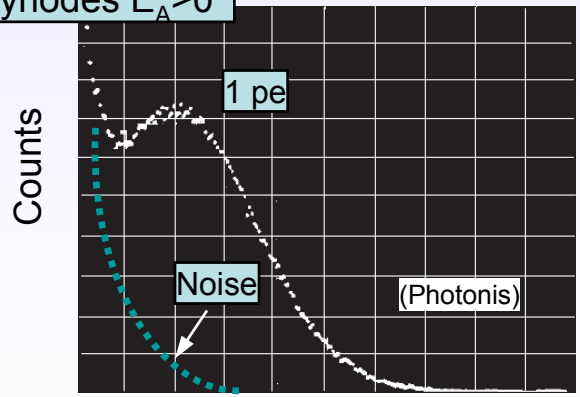

Pulse height

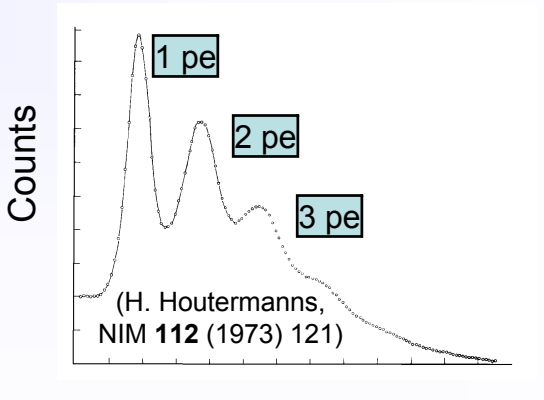

Pulse height

Dynode configurations of PMT's

Traditional

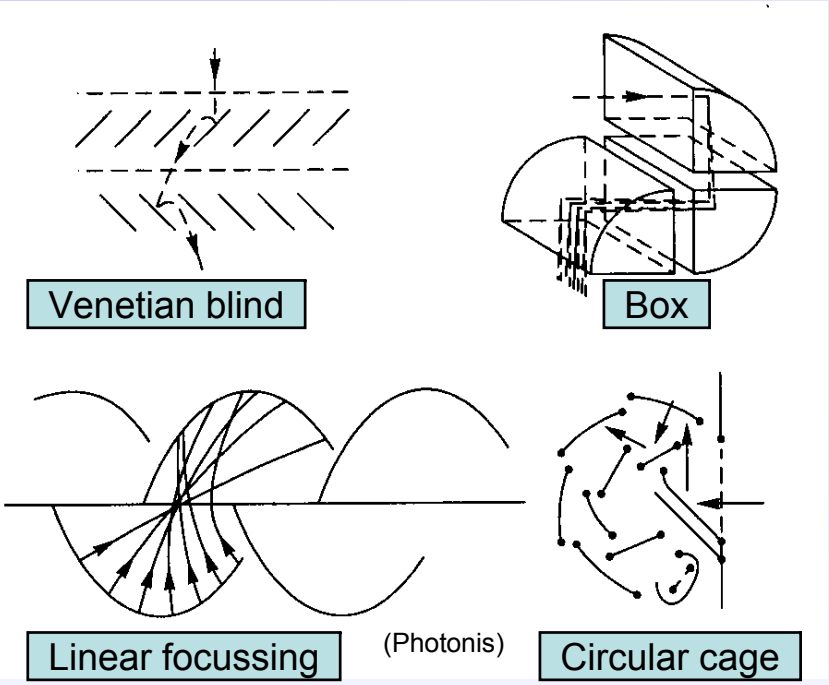

Position-sensitive

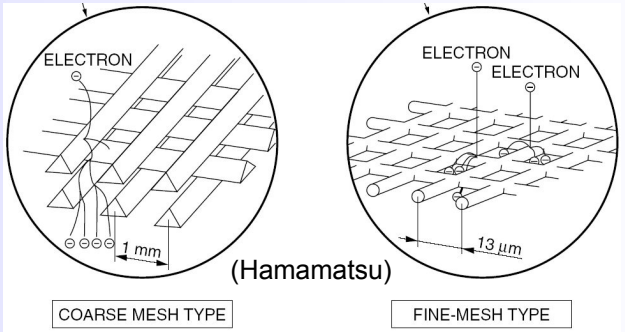

Mesh

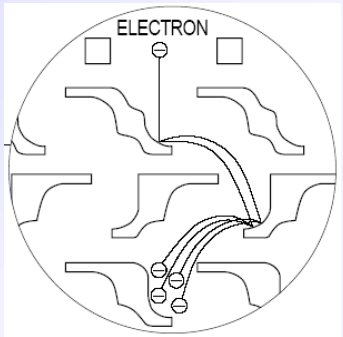

Metal-channel (fine-machining techniques)

(Hamamatsu)

- "Fast" PMT's require well-designed input electron optics to limit (e) chromatic and geometric aberrations → transit time spread < 200 ps;
- PMT's are in general very sensitive to magnetic fields, even to earth field (30-60 μT). Magnetic shielding required.

Multi-anode and flat-panel PMT's

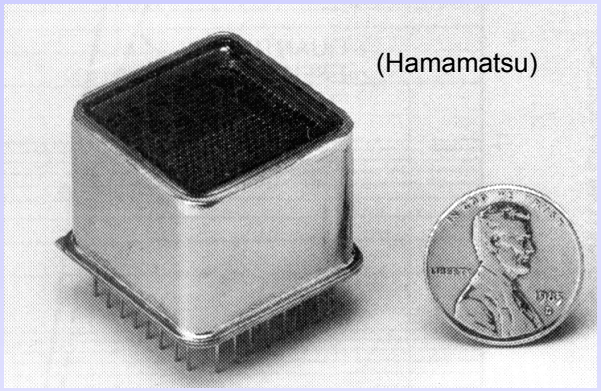

Multi-anode (Hamamatsu H7546)

- Up to 8 × 8 channels (2 × 2 mm^2 each);
- Size: 28 × 28 mm^2;
- Active area 18.1 × 18.1 mm^2 (41%);
- Bialkali PC: QE ≈ 20% @ λ_{max} = 400 nm;
- Gain ≈ 3 10^5;
- Gain uniformity typ. 1 : 2.5;
- Cross-talk typ. 2%

Cherenkov rings from
3 GeV/c π^- through aerogel

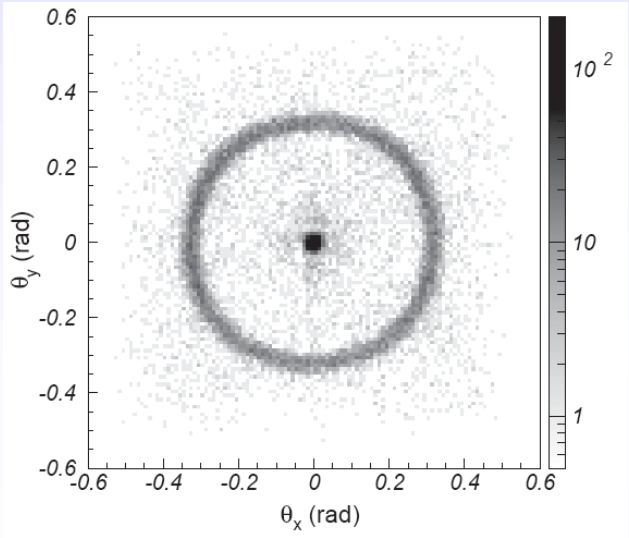

(T. Matsumoto et al., NIMA **521** (2004) 367)

Flat-panel (Hamamatsu H8500):

- 8 x 8 channels (5.8 x 5.8 mm^2 each);
- Excellent surface coverage (89%)

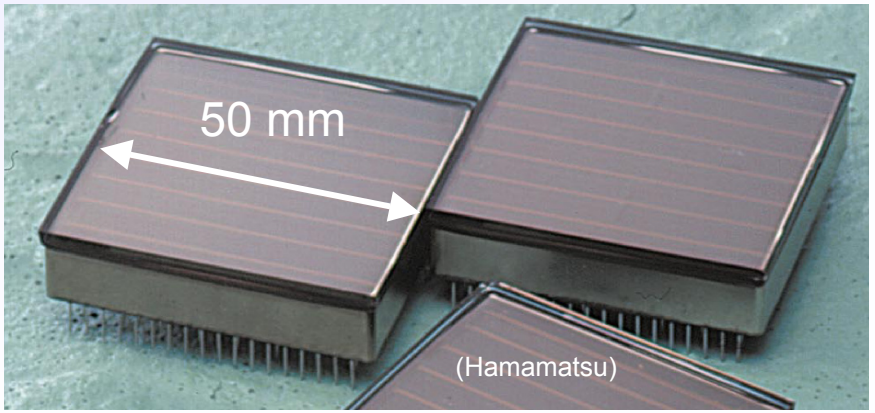

Image intensifiers

Basic principle:

- Vacuum photon detectors amplifying low light-level *image* to observable levels;
- Input: collection lens, optical window, photo-cathode;
- Gain: achieved by high voltage and possibly by additional imaging electron multiplier;
- Output: phosphor on optical window, ocular, observer (eye, CCD)

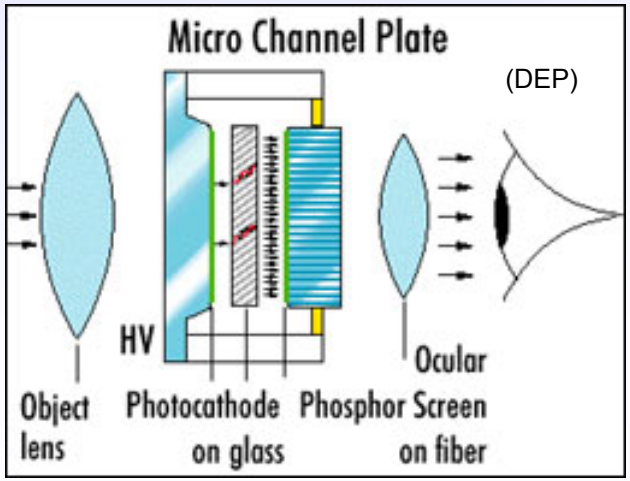

Image intensifier generations

Gen. I - electrostatic focussing:

- high image resolution;
- wide dynamic range;
- low noise;

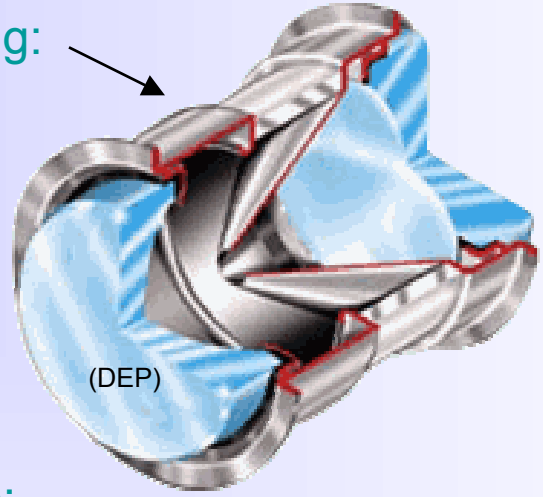

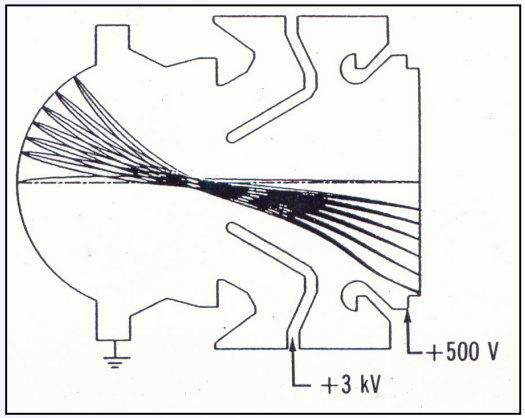

(I. P. Csorba, Image Tubes, Sams (1985))

Gen. II - Micro Channel Plate:

- worse resolution;
- much higher gain;

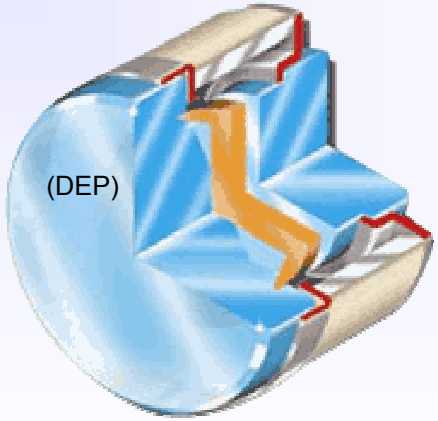

Gen. III – GaAs photo-cathode;

- enhanced sensitivity in near infrared;

Phosphor screens

extra slide not shown

Principle:

- absorb electrons;
- emit light on a characteristic λ of their material;

Spectral response:

- originally adapted to human eye response;
- must now match solid-state sensor response (e.g. CCD's);

Decay time:

- short (<100ns) for e.g. high-speed CCD's to minimize afterglow;
- long (~1ms) for night-vision and surveillance to minimize flicker;

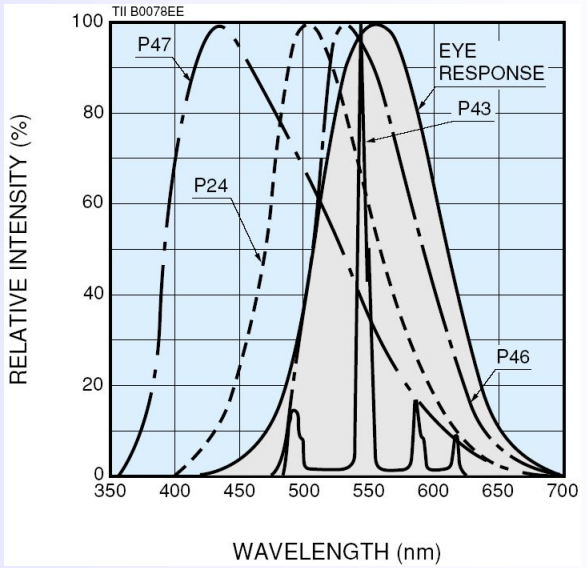

(Hamamatsu)

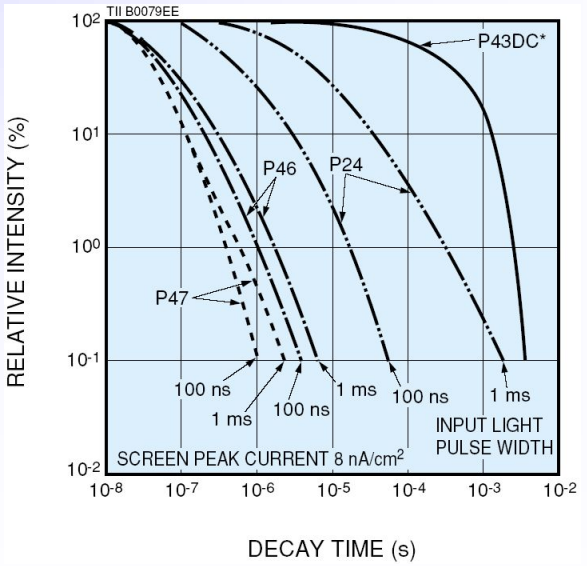

(Hamamatsu)

The Micro Channel Plate (MCP)

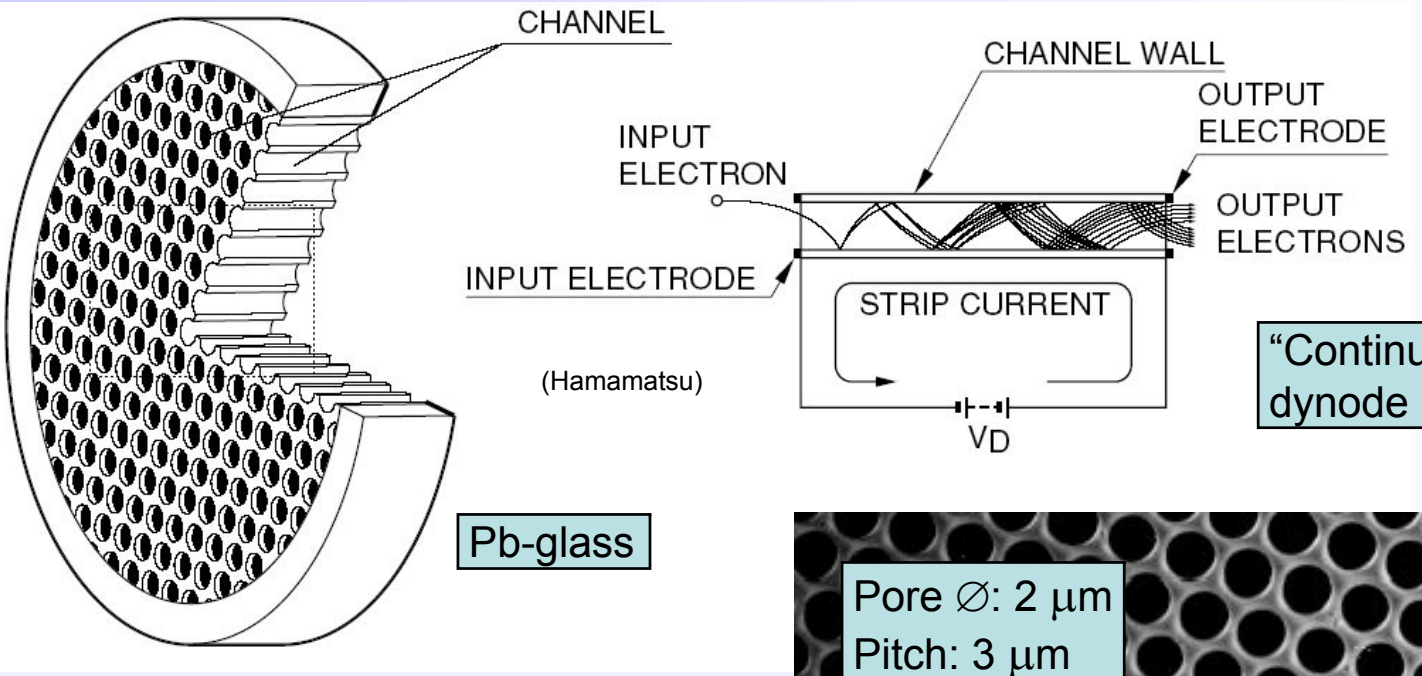

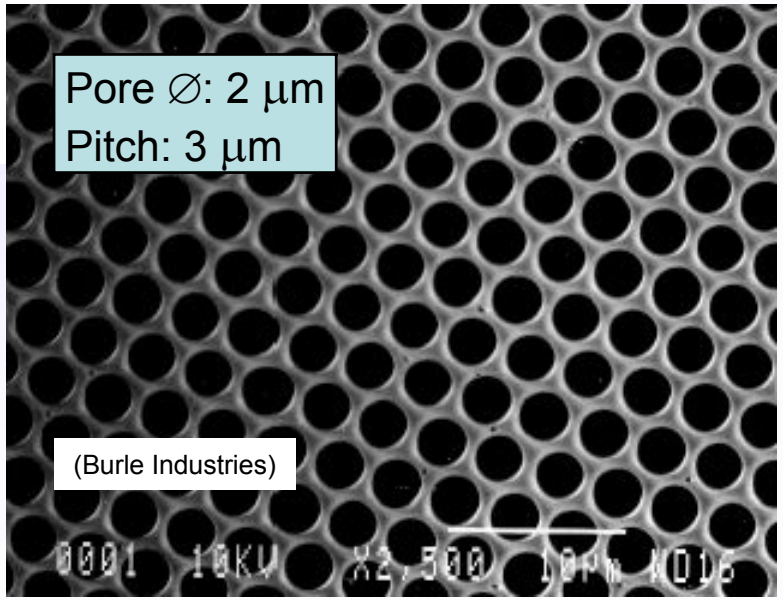

Kind of 2D PMT:

+ high gain up to 5 10^4;
+ fast signal (transit time spread ~50 ps);
+ less sensitive to B-field (0.1 T);
- limited lifetime (0.5 C/cm^2);
- limited rate capability (μA/cm^2);

Solid-state photon detectors

Photodiodes:

- P(I)N type (see lecture 2b);
- p layer very thin (<1 μm), as visible light is rapidly absorbed by silicon (see next slide);
- High QE (80% @ $\lambda \approx 700$nm);
- No gain: cannot be used for single photon detection;

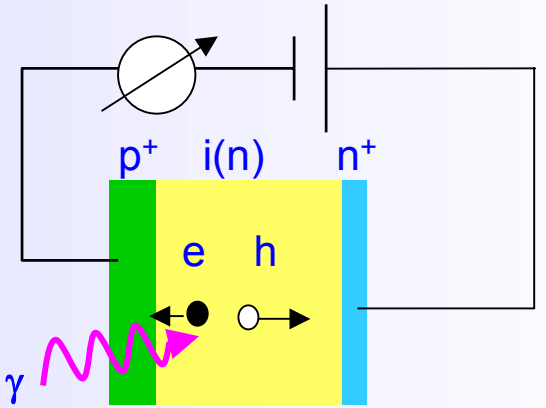

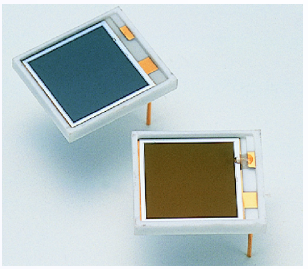

Avalanche photodiode:

- High reverse bias voltage: typ. 100-200 V

⇒ due to doping profile, high internal field and avalanche multiplication;

- High gain: typ. 100-1000;
- Used in CMS ECAL;

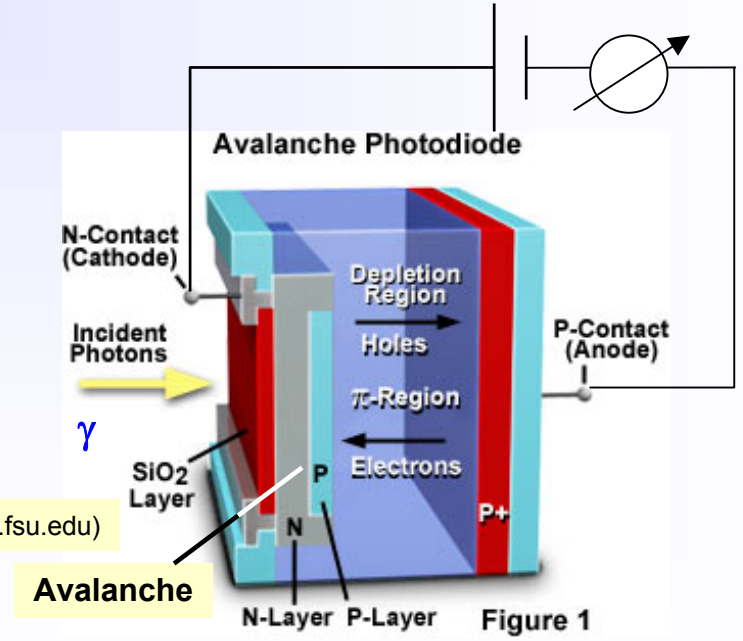

(http://micro.magnet.fsu.edu)

Figure 1

Light absorption in Silicon

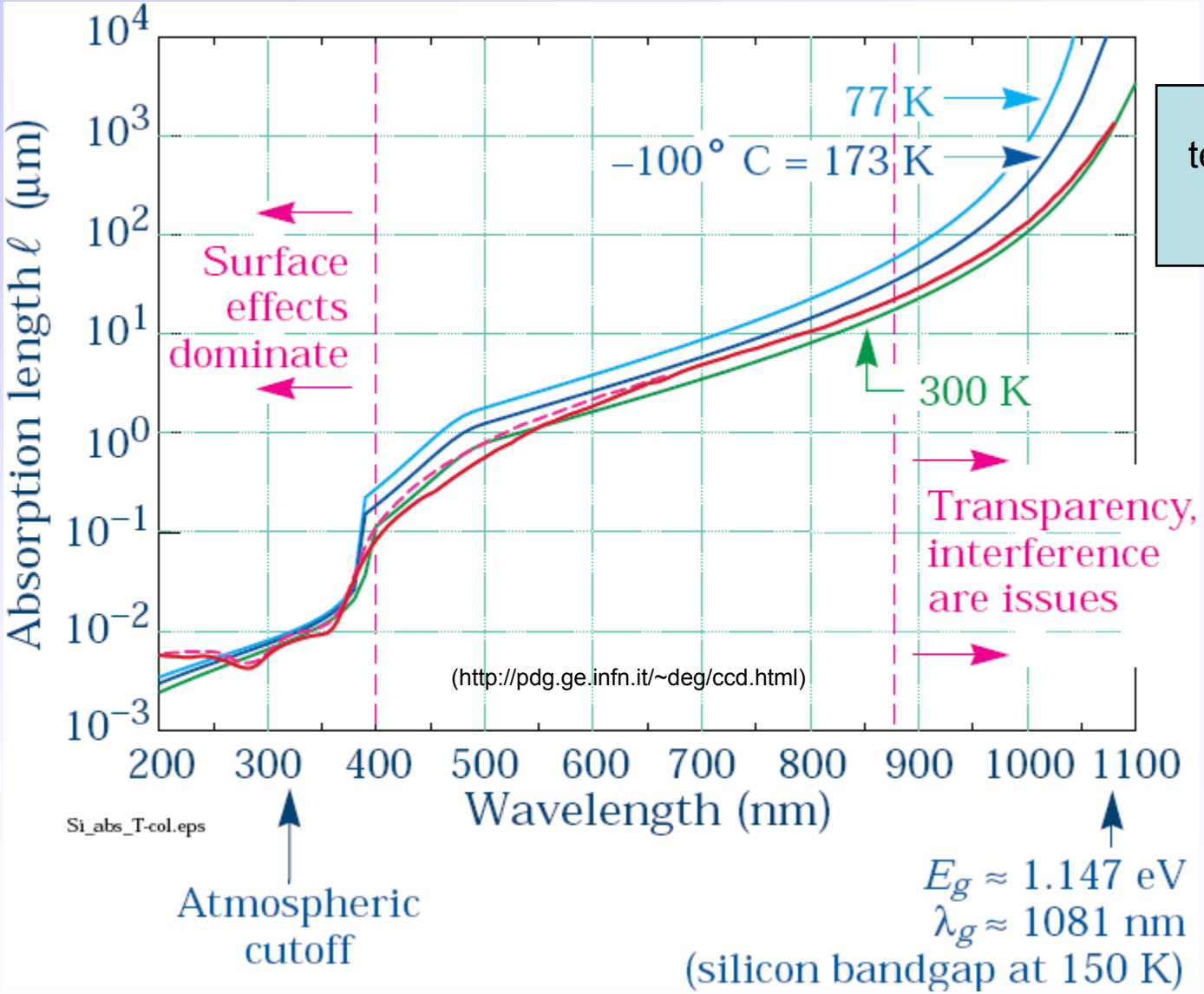

At long λ, temperature effects dominate

Many more types exist ...

Non-exhaustive list:

- Visible Light Photon Counter (VLPC);
- Silicon Photo-Multiplier (Si-PMT);
- Strip, pad and pixel arrays;
- CCD's:
  - conventional, front-illuminated;
  - thinned, back-illuminated;
  - fully-depleted, back-illuminated;

  (see a detailed example of the latter 2 for astronomical applications in the next slides)

Visible Light Photon Counter

extra slide not shown

Visible Light Photon Counter (VLPC):

- Originally developed by Rockwell;
- Operation at low bias voltage (7V);
- High IR sensitivity:

$\Rightarrow$ *requires cooling at liquid He T° (7K)!*

- Q.E. $\approx$ 70% around 500 nm;
- Gain up to 50.000 !
- used in the D0 Central Scintillating Fibre Tracker

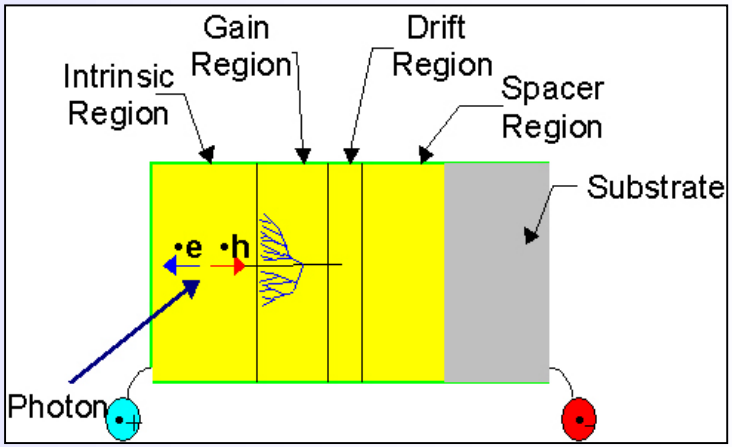

(http://d0server1.fnal.gov/projects/scifi/pictures/vlpc_related.html)

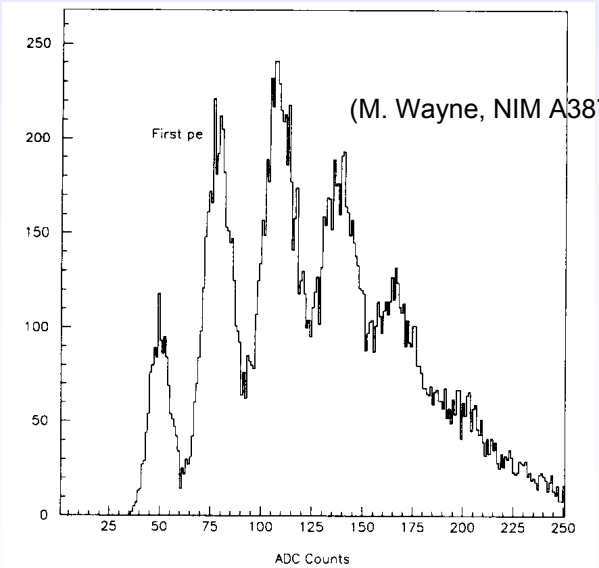

(M. Wayne, NIM A387 (1997) 278)

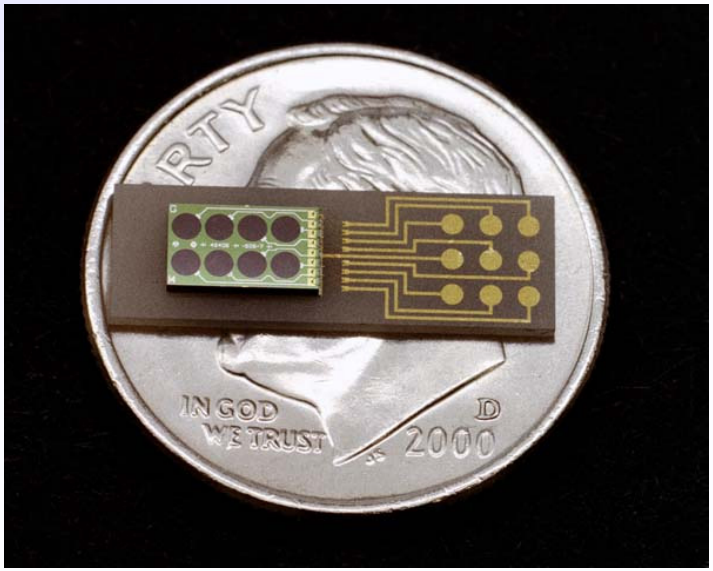

Silicon Photo-Multiplier

extra slide not shown

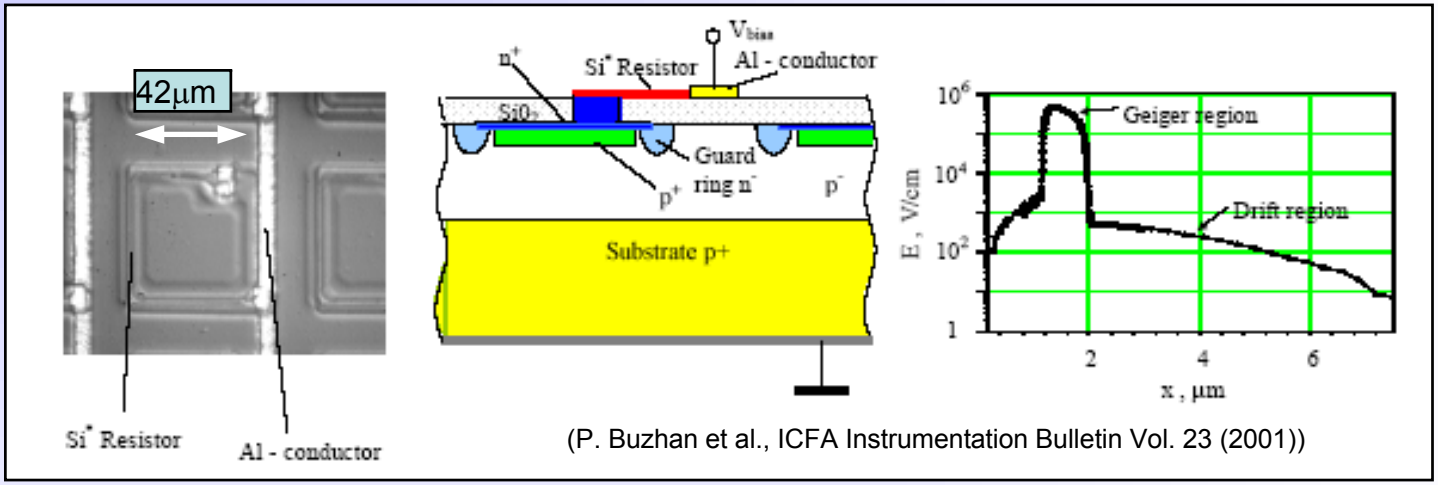

(P. Buzhan et al., ICFA Instrumentation Bulletin Vol. 23 (2001))

Kind of APD array operating in Geiger mode

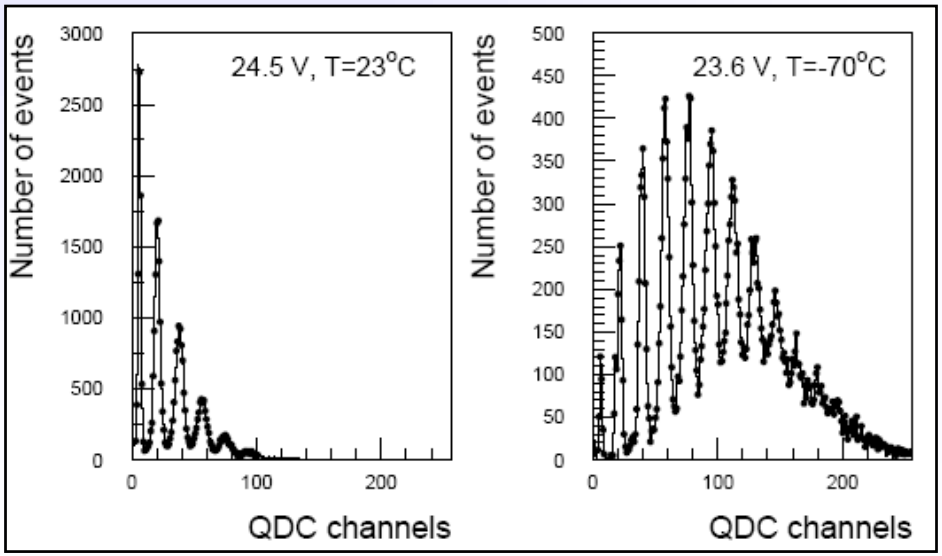

Back-illuminated fully depleted CCD

Front-illuminated CCD	Back-illuminated thinned CCD	Back-illuminated fully depleted CCD

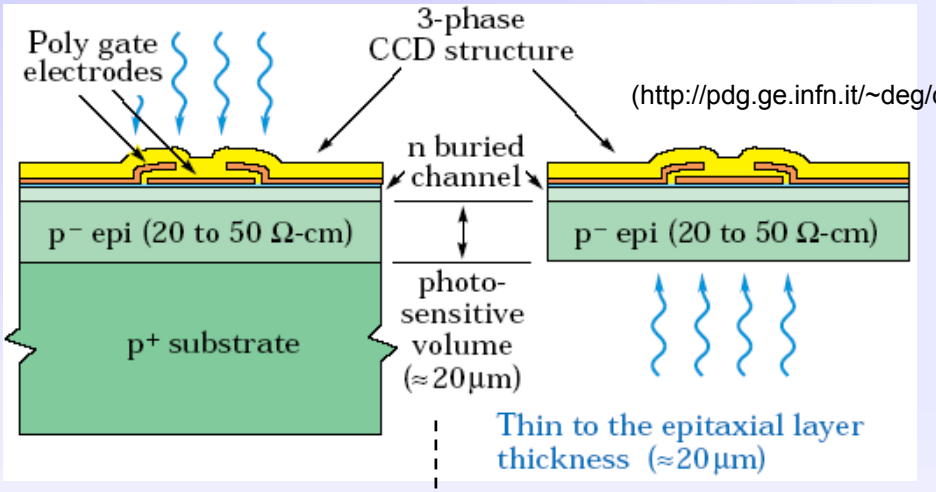

(http://pdg.ge.infn.it/~deg/ccd.html)

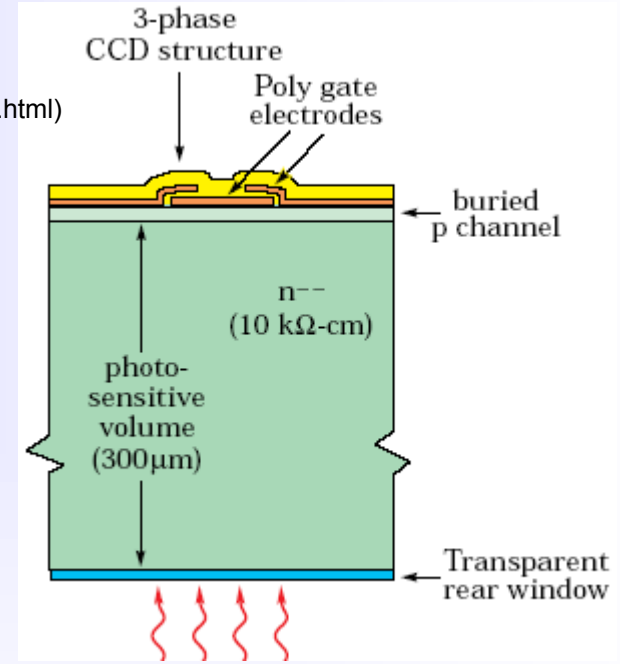

-poor response in blue (poly-Si) and IR (thin epitaxial layer);
-interference (gate);

-thinning difficult, expensive and not flat;
-poor IR response;
-fringing;
-lateral diffusion ⇒ degraded PSF;
-charge build-up at rear surface;

+conventional MOS process;
+full QE up to λ=1μm, (no fringing);
+good blue response;
-enhanced sensitivity to radiation

Measured QE curves

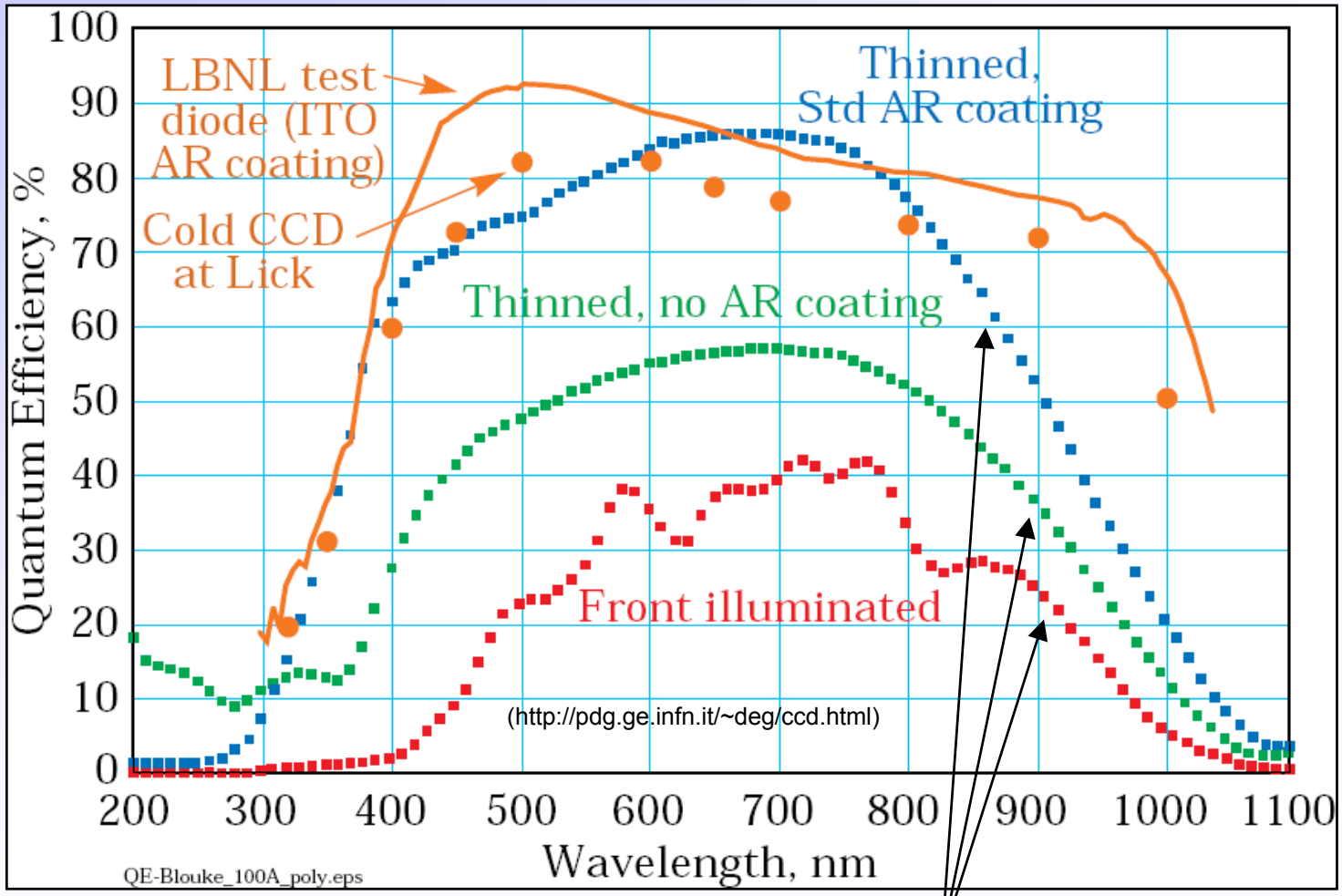

(http://pdg.ge.infn.it/~deg/ccd.html)

(M. Blouke and M. Nelson, SPIE **1900** (1993), 228-240)

And the result is ...

Dumbbell Nebula in Vulpecula (M27, NGC 6853)

(http://antwrp.gsfc.nasa.gov/apod/ap981009.html)

FORS false color image using a Tektronix back-illuminated 2k×2k CCD with 24μm pixels thinned and anti-reflection coated.
This image was obtained on ESO 8.2-m VLT Unit Telescope (UT) 1 on September 28, 1998.

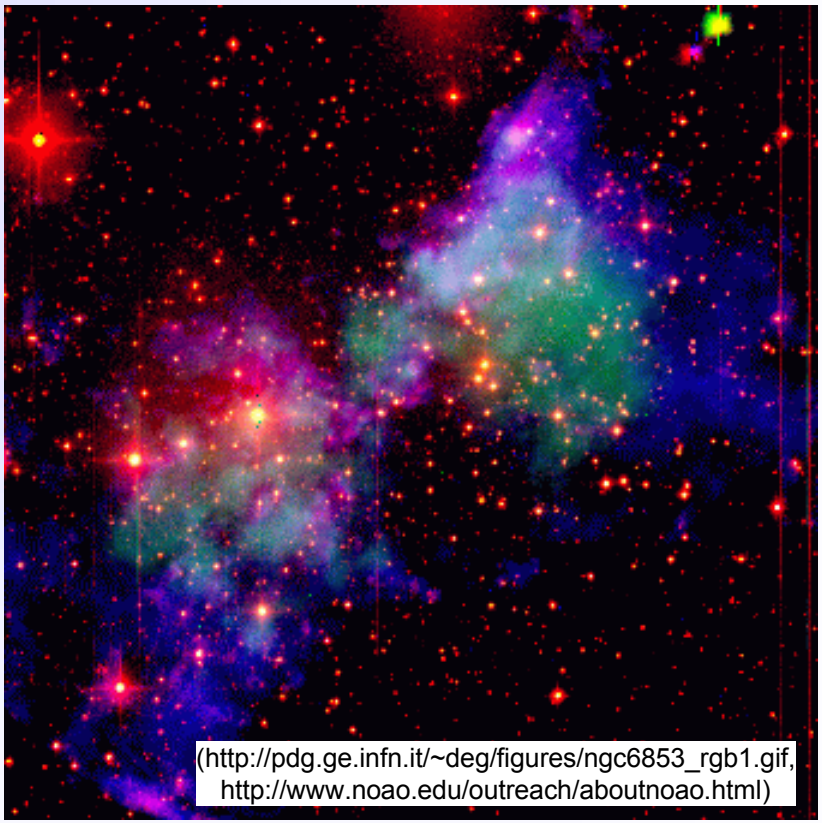

(http://pdg.ge.infn.it/~deg/figures/ngc6853_rgb1.gif, http://www.noao.edu/outreach/aboutnoao.html)

NOAO false color image using a back-illuminated fully depleted 2k×2k CCD with 15μm pixel.
This image was obtained on WIYN 3.5-m Telescope on June 7, 2001.

Hybrid Photon Detectors (HPD's)

Basic principle:

- Combination of vacuum photon detectors and solid-state technology;
- Input: collection lens, (active) optical window, photo-cathode;
- Gain: achieved *in one step* by energy dissipation of keV pe's in solid-state detector anode; this results in low gain fluctuations;
- Output: direct electronic signal;
- Encapsulation in the tube implies:
  - compatibility with high vacuum technology (low outgassing, high T° bake-out cycles);
  - internal (for speed and fine segmentation) or external connectivity to read-out electronics;
  - heat dissipation issues;

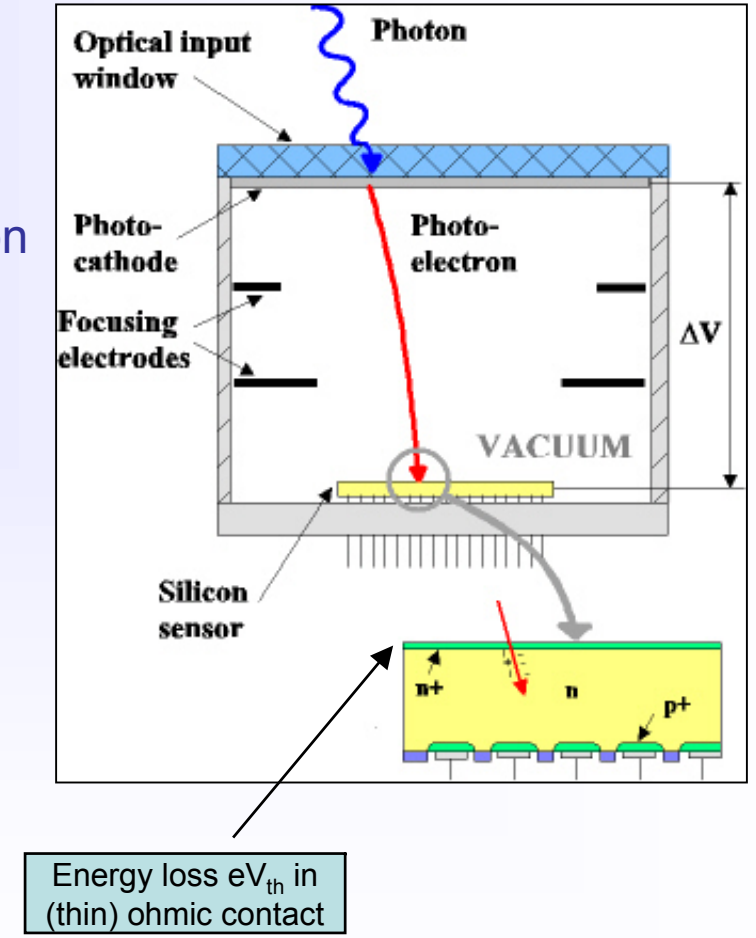

Energy resolution of HPD's

Basic properties:

- Photo-emission from photo-cathode;
- Photo-electron acceleration to $\Delta V \approx$ 10-20kV;
- Energy dissipation through ionization and phonons (W_{Si}=3.6eV to generate 1 e-h pair in Si) with low fluctuations (Fano factor F ≈ 0.12 in Si);
- Gain *M*: $M = \frac{e(\Delta V - Vth)}{W_{Si}}$
- Gain fluctuations σ_M: $\sigma_M = \sqrt{F \times M}$

  $\Rightarrow$ dominated by electronics
- Example: ΔV = 20kV

  $\Rightarrow M \approx 5000$ and $\sigma_M \approx 25$
- suited for single photon detection with high resolution;

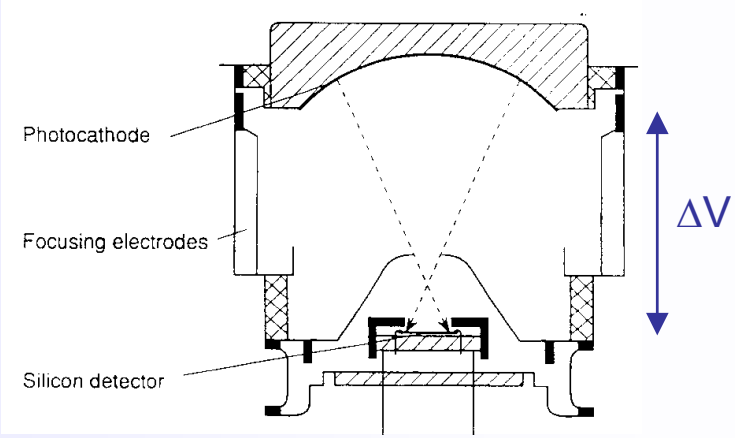

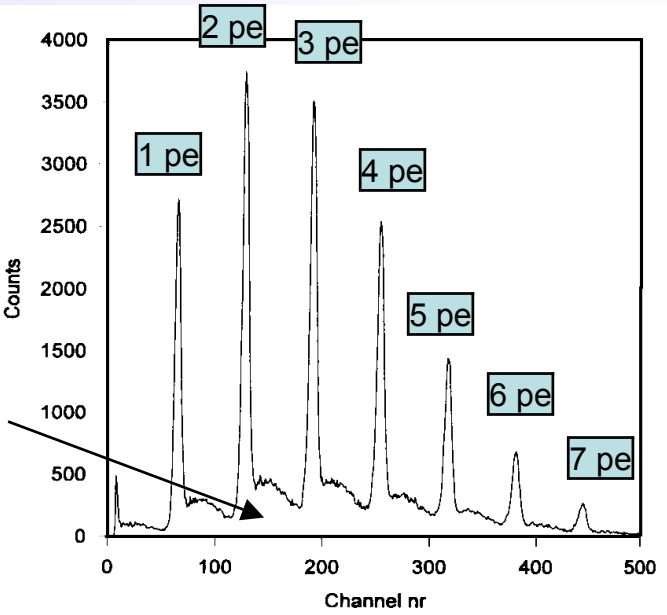

Background from electron back-scattering at Si surface

(C.P. Datema et al., NIM A 387(1997) 100)

Multi-pixel proximity-focussed HPD

DEP-CMS HCAL example:

- B=4T ⇒ proximity-focussing with 3.35mm gap and HV=10kV;
- Minimize cross-talks:
  - pe back-scattering: align with B;
  - capacitive: Al layer coating;
  - internal light reflections: a-Si:H AR coating optimized @ λ = 520nm (WLS fibres);
- Results in linear response over a large dynamic range from minimum ionizing particles (muons) up to 3 TeV hadron showers;

http://cmsinfo.cern.ch/Welcome.html/CMSdetectorInfo/CMShcal.html

Possible cross-talks

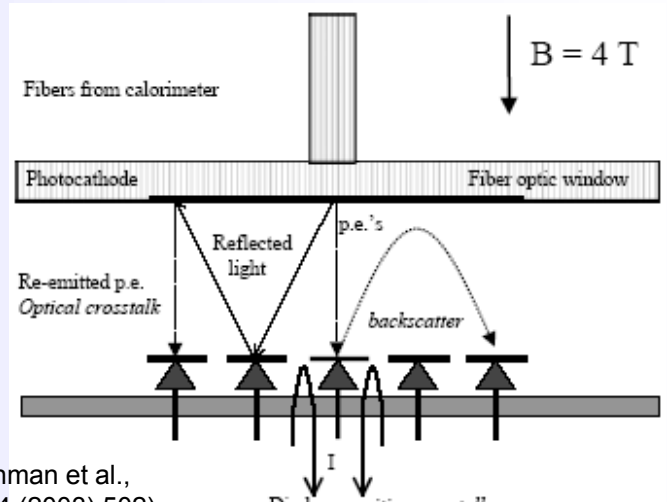

(P. Cushman et al., NIM A 504 (2003) 502)

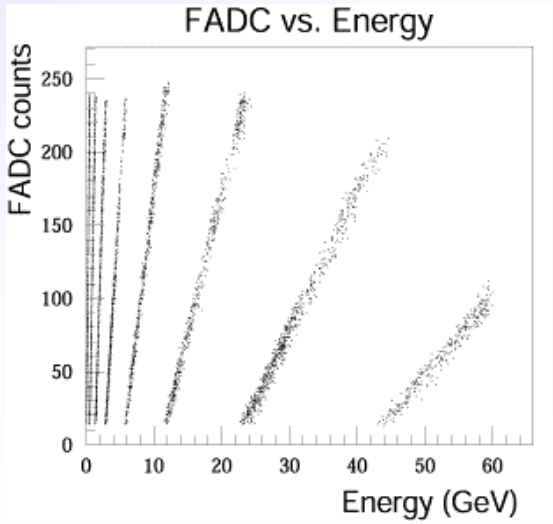

Various kinds of commercial HPD's

extra slide not shown

Single-diode cross-focussing

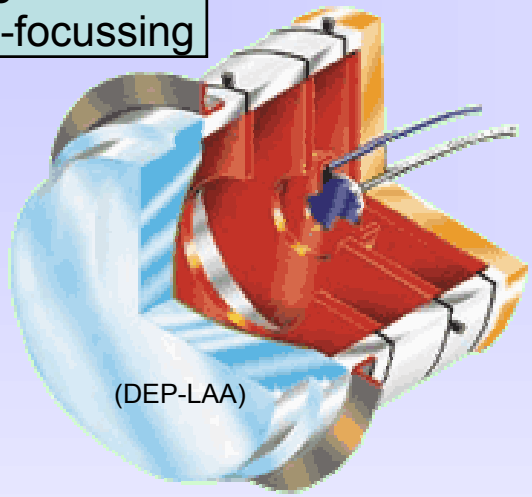

(DEP-LAA)

Multi-pixel proximity-focussing

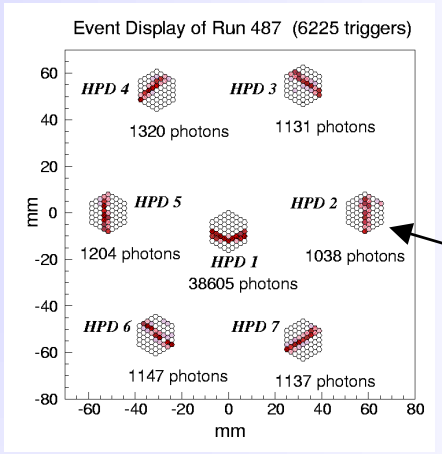

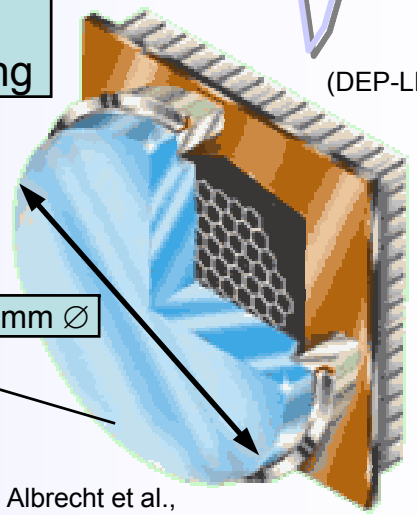

(DEP-LHCb)

(E. Albrecht et al., NIMA A 411 (1998) 249-264)

Single avalanche diode HPD

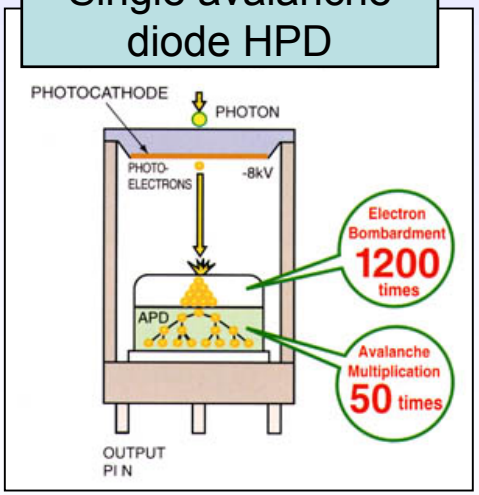

(Hamamatsu)

DEP-LHCb development:

- Multi-alkali photo-cathode;
- Commercial anode with 61 2mm-pixels; vacuum feed-throughs to external analog (VA2) readout electronics;
- Proximity-focussing electron optics;
- Poor intrinsic active area coverage (~50%);

Various kinds of commercial HPD's

extra slide not shown

Multi-pixel, cross-focussing

(DEP-LHCb)

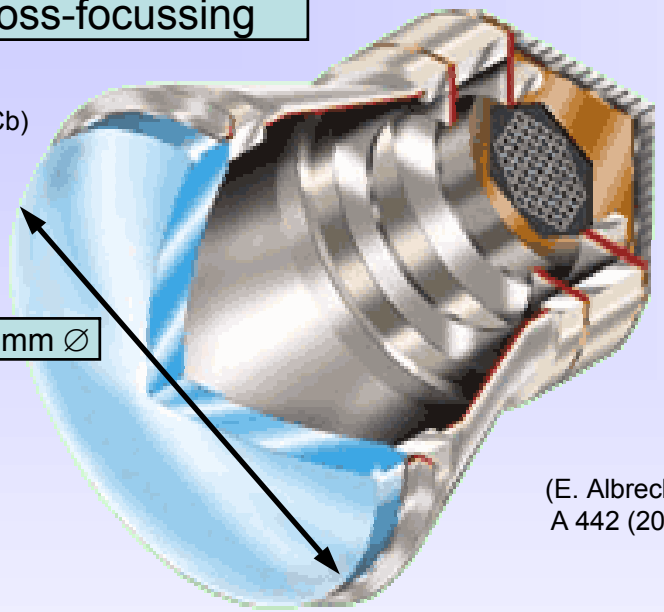

(E. Albrecht et al., NIMA A 442 (2000) 164-170)

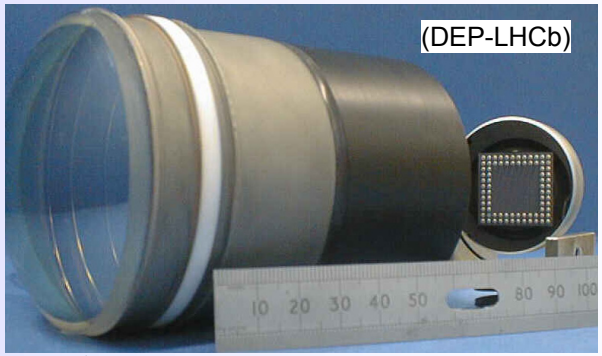

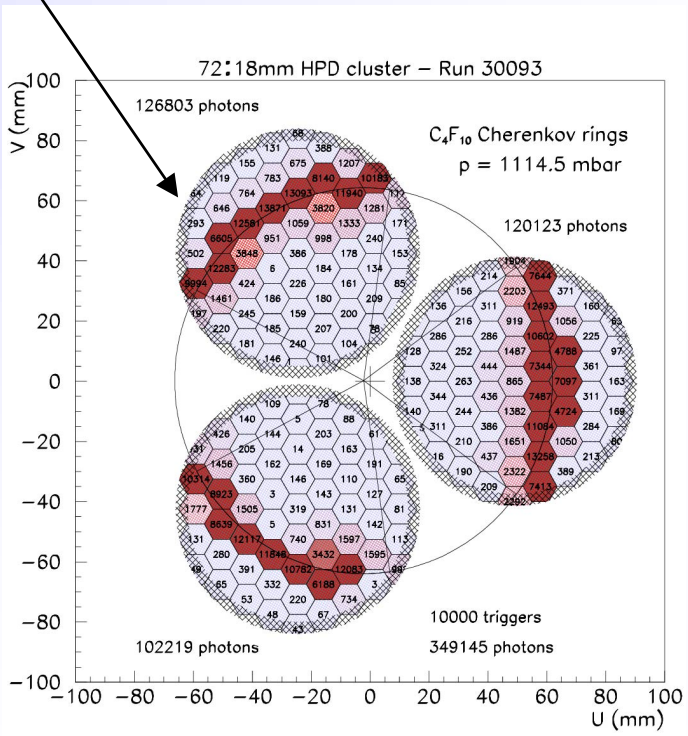

DEP-LHCb development:

- Commercial anode;
- Cross-focussing electron optics (de-magnification by ~5);
- High intrinsic active area coverage (83%);

Electron-bombarded CCD (EBCCD)

EBCCD
proximity-focussed

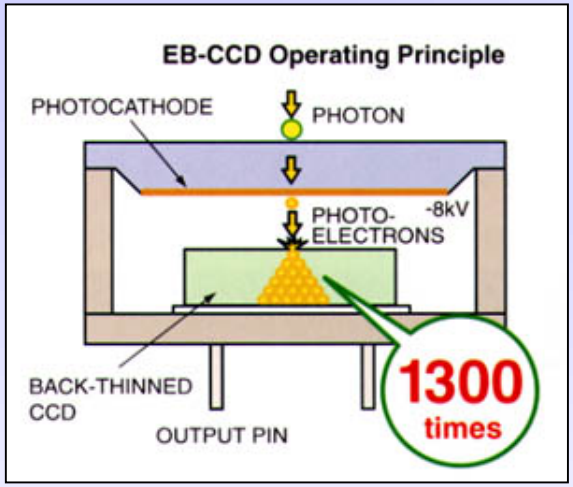

(Hamamatsu)

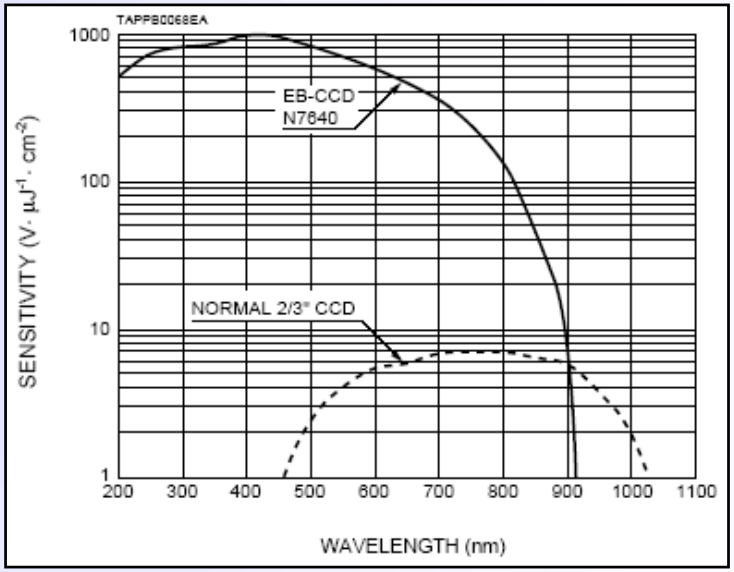

Commercial 2/3”
CCD

Hamamatsu N7640
EB-CCD

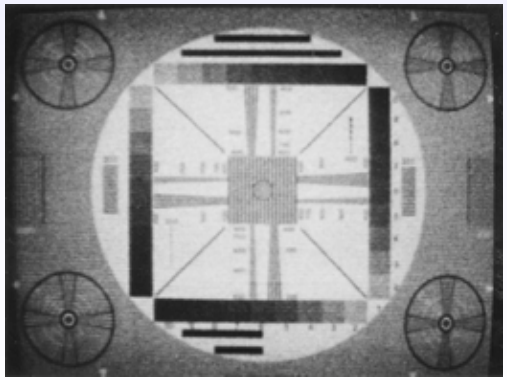

Object illuminance: 0.1lx

ISPA-tube

Imaging with Silicon Pixel Array:

- Pixel array sensor bump-bonded to binary electronic chip, developed for tracking (CERN-RD19);
- Flip-chip assembly encapsulated inside vacuum tube using standard parts, commercial ceramic carriers and packaging techniques;
- First ISPA prototype (1994) used to read small-diameter scintillating fibres developed for tracking (CERN-RD7);
- Spin-off applications for beta- and gamma-detection (quartz and YAP-crystal windows)

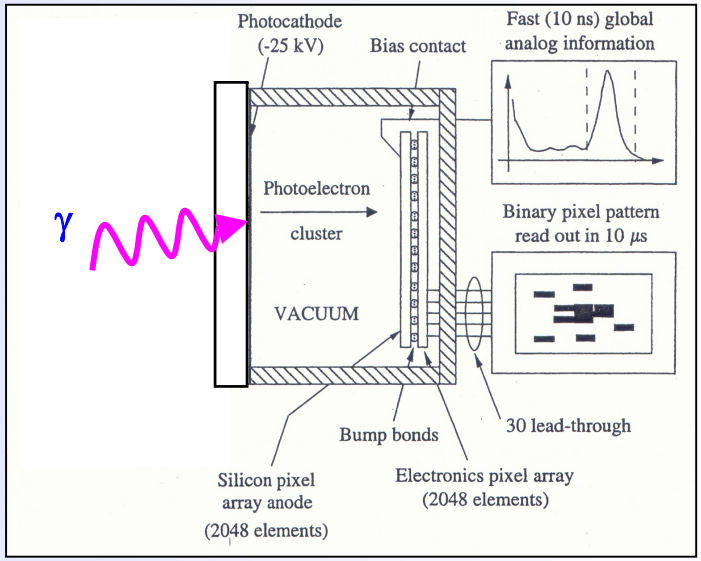

(T. Gys et al., NIMA 355 (1995) 386-389)

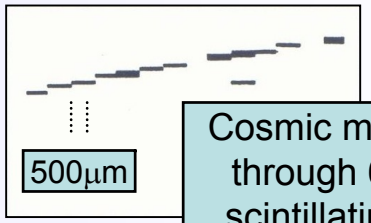

Cosmic muon track through 60μm ∅ scintillating fibres

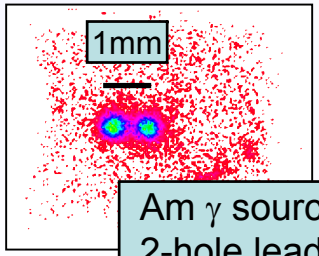

Am γ source through a 2-hole lead collimator

(F. Cindolo et al., IEEE TNS , Vol. 50, No. 1, February 2003, 126-132)

Pixel-HPD's for LHCb RICH's

Industry-LHCb development:

- LHCb-dedicated pixel array sensor bump-bonded to binary electronic chip (in coll. w. ALICE-ITS), specially developed high T° bump-bonding;
- Flip-chip assembly encapsulated inside vacuum tube using full-custom ceramic carrier;

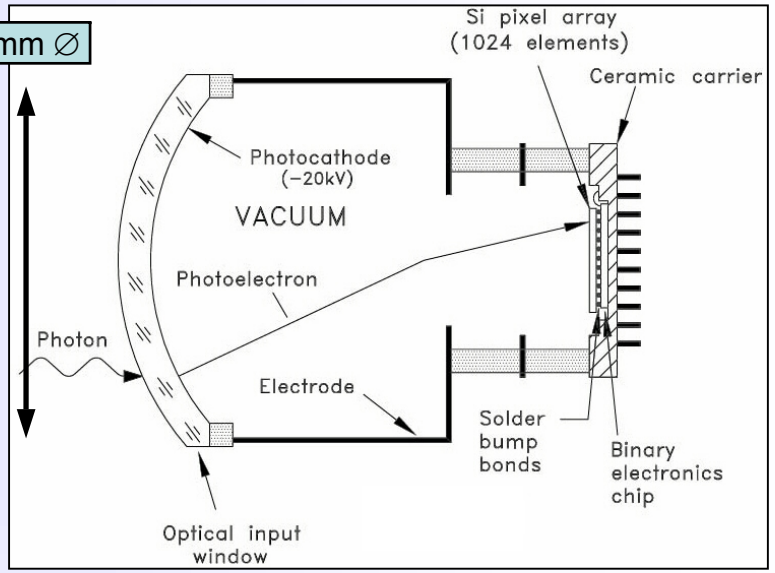

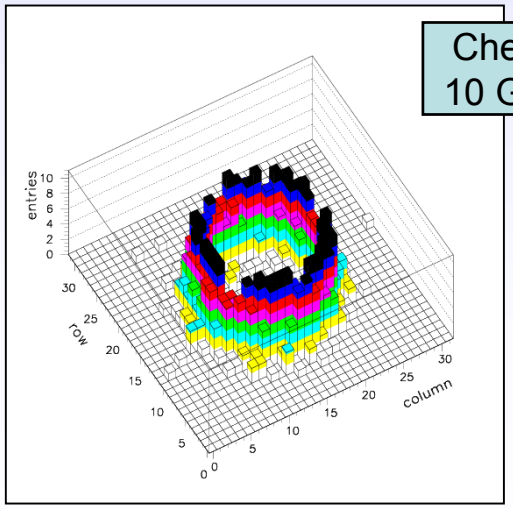

Cherenkov rings from 10 GeV/c π^- through air

(M. Moritz et al., IEEE TNS Vol. 51, No. 3,, June 2004, 1060-1066)

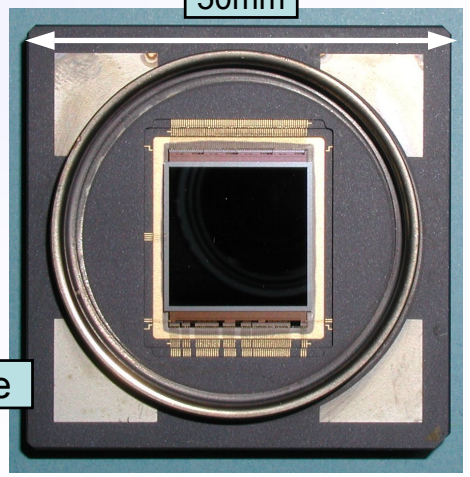

Pixel-HPD anode

The pad HPD for RICH detectors

extra slide not shown

Full in-house (LHCb, CERN, Bologna, CdF) development:

- Aim for active area > 80%;
- Bi-alkali photo-cathode;
- "Fountain" focussing electron optics (de-magnification ~2.4);
- Si detector: 16 × 128 = 2048 pads (~1 × 1 mm^2 each);
- Analogue electronics (16 VA3 chips) encapsulated inside vacuum tube;
- Standard Al wedge bonding;

(LHCb 98-007, RICH)

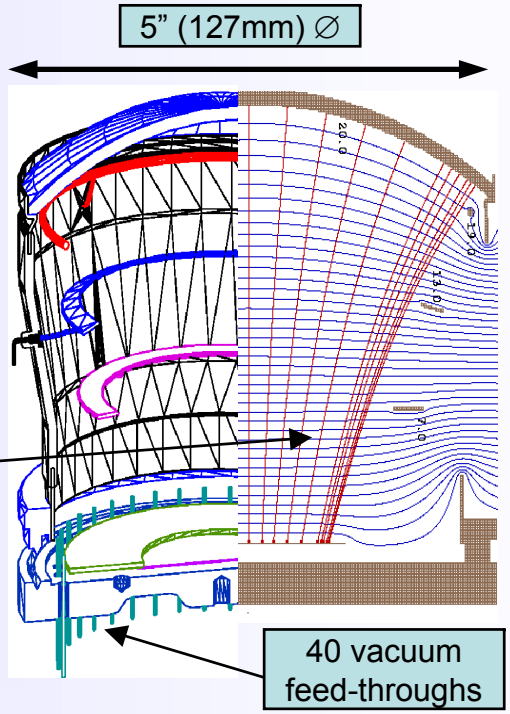

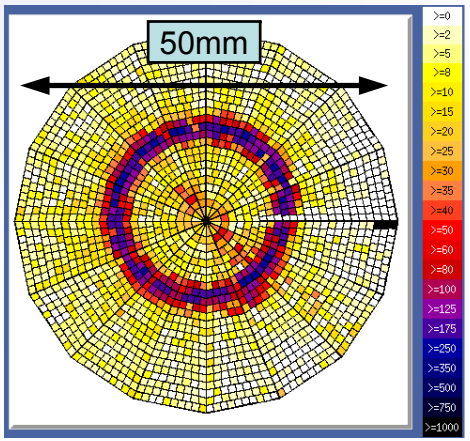

Hybrid MCP for adaptive optics (AO)

extra slide not shown

Development of next-generation astronomical AO:

- Alternative to replace more conventional high-speed CCD's;
- Aim for IR response, ultra-low noise and several kHz frame-rates;
- GaAs photo-cathode;
- Proximity-focussing electron optics;
- High-gain wide dynamic range MCP;
- Anode: Medipix2 photon-counting chip used both as direct electron detector (55μm pixels) and FE readout electronics;

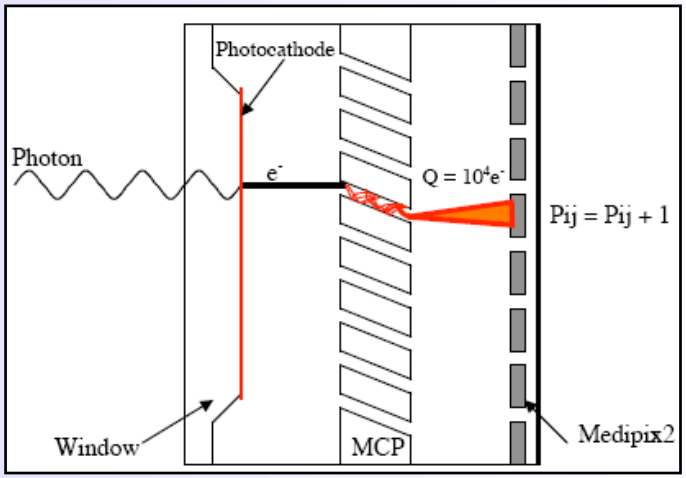

(J. Vallerga et al., Proc. SPIE, vol. 5490 (2004) 1256-1267)

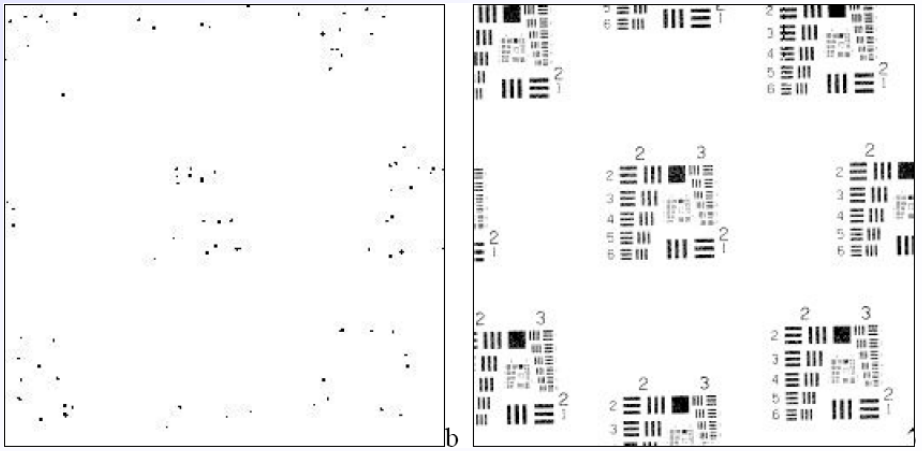

Images of USAF test pattern,
100ms (left) and 100s (right) exposures,
50k MCP gain

Literature

Non-exhaustive list:

- www.photonis.com: “Photomultiplier tubes, principles and applications”;
- www.hamamatsu.com;
- www.dep.nl;
- A.H. Sommer, ”Photoemissive materials”, J. Wiley & Sons (1968);
- H. Bruining, “Physics and Applications of Secondary Electron Emission”, Pergamon Press (1954);
- I. P. Csorba, “Image Tubes”, Sams (1985);
- Proceedings of the Beaune Conferences (1996-1999-2002) on “New Developments in Photo-detection”, published in NIMA;

Outline

- **Lecture 1 - Introduction** — C. Joram, L. Ropelewski
- **Lecture 2 - Tracking Detectors** — L. Ropelewski, M. Moll
- **Lecture 3 - Scintillation and Photodetection** — C. D'Ambrosio, T. Gys
- **Lecture 4 – Calorimetry** — C. Joram
  - Calorimetry - Basic principles
    - Interaction of charged particles and photons
    - Electromagnetic cascades
    - Nuclear interactions
    - Hadronic cascades
  - Homogeneous calorimeters
  - Sampling calorimeters
- **Lecture 5 - Particle ID, Detector Systems** — C. Joram, C. D'Ambrosio

Calorimetry

Calorimetry = Energy measurement by total absorption, usually combined with spatial reconstruction.

latin: calor = heat

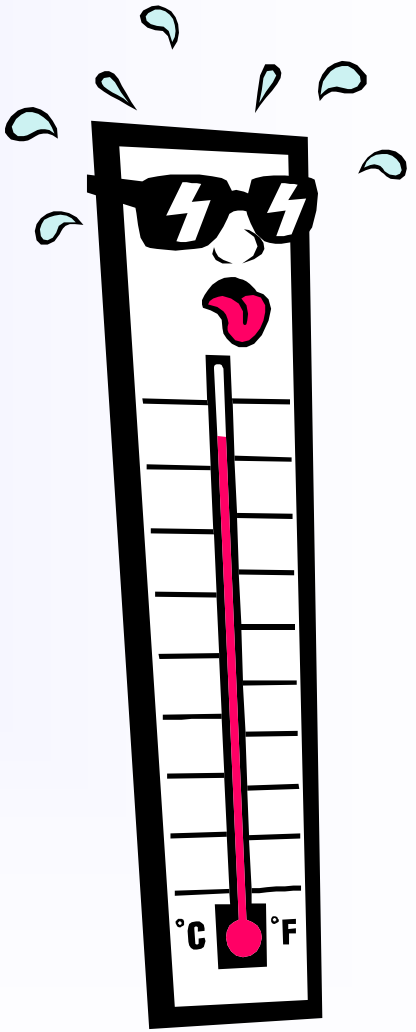

- LHC beam: Total stored beam energy
  E = 10^{14} protons $\times$ $14 \cdot 10^{12}$ eV $\approx 1 \cdot 10^{8}$ J
- Which mass of water M_{water} could one heat up (ΔT = 100 K) with this amount of energy (c_{water} = 4.18 J g^{-1} K^{-1}) ?
  $M_{water} = E / (c\Delta T) =$ 239 kg
- What is the effect of a 1 GeV particle in 1 liter water (at 20° C)?
  $\Delta T = \mathrm{E} / (\mathrm{c} \cdot M_{water})$ = $3.8 \cdot 10^{-14}$ K !

There must be more sensitive methods than measuring ΔT !

Calorimetry

- Basic mechanism for calorimetry in paricle physics: formation of
  - ⇨ electromagnetic
  - ⇨ or hadronic showers.
- Finally, the energy is converted into ionization or excitation of the matter.

- Calorimetry is a “destructive” method. The energy and the particle get absorbed!
- Detector response $\propto$ E
- Calorimetry works both for
  - ⇨ charged ($e^{\pm}$ and hadrons) → Complementary information to p-measurement
  - ⇨ and neutral particles (n,γ) → Only way to get direct kinematical information for neutral particles

Interaction of charged particles

Energy loss by Bremsstrahlung

Radiation of real photons in the Coulomb field of the nuclei of the absorber medium

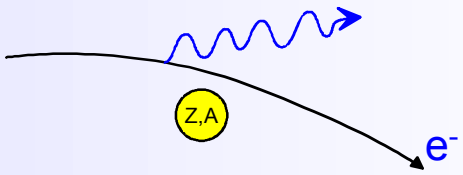

$$-\frac{dE}{dx} = 4\alpha N_A \frac{Z^2}{A} z^2 \left(\frac{1}{4\pi\varepsilon_0}\frac{e^2}{mc^2}\right)^2 E \ln\frac{183}{Z^{1/3}} \propto \frac{E}{m^2}$$

Effect plays a role only for $e^{\pm}$ and ultra-relativistic μ (>1000 GeV)

For electrons: $-\frac{dE}{dx} = 4\alpha N_A \frac{Z^2}{A} r_e^2 E \ln\frac{183}{Z^{1/3}}$

$$-\frac{dE}{dx} = \frac{E}{X_0} \quad \Rightarrow \quad E = E_0\, e^{-x/X_0}$$

$$X_0 = \frac{A}{4\alpha N_A Z^2 r_e^2 \ln\frac{183}{Z^{1/3}}}$$

radiation length [g/cm^2]

(divide by specific density to get X_0 in cm)

Interaction of charged particles

Critical energy E_c

$$\left.\frac{dE}{dx}(E_c)\right|_{Brems} = \left.\frac{dE}{dx}(E_c)\right|_{ion}$$

For electrons one finds approximately:

$$E_c^{solid+liq} = \frac{610MeV}{Z+1.24} \qquad E_c^{gas} = \frac{710MeV}{Z+1.24}$$

$E_c(e^-)$ in Cu(Z=29) = 20 MeV

For muons $E_c \approx E_c^{elec}\left(\frac{m_\mu}{m_e}\right)^2$

$E_c(\mu)$ in Cu $\approx$ 1 TeV

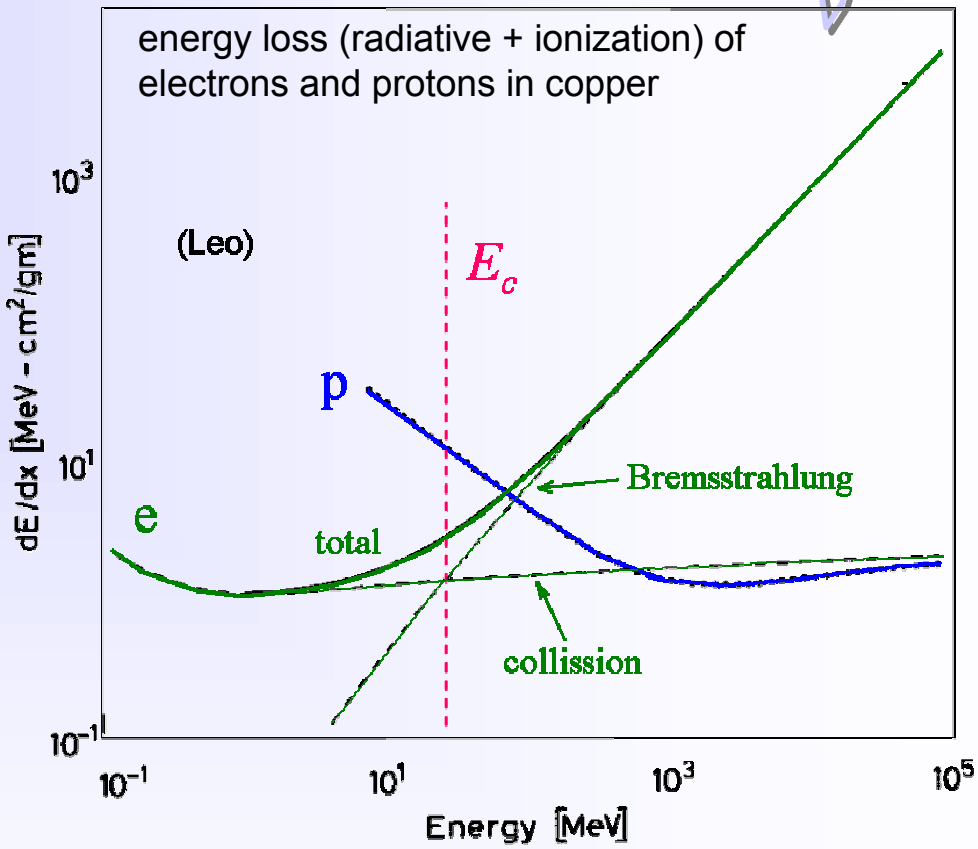

Unlike electrons, muons in multi-GeV range can traverse thick layers of dense matter.
Find charged particles traversing the calorimeter ? → most likely a muon → Particle ID

Interaction of photons

In order to be detected, a photon has to create charged particles and / or transfer energy to charged particles

- **Photo-electric effect:** (already met in photocathodes of photodetectors)

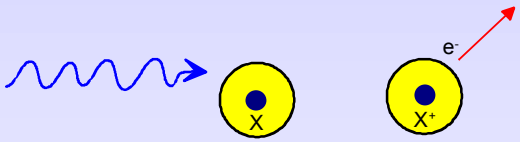

Only possible in the close neighborhood of a third collision partner → photo effect releases mainly electrons from the K-shell.

$$\gamma + \text{atom} \rightarrow \text{atom}^{+} + e^{-}$$

Cross section shows strong modulation if $E_\gamma \approx E_{shell}$

$$\sigma^{K}_{photo} = \left(\frac{32}{\varepsilon^7}\right)^{\frac{1}{2}} \alpha^4 Z^5 \sigma^{e}_{Th} \qquad \varepsilon = \frac{E_\gamma}{m_e c^2} \qquad \sigma^{e}_{Th} = \frac{8}{3}\pi r_e^2 \quad \text{(Thomson)}$$

At high energies ($\varepsilon >> 1$)

$$\sigma^{K}_{photo} = 4\pi r_e^2 \alpha^4 Z^5 \frac{1}{\varepsilon} \qquad \boxed{\sigma_{photo} \propto Z^5}$$

Interaction of photons

Compton scattering:

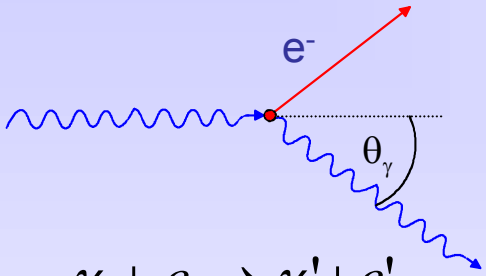

$$\gamma + e \rightarrow \gamma' + e'$$

$$E'_\gamma = E_\gamma \frac{1}{1+\varepsilon\left(1-\cos\theta_\gamma\right)}$$

$$E_e = E_\gamma - E'_\gamma$$

Assume electron as quasi-free.

Klein-Nishina $\frac{d\sigma}{d\Omega}(\theta,\varepsilon)$

Compton cross-section (Klein-Nishina)

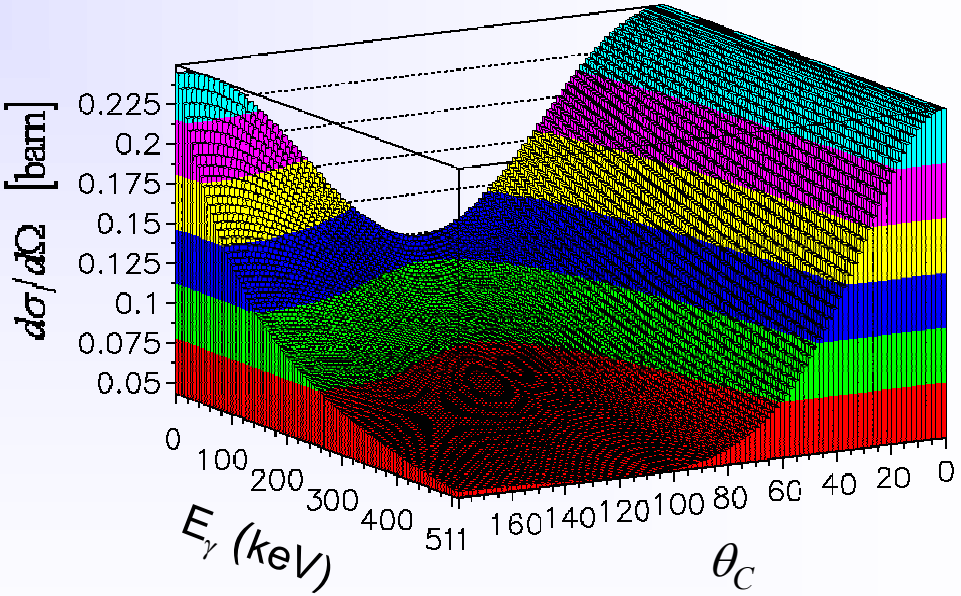

At high energies approximately

$$\sigma_c^e \propto \frac{\ln\varepsilon}{\varepsilon}$$

Atomic Compton cross-section:

$$\sigma_c^{atomic} = Z \cdot \sigma_c^e$$

Interaction of photons

Pair production

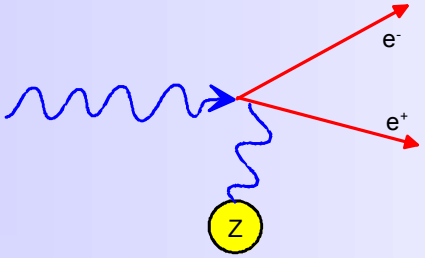

$$\gamma + nucleus \rightarrow e^+e^- + nucleus$$

Only possible in the Coulomb field of a nucleus (or an electron) if $E_\gamma \geq 2m_e c^2$

Cross-section (high energy approximation)

$$\sigma_{pair} \approx 4\alpha r_e^2 Z^2 \left(\frac{7}{9}\ln\frac{183}{Z^{\frac{1}{3}}}\right)$$

independent of energy !

$$\approx \frac{7}{9}\frac{A}{N_A}\frac{1}{X_0}$$

$$\approx \frac{A}{N_A}\frac{1}{\lambda_{pair}}$$

$$\lambda_{pair} = \frac{9}{7}X_0$$

Energy sharing between e^+ and e^- becomes asymmetric at high energies.

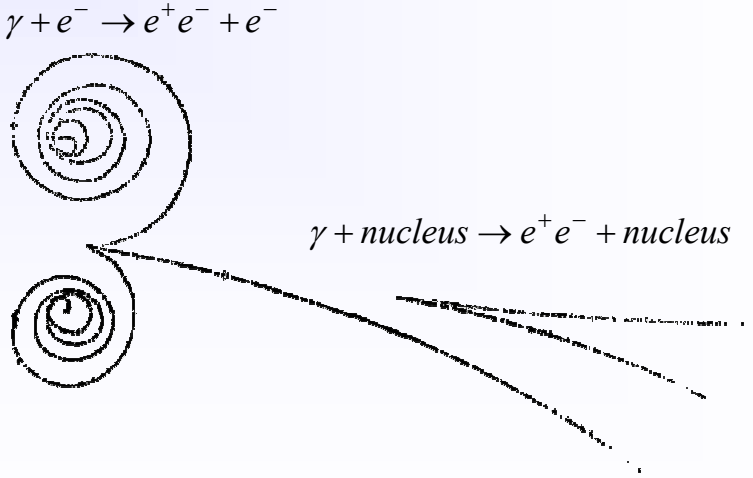

Interaction of photons

In summary: $I_\gamma = I_0 e^{-\mu x}$

μ: mass attenuation coefficient $\mu_i = \frac{N_A}{A}\sigma_i \quad \left[cm^2/g\right]$ $\mu = \mu_{photo} + \mu_{Compton} + \mu_{pair} + \ldots$

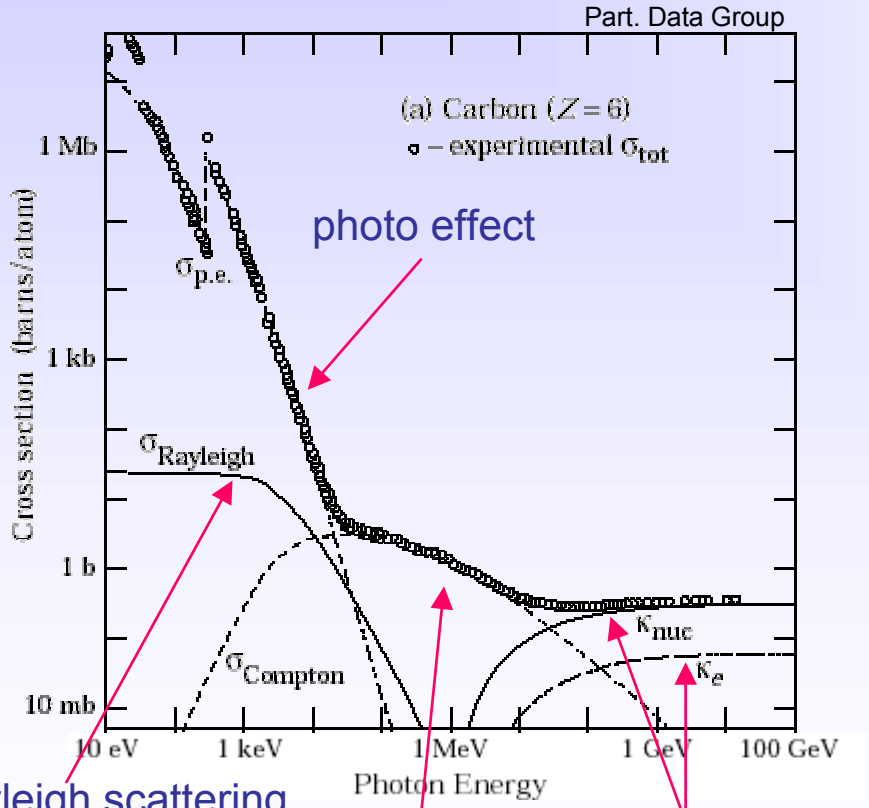

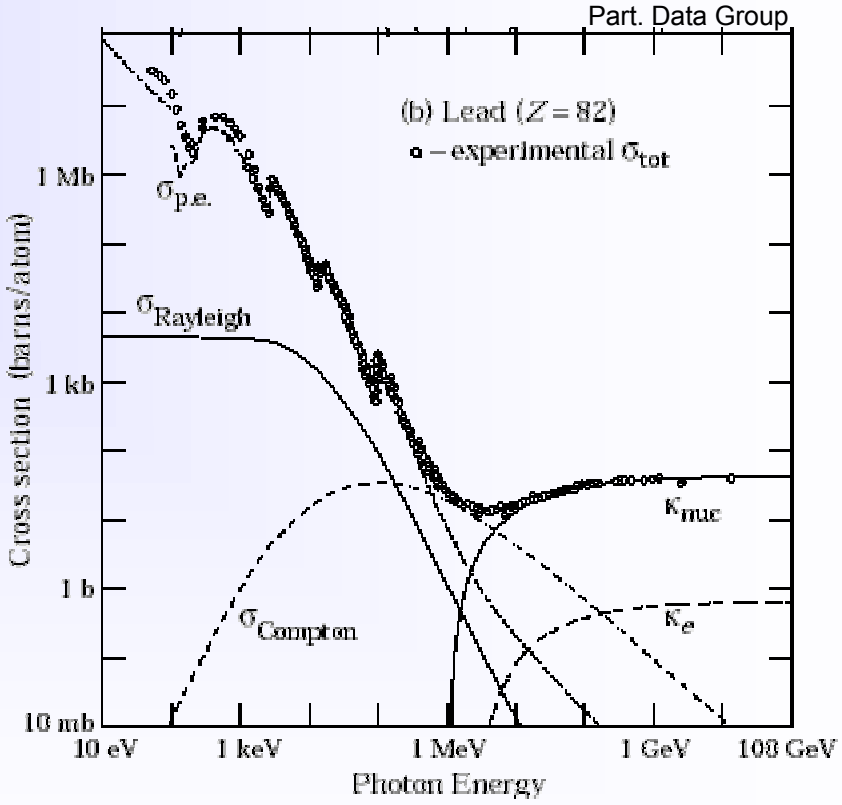

Reminder: basic electromagnetic interactions

e^+ / e^-

- Ionisation

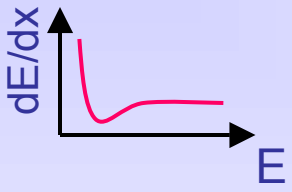

- Bremsstrahlung

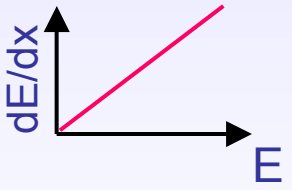

γ

- Photoelectric effect

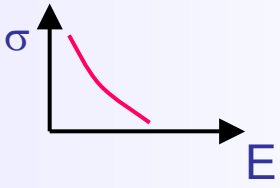

- Compton effect

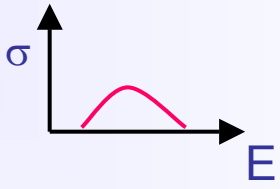

- Pair production

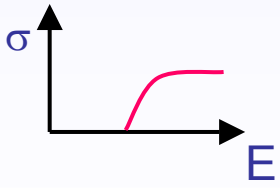

Electromagnetic cascades (showers)

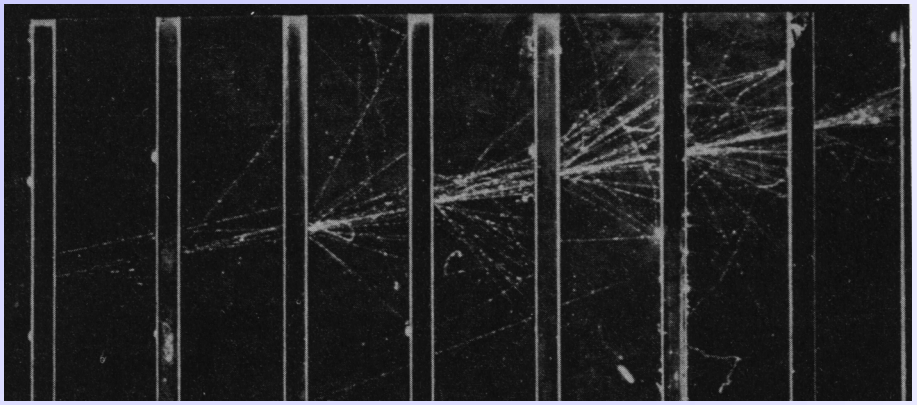

Electron shower in a cloud chamber with lead absorbers

Simple qualitative model

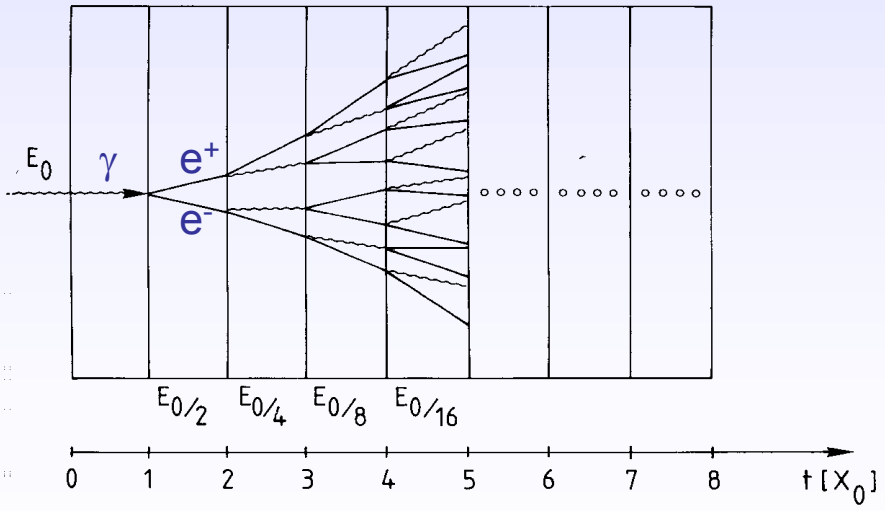

- Consider only Bremsstrahlung and (symmetric) pair production.
- Assume: $X_0 \sim \lambda_{pair}$

$$N(t) = 2^t \qquad E(t)/particle = E_0 \cdot 2^{-t}$$

Process continues until $E(t) < E_c$

$$N^{total} = \sum_{t=0}^{t_{max}} 2^t = 2^{(t_{max}+1)} - 1 \approx 2 \cdot 2^{t_{max}} = 2\frac{E_0}{E_c}$$

$$t_{max} = \frac{\ln E_0/E_c}{\ln 2}$$

After $t = t_{max}$ the dominating processes are ionization, Compton effect and photo effect → absorption of energy.

Electromagnetic cascades

Longitudinal shower development

$$\frac{dE}{dt} \propto t^{\alpha} e^{-t}$$

Shower maximum at $t_{\max} = \ln \frac{E_0}{E_c} \frac{1}{\ln 2}$

95% containment $t_{95\%} \approx t_{\max} + 0.08Z + 9.6$

Size of a calorimeter grows only logarithmically with E_0

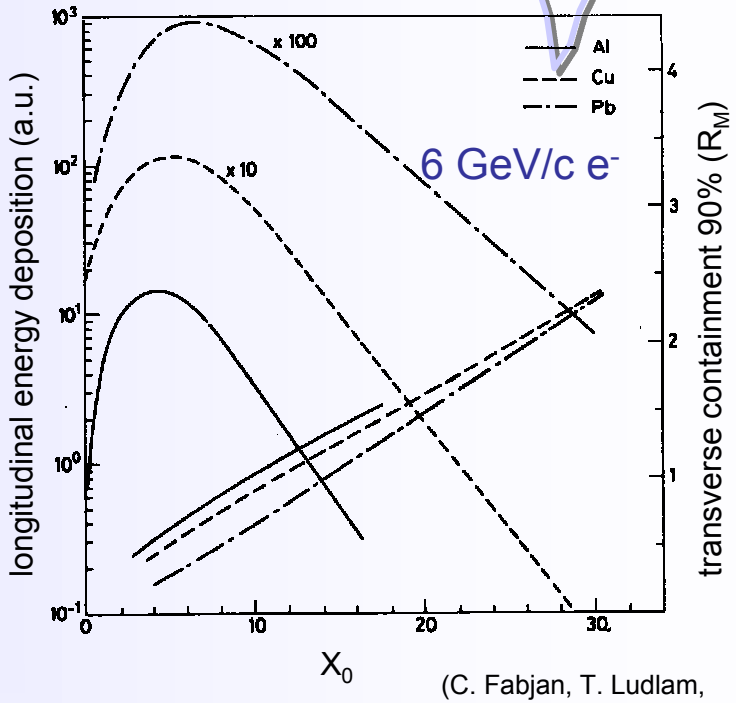

(C. Fabjan, T. Ludlam, CERN-EP/82-37)

Transverse shower development

95% of the shower cone is located in a cylinder with radius 2 R_M

Molière radius $R_M = \frac{21\,\text{MeV}}{E_c} X_0 \quad [g/cm^2]$

Example: E_0 = 100 GeV in lead glass

E_c=11.8 MeV $\rightarrow$ $t_{max} \approx 13$, $t_{95\%} \approx 23$

$X_0 \approx 2$ cm, $R_M = 1.8 \cdot X_0 \approx 3.6$ cm

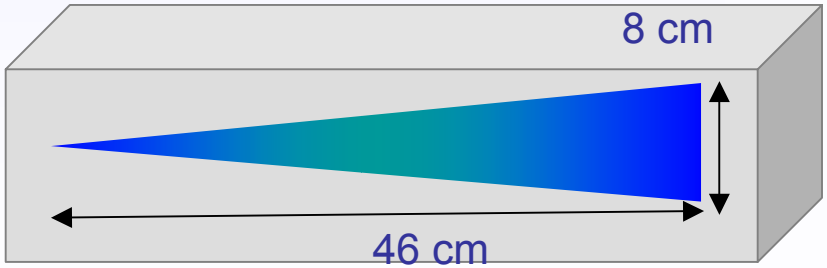

Energy resolution of a calorimeter

$N^{total} \propto \frac{E_0}{E_c}$ total number of track segments

$T \propto \frac{E_0}{E_c} X_0$ total track length

$T_{\det} = F(\xi) T \qquad \zeta \propto \frac{E_{cut}}{E_c}$ detectable track length (above energy E_{cut})

$\frac{\sigma(E)}{E} \propto \frac{\sigma(T_{\det})}{T_{\det}} \propto \frac{1}{\sqrt{T_{\det}}} \propto \frac{1}{\sqrt{E_0}}$ holds also for hadron calorimeters

More general: $\frac{\sigma(E)}{E} = \frac{a}{\sqrt{E}} \oplus b \oplus \frac{c}{E}$

Also spatial and angular resolution scale like $1/\sqrt{E}$

stochastic term
(see above)

'constant term'

- inhomogenities
- bad cell inter-calibration
- non-linearities

Quality factor !

'noise term'

- Electronic noise
- radioactivity
- pile up

Nuclear Interactions

The interaction of energetic hadrons (charged or neutral) with matter is determined by inelastic nuclear processes.

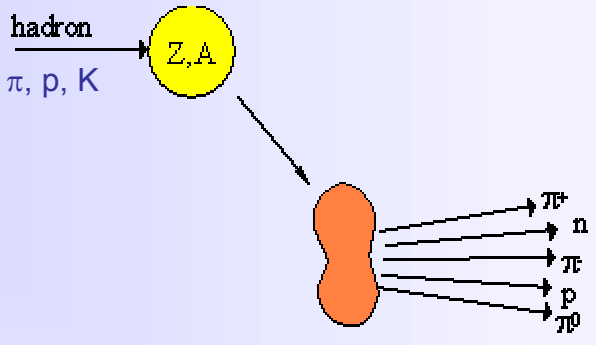

Excitation and finally break-up of nucleus
→ nucleus fragments
+ production of secondary particles.

multiplicity ∝ ln(*E*)

$p_t \approx 0.35$ GeV/c

For high energies (>1 GeV) the cross-sections depend only little on the energy and on the type of the incident particle (π, p, K…).

$$\sigma_{inel} \approx \sigma_0 A^{0.7} \qquad \sigma_0 \approx 35\ mb$$

In analogy to X_0 a hadronic absorption length can be defined

$$\lambda_a = \frac{A}{N_A \sigma_{inel}} \propto A^{\frac{1}{4}} \quad \text{because} \quad \sigma_{inel} \approx \sigma_0 A^{0.7}$$

similarly a hadronic interaction length

$$\lambda_I = \frac{A}{N_A \sigma_{total}} \propto A^{\frac{1}{3}} \qquad \lambda_I < \lambda_a$$

Interaction of charged particles

Material	Z	A	ρ [g/cm^3]	X_0 [g/cm^2]	λ_I [g/cm^2]
Hydrogen (gas)	1	1.01	0.0899 (g/l)	63	50.8
Helium (gas)	2	4.00	0.1786 (g/l)	94	65.1
Beryllium	4	9.01	1.848	65.19	75.2
Carbon	6	12.01	2.265	43	86.3
Nitrogen (gas)	7	14.01	1.25 (g/l)	38	87.8
Oxygen (gas)	8	16.00	1.428 (g/l)	34	91.0
Aluminium	13	26.98	2.7	24	106.4
Silicon	14	28.09	2.33	22	106.0
Iron	26	55.85	7.87	13.9	131.9
Copper	29	63.55	8.96	12.9	134.9
Tungsten	74	183.85	19.3	6.8	185.0
Lead	82	207.19	11.35	6.4	194.0
Uranium	92	238.03	18.95	6.0	199.0

For Z > 6: $\lambda_I > X_0$

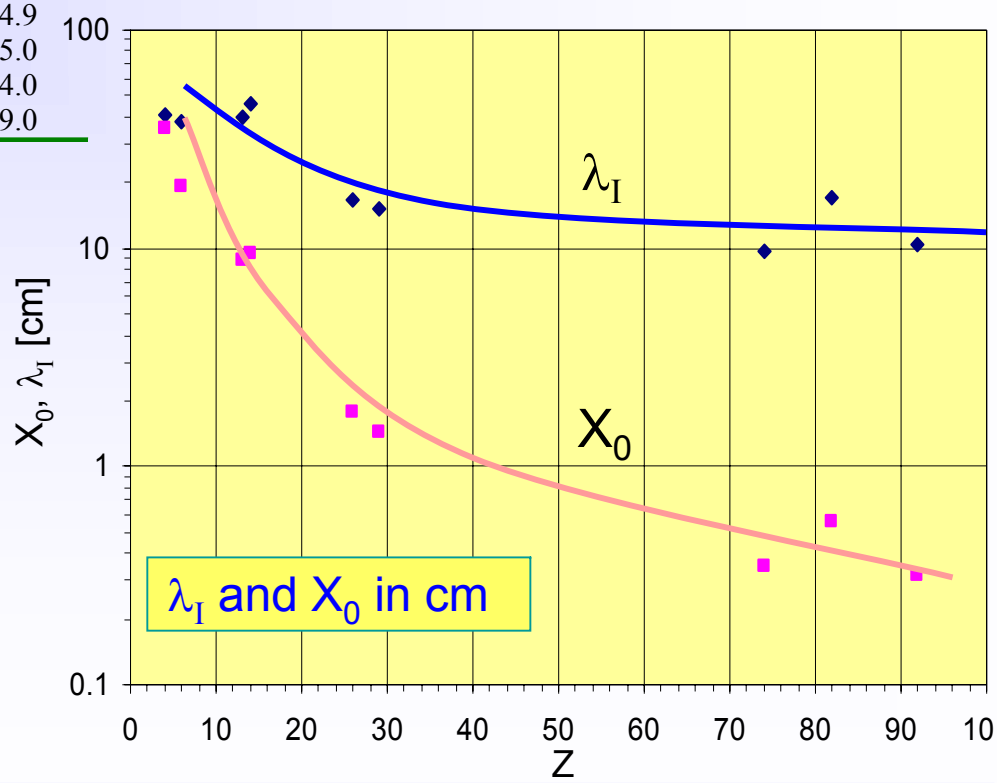

Interaction of neutrons and neutrinos

Interaction of neutrons

Neutrons have no charge, i.e. their interaction is based only on strong (and weak) nuclear force. To detect neutrons, we have to create charged particles.
Possible neutron conversion and elastic reactions …

$n + {}^{6}Li \rightarrow \alpha + {}^{3}H$
$n + {}^{10}B \rightarrow \alpha + {}^{7}Li$ } $E_n < 20$ MeV
$n + {}^{3}He \rightarrow p + {}^{3}H$

$n + p \rightarrow n + p$ $E_n < 1$ GeV

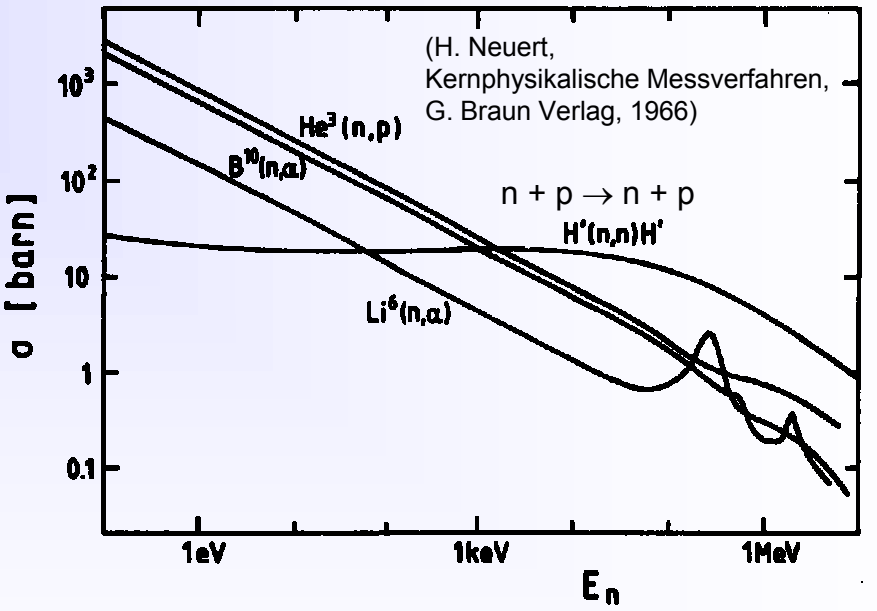

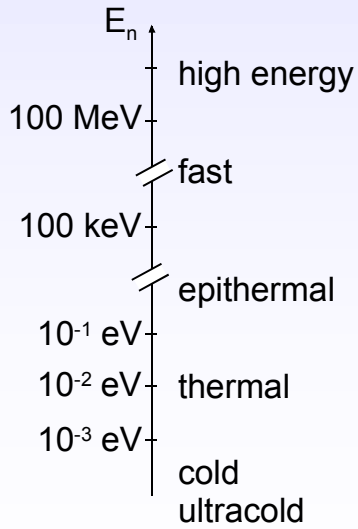

In addition there are …
- neutron induced fission $E_n \approx E_{th} \approx 1/40$ eV
- inelastic reactions → hadronic cascades (see below) $E_n > 1$ GeV

Interaction of neutrons and neutrinos

Interaction of neutrinos

Neutrinos interact only weakly → tiny cross-sections. For their detection we need again first a charged particle. Possible detection reactions:

$\nu_\ell + n \rightarrow \ell^- + p \quad \ell = e, \mu, \tau$

$\bar{\nu}_\ell + p \rightarrow \ell^+ + n \quad \ell = e, \mu, \tau$

The cross-section for the reaction $\nu_e + n \rightarrow e^- + p$ is of the order of 10^{-43} cm^2 (per nucleon, $E_\nu \approx$ few MeV).

→ detection efficiency $\varepsilon_{\text{det}} = \sigma \cdot N^{surf} = \sigma \cdot \rho \frac{N_A}{A} d$

1 m Iron: $\varepsilon_{\text{det}} \approx 5 \cdot 10^{-17}$

1 km water: $\varepsilon_{\text{det}} \approx 6 \cdot 10^{-15}$

Neutrino detection requires big and massive detectors (ktons - Mtons) and very high neutrino fluxes (e.g. 10^{20} ν / yr).

In collider experiments fully hermetic detectors allow to detect neutrinos indirectly:

- sum up all visible energy and momentum.
- attribute missing energy and momentum to neutrino.

Hadronic cascades

Various processes involved.
Much more complex than electromagnetic cascades.

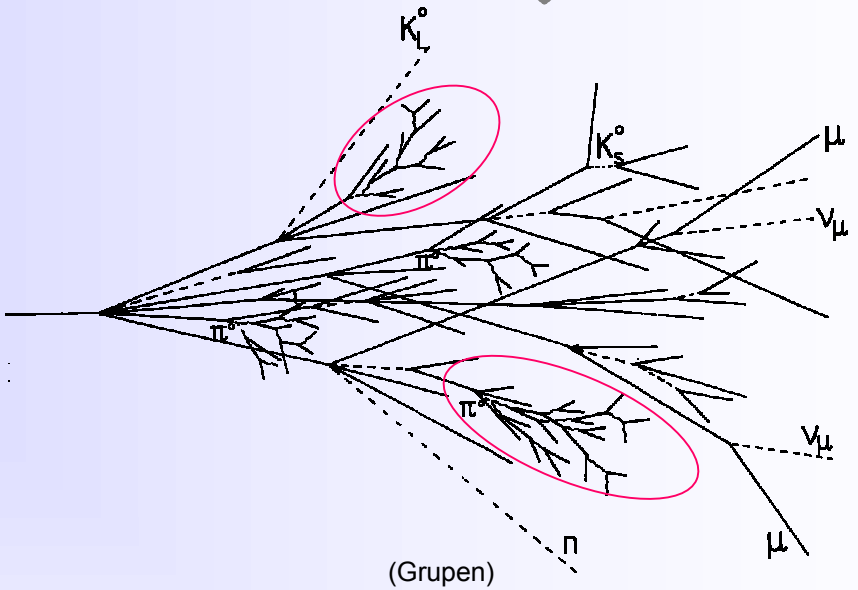

(Grupen)

A hadronic shower contains two components:

hadronic + **electromagnetic**

- charged hadrons p,$\pi^{\pm}$,$K^{\pm}$,
- nuclear fragmets ….
- breaking up of nuclei (binding energy)
- neutrons, neutrinos, soft γ's, muons

neutral pions $\rightarrow 2\gamma$

$\rightarrow$ electromagnetic cascades

$$n(\pi^0) \approx \ln E(GeV) - 4.6$$

example $E = 100$ GeV: $n(\pi^0) \approx 18$

invisible energy $\rightarrow$ large energy fluctuations $\rightarrow$ limited energy resolution

Hadronic cascades

- Longitudinal shower development

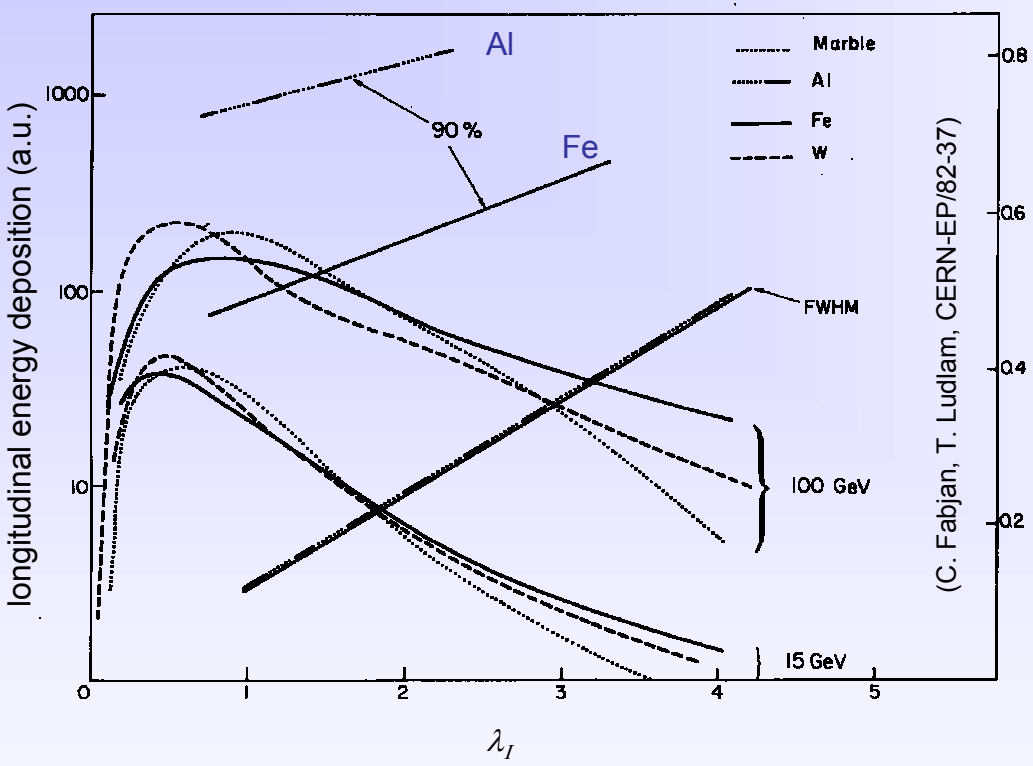

$$t_{\max}[\lambda_I] \approx 0.2 \ln E[GeV] + 0.7$$
$$t_{95\%}[cm] \approx a \ln E + b$$

Ex.: 100 Gev in iron (λ_i =16.7 cm)

a = 9.4, b = 39
→ t_{max} = 1.6 λ_i = 27 cm
→ $t_{95\%}$ = 4.9 λ_i = 80 cm

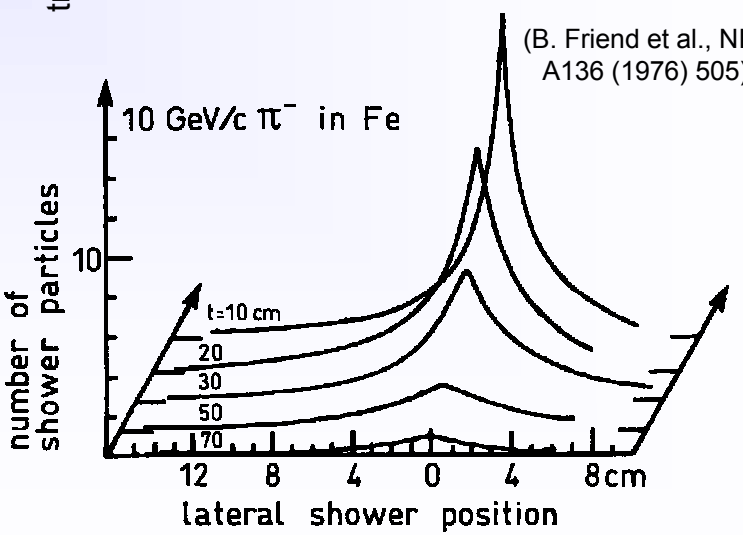

- Laterally shower consists of core + halo.
  95% containment in a cylinder of radius λ_I.

Hadronic showers are much longer and broader than electromagnetic ones !

Hadronic cascades

The concept of compensation

A hadron calorimeter shows in general different efficiencies for the detection of the hadronic and electromagnetic components ε_h and ε_e.

$$R_h = \varepsilon_h E_h + \varepsilon_e E_e$$

ε_h: hadron efficiency
ε_e: electron efficiency

The fraction of the energy deposited hadronically depends on the energy (remember n(π^0))

$$\frac{E_h}{E} = 1 - f_{\pi^0} = 1 - k \ln E \ \ (GeV) \qquad k \approx 0.1$$

$\rightarrow$ Response of calorimeter to hadron shower becomes non-linear

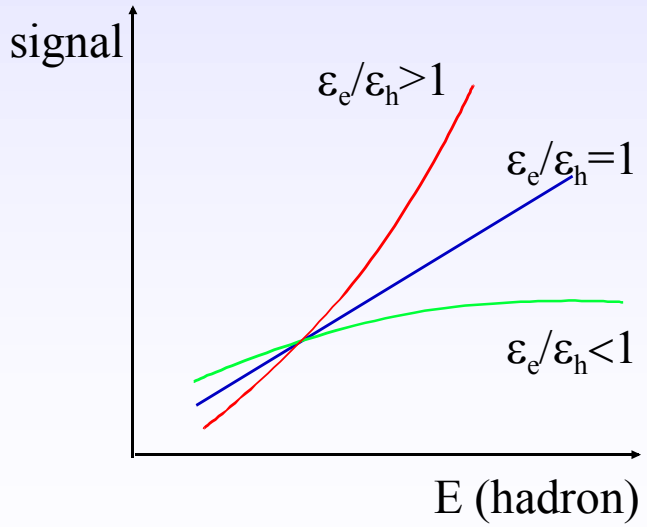

(Schematically after Wigmans R. Wigmans NIM A 259 (1987) 389)

Energy resolution degraded !

$$\frac{\sigma(E)}{E} = \frac{a}{\sqrt{E}} + b \cdot \left| \frac{\varepsilon_e}{\varepsilon_h} - 1 \right|$$

Hadronic cascades

How to achieve compensation?

increase ε_h : use Uranium absorber → amplify neutron and soft γ component by fission + use hydrogeneous detector → high neutron detection efficiency

decrease ε_e : combine high Z absorber with low Z detectors. Suppressed low energy γ detection ($\sigma_{photo} \propto Z^5$)

offline compensation : requires detailed fine segmented shower data → event by event correction.

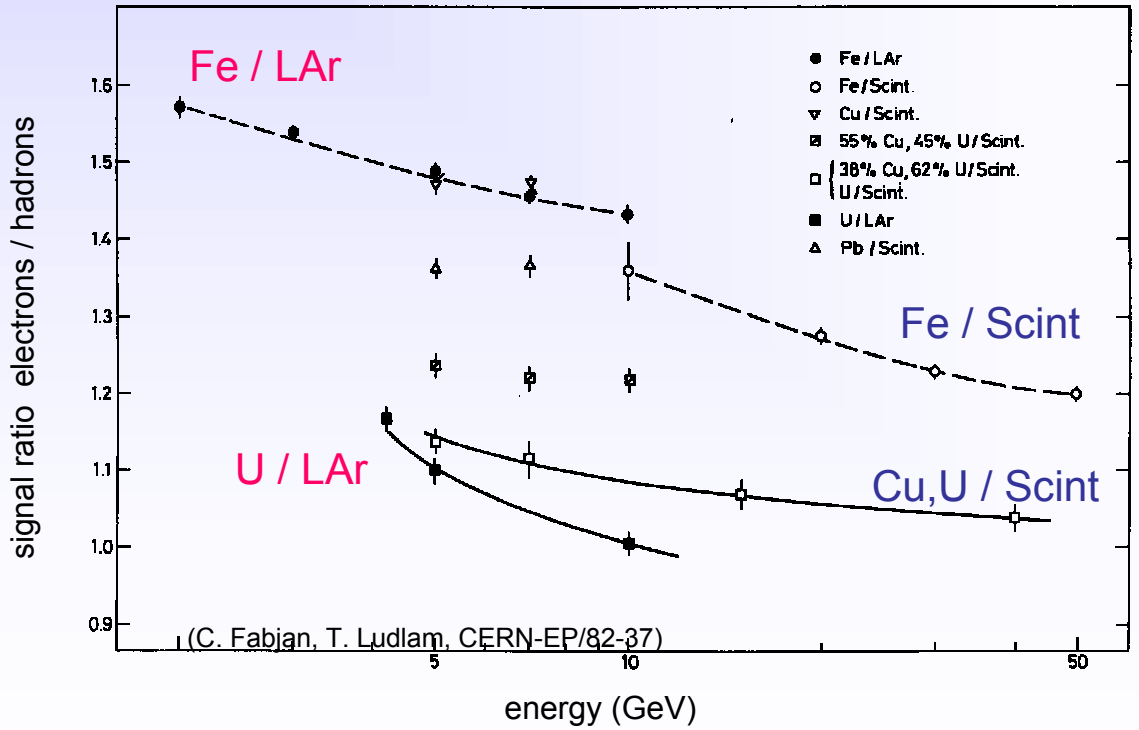

Calorimeter types

Homogeneous calorimeters: Detector = absorber

- ⇨ good energy resolution
- ⇨ limited spatial resolution (particularly in longitudinal direction)
- ⇨ only used for electromagnetic calorimetry

Two main types:

1. Scintillators →

Scintillator	Density [g/cm^3]	X_0 [cm]	Light Yield γ/MeV (rel. yield*)	τ_1 [ns]	λ_1 [nm]	Rad. Dam. [Gy]	Comments
NaI (Tl)	3.67	2.59	4×10^4	230	415	≥10	hydroscopic, fragile
CsI (Tl)	4.51	1.86	5×10^4 (0.49)	1005	565	≥10	Slightly hygroscopic
CSI pure	4.51	1.86	4×10^4 (0.04)	10 36	310 310	10^3	Slightly hygroscopic
BaF_2	4.87	2.03	10^4 (0.13)	0.6 620	220 310	10^5	
BGO	7.13	1.13	8×10^3	300	480	10	
$PbW0_4$	8.28	0.89	≈100	440 broad band 530 broad band		10^4	light yield =f(T)

2. Cherenkov devices ↘

* Relative light yield: rel. to NaI(Tl) readout with PM (bialkali PC)

Material	Density [g/cm^3]	X_0 [cm]	n	Light yield [p.e./GeV] (rel. p.e.*)	λ_{cut} [nm]	Rad. Dam. [Gy]	Comments
SF-5 Lead glass	4.08	2.54	1.67	600 (1.5×10^{-4})	350	10^2	
SF-6 Lead glass	5.20	1.69	1.81	900 (2.3×10^{-4})	350	10^2	
PbF_2	7.66	0.95	1.82	2000 (5×10^{-4})		10^3	Not available in quantity

In both cases the signal consists of photons. Readout via photomultiplier, -diode/triode, APD, HPD

Example ECAL - homogeneous

OPAL Barrel + end-cap electromagnetic calorimeter: lead glass + pre-sampler

(OPAL collab. NIM A 305 (1991) 275)

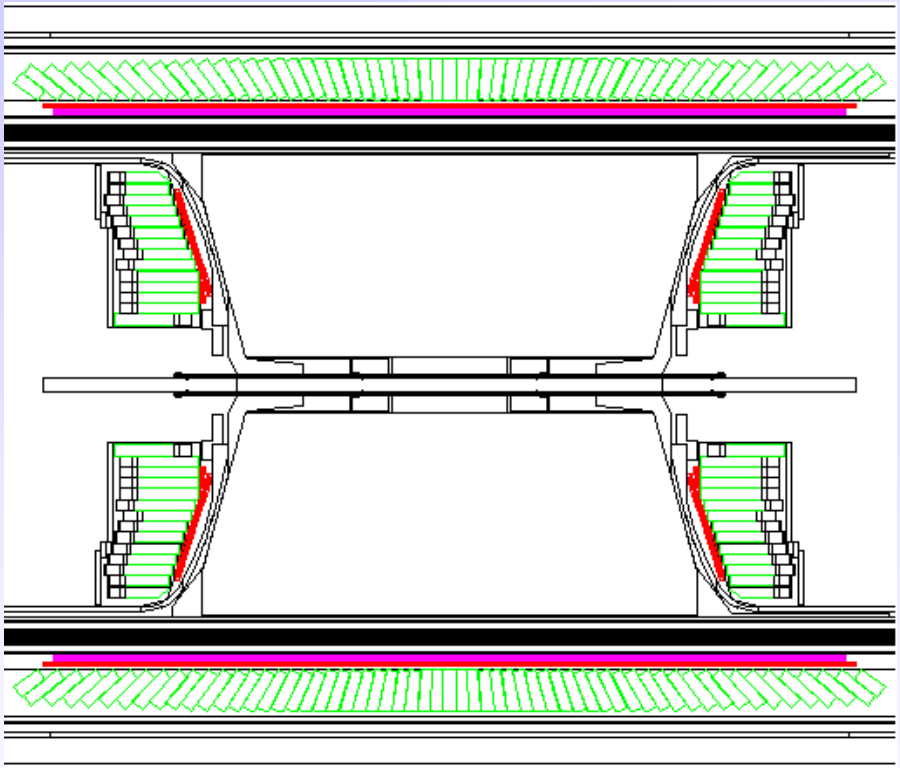

≈10500 blocks (10 x 10 x 37 cm^3, 24.6 X_0), PM (barrel) or PT (end-cap) readout.

$$\sigma(E)/E = 0.06/\sqrt{E} \oplus 0.002$$

Spatial resolution (intrinsic) ≈ 11 mm at 6 GeV

Principle of pre-sampler or pre-shower detector

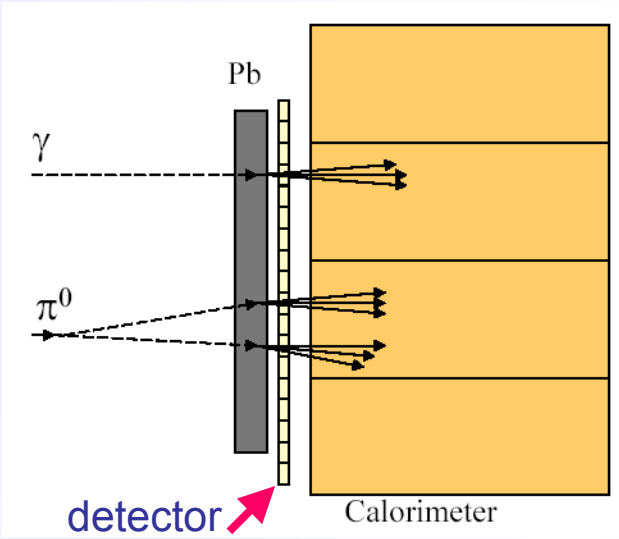

Sample first part of shower with high granularity. Useful for γ/π^0, e/γ, $e/\pi^{\pm}$ discrimination.

Usually gas or, more recently, Si detectors.

Example ECAL - homogeneous

BABAR (SLAC)

6580 CsI(Tl) crystals with
Si-PD readout

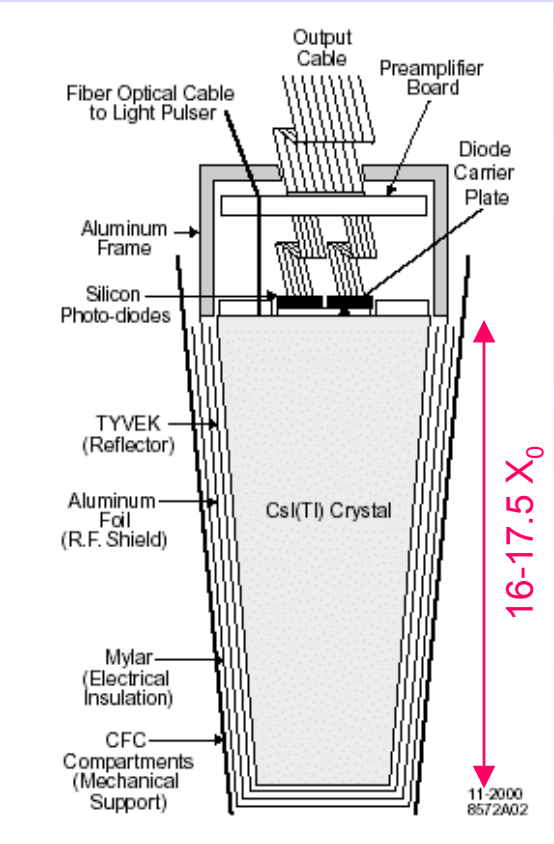

M. Kocian et al. (CALOR 2002)

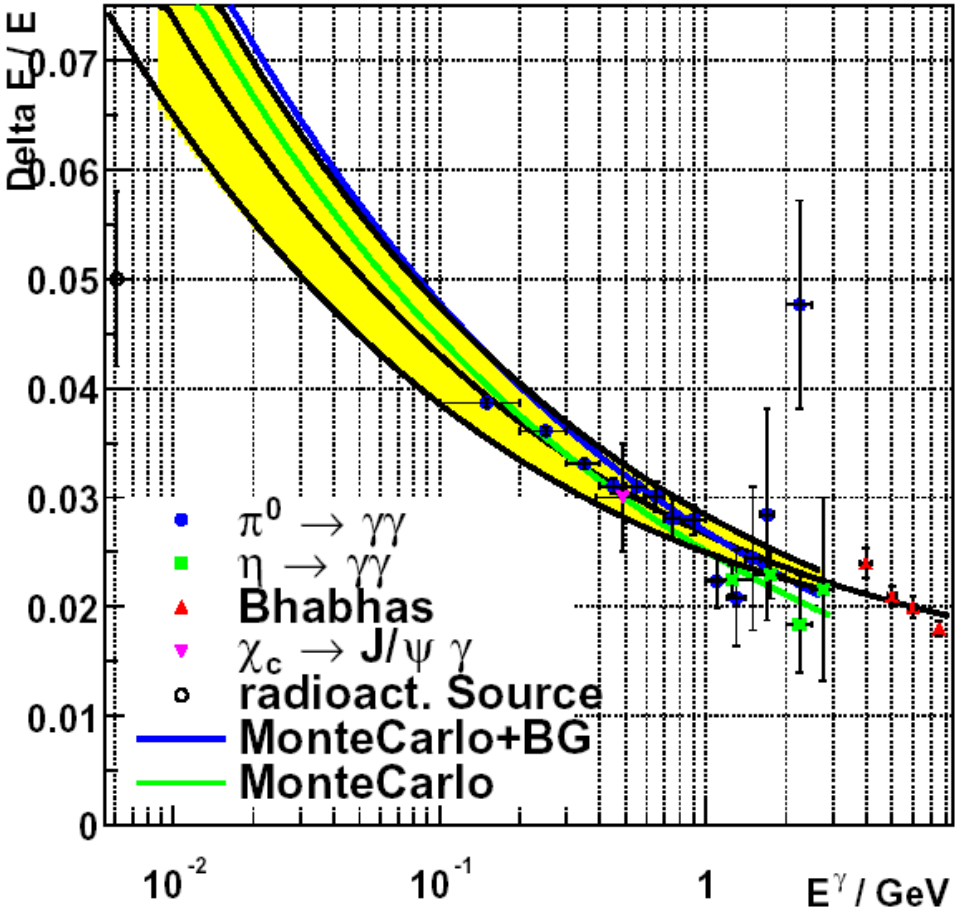

$$\frac{\sigma_E}{E} = \frac{\sigma_1}{\sqrt[4]{E}} \oplus \sigma_2$$

$\sigma_1 = (2.30 \pm 0.03 \pm 0.3)\%$

$\sigma_2 = (1.35 \pm 0.08 \pm 0.2)\%$

resolution drops only with $\sqrt[4]{E}$!

Sampling calorimeters

- **Sampling calorimeters** = Absorber + detector (gaseous, liquid, solid)

- MWPC, streamer tubes
- warm liquids (TMP = tetra-methylpentane, TMS = tetra-methylsilane)
- cryogenic noble gases: mainly LAr (Lxe, LKr)
- scintillators, scintillation fibres, silicon detectors

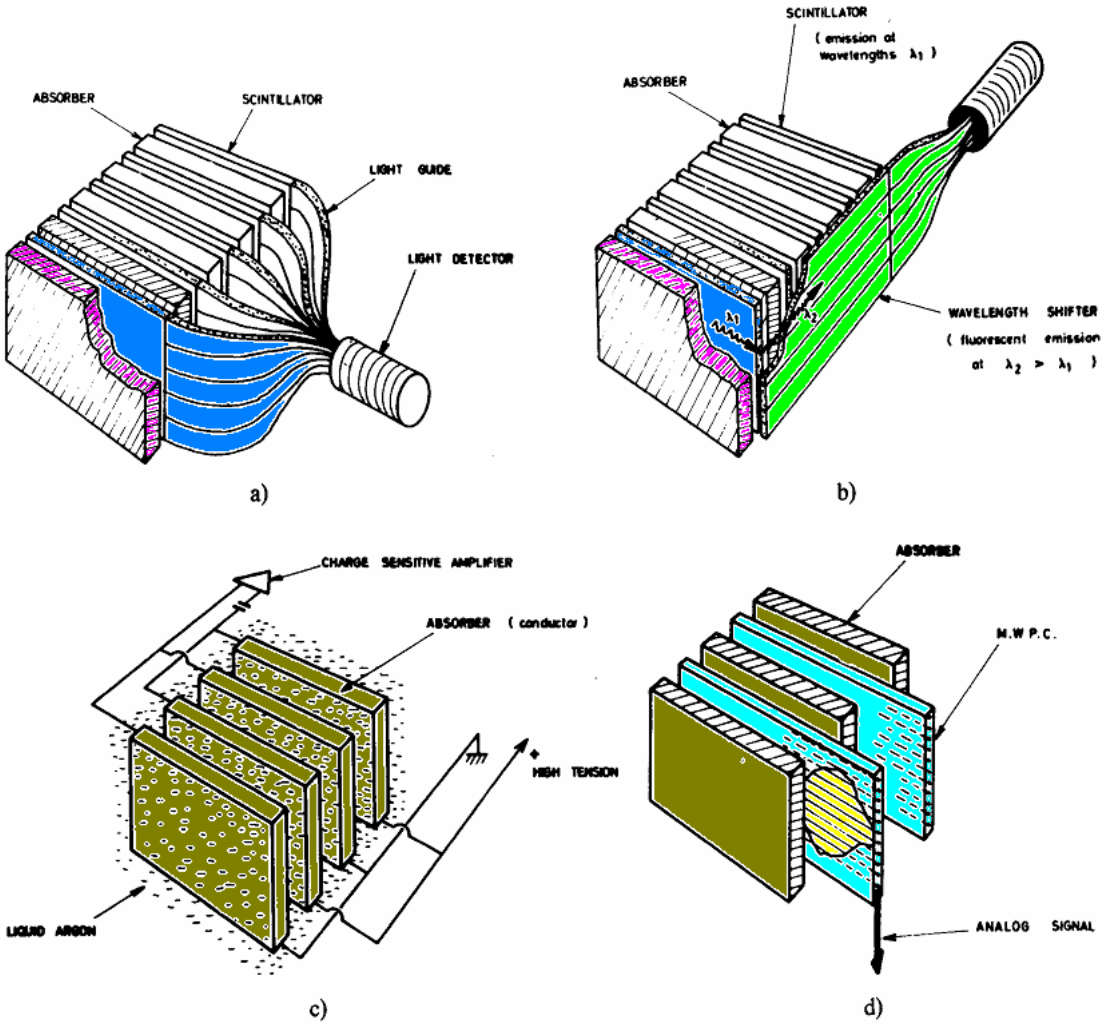

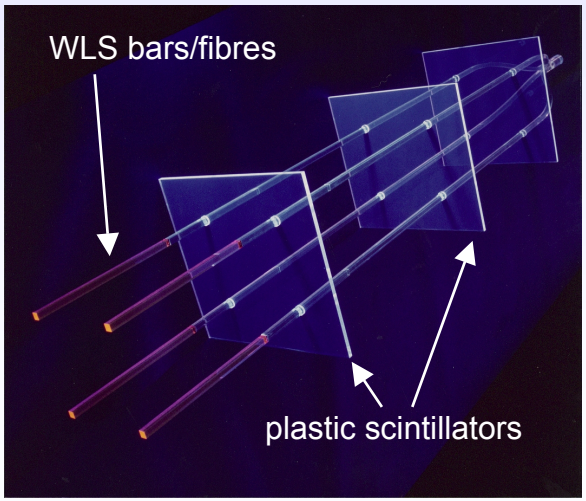

'Shashlik' readout

Sampling calorimeters

Sampling fluctuations

$$N = \frac{T_{\text{det}}}{d}$$ Detectable track segments

$$= F(\xi)\frac{E}{E_c}\frac{X_0}{d} \quad \rightarrow \quad \frac{\sigma(E)}{E} \propto \frac{\sqrt{N}}{N} \propto \frac{1}{\sqrt{F(\xi)}}\sqrt{\frac{E_c}{E}}\sqrt{\frac{d}{X_0}}$$

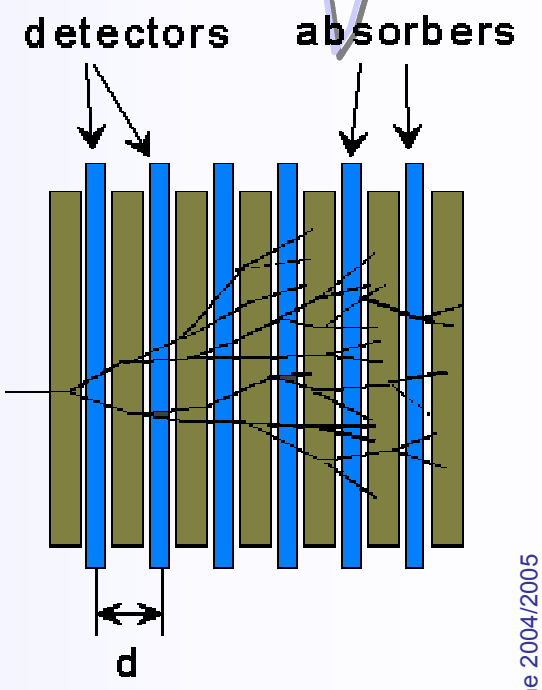

Pathlength fluctuations + Landau fluctuations

wide spread angular distribution of (low energy) $e^{\pm}$

In thin gas detector layers the deposited energy shows typical Landau tails

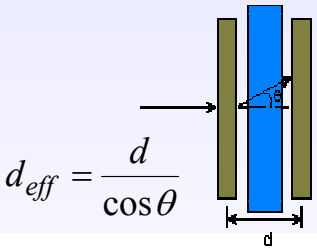

$$d_{eff} = \frac{d}{\cos\theta}$$

(C. Fabjan, T. Ludlam, CERN-EP/82-37)

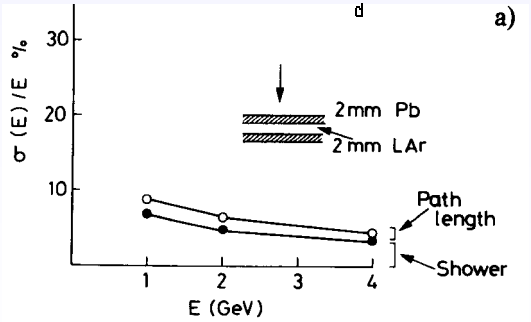

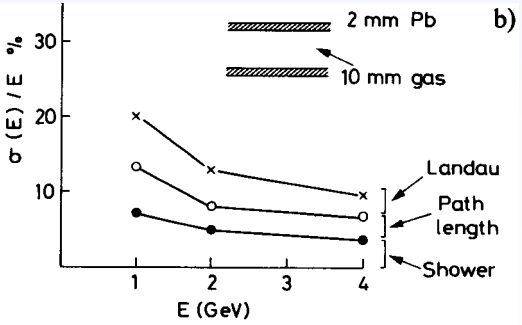

Example ECAL - sampling

Example of a sampling ECAL: DELPHI High Density Projection Chamber (HPC)

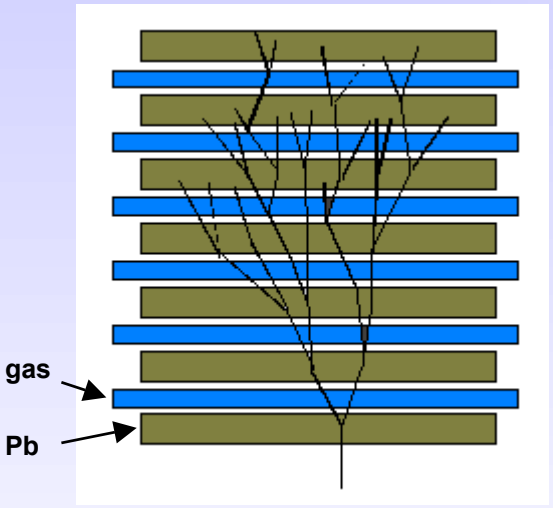

(H.G. Fischer and O. Ullaland, IEEE NS-27 (1980), 38)

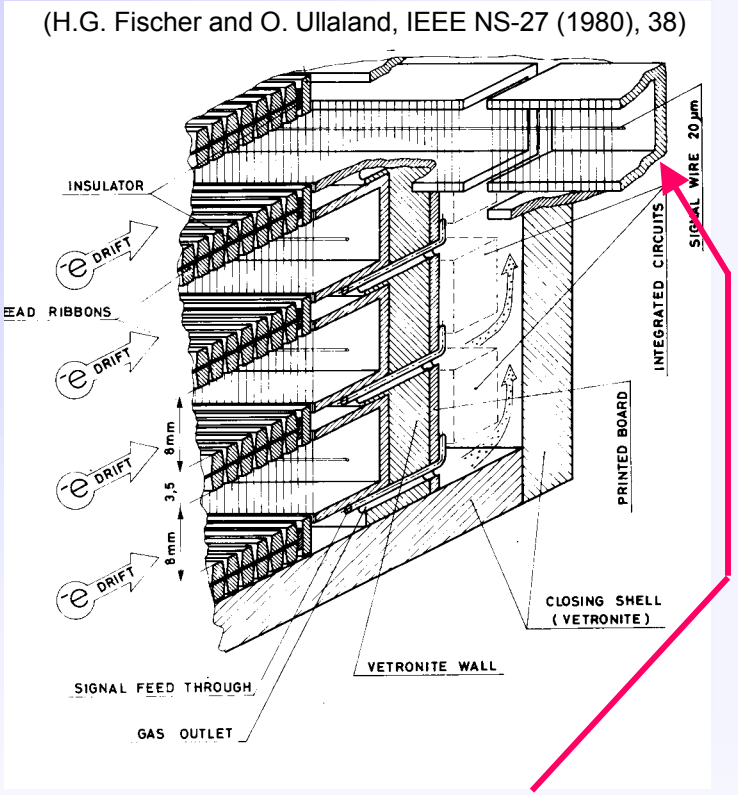

Segmented cathodes + drift times ('TPC')
→ full 3D reconstruction of shower

Transversal charge distribution in the DELPHI HPC

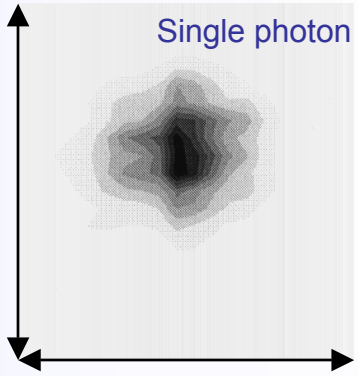

$\Delta\varphi \times \Delta\theta = 1^\circ \times 1^\circ$

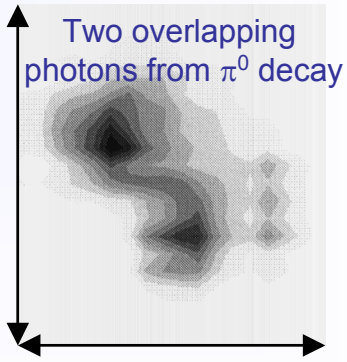

$\Delta\varphi \times \Delta\theta = 1^\circ \times 1^\circ$

(A. Algeri et al. CERN-PPE/95-04)

$$\sigma(E)/E = 0.32/\sqrt{E} \oplus 0.043$$

$$\sigma_\varphi = 1.7 \text{ mrad}, \sigma_\theta = 1.0 \text{ mrad}$$

(HPC was placed behind massive RICH detector !)

CERN Academic Training Programme 2004/2005

Example ECAL - sampling

ATLAS electromagnetic Calorimeter

Accordion geometry absorbers immersed in Liquid Argon

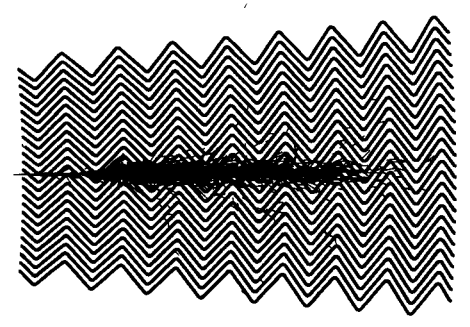

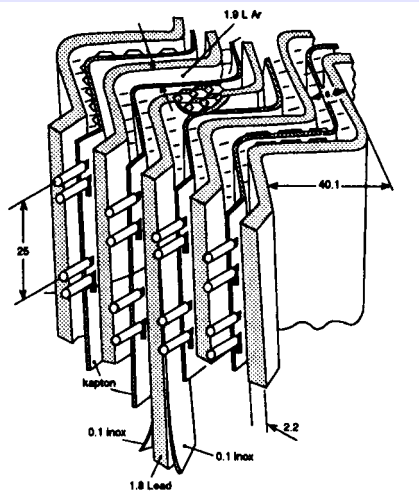

Liquid Argon (90K)

+ lead-steal absorbers (1-2 mm)

+ multilayer copper-polyimide readout boards

→ Ionization chamber.

1 GeV E-deposit → 5 x10^6 e^-

- Accordion geometry minimizes dead zones.
- Liquid Ar is intrinsically radiation hard.
- Readout board allows fine segmentation (azimuth, pseudo-rapidity and longitudinal) acc. to physics needs

Test beam results $\sigma(E)/E = 9.24\%/\sqrt{E} \oplus 0.23\%$

Spatial resolution ≈ 5 mm / √E

Example HCAL - sampling

CMS Hadron calorimeter

Brass absorber + plastic scintillators

2 x 18 wedges (barrel)
+ 2 x 18 wedges (endcap)
~ 1500 T absorber
5.8 λ_i *at* $\eta = 0$.

Scintillators fill slots and are read out via WLS fibres by HPDs (B = 4T!)

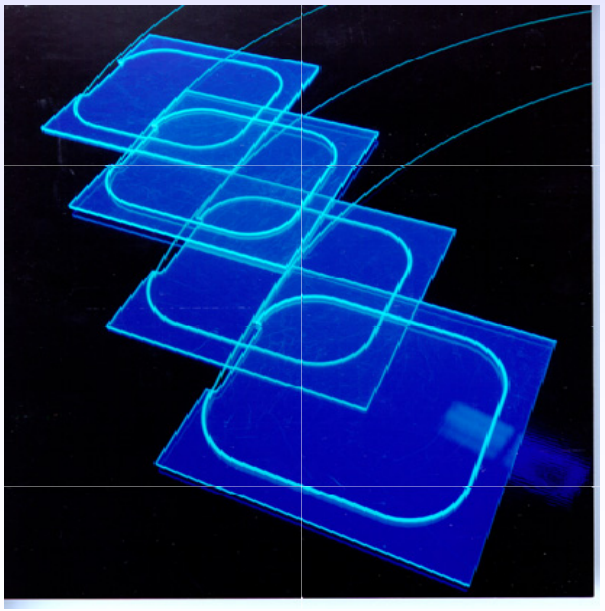

Test beam resolution for single hadrons

$$\frac{\sigma_E}{E} = \frac{65\%}{\sqrt{E}} \oplus 5\%$$

Outline

- **Lecture 1 - Introduction** — C. Joram, L. Ropelewski
- **Lecture 2 - Tracking Detectors** — L. Ropelewski, M. Moll
- **Lecture 3 - Scintillation and Photodetection** — C. D'Ambrosio, T. Gys
- **Lecture 4 – Calorimetry** — C. Joram
- **Lecture 5a - Particle Identification** — C. Joram
  - dE/dx measurement
  - Time of flight
  - Cherenkov detectors
  - Transition radiation detectors
- **Lecture 5b - Detector Systems / Design** — C. D'Ambrosio

Particle Identification

Particle identification is an important aspect of high energy physics experiments.

Some physical quantities are only accessible with sophisticated particle identification (B-physics, CP violation, rare exclusive decays).

One wants to discriminate: π/K, K/p, e/π, γ/π^0 ….

The applicable methods depend strongly on the interesting energy domain.

Depending on the physics case either ε_{xx} or ε_{xy} has to be optimized:

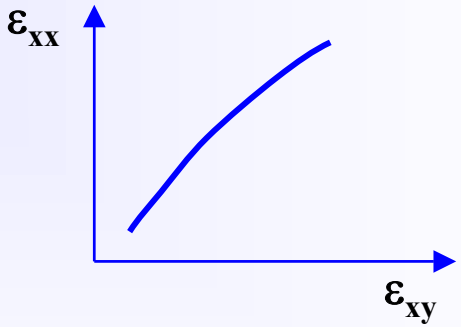

Efficiency: $\varepsilon_{xx} = N_x^{tag} / N_x$

Misidentification: $\varepsilon_{xy} = N_y^{x-tag} / N_y$

Rejection: $R_{xy} = \varepsilon_{xx} / \varepsilon_{xy}$

The performance of a detector can be expressed in terms of the resolving power $D_{x,y}$

$$D_{x,y} = \frac{S_x - S_y}{\sigma_S}$$

S_x and S_y are the signals provided by the detector for particles of types x and y with a resolution σ_S.

Particle Identification - an example

A 'charmless' B decay:

$$B^- \rightarrow K^{*}\pi^-$$
$$\downarrow$$
$$K\pi$$

1 K + 2 π
in final state

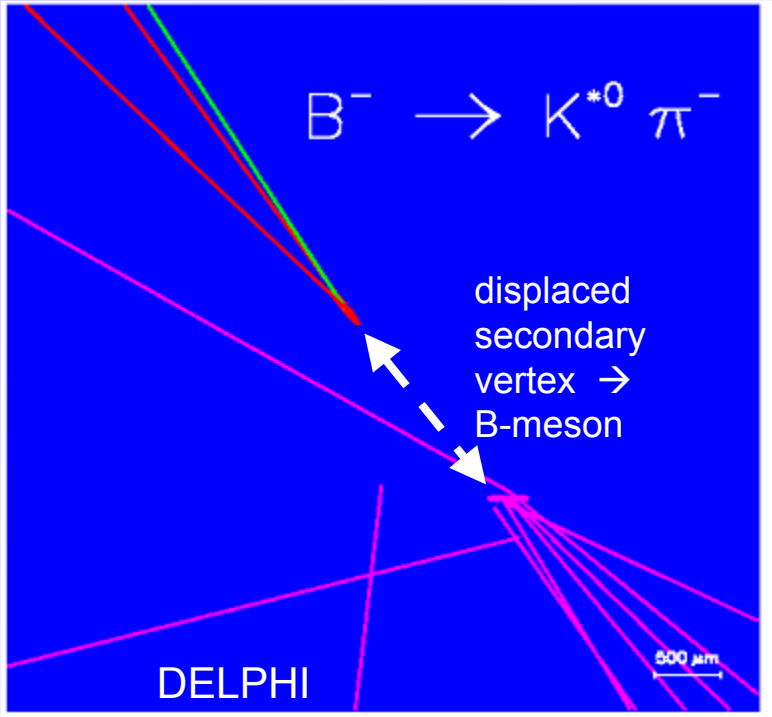

Who is who ?

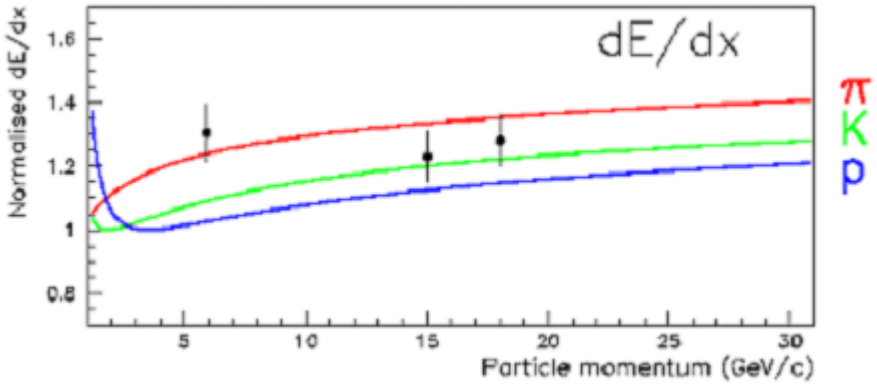

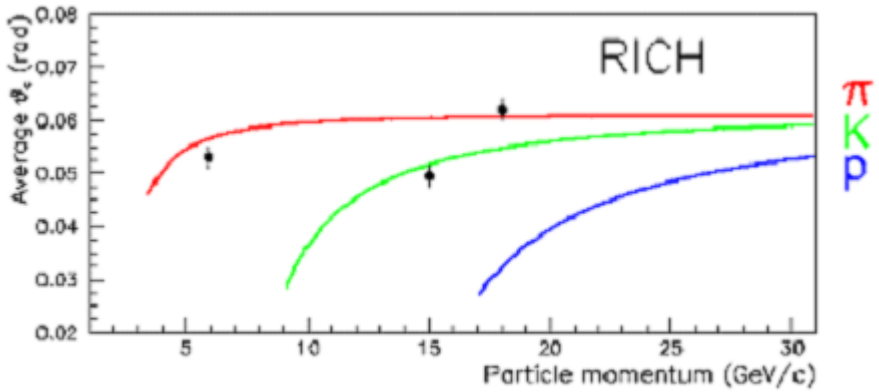

Particle ID through dE/dx

$$p = m_0 \beta\gamma c$$
$$\frac{dE}{dx} \propto \frac{1}{\beta^2} \ln\left(\beta^2\gamma^2\right)$$

Simultaneous measurement of *p* and *dE/dx* defines mass m_0, hence the particle identity

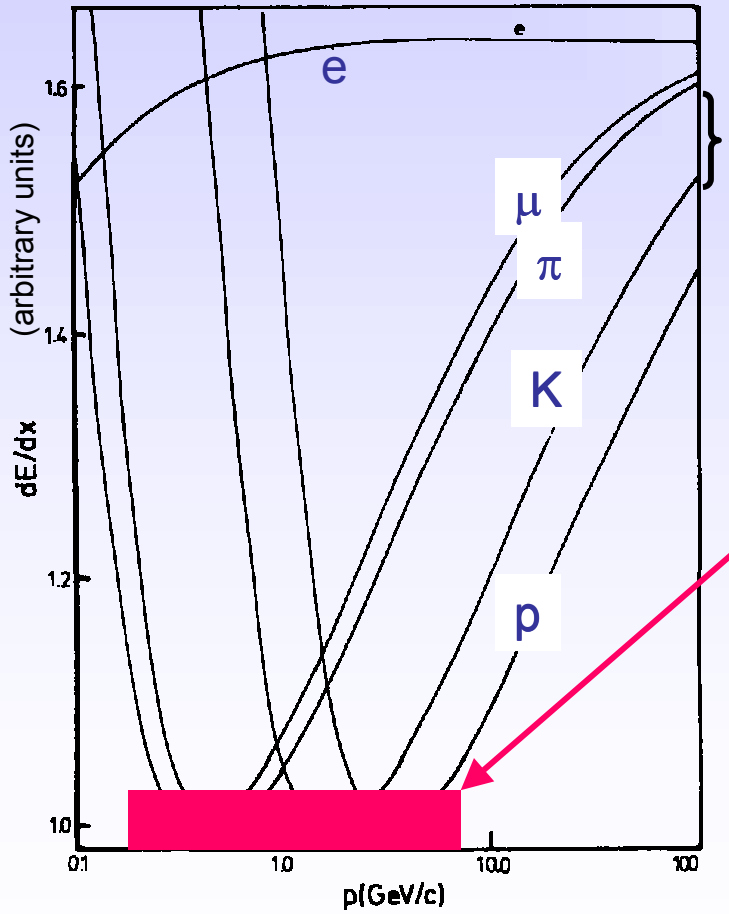

π/K separation (2σ) requires a *dE/dx* resolution of < 5%

Not so easy to achive !

- dE/dx is very similar for minimum ionising particles.
- Energy loss fluctuates and shows Landau tails.

Average energy loss for e, μ, π, K, p in 80/20 Ar/CH_4 (NTP)
(J.N. Marx, Physics today, Oct.78)

Particle ID through dE/dx

How to reduce fluctuations ?

- subdivide track in several dE/dx samples
- calculate truncated mean, i.e. ignore samples with (e.g. 40%) highest values
- Also increased gas pressure can improve resolution (→ higher primary statistics), but it reduces the rel. rise due to density effect !

Don't cut the track into too many slices ! There is an optimum for a given track length L.

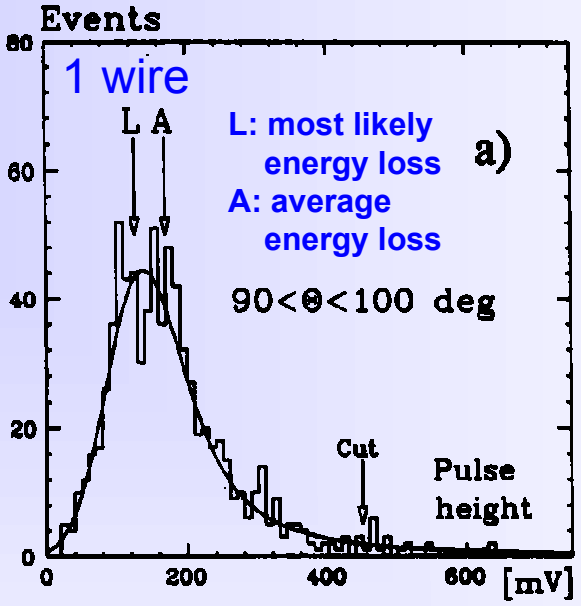

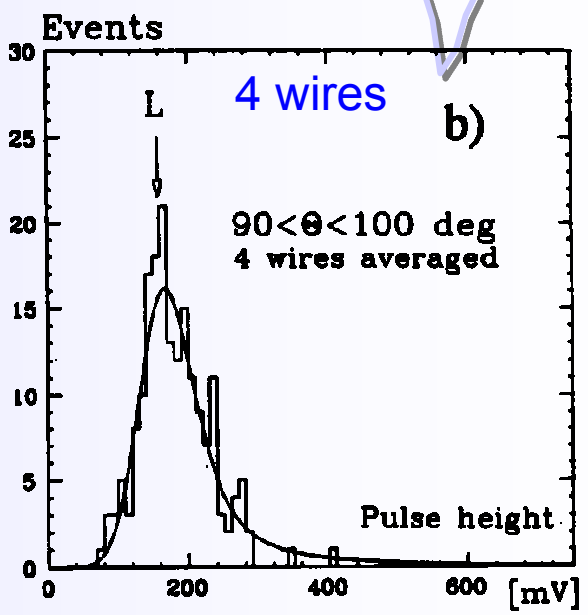

(B. Adeva et al., NIM A 290 (1990) 115)

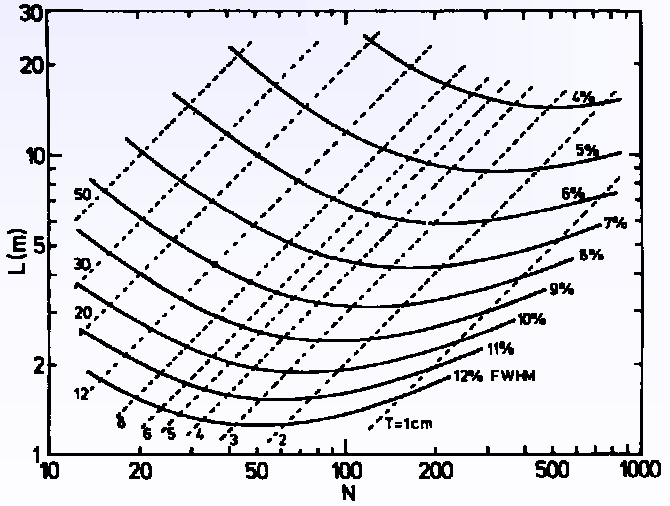

(M. Aderholz, NIM A 118 (1974), 419)

Example ALEPH TPC

- Gas: Ar/CH4 90/10
- $N_{samples}$ = 338
- wire spacing 4 mm
- dE/dx resolution
  ~5% for m.i.p.'s

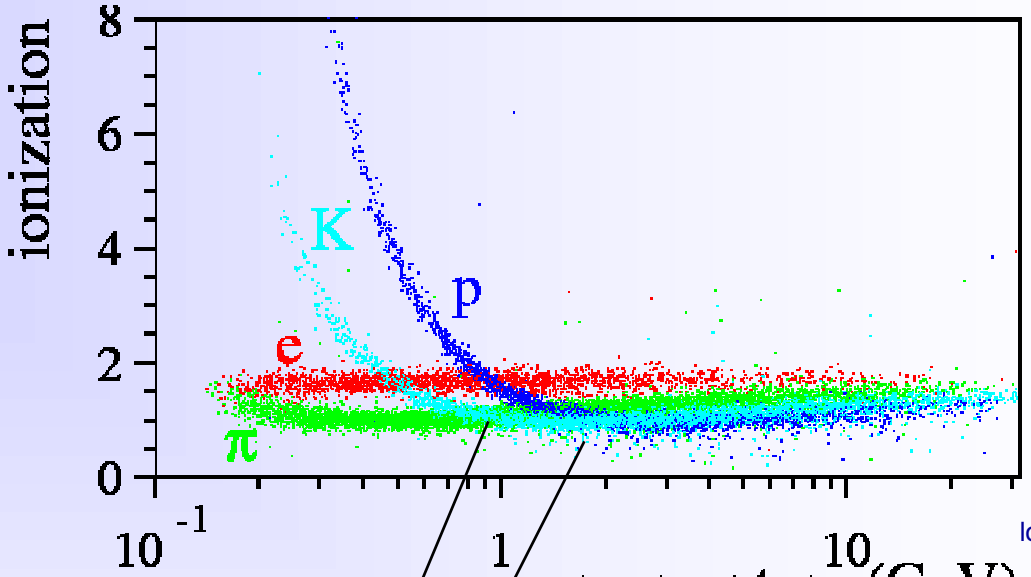

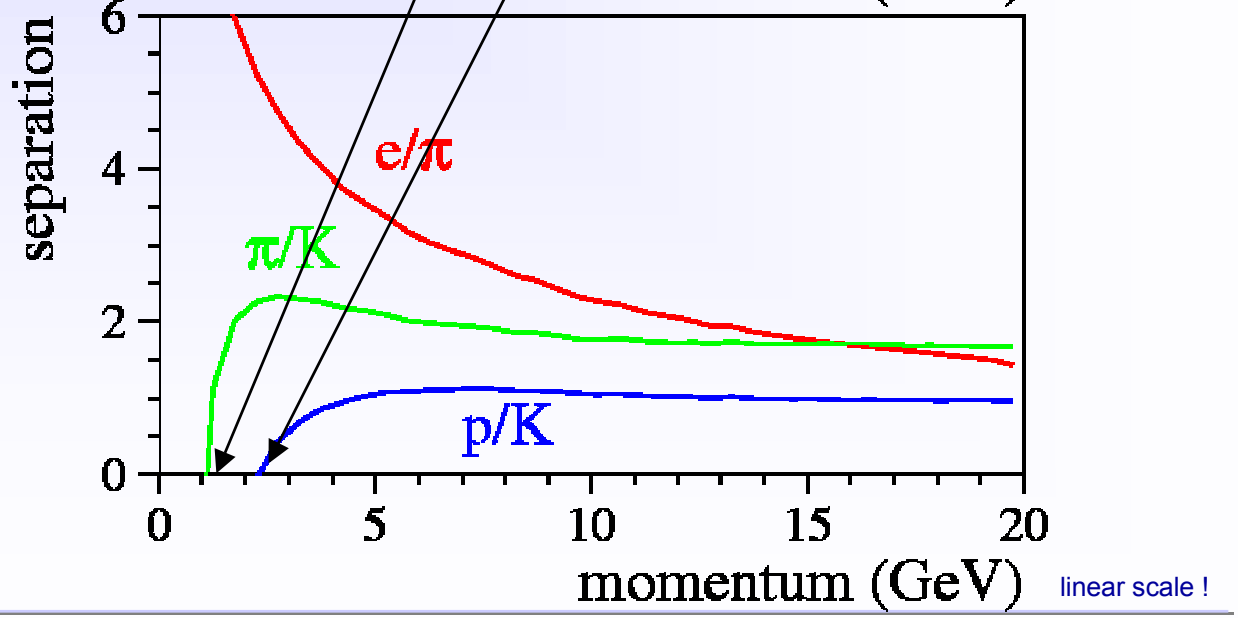

High resolution dE/dx by cluster counting

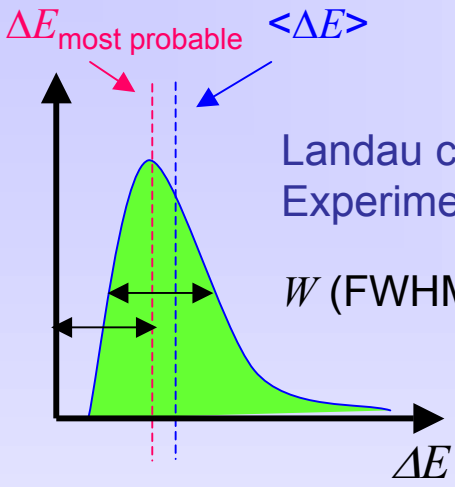

Landau curve
Experimental observation (first order)

W (FWHM) $\approx \Delta E_{\text{m.p.}}$

Remember (lecture 2a): the number of primary electron - ion pairs is Poisson distributed !
What would be the resolution in ΔE if we could count the clusters ?

1 cm Ar $\rightarrow n_{primary} \approx 28$

$$\frac{W}{\Delta E_{m.p.}} = 2.35\frac{\sqrt{n_{primary}}}{n_{primary}} = 0.44$$

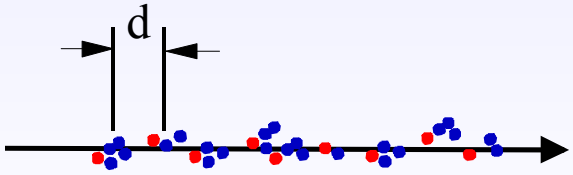

Average distance d $\approx$ 360 μm $\rightarrow \Delta t = d/v_{\text{drift}} \approx$ few ns

In addition diffusion $\rightarrow$ washes out clusters

Principle of cluster counting has been demonstrated to work - Time Expansion Chamber - but never successfully applied in a particle physics experiment. (A.H. Walenta, IEEE NS-26, 73 (1979))

High resolution dE/dx by cluster counting

Cluster counting with a hybrid gas detector: pixel readout chip + micromegas

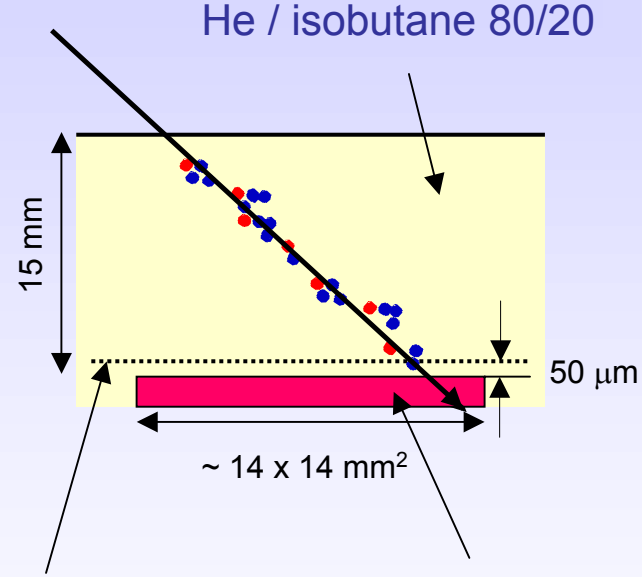

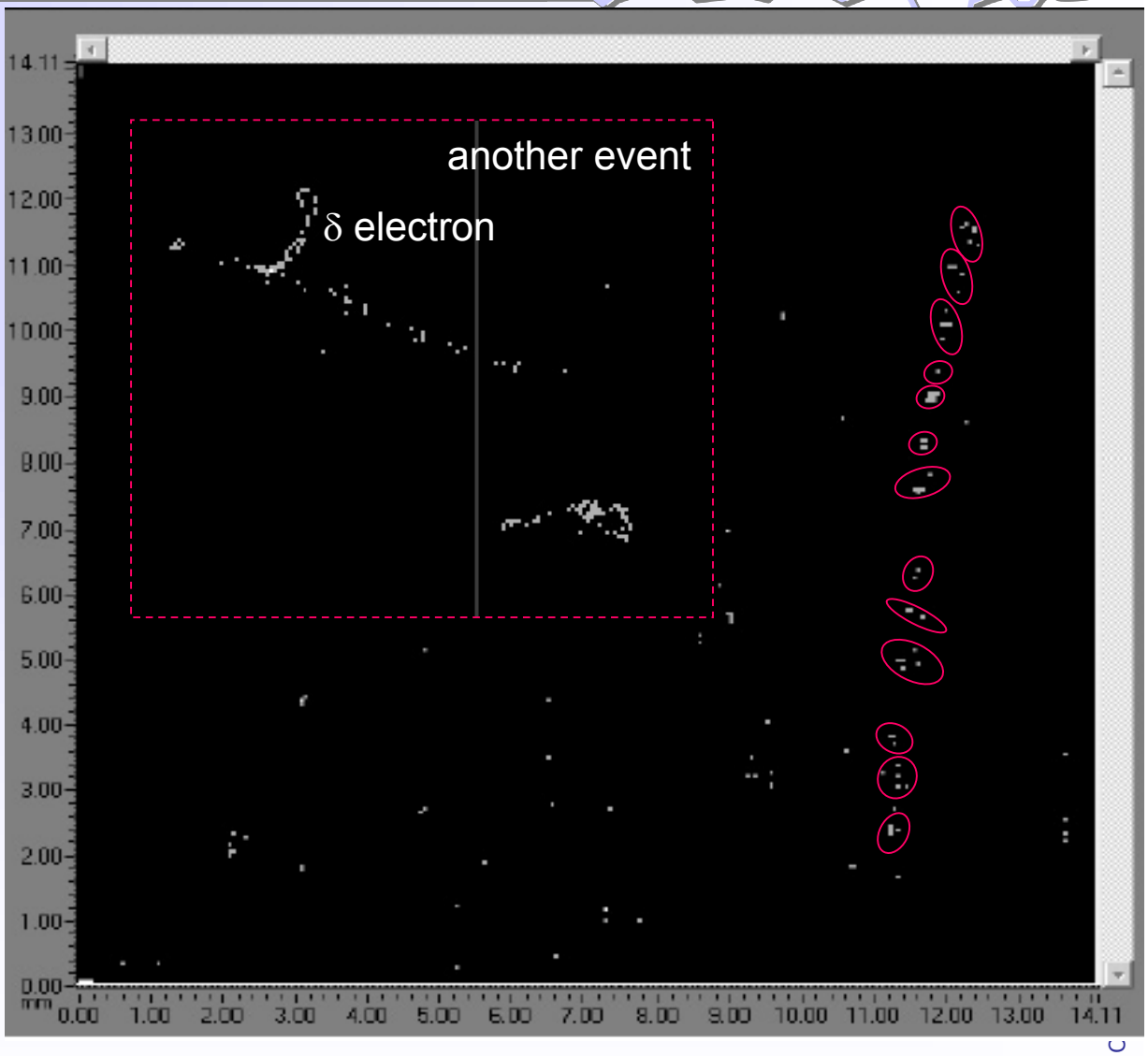

M. Campbell et al., NIM A 540 (2005) 295

track by cosmic particle (mip): 0.52 clusters / mm, ~3 e^-/cluster

Particle ID using Time Of Flight (TOF)

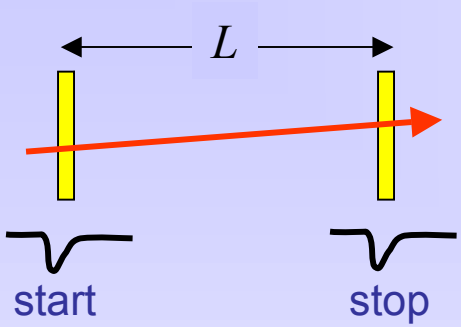

$$t = \frac{L}{\beta c} \longrightarrow \beta = \frac{L}{tc}$$

Combine TOF with momentum measurement

$$p = m_0 \beta\gamma \longrightarrow m_0 = p\sqrt{\frac{c^2 t^2}{L^2} - 1}$$

Mass resolution $\frac{dm}{m} = \frac{dp}{p} + \gamma^2\left(\frac{dt}{t} + \frac{dL}{L}\right)$

TOF difference of 2 particles as *f(p)*

$$\Delta t = \frac{L}{c}\left(\frac{1}{\beta_1} - \frac{1}{\beta_2}\right)$$

$$= \frac{L}{c}\left(\sqrt{1 + m_1^2 c^2 / p^2} - \sqrt{1 + m_2^2 c^2 / p^2}\right)$$

$$\approx \frac{Lc}{2p^2}\left(m_1^2 - m_2^2\right)$$

Δt for L = 1 m path length

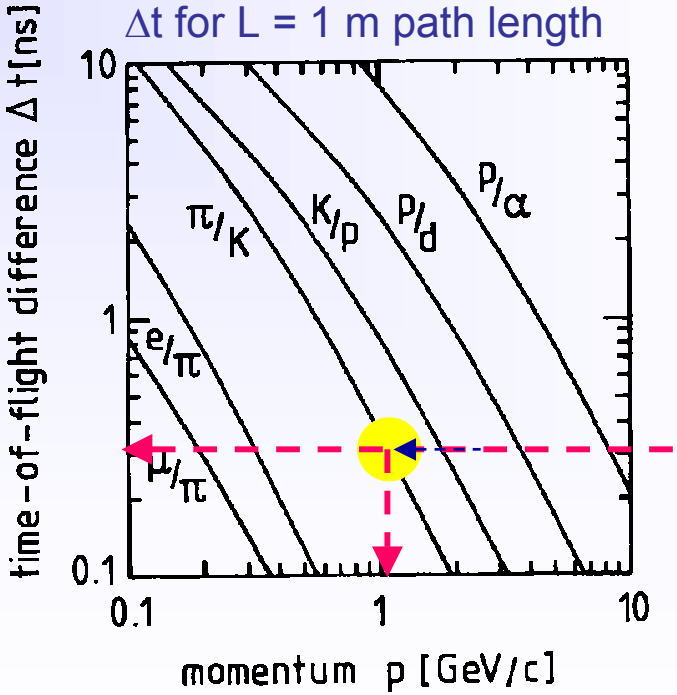

σ_t = 300 ps
π/K separation
up to 1 GeV/c

Example: NA49 Heavy Ion experiment

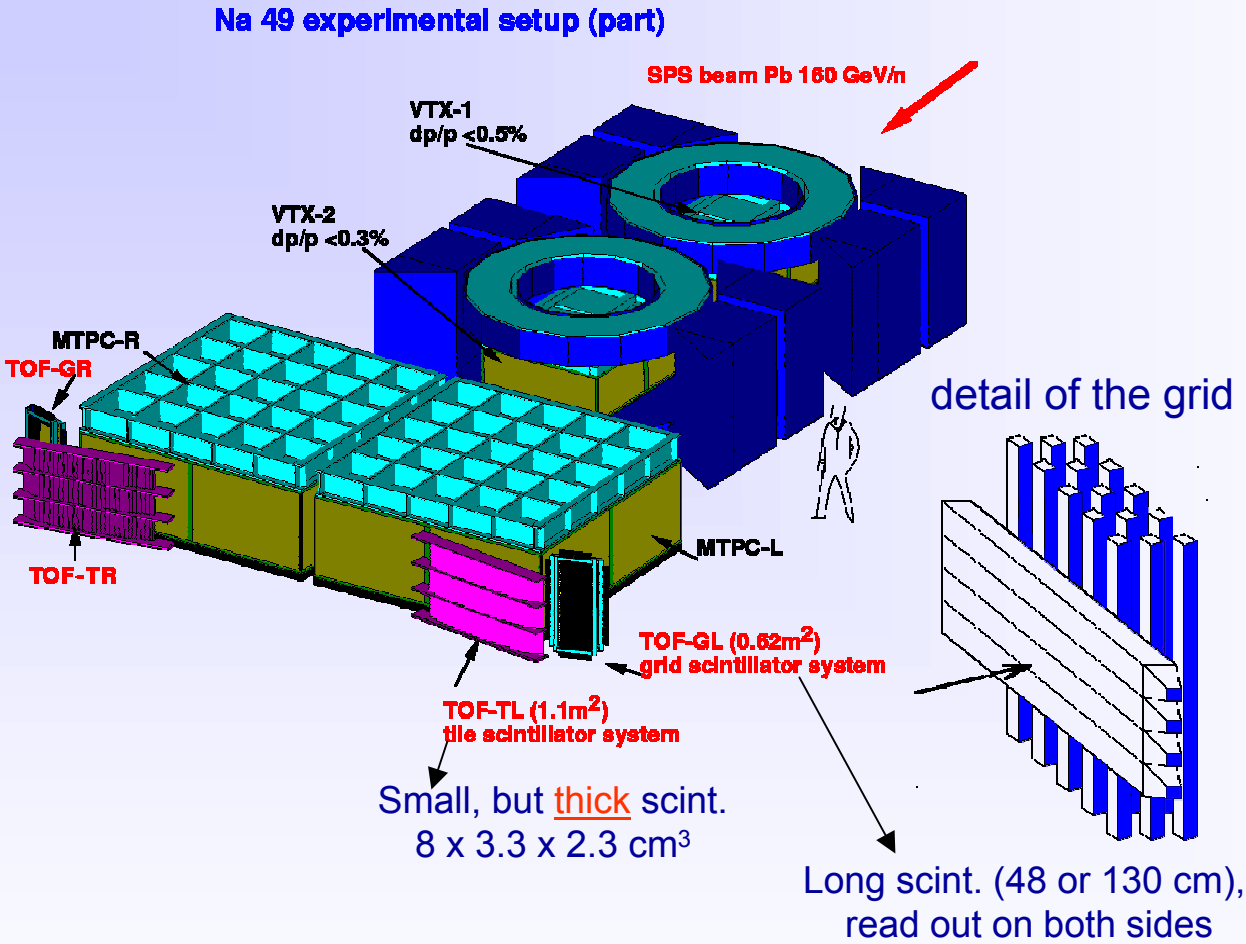

High resolution TOF requires

- fast detectors (plastic scintillator, gaseous detectors, e.g. RPC (ALICE)),
- appropriate signal processing (constant fraction discrimination, corrections)
- continuous stability monitoring.

Example: NA49 Heavy Ion experiment

System resolution of the tile stack

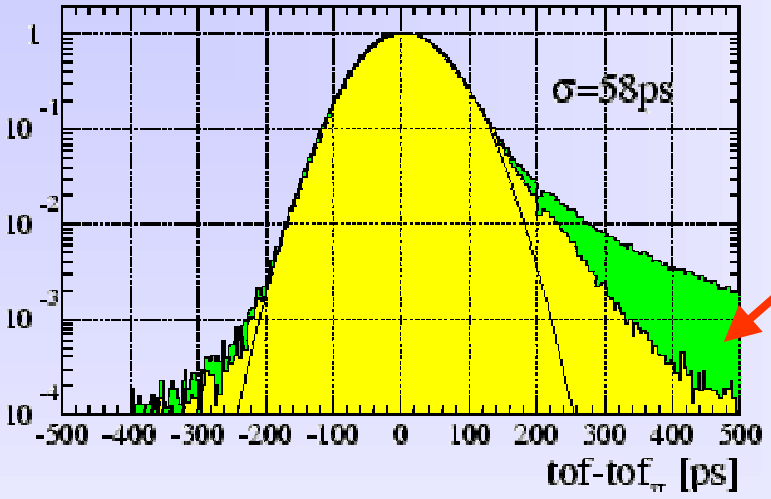

From γ conversion in scintillators

NA49 combined particle ID: TOF + dE/dx (TPC)

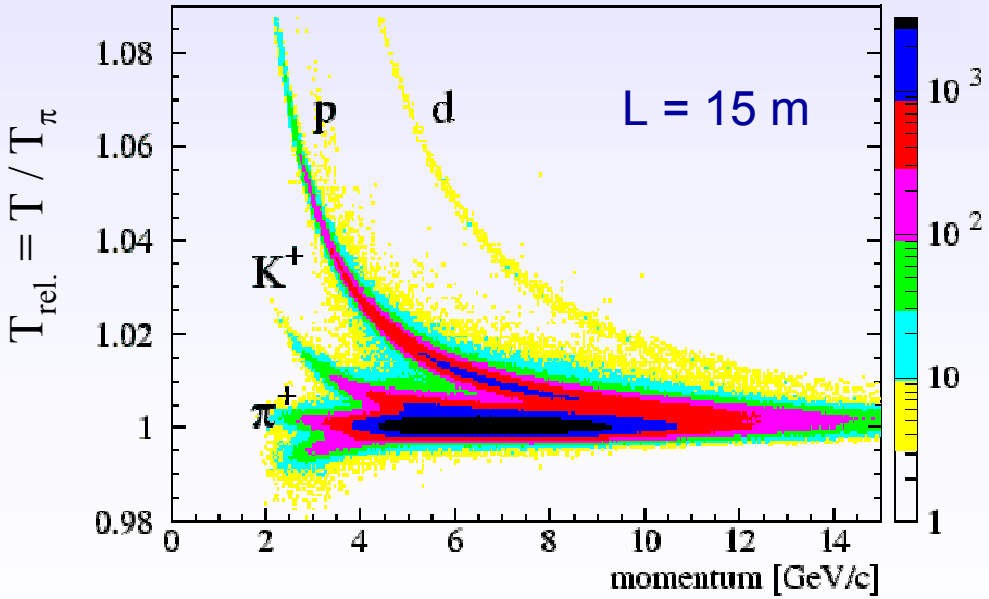

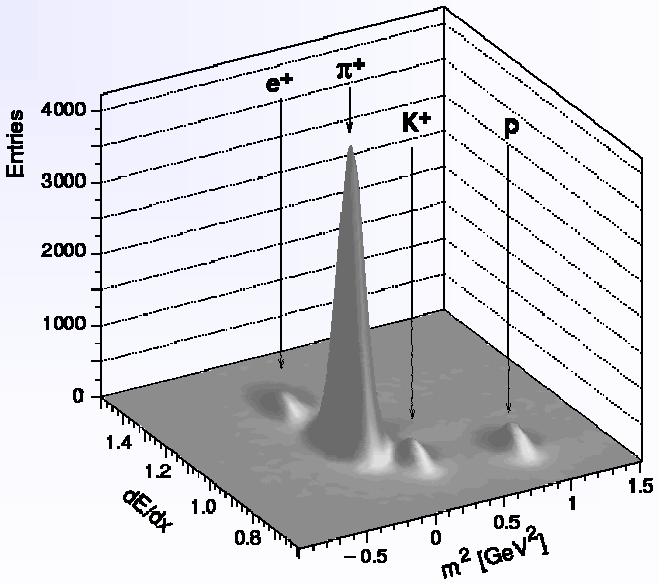

back to ... Interaction of charged particles

Remember energy loss due to ionisation…

There are other ways of energy loss !

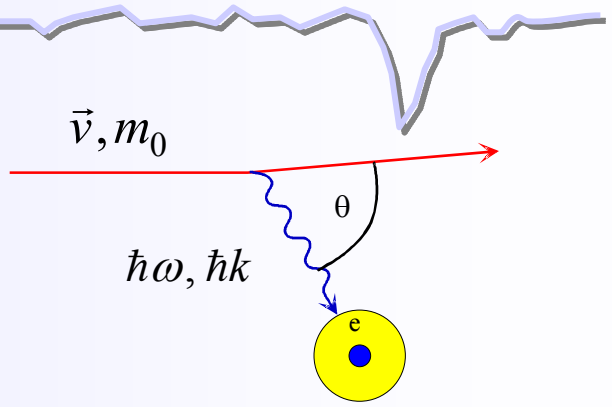

A photon in a medium has to follow the dispersion relation

$$\omega = 2\pi\nu = 2\pi\frac{c/n}{\lambda} = k\frac{c}{n} \qquad \omega^2 - \frac{k^2c^2}{\varepsilon} = 0 \qquad \varepsilon = n^2$$

Optical behaviour of medium is characterized by the dielectric constant ε

$\mathrm{Re}\sqrt{\varepsilon} = n$

Refractive index

$\mathrm{Im}\,\varepsilon = k$

Absorption parameter

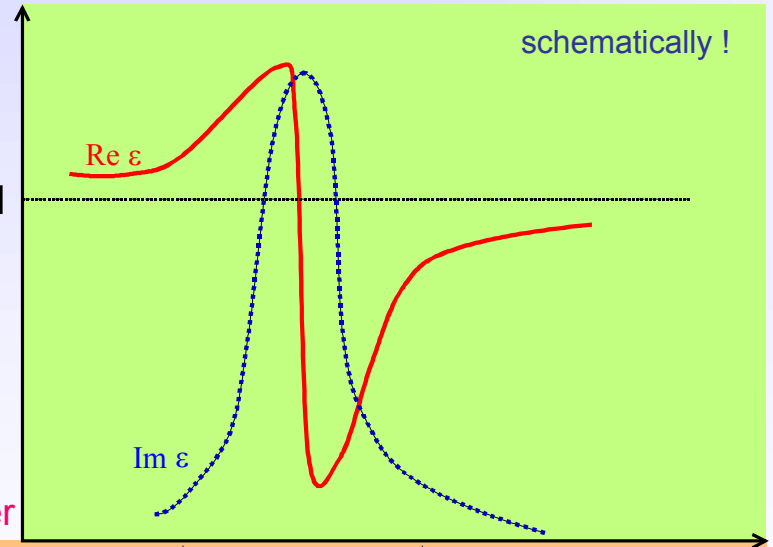

regime:	optical	absorptive	X-ray
effect:	Cherenkov radiation	ionisation	transition radiation

Assuming soft collisions + energy and momentum conservation → emission of real photons:

$$\omega \cong \vec{v}\cdot\vec{k} = v\cdot k\cos\theta$$

$$\rightarrow \quad \cos\theta = \frac{\omega}{vk} = \frac{1}{n\beta} = \frac{1}{\beta\sqrt{\varepsilon}}$$

Emission of photons if

$$\beta = 1/n\cdot\cos\theta \qquad \beta \geq 1/n$$

A particle emits real photons in a dielectric medium if its speed $\beta\cdot c$ is greater than the speed of light in the medium c/n

Cherenkov radiation

Cherenkov radiation is emitted when a charged particle passes through a dielectric medium

with velocity $\beta \geq \beta_{thr} = \frac{1}{n}$ n : refractive index

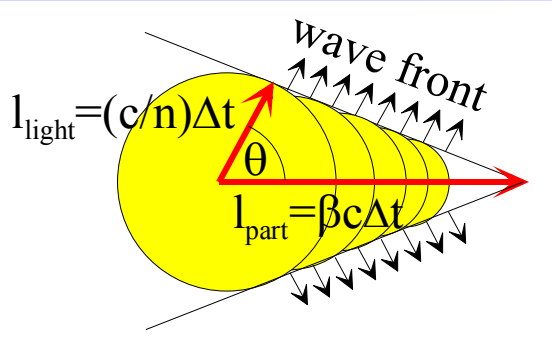

$$\cos\theta_C = \frac{1}{n\beta}$$
$$\text{with} \quad n = n(\lambda) \geq 1$$

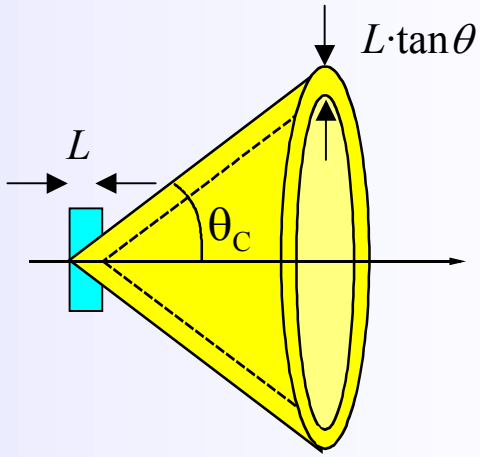

- $\beta_{thr} = \frac{1}{n} \rightarrow \theta_C \approx 0$ Cherenkov threshold
- $\theta_{\max} = \arccos\frac{1}{n}$ 'saturated' angle (β=1)

Number of emitted photons per unit length and unit wavelength interval

$$\frac{d^2N}{dxd\lambda} = \frac{2\pi z^2\alpha}{\lambda^2}\left(1-\frac{1}{\beta^2n^2}\right) = \frac{2\pi z^2\alpha}{\lambda^2}\sin^2\theta_C$$

$$\frac{d^2N}{dxd\lambda} \propto \frac{1}{\lambda^2} \quad \text{with} \quad \lambda = \frac{c}{\nu} = \frac{hc}{E} \quad \frac{d^2N}{dxdE} = const.$$

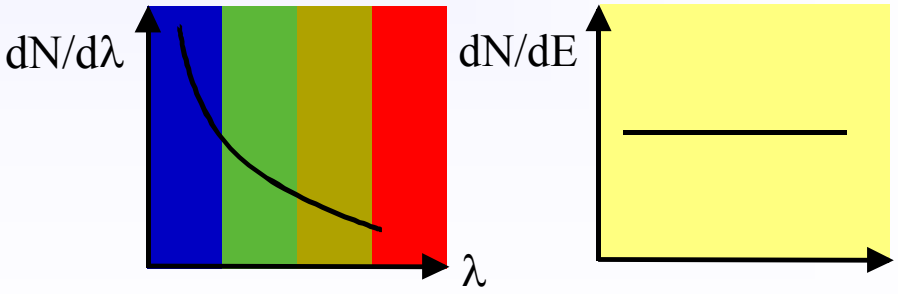

Cherenkov detectors

medium	n	θ_{max} (deg.)	N_{ph} (eV^{-1} cm^{-1})
air*	1.000283	1.36	0.208
isobutane*	1.00127	2.89	0.941
water	1.33	41.2	160.8
quartz	1.46	46.7	196.4

*NTP

- Energy loss by Cherenkov radiation small compared to ionization (≈0.1%)
- Cherenkov effect is a very weak light source

→ need highly sensitive photodetectors

Number of detected photo electrons $N_{p.e.} = L \sin^2\theta \underbrace{\frac{\alpha}{\hbar c}\int_{E_1}^{E_2} \varepsilon_Q(E) \prod_i \varepsilon_i(E) dE}_{N_0 = 370 \cdot eV^{-1} \cdot cm^{-1} \langle \varepsilon_{total} \rangle \Delta E}$

$\Delta E = E_2 - E_1$ is the width of the sensitive range of the photodetector (photomultiplier, photosensitive gas detector...)

N_0 is also called figure of merit (~ performance of the photodetector)

Example: for a detector with $\langle \varepsilon_{total} \rangle \cdot \Delta E = 0.2 \cdot 1\, eV \quad L = 1\, cm$

and a Cherenkov angle of $\theta_C = 30^\circ$

one expects $N_{p.e.} = 18$ photo electrons

Cherenkov detectors

Detectors can exploit ...

1. $N_{ph}(\beta)$ → threshold detector (do not measure θ_C)
2. $\theta(\beta)$ → differential and Ring Imaging Cherenkov detectors "RICH"

Threshold Cherenkov detectors

$$N_{ph} \approx 1 - \frac{1}{n^2\beta^2} = 1 - \frac{1}{n^2} \cdot \left(1 + m^2/p^2\right)$$

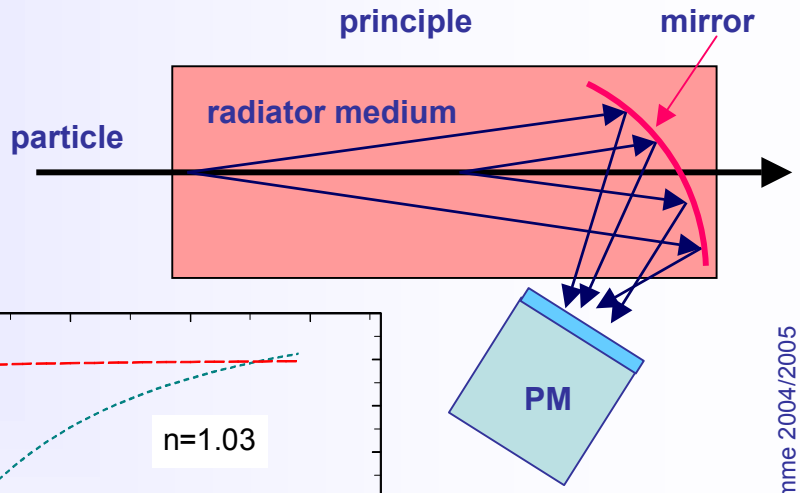

Example: study of an Aerogel threshold detector for the BELLE experiment at KEK (Japan)

Goal: π/K separation

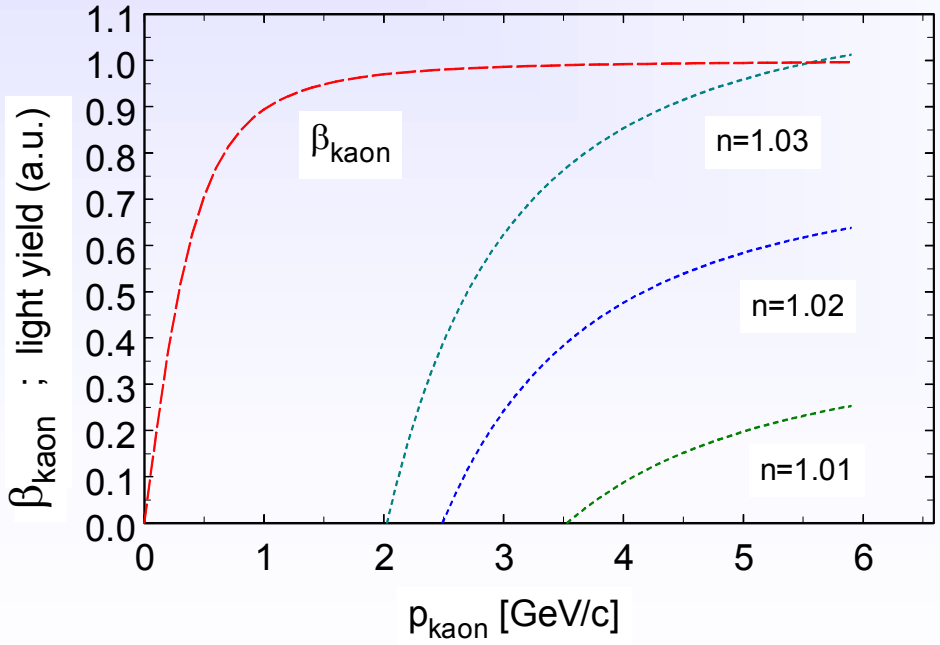

Ring Imaging Cherenkov detectors (RICH)

RICH detectors determine θ_C by intersecting the Cherenkov cone with a photosensitive plane

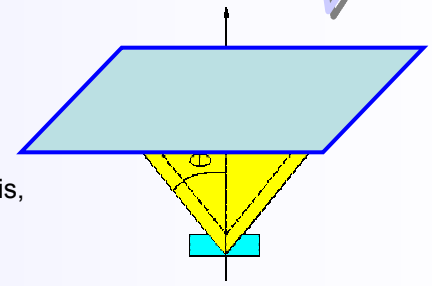

(J. Seguinot, T. Ypsilantis, NIM 142 (1977) 377)

→ requires large area photosensitive detectors, e.g.

- wire chambers with photosensitive detector gas
- PMT arrays

DELPHI

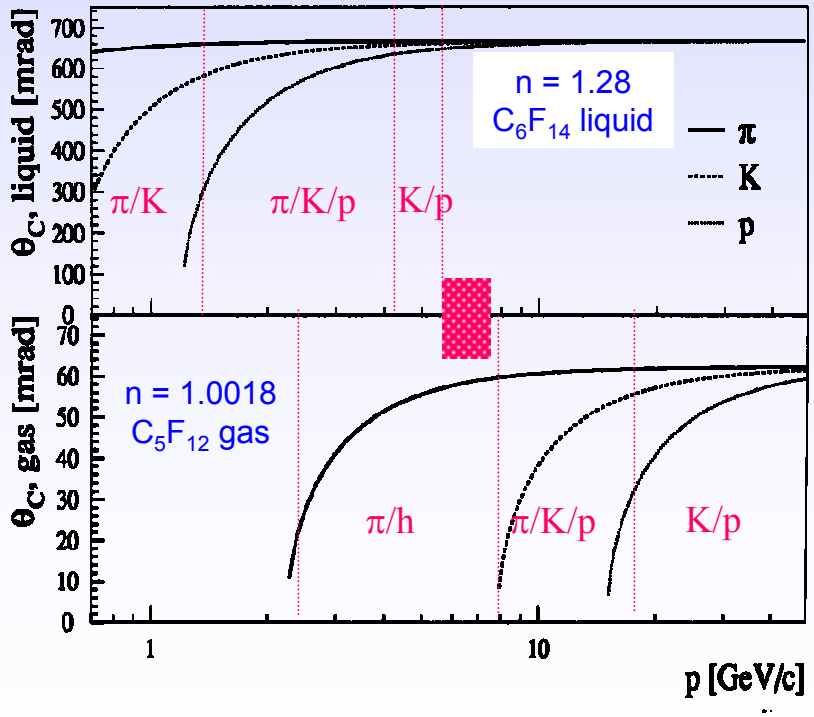

$$\theta_C = \arccos\left(\frac{1}{n\beta}\right) = \arccos\left(\frac{1}{n}\cdot\frac{E}{p}\right)$$

$$= \arccos\left(\frac{1}{n}\cdot\frac{\sqrt{p^2+m^2}}{p}\right)$$

$$\cos\theta_C = \frac{1}{n\beta} \quad \rightarrow \quad \frac{\sigma_\beta}{\beta} = \tan\theta\cdot\sigma_\theta$$

Detect $N_{p.e.}$ photons (photoelectrons) →

$$\sigma_\theta \approx \frac{\sigma_\theta^{p.e.}}{\sqrt{N_{p.e.}}}$$

→ minimize $\sigma_\theta^{p.e.}$

→ maximize $N_{p.e.}$

Ring Imaging Cherenkov detectors (RICH)

Reconstruction and resolution of Cherenkov angle

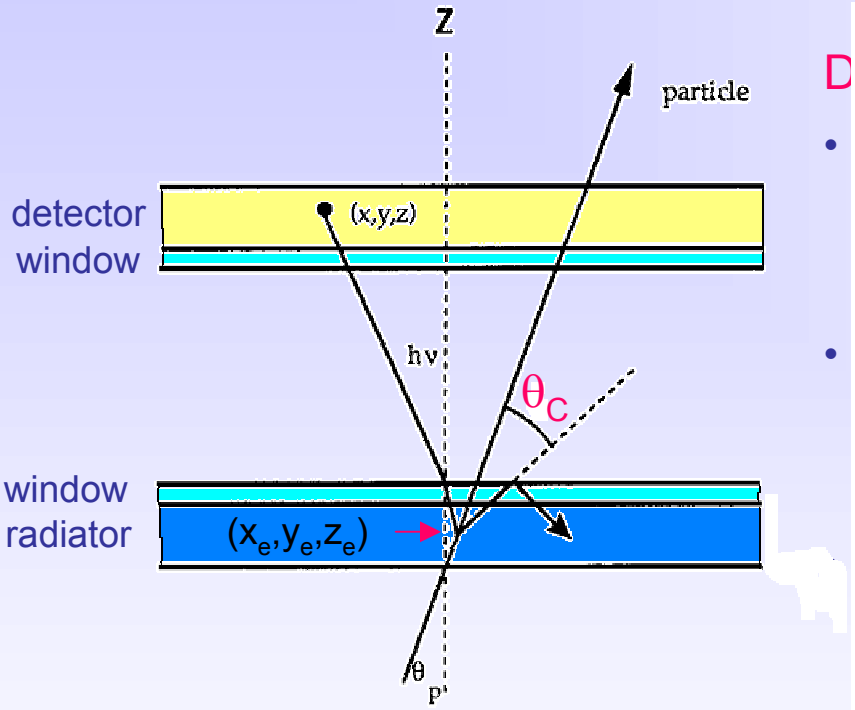

Determination of θ_C requires:

- Space point of the detected photon (x,y,z)
  - photodetector granularity (σ_x, σ_y), depth of interaction (σ_z)
- Emission point (x_e,y_e,z_e)
  - keep radiator thin or use focusing mirror
- Particle direction θ_p, ϕ_p
  - RICH requires good tracker

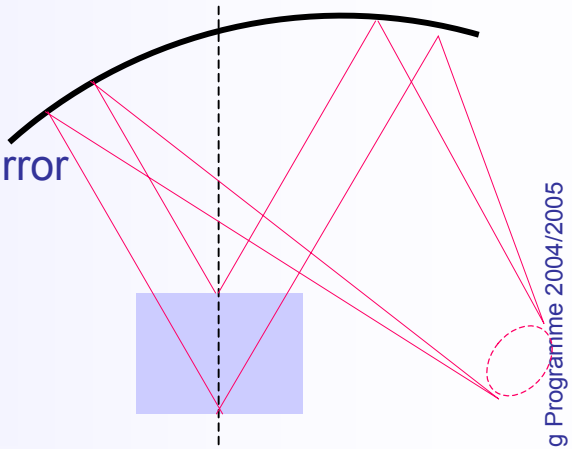

- the chromatic error - an 'irreducible' error

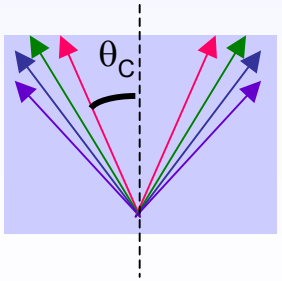

$$n_{rad} = n(E)$$

$$\sigma_\theta^c = \frac{1}{n \tan\theta}\sigma_n = \frac{1}{n \tan\theta}\frac{dn}{dE}\sigma_E$$

σ_E is related to the sensitivity range of the photodetector ΔE

$\Delta E \uparrow \rightarrow N_{pe} \uparrow$ good $\quad \sigma_E \uparrow$ bad

$\Delta E \downarrow \rightarrow N_{pe} \downarrow$ bad $\quad \sigma_E \downarrow$ good

Ring Imaging Cherenkov detectors (RICH)

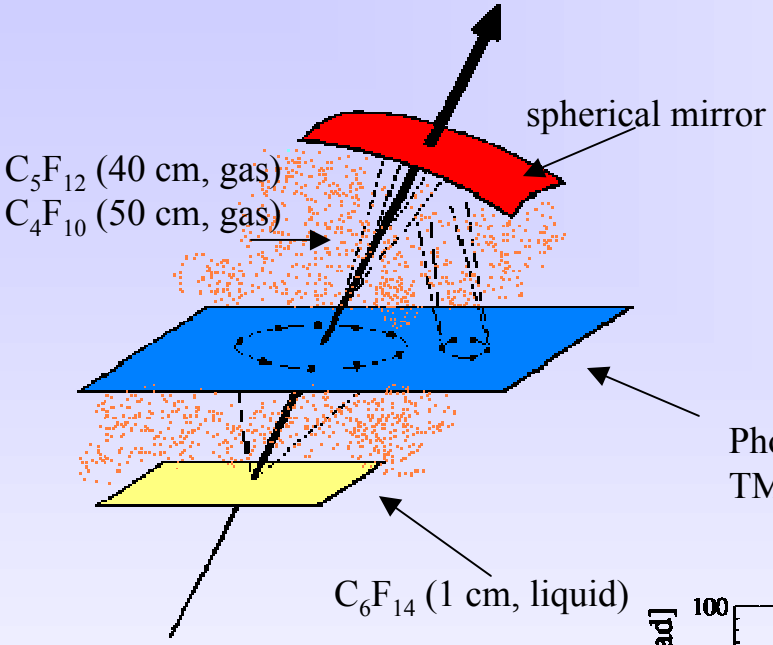

DELPHI and SLD:
A RICH with two radiators and a common photodetector plane
→ covers a large momentum range.
→ π/K/p separation 0.7 - 45 GeV/c:

(W. Adam et al. NIM A 371 (1996) 240)

Two particles from a hadronic jet (Z-decay) in the DELPHI gas and liquid radiator.
Circles show hypotheses for π and K

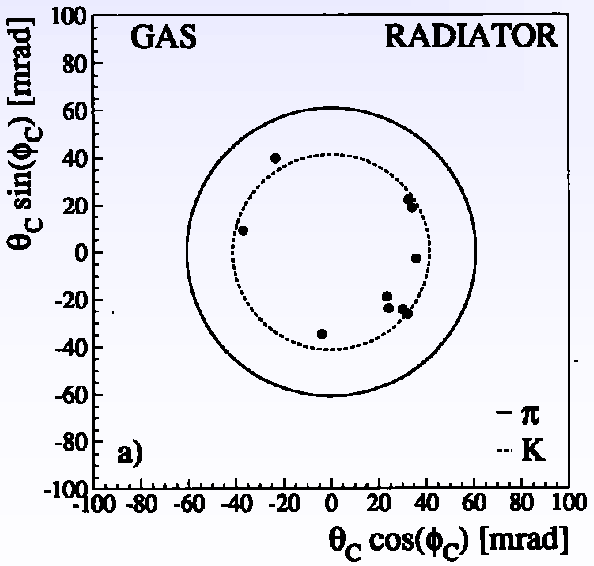

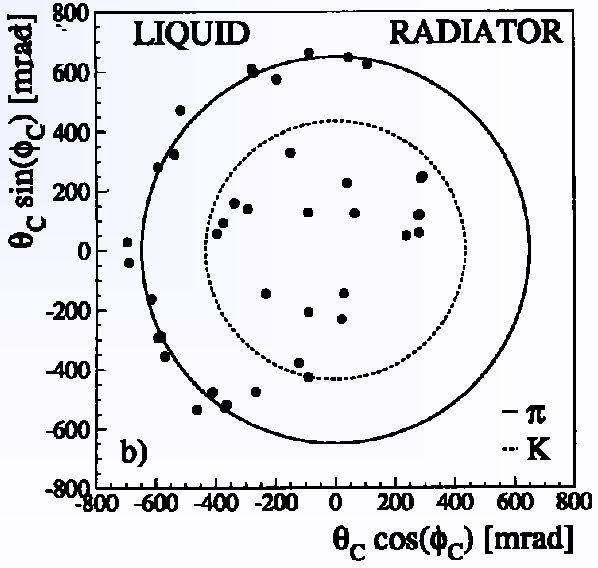

2 RICH detectors in LHCb

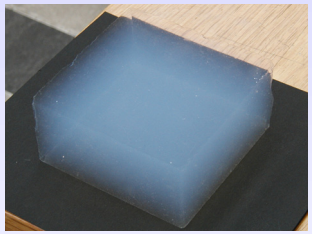

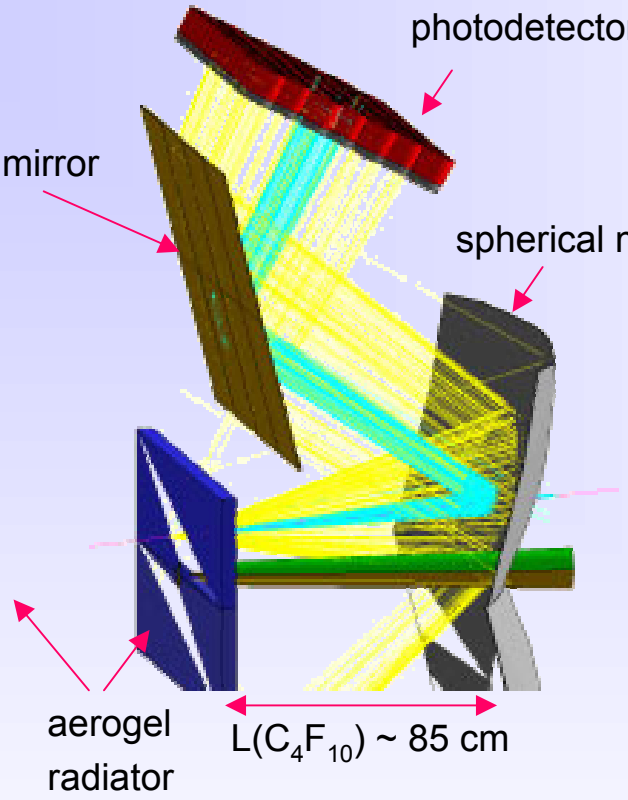

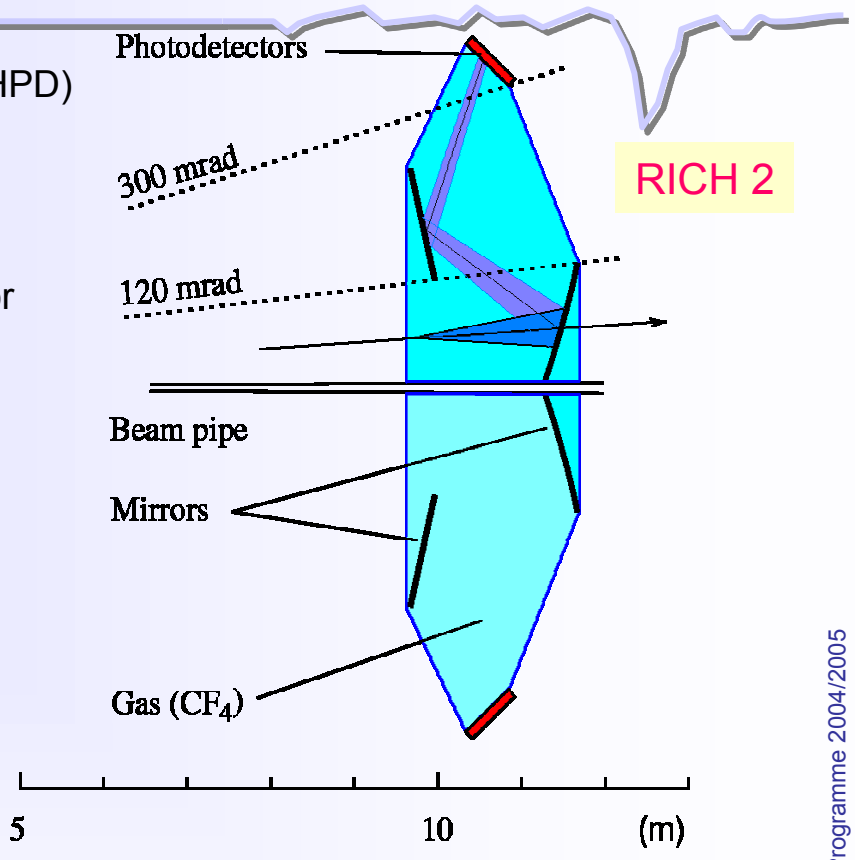

radiator	C_4F_{10}	aerogel
θ	3.03°	13.8°
n	1.0014	1.03
p_{thresh} (π)	2.6	0.6 GeV/c
$N_{p.e.}$	31	6.8
σ_θ	1.29	2.19 mrad
p (3σ)	56	13.5 GeV/c

radiator	CF_4
θ	1.8°
n	1.0005
p_{thresh} (π)	4.4 GeV/c
$N_{p.e.}$	23
σ_θ	0.6 mrad
p (3σ)	98.5 GeV/c

2 RICH detectors in LHCb

RICH 2

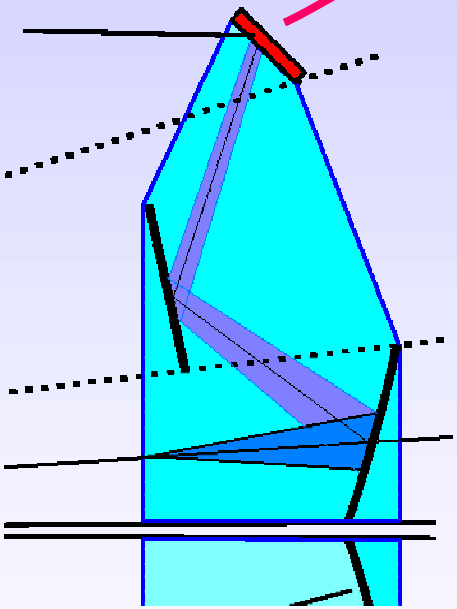

photodetector plane

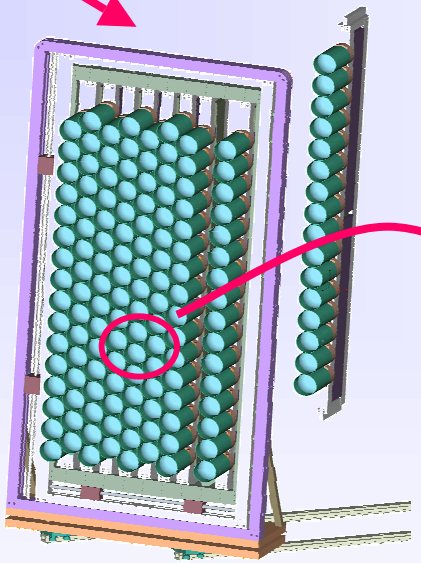

beam test in 2004 with 6 HPDs

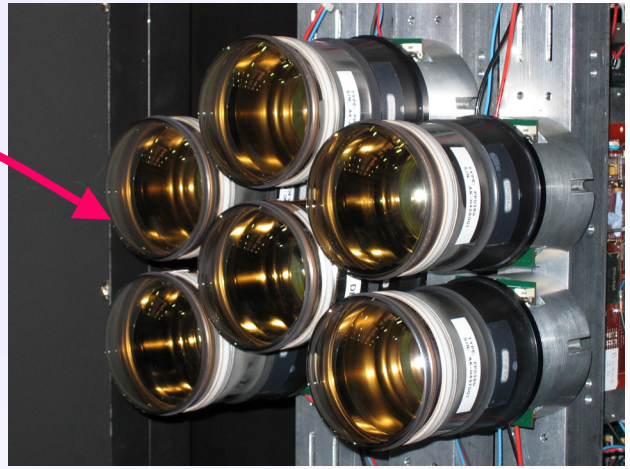

2 RICH detectors in LHCb

Beam test results with C_4F_{10} radiator gas (autumn 2004).

Single pion (10 GeV/c)

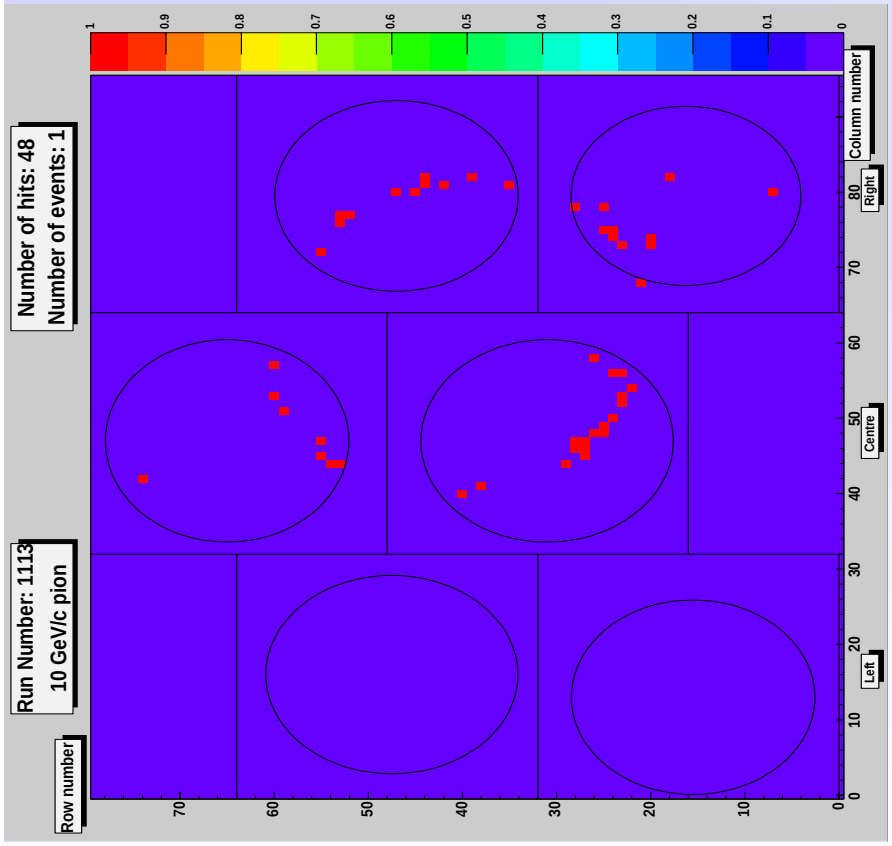

Superimposed events (100 k pions, 10 GeV/c)

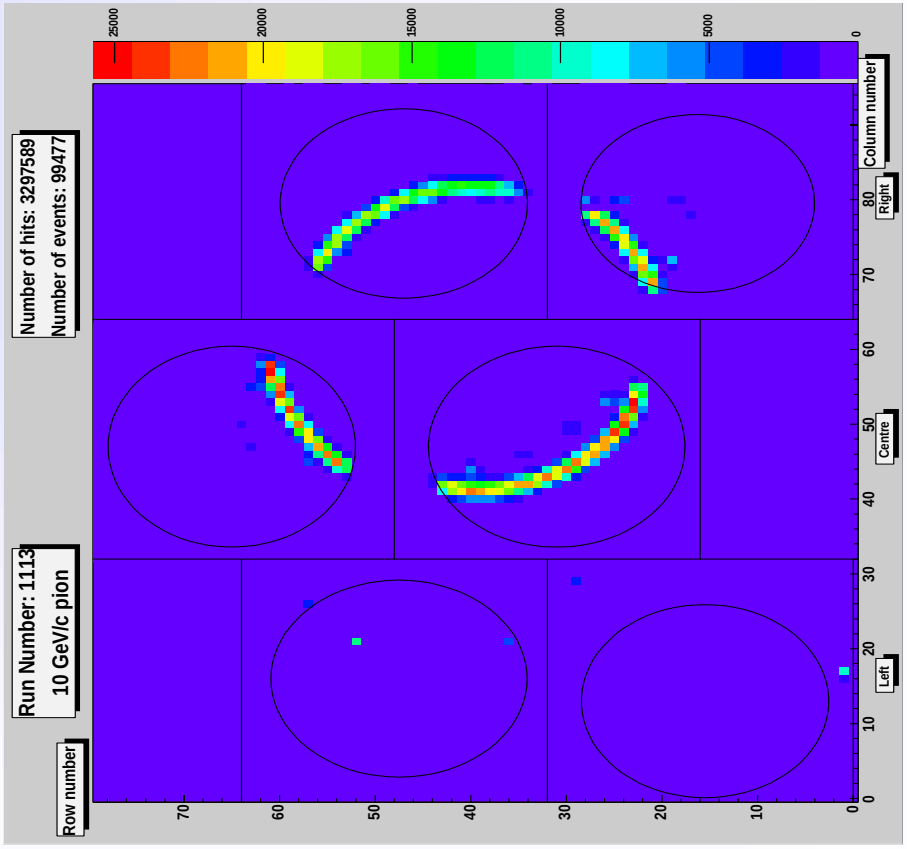

Particle ID by Transition radiation

(there is an excellent review article by B. Dolgoshein (NIM A 326 (1993) 434))

Transition Radiation was predicted by Ginzburg and Franck in 1946

TR is electromagnetic radiation emitted when a charged particle traverses a medium with a discontinuous refractive index, e.g. the boundaries between vacuum and a dielectric layer.

TR is also called sub-threshold Cherenkov radiation

A (too) simple picture

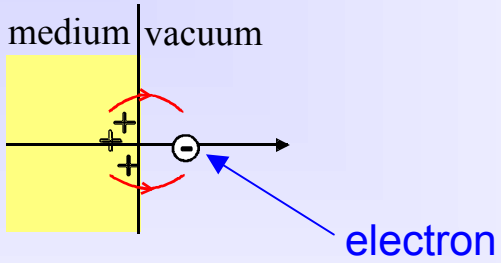

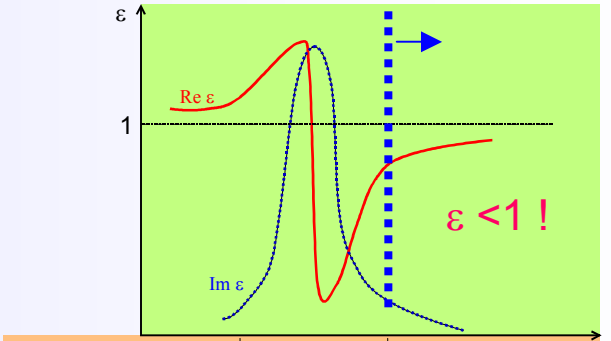

regime:	optical	absorptive	X-ray
effect:	Cherenkov radiation	ionisation	transition radiation

A correct relativistic treatment shows that…
(G. Garibian, Sov. Phys. JETP63 (1958) 1079)

- Radiated energy per medium/vacuum boundary

$$W = \frac{1}{3}\alpha\hbar\omega_p\gamma \qquad \boxed{W \propto \gamma} \longrightarrow$$

only high energetic e± emit TR of detectable intensity.
→ particle ID

$$\omega_p = \sqrt{\frac{N_e e^2}{\varepsilon_0 m_e}} \qquad \begin{pmatrix}\text{plasma}\\ \text{frequency}\end{pmatrix} \qquad \hbar\omega_p \approx 20\text{eV} \ \text{(plastic radiators)}$$

Particle ID by Transition radiation

- Number of emitted photons / boundary is small $N_{ph} \approx \frac{W}{\hbar\omega} \propto \alpha \approx \frac{1}{137}$

  → Need many transitions → build a stack of many thin foils with gas gaps

- Emission spectrum of TR = f(material, γ)

  Typical energy: $\hbar\omega \approx \frac{1}{4}\hbar\omega_p\gamma$

  → photons in the keV range

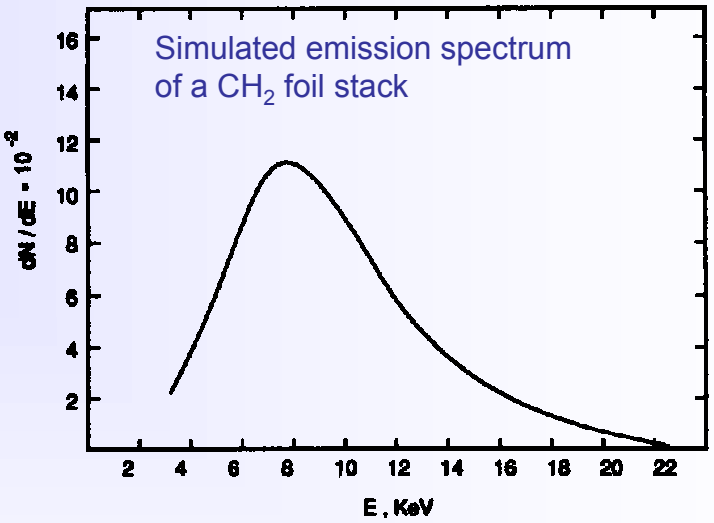

- X-rays are emitted with a sharp maximum at small angles $\theta \propto 1/\gamma$

  → TR stay close to track

- Particle must traverse a minimum distance, the so-called formation zone Z_f, in order to efficiently emit TR.

$$Z_f = \frac{2c}{\omega(\gamma^{-2} + \theta^2 + \xi^2)}, \quad \xi = \omega_p / \omega$$

Z_f depends on the material (ω_p), TR frequency (ω) and on γ.

$Z_f(air)$ ~ mm, $Z_f(CH_2)$ ~ 20 μm → important consequences for design of TR radiator.

Particle ID by Transition radiation

TR Radiators:

- stacks of thin foils made out of CH_2 (polyethylene), $C_5H_4O_2$ (Mylar)
- hydrocarbon foam and fiber materials

  Low Z material preferred to keep re-absorption small ($\propto Z^5$)

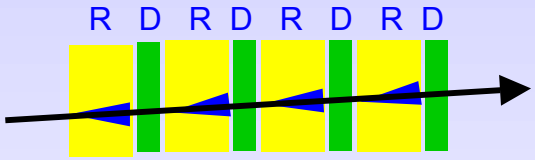

alternating arrangement of radiators stacks and detectors
→ minimizes reabsorption

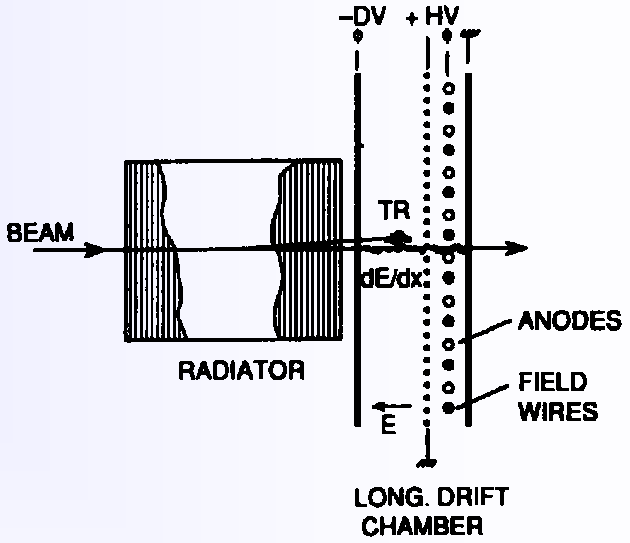

TR X-ray detectors:

- Detector should be sensitive for $3 \leq E_\gamma \leq 30$ keV.
- Mainly used: Gas detectors: MWPC, drift chamber, straw tubes…
- Detector gas: $\sigma_{\text{photo effect}} \propto Z^5$

  → gas with high Z required, e.g. Xenon (Z=54)
- Intrinsic problem: detector "sees" TR and dE/dx

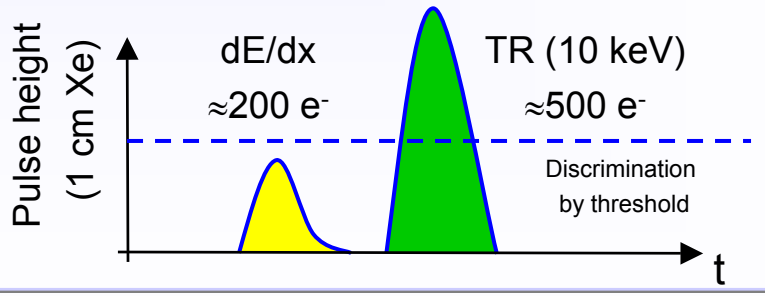

Particle ID by Transition radiation

The ATLAS Transition Radiation Tracker (TRT)

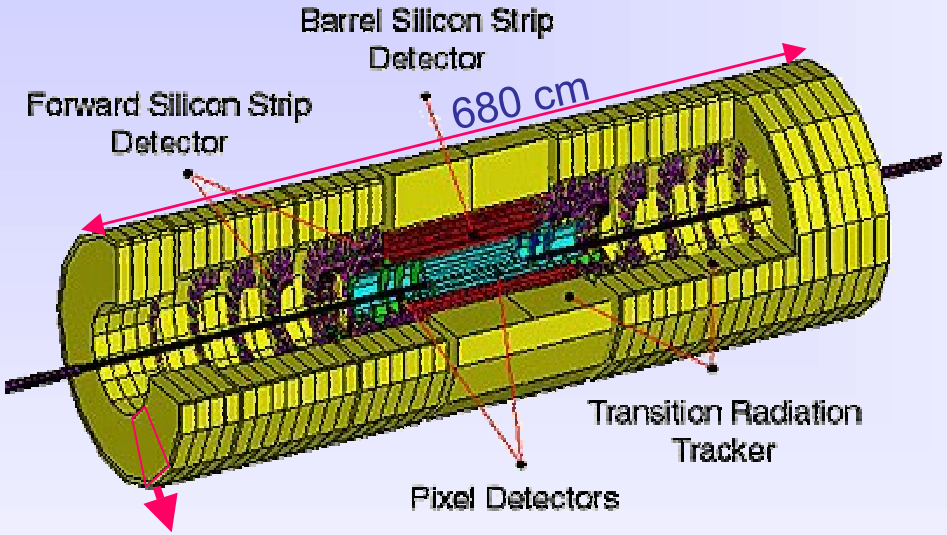

photo of an endcap TRT sector.

Straw tubes (d = 4mm) based tracking chamber with TR capability for electron identification.

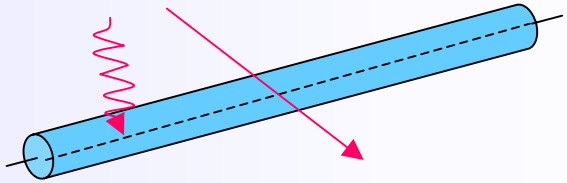

Active gas is $Xe/CO_2/O_2$ (70/27/3) operated at ~$2x10^4$ gas gain;
drift time ~ 40ns (fast!)

Radiators

- Barrel: Propylen fibers
- Endcap: Propylen foils
  d=15 μm with 200 μm spacing.

Counting rate ~ 6-18 MHz at LHC design luminosity 10^{34} $cm^{-2}s^{-1}$

ALICE TRD

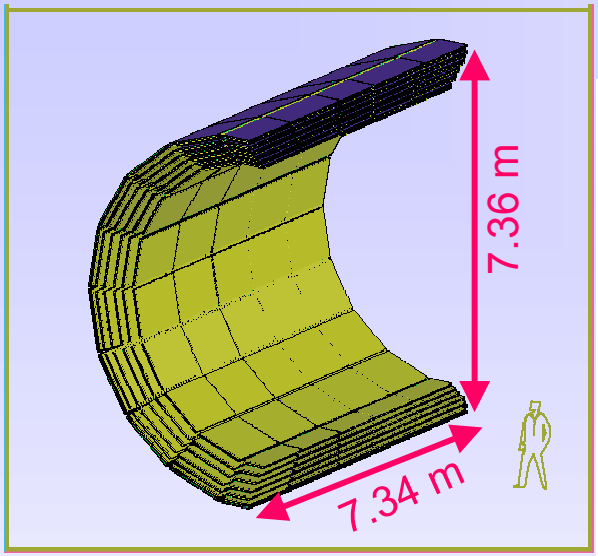

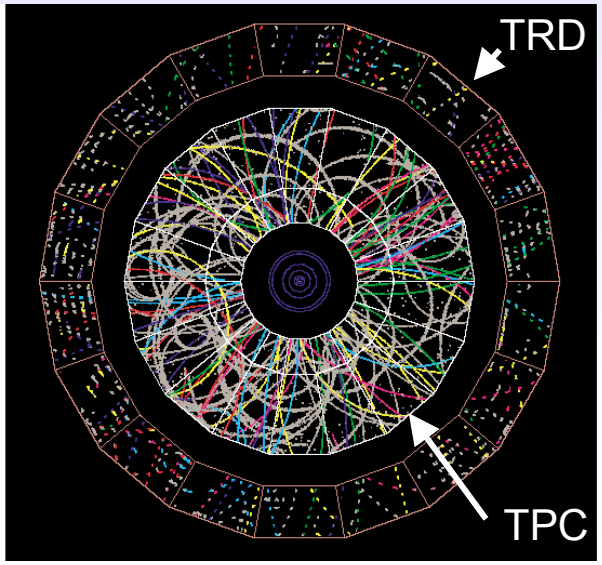

Time Expansion Chamber with Xe/CO_2 gas (85%-15%)

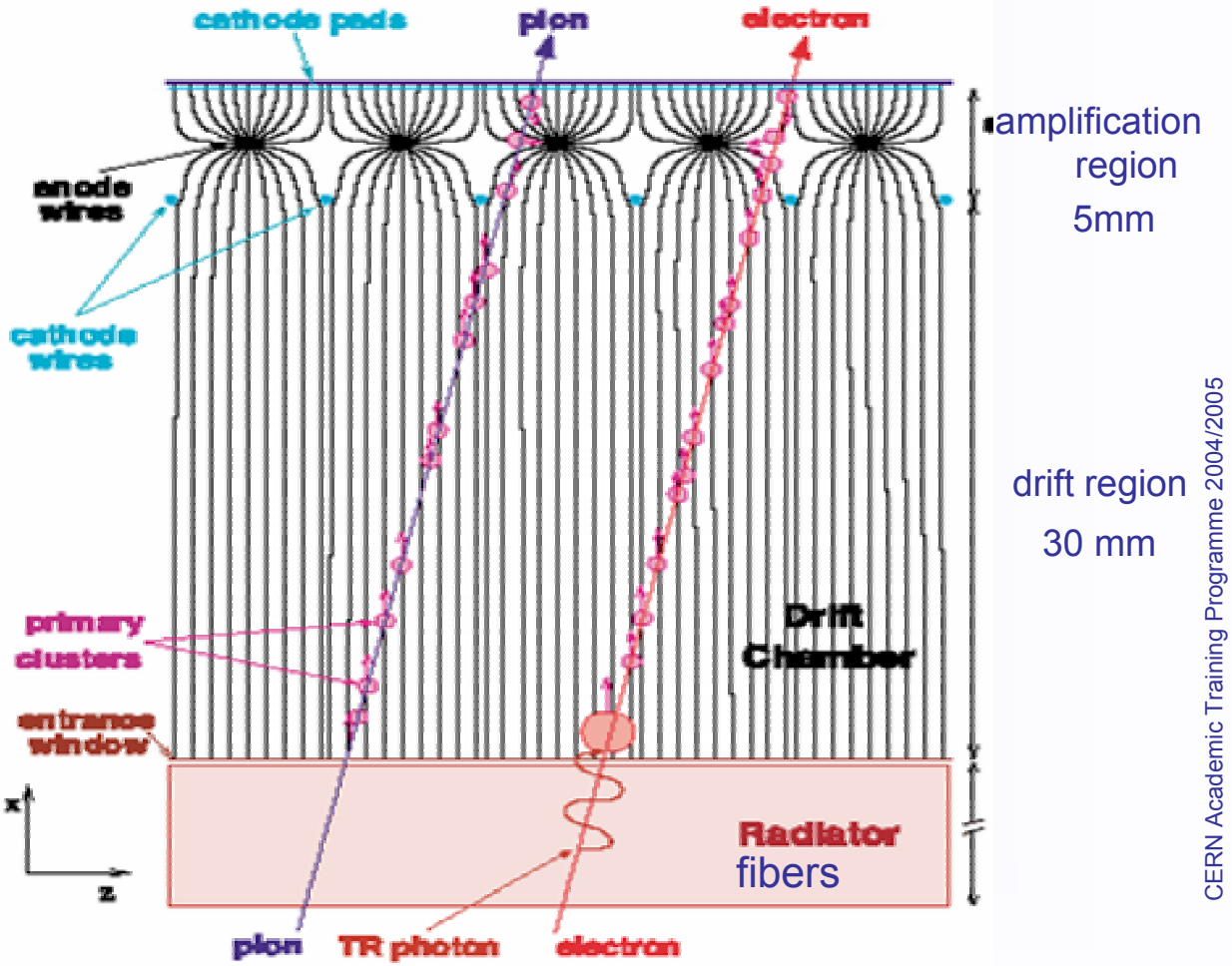

ALICE TRD performance

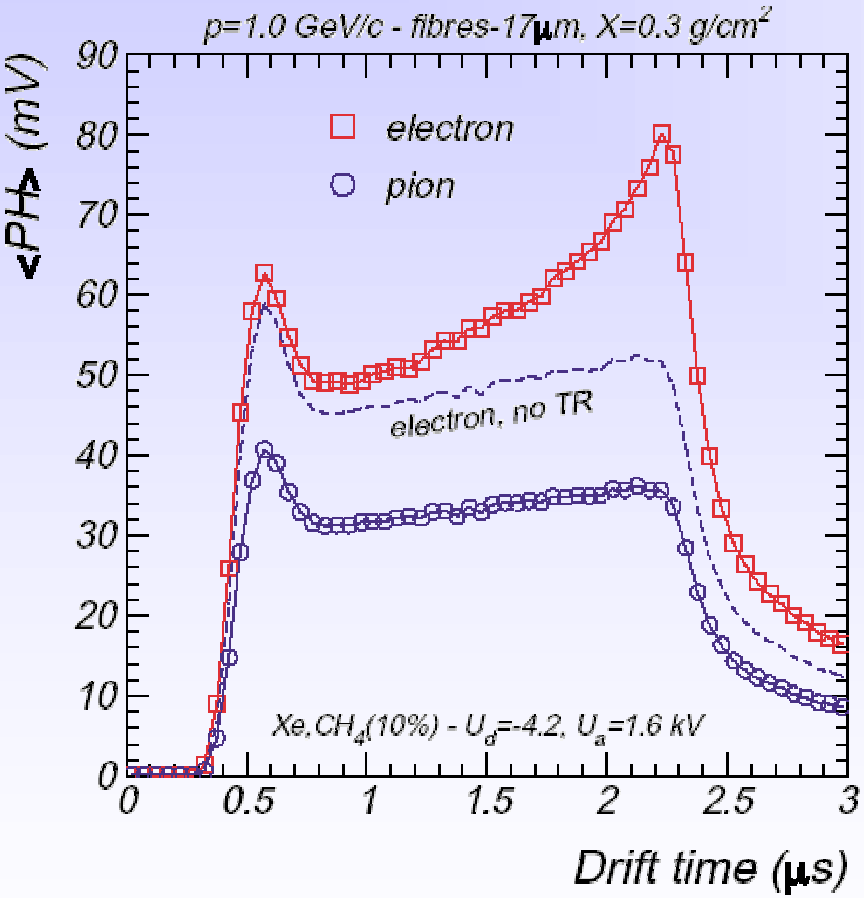

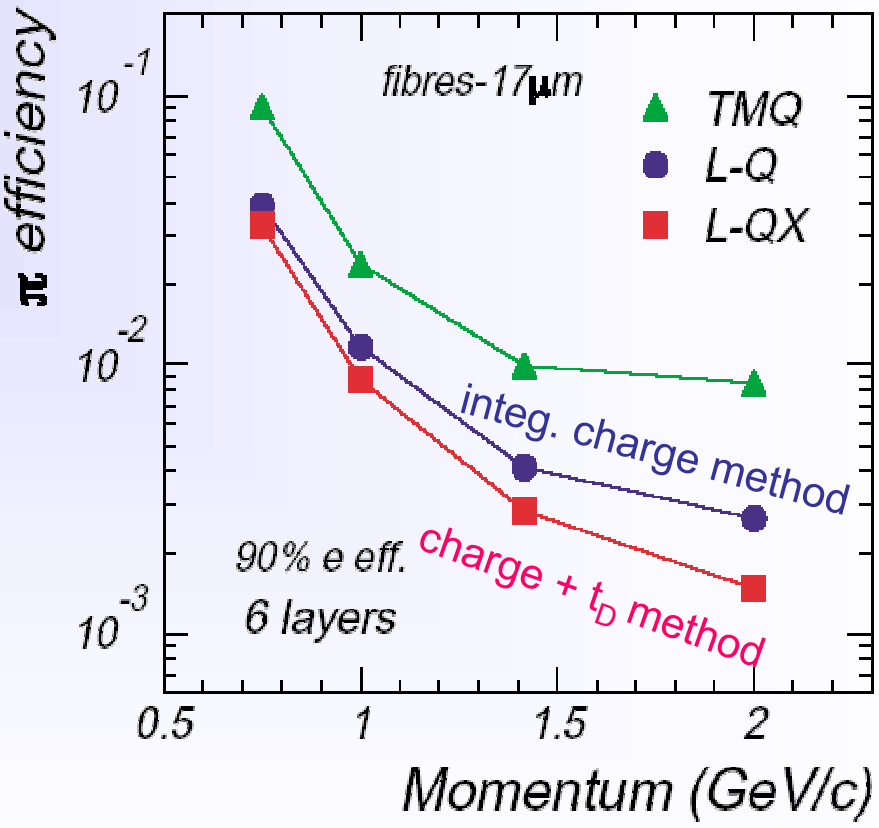

Particle ID by Transition radiation

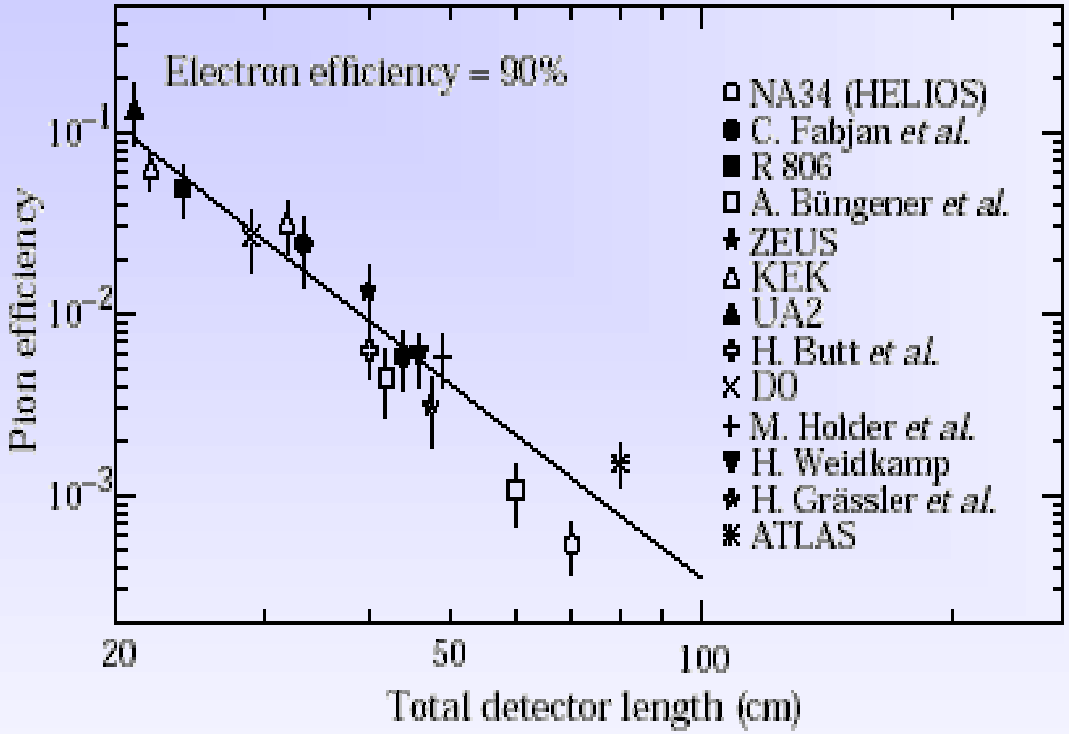

Rejection Power : $R_{\pi/e} = \varepsilon_\pi/\varepsilon_e$ (90%)

one order of magnitude in Rejection Power is gained when the TRD length is increased by ~ 20 cm

Particle Identification

Summary:

- A number of powerful methods are available to identify particles over a large momentum range.
- Depending on the available space and the environment, the identification power can vary significantly.

- A very coarse plot ….

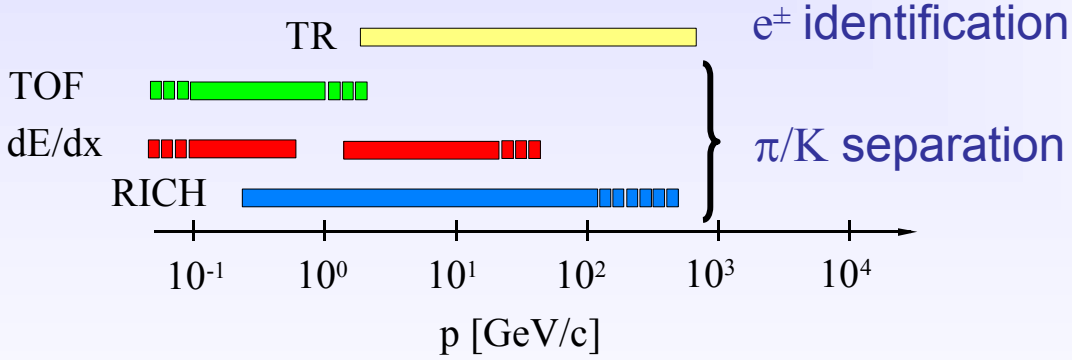

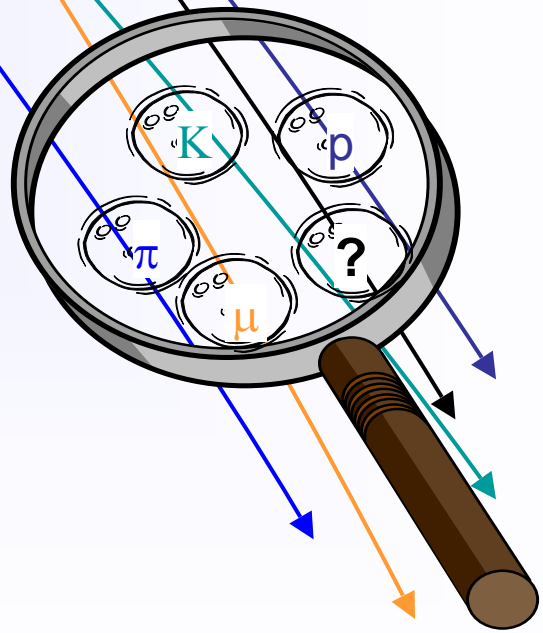

Basic principles of detector design

By C. D'Ambrosio (CERN)

Geneva, 15 April 2005

Outline

Lecture 1 - Introduction C. Joram, L. Ropelewski

Lecture 2 - Tracking Detectors L. Ropelewski, M. Moll

Lecture 3 - Scintillation and Photodetection C. D'Ambrosio, T. Gys

Lecture 4 - Calorimetry, Particle ID C. Joram

Lecture 5 - Particle ID, Detector Design C. Joram, C. D'Ambrosio

5a – Particle Identification

5b – Detector Design

- **Basic connections between accelerator and detector**
- **Vertex and momentum measurements (in solenoid systems)**
- **Dose generated and occupancy**
- **A Decalogue**

Principles of Detector Design

Designing a detector is exciting
(one of the best part of the whole story!)

I shall try to give you a fade feeling of what a process lasting years is, and a few tools and basic principles, for a "back of the envelope" design.

Important before starting: Given an accelerator

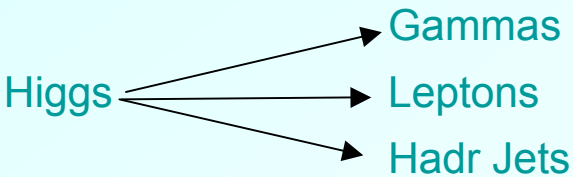

Sparticles…..

Rare mesons….

Etc

What we want to measure (signatures)
How we can measure (detector)

But a lot is simply not known, therefore, **stick to general assumptions and design for surprises.**

Introduction 2

The classic quantities to measure are:

Trajectory, Charge, Momentum, Velocity, Energy

In order to :

identify particle, calculate mass, recover intermediate processes, decays, etc.

Most basic for a detector design:

Cost of experiment goes with **~volume**

As little as possible material in front of the calorimeter

As much as possible in front of the muon chambers

Hermetic but easy to dismount

Introduction

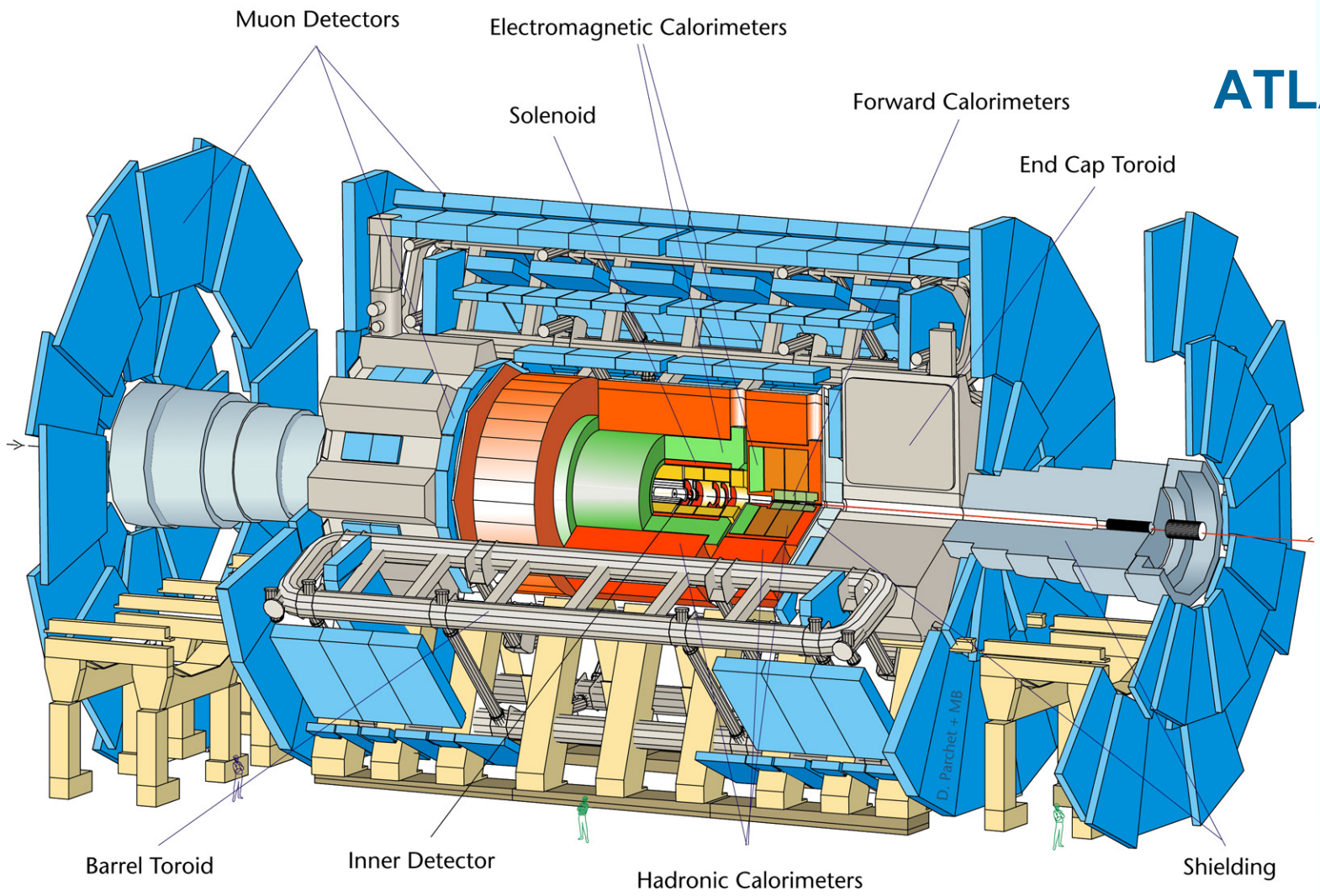

Introduction 1

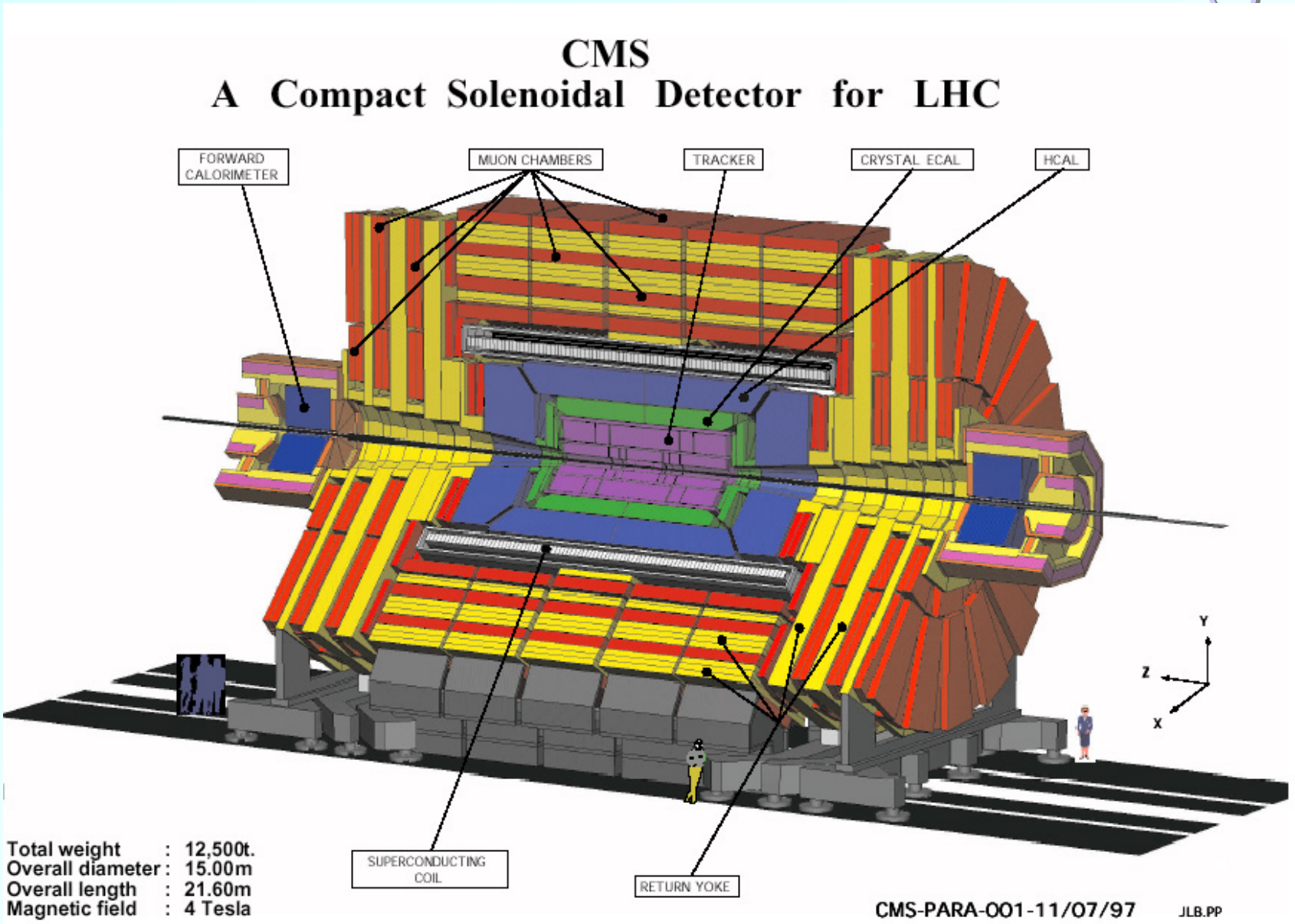

List of relevant parameters, their units and symbols

Accelerator parameters		Symbol
Centre of mass energy	TeV	E_{CM}
Full beam crossing angle	μrad	α
Beam radius (68 % of particles)	μm	σ_x
Bunch length (68 % of particles)	m	σ_b
Time between two bunches	ns	t_b
Interaction parameters		
Standard luminosity	$cm^{-2}s^{-1}$	L_0
Length of luminous region	m	l^*
Inelastic cross-section	cm^2	σ_{inel}
Avr. Nr of charged part. per unit of rap. and per event		H
Distribution of vertices per mm		$n_v(z)$
Avr. Nr of vertices per bunch crossing		$\langle n_v \rangle$
Avr. Nr of vertices per mm (for 68 % of interaction)	mm^{-1}	$\langle n_v^* \rangle$
Momentum, trans. Mom. and avr. trans. Mom.	GeV/c	p, p_t, $\langle p_t \rangle$

Detector parameters		
Det. precision in (r,z)-plane	μm	σ_z
Det. precision in (r,φ)-plane	μm	σ_φ
Distance from the beam axis	m	r
Distance between outer- and inner det. shells	m	Δr_t
Number of hits		N
Multiple scattering angle	rad	θ_{ms}
Thickness of det. in unit of radiation length		t
Thickness of det. to achieve one hit in unit of rad. length		t_0
Det. precision on the beam axis (z-axis)	mm	δz
Total and transverse Mom. resolution		$\delta p/p$, $\delta p_t/p_t$

Disclaimer

- In this "walkthrough", we will concentrate mainly on the "central" trackers design: this is roughly the region up to $\eta = 2$, $\eta = -\ln\tan(\theta/2)$ (η is the pseudo rapidity and θ the polar angle with origin at the interaction point).
- Also, we will be talking mostly of charged particles. In principle, all the gammas produced are traversing the "inner region" (before the calorimeters) unconverted. Neutrons constitute an important source of noise and rad. Dose.
- Fraction of converted gammas or hadrons before the calorimeter

$$f_{conv} \sim 1 - e^{-t} \quad where \quad t \equiv material\ in\ units\ \ of\ \ X_0\ or\ \lambda_I$$

- Whenever we talk of "xxx-like detector", it means that our results may not coincide with the actual xxx detector.
- Nothing about calorimeter design and neither about trigger aspects.
- We will have to be short, therefore you will have to accept for good a lot of things that you should not to…

- Apologies…, I have given to the lecture a fairly personal cut. I trust the interested people will find the remaining information!

Layout

- **Basic connections between accelerator and detector**
  - Luminosity, interaction region and implications on the detector design
  - Scaling of physical quantities with the center of mass energy
- **Vertex and momentum measurements (in solenoid systems)**
  - Basic tools for the calculation of vertex and momentum resolutions in detector systems
  - The example of a CMS-like detector in a LHC-like accelerator
- **Dose generated and occupancy**
  - Charged and neutral particles
  - Detector Occupancy
  - Magnetic field effects on dose and occupancy
- **Conclusions**

http://ph-dep-dt2.web.cern.ch/ph-dep-dt2/lectures_PD_2005.htm or

http://user.web.cern.ch/User/Welcome.html

Luminosity and Interaction Region

Luminosity and Interaction Region

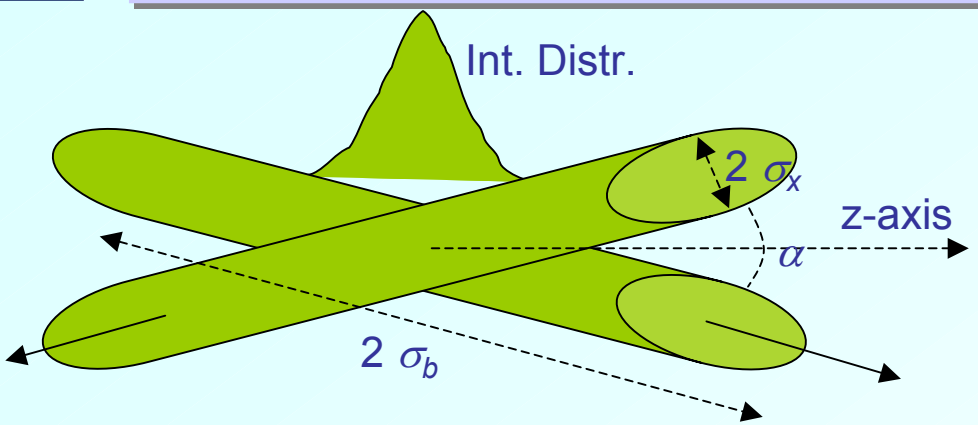

$$\langle n_v \rangle = \sigma_{inel} t_b L_0$$

$$\langle n_v^* \rangle = \frac{0.68 \langle n_v \rangle}{l^*} \quad [mm^{-1}]$$

$$L_0 = \frac{N^2}{4\pi\sigma_x^2 t_b} \frac{F^2}{q} \quad [cm^{-2}s^{-1}]$$

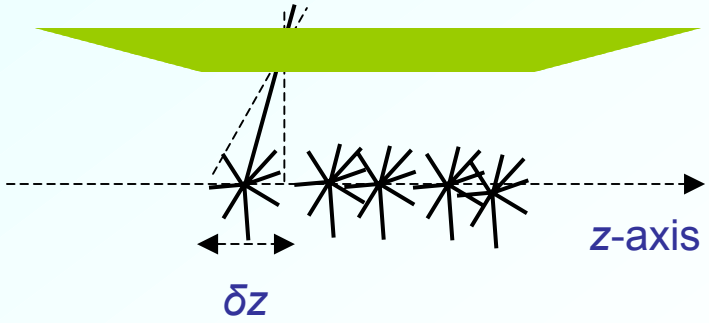

$$q = \sqrt{1 + \left(\frac{\alpha}{2}\frac{\sigma_b}{\sigma_x}\right)^2}$$

$$2.36\ \delta z \cdot \langle n_v^* \rangle < 0.5 \qquad (1)$$

$$l^* = \frac{q}{\sqrt{2}\sigma_b}$$

δz is the min. required detector precision on the beam axis. This inequality relates a collider quantity, $\langle n_v^* \rangle$,to a detector quantity, *δz* : it tells us, how good our tracking system has to be to distinguish adjacent interaction vertices.

Interaction Region Parameters

σ_b [m]	σ_x [μm]	α [μrad]	σ_{inel} [mb]	t_b [ns]	L_0 [cm^{-2}s^{-1}]	$\langle n_v \rangle$	$\langle n^*_v \rangle$ **[mm^{-1}]**	l^* [m]	δz **[mm]**	Collider E_{cm} [TeV]
0.38	30	0	56	400	$1 \cdot 10^{-32}$	2.24	**0.003**	0.54	**74.8**	Tevatron 1.8
0.076	15	300	80	25	$1 \cdot 10^{-34}$	20	**0.159**	0.085	**1.33**	LHC 14
75	15	500	80	25	$1 \cdot 10^{-35}$	200	**1.603**	0.085	**0.13**	SLHC 15
0.076	15	300	80	25	$1 \cdot 10^{-35}$	200	**1.59**	0.086	**0.13**	SLHC 15
0.06	5	50	130	20	$1 \cdot 10^{-34}$	26	**0.22**	0.081	**0.97**	VLHC 200

Scaling Relations

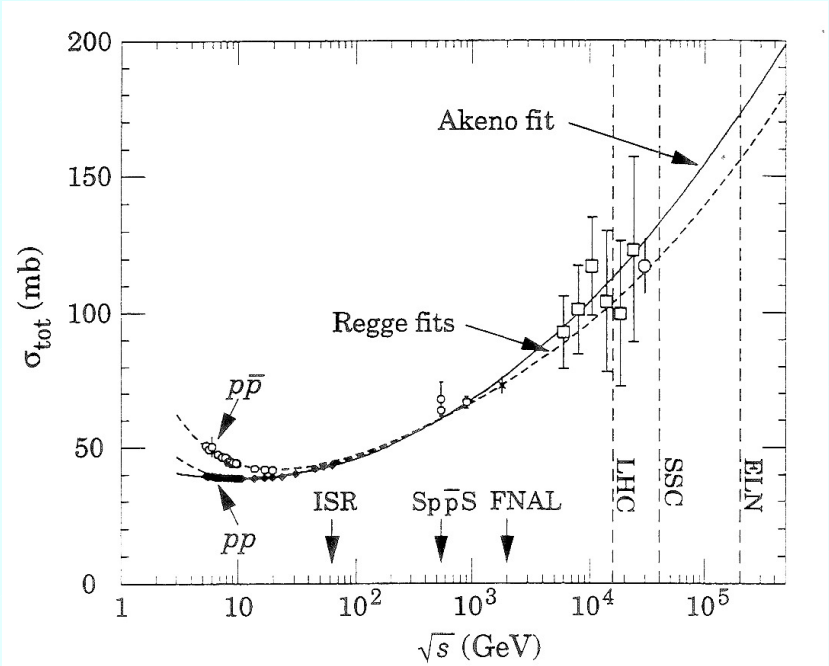

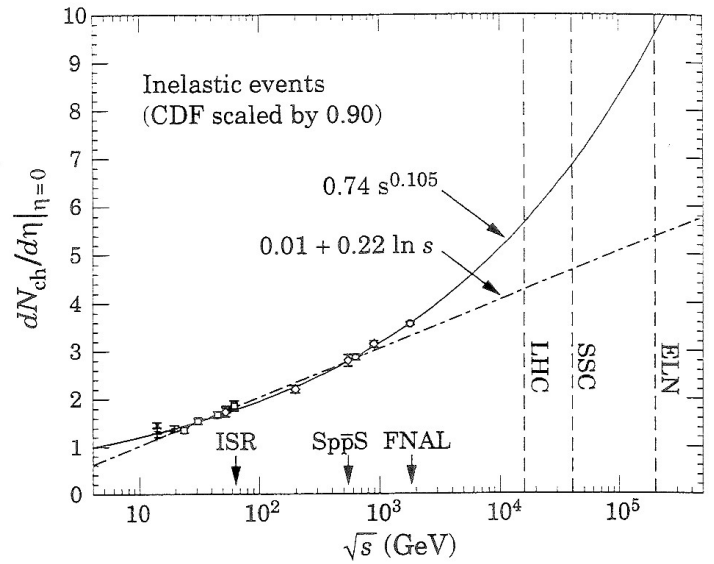

G. 2. Data and extrapolations of $dN_{ch}/d\eta|_{\eta=0}$.

Remember $\sigma_{tot} \sim 1/4\sigma_{elas} + 3/4\sigma_{inel}$

$$\langle p_t \rangle \approx 0.44 + 0.071 \log \sqrt{s}$$

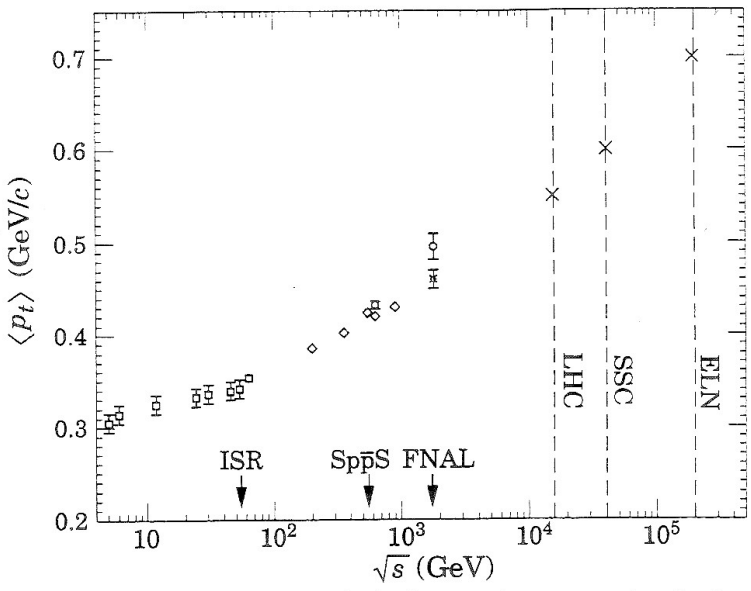

From D. E. Groom, in *Supercolliders and Superdetectors: Proc. Of the 19th and 25th Workshops*, ed. W.A. Barletta and H. Leutz, Erice, 17-22 Nov. 1992

Table of scaled parameters

E_{cm} [TeV]	σ_{inel} [mb]	Integ. L_0 [fb^{-1}]]	L_0 [$cm^{-2}s^{-1}$]	$\langle p_t \rangle$ [GeV/c]	H_{ch}	$\langle n_v \rangle$	N_{ch}*	Collider
1.8	56	***	$1 \cdot 10^{-32}$	0.46	4	2.24	18	**Tevatron**
14	80	10 - 100	$1 \cdot 10^{-34}$	0.55	7	20	280	**LHC**
15	80	100 -1000	$1 \cdot 10^{-35}$	0.55	7	200	2800	**SLHC**
200	130	10 - 100	$1 \cdot 10^{-34}$	0.70	11	26	572	**VLHC (Elo)**

*for a coverage of $\eta_{max} = 2$

Meanwhile keep in mind that, other than the N_{ch} produced, we also have neutral particles and gammas. And that the vast majority of events represents NOISE for us.

A CMS-Like Detector

(mostly tracking)

Solenoidal detector system

Let us now get on with the **solenoidal system**

Of course, we need the magnetic field (***B***) to measure the **momentum** (of charged particles).

We also try to place the big solenoid after the calorimeter to preserve its energy resolution (see Christian's lecture 4a, CMS choice):

We like the Higgs to $\gamma\gamma$ signature

We also like the Higgs to ZZ to 4 muons signature:

We build a robust muon detector outside the coil, with "integrated" return yoke, to have **transverse momentum** measurement from the **beam axis to the last muon chamber**.

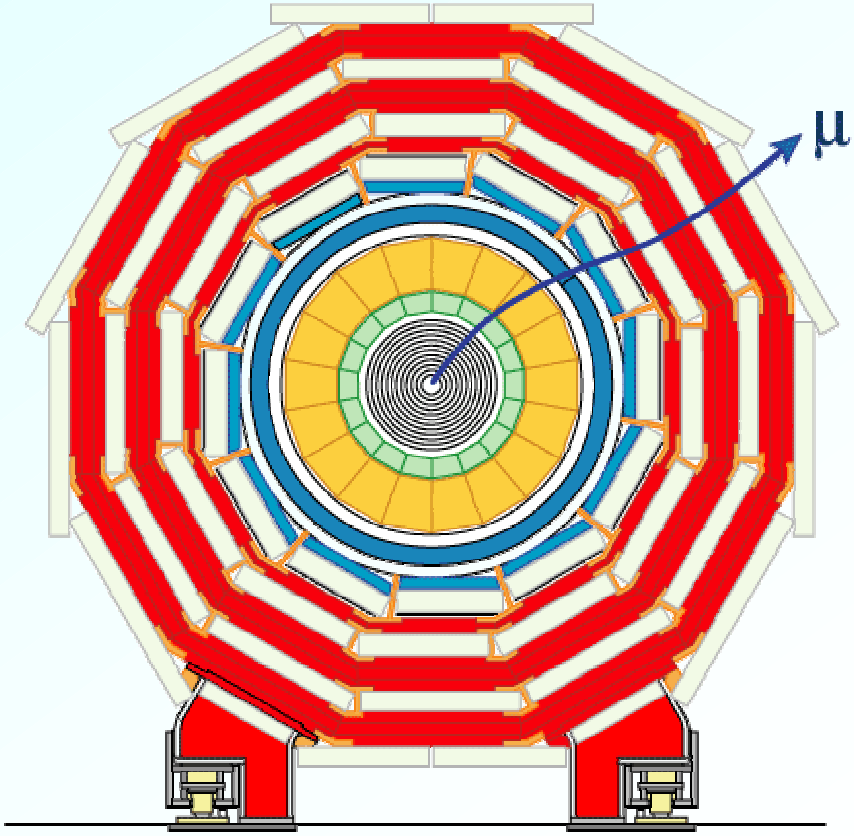

CMS front view

(from CMS home page)

Vertex Resolution in solenoid systems 1

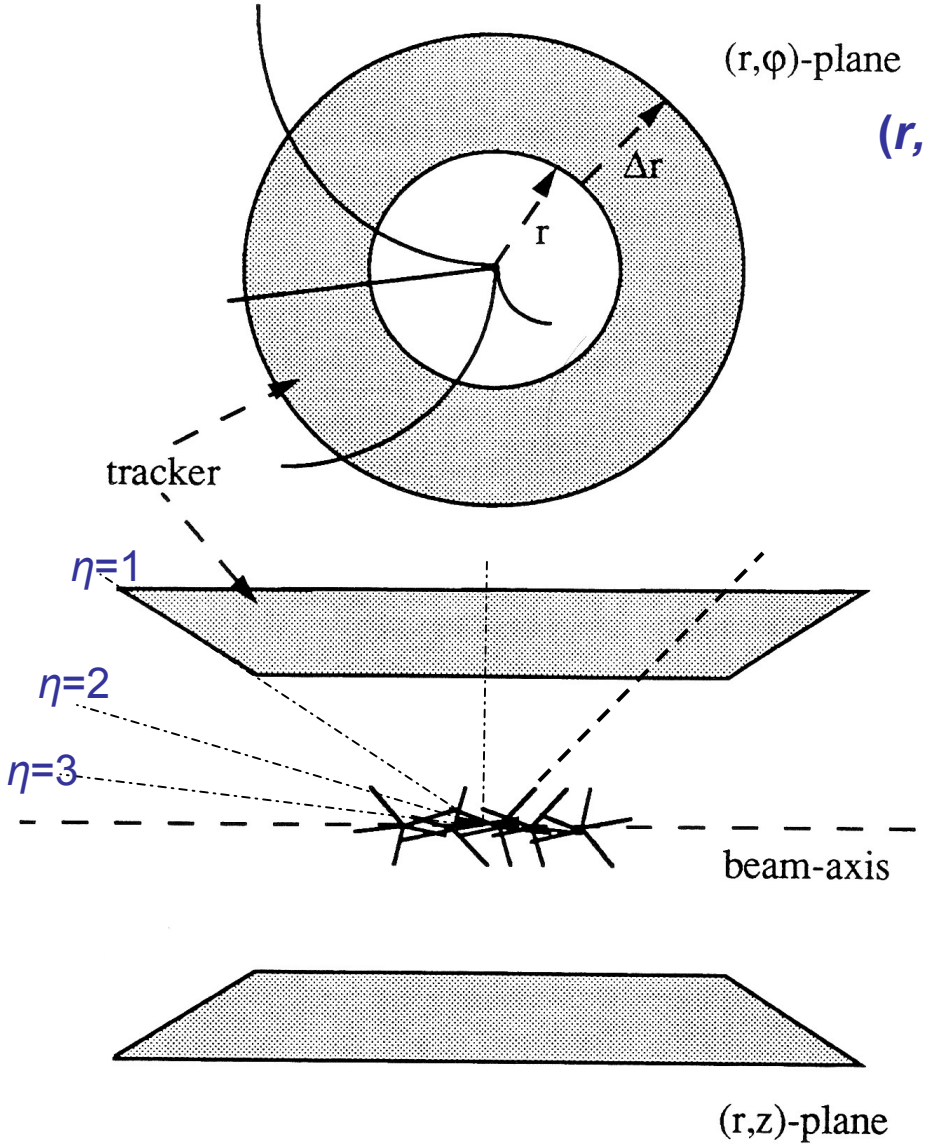

(*r*,*φ*)- and (*r*,*z*)- views of a schematic tracker:

In the (*r*,*φ*)-plane, the beam constraint provides enough precision on the primary vertex position;

on the contrary, in the (*r*,*z*)-plane the production of multi-vertices in the luminous region asks for a high detector resolution (**2.36*δz***) in the z-coordinate.

Vertex Resolution in solenoid systems 2

If we follow an old work from Monsieur Gluckstern, we find that:

$$\delta z^2 \approx \frac{\sigma_z^2}{N}\left[\frac{5}{2} + 6\frac{r}{\Delta r} + 6\left(\frac{r}{\Delta r}\right)^2\right] + N\left(r\frac{0.0136}{p}\sqrt{t_0}\right)^2 \quad (2)$$

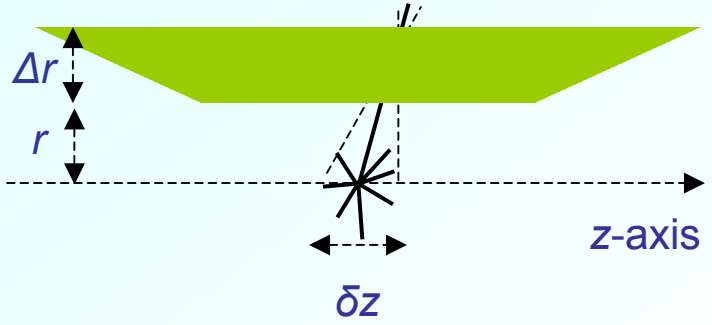

And, for a system where $r/\Delta r$ ~1, N=16, σ_z =1 mm and t_0 is the minimum layer thickness to achieve one hit (you will understand why I am taking these values in a moment)

$$\delta z \approx 1\,mm + mult.\,scatt.\,error$$

Sufficient for the LHC requirement on δz.

For a CMS-like det., this could be achieved with the muon chambers alone, if we manage to keep low the multiple scattering error….

By the way, if you are interested, here the complete formulas for the (r,z)-plane measuring error:

$$\delta z^2 = \frac{F_2}{F_0F_2 - F_1^2} \quad with \quad F_i = \sum_1^N \beta_n x_n^i$$

$$\sigma_{sl}^2 = \frac{F_0}{F_0F_2 - F_1^2} \quad and \quad \beta_n = \frac{\alpha_n}{\varepsilon_n^2}$$

Not difficult to calculate for the (r,φ)-plane

Vertex Resolution in solenoid systems 3

The δz is completely smeared by the mult. scatt. error due to the material of and in front of the muon system :

$$\delta z \approx (1\,mm) \oplus N\left(r\,\frac{0.0136}{p}\sqrt{t_0}\right) \oplus \left(r\,\frac{0.0136}{p}\sqrt{t_{inner}}\right) = (1\,mm) \oplus (11\,mm) \oplus (14\,mm)$$

Therefore, a good tracker is mandatory.

For a four shell tracker:

$$\delta z \approx (0.6\,mm) \oplus \left(\frac{3.4\,mm}{p}\right)$$

for $r/\Delta r$ ~0.35/1 ($r+\Delta r$ =1.35 m), N=16, σ_z =1 mm and t_0 ~2 % of X_0 , (see Eq. 2)

For SuperLHC, this would not be enough. Can we go closer ?
We must consider dose and occupancy.

Momentum Resolution in solenoid systems 1

Transverse slice through CMS detector

Click on a particle type to visualise that particle in CMS

Press "escape" to exit

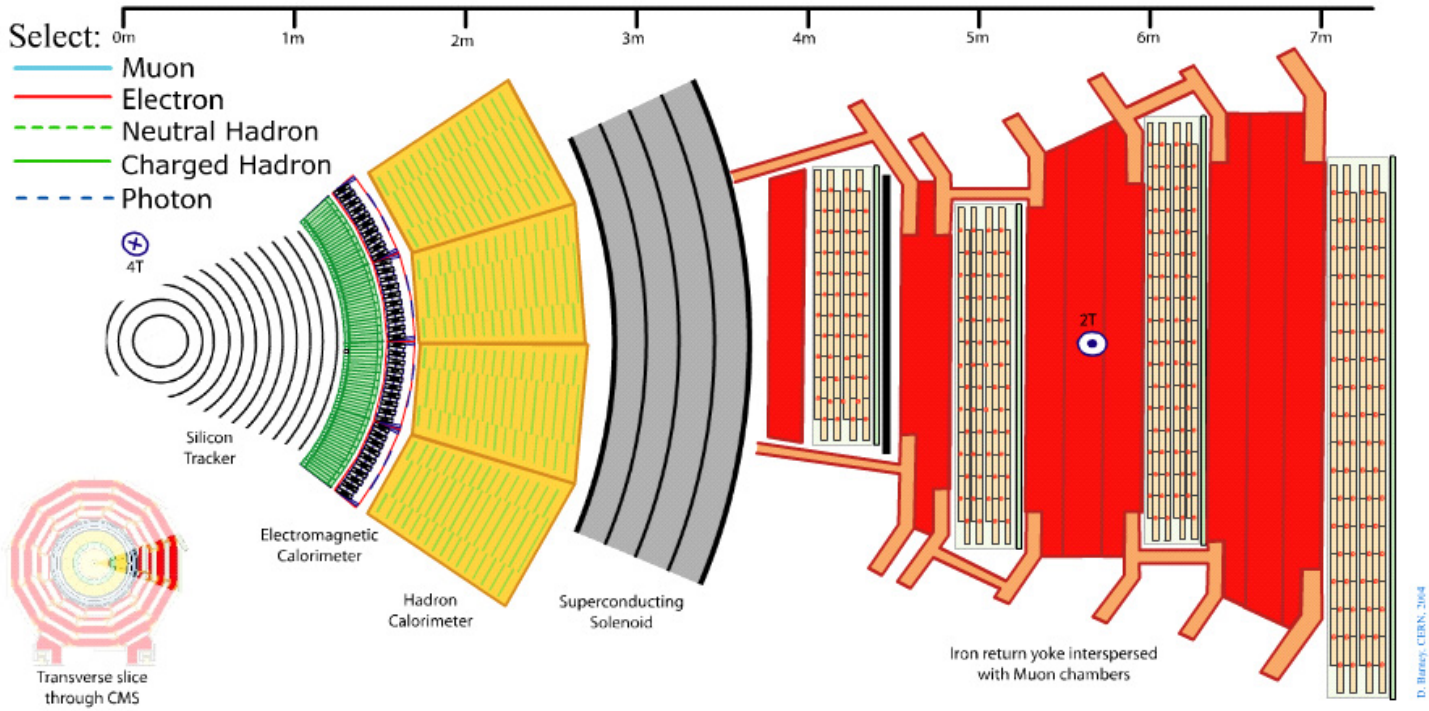

From CMS home page

Momentum Resolution in solenoid systems 2

For H to ZZ to 4 muons, in a CMS-like system with only muon chambers, the mom. resolut. is:
In the (r,φ)-plane, p_t resolution* (remember Christian's lecture 1a),

$$\left(\frac{\delta p_t}{p_t}\right) = \left\{\left(\frac{363}{N}\right)^{1/2}\left(\frac{\sigma_\varphi}{\Delta r_m^2}\right)\left(\frac{p\sin\theta}{0.3B}\right)\right\}_{curv} \oplus \left\{10\cdot\left(\frac{0.016\sin\theta}{0.3B\Delta r_m}\right)\right\}_{ms}$$

For a 45° muon track at 50 GeV/c, B=2T, Δr_m =4 m, $\sigma_{\varphi,z}$=1 mm and N=16

$$\sim (1.8\,\mathrm{x}\,10^{-2}) \oplus (4.7\,\mathrm{x}\,10^{-2})$$

curvature error, plus ~100 X_0 of multiple scattering

In the (r,z)-plane, $p_{//}$ resolution*,

$$\left(\frac{\delta p_{//}}{p_{//}}\right) = \left\{\left(\frac{7.3}{N}\right)^{1/2}\left(\frac{\sigma_z\cos\theta}{\Delta r_m}\right)\right\}_{slope} \oplus \left\{\left(\frac{100}{\sin\theta}\right)^{1/2}\cdot\left(\frac{0.014}{p\tan\theta}\right)\right\}_{ms}$$

$$\sim (0.012\,\mathrm{x}\,10^{-2}) \oplus (0.028\,\mathrm{x}\,10^{-2})$$

slope error, plus ~100 X_0 of multiple scattering

*thanks again to M. Gluckstern, we can calculate the numerators of $(G_{c,sl}/N)^{1/2}$, for any disposition of our det. layers. They range from 256 to 720 for G_c and from 2 to 12 for G_{sl}, if the precisions are the same everywhere.

Momentum Resolution in solenoid systems 3

For the tracker alone, the momentum resolution is:
In the (r,φ)-plane, p_t resolution ,

$$\left(\frac{\delta p_t}{p_t}\right) = \left\{\left(\frac{250}{N+1}\right)^{1/2}\left(\frac{\sigma_\varphi}{(r+\Delta r)^2}\right)\left(\frac{p\sin\theta}{0.3B}\right)\right\}_{curv} \oplus \left\{0.56\cdot\left(\frac{0.016\sin\theta}{0.3B(r+\Delta r)}\right)\right\}_{ms}$$

For 45° tracks, B = 4 T,
$r/\Delta r$ ~ 0.35/1 ($r+\Delta r$ = 1.35 m),
$\sigma_{\varphi,z}$= 1 mm and N = 17,
beam axes point ~ 0.020 mm
and t_0 ~ 2 % of X_0.

In the (r,z)-plane, $p_{//}$ resolution,

$$\left(\frac{\delta p_{//}}{p_{//}}\right) = \left\{\left(\frac{7}{N}\right)^{1/2}\left(\frac{\sigma_z\cos\theta}{\Delta r}\right)\right\}_{slope} \oplus \left\{\left(\frac{0.3}{\sin\theta}\right)^{1/2}\cdot\left(\frac{0.014}{p\tan\theta}\right)\right\}_{ms}$$

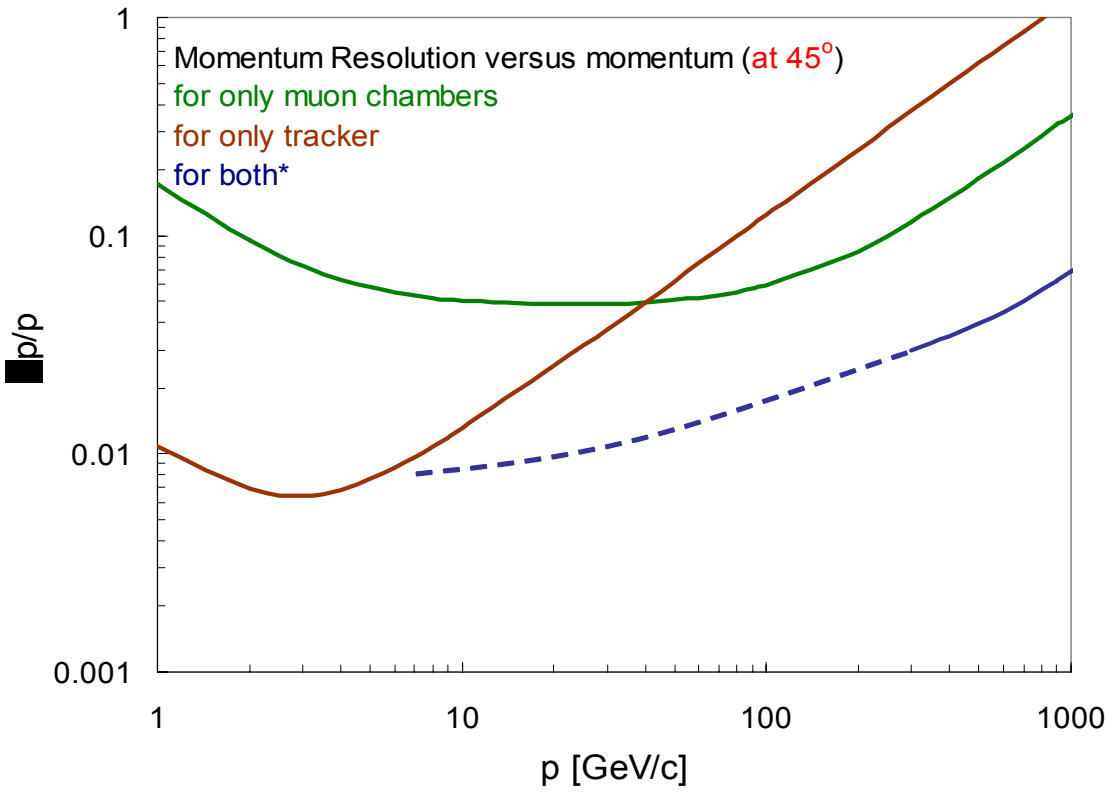

- Given our solenoid, we have roughly defined:
  - our muon detection system (cell precision, number of hits, positions);
  - our inner tracker and calorimeters;
- We have calculated rough estimations for the values of δz, *dp/p.*

But, can our detectors cope with radioactivity dose ?

And will they not be flooded with particles ?

CMS: H → ZZ → 2e 2μ (from J. Virdee, HIP-27 Aug 03)

20 pileup events/crossing superposed on the one of interest

Only tracks with p_t> 2 GeV/c are shown

Single event

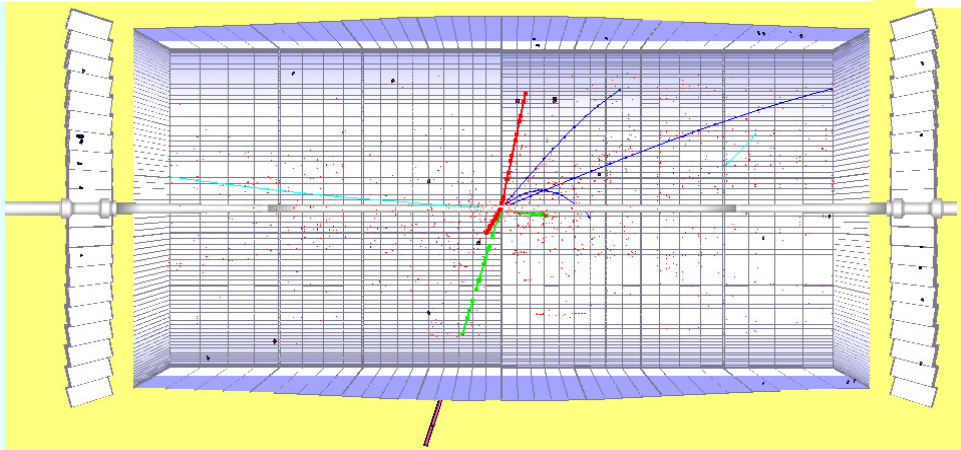

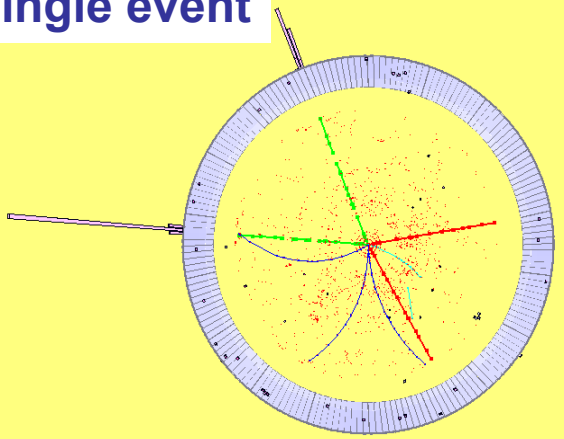

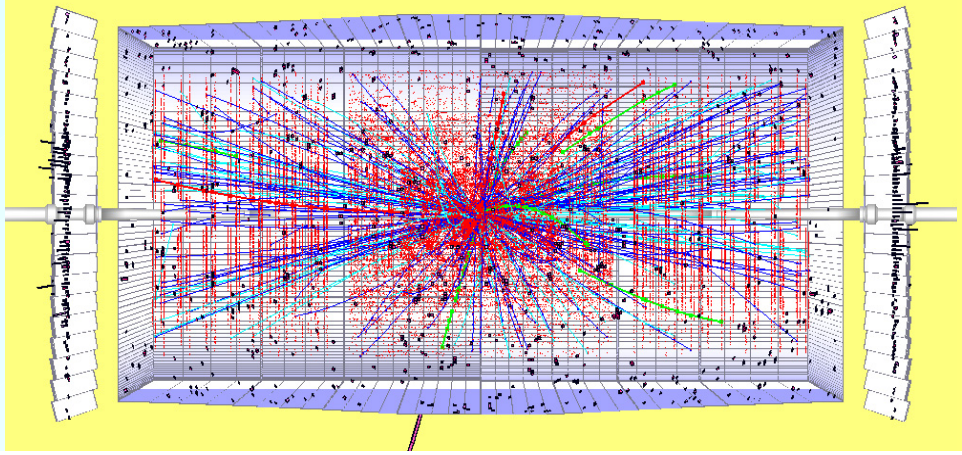

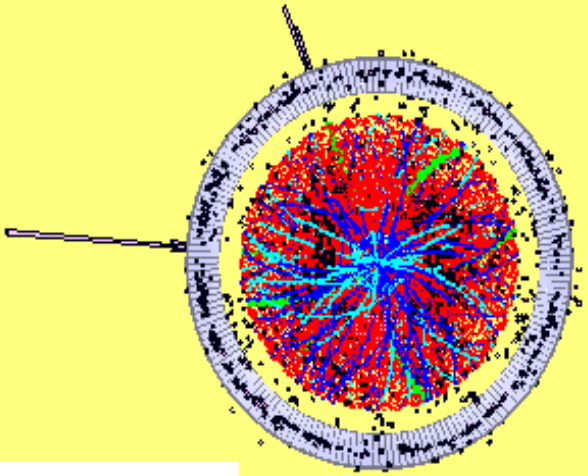

+ 20 pileup events i.e. L =10^{34} and 25 ns bunch spacing

Dose and Occupancy

Dose generated and occupancy 1

The dose experienced by a thin absorber, placed around the interaction point and due to charged particles, depends only on r^{-2} (r is the distance to the beam axes). Therefore, the average dose experienced by a thin cylindrical shell placed at distance r from the beam axis (central tracker arrangement) can be written as:

$$D_{ch}[Gy\ yr^{-1}] \approx \frac{C}{2\pi r^2} \quad where\ C = 3.2 \cdot 10^{-7}\ H\langle n_v \rangle t_b^{-1}$$

For a year of 10^7 s.

For LHC, $H\langle n_v \rangle t_b^{-1} = 5.6 \cdot 10^9$, therefore $C = 1800\,[m^{-2}]$.

The albedo neutron flux is roughly constant in the inner cavity and can be estimated between 10^{13} – 10^{14} $cm^{-2}yr^{-1}$. The dose induced will depend on the material, its thickness and neutron cross section (energy dep.). A rule of thumb would give a 100 – 1000 Gy/yr.

Dose generated and occupancy 2

Adding a magnetic field, produces three major effects:

Charged particles start curling: Low p_t will curl and stay inside the inner region, while high pt will escape and continue to the calorimeter. Therefore the dose is increases at low radii and decreases at large radii (remember, $r = p_t / (0.15\ B)$).

Charged pions (half of the particles produced, considering double counts from neutral pions) will decay inside or outside the tracker acceptance η_{max}: contributing with a different weight to the dose, which will now depend also on η.

The calorimeter (or the magnet) position will influence the inner tracker dose.

$$D_{ch}[Gy\ yr^{-1}] \approx \frac{C}{2\pi r^2} \cdot F(x,\eta) \quad where\ x = 2\frac{p_t}{\langle p_t \rangle} = \frac{0.3Br}{\langle p_t \rangle}$$

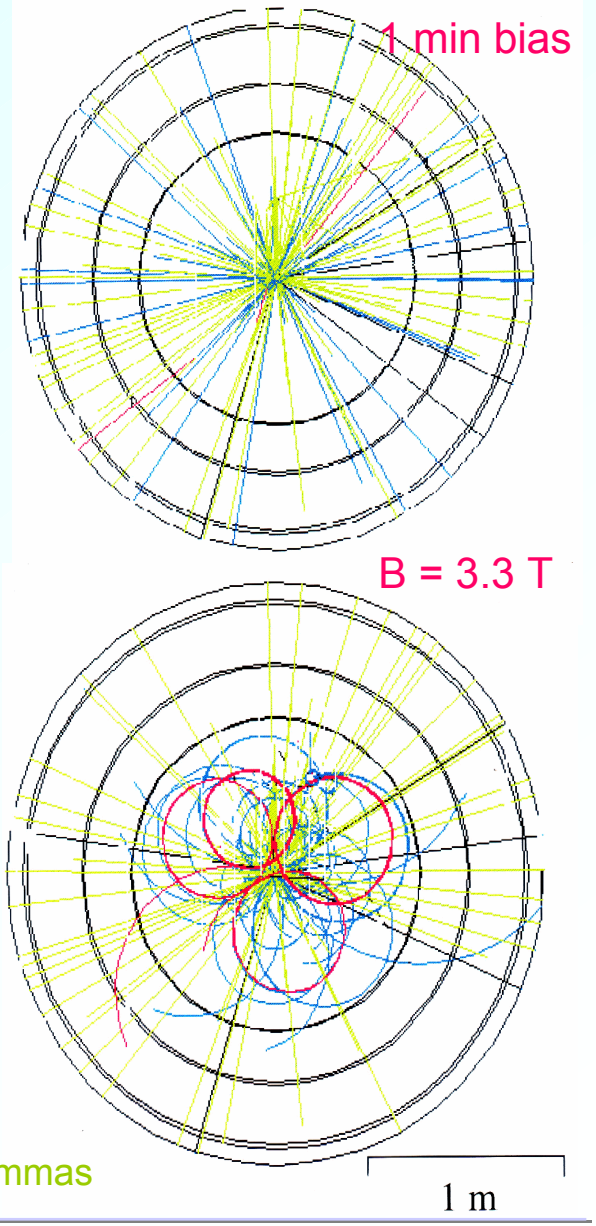

Blue, charged hadrons Red, charged leptons Green, gammas

Dose generated and occupancy 3

$$D_{ch}[Gy\ yr^{-1}] \approx \frac{C}{2\pi r^2} \cdot F(x,\eta) \quad where\ x = 2\frac{p_t}{\langle p_t \rangle} = \frac{0.3Br}{\langle p_t \rangle}$$

$\langle p_t \rangle \approx 0.44 + 0.07 \log E_{cm}$ you already saw this one

$$F(x,\eta) = 2\langle n_c \rangle \int_{x_r}^{x_c} f(x')dx' + \int_{x_c}^{\infty} f(x')dx' =$$

$$= 2\langle n_c \rangle \left[(1+x_r)e^{-x_r} - (1+x_c)e^{-x_c} \right] + (1+x_c)e^{-x_c}$$

$f(x) = x\,e^{-x}$ is a rough distribution of p_t with $<p_t>$

$$\langle n_c \rangle = \frac{1}{\pi} \frac{\sinh\eta_{\max}}{\eta_{\max}} \left\{ \frac{\eta_0}{\sinh\eta_0} + \ln\left[\frac{\tanh\left(\frac{\eta_{\max}}{2}\right)}{\tanh\left(\frac{\eta_0}{2}\right)} \right] \right\}$$

x_r and x_c are the x equivalent to the tracker inner radius and the calorimeter starting position

$<n_c>$ is the average number of curls per produced particle (note it is independent of p_t)

η_{max} is the max. coverage of the tracker shells and η_0 *is* the pseudorapidity, inside which particles decay in the tracker

Dose generated and occupancy 4

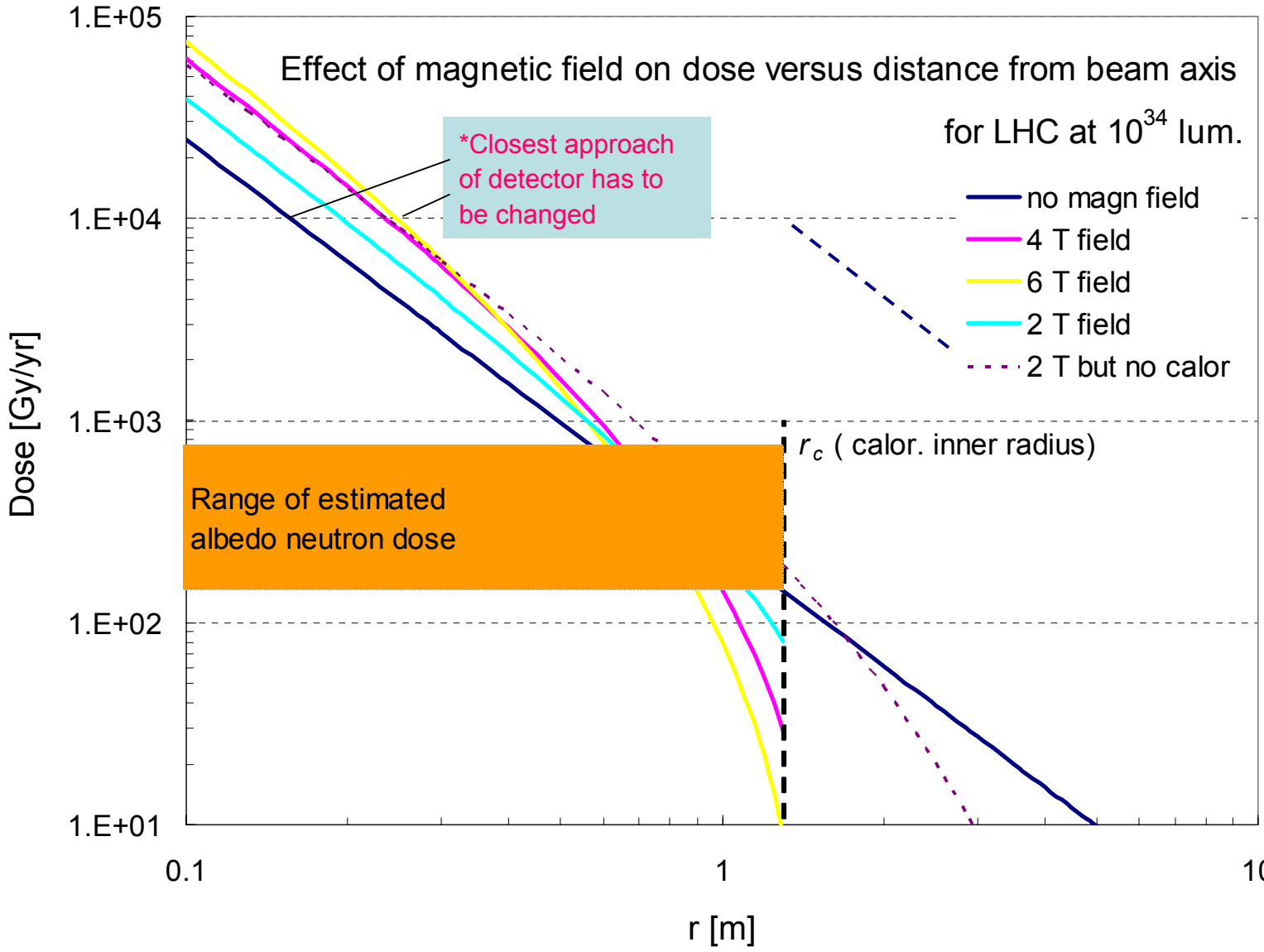

For SLHC, just multiply the left-hand scale by 10!

Note the effect of the calorimeter.

*for a detector withstanding a max. dose of 10 kGy/yr

Dose generated and occupancy 5

The occupancy (O_{ch}) of a detector with a cylindrical shell shape, placed at a distance r from the beam axis, is defined as the number of occupied detector cells divided by the their total number and multiplied by their time response in two-bunch crossing time units (t_b).

$$O_{ch} = \frac{\langle n_v \rangle H}{2\pi r^2} \frac{t_{dr}}{t_b} (\Delta\varphi \Delta z) \approx 3.1 \cdot 10^6 \; n \; t_b D_{ch} (\Delta\varphi \Delta z)$$

and it is proportional to the charged particle dose, for thin detector shells.

($\Delta\varphi \; \Delta z$) – in mm^2 - is the detector cell segmentation.

For our detector (slide 5b/19):

$$O_{ch} \approx 3.1 \cdot 10^{-4}$$

At a distance of 0.35 m from the beam axes.

The decalogue of the detector designer:

If you want to have fun with your next collider detector (mostly trackers) design:

1) Check what signatures have significance (ask your preferred theoretician);
2) Have a look at the interaction region and estimate your minimal δz;
3) Fix your detector cell size (with precisions σ_φ, σ_z);
4) Go for a magnet (or none?) and decide which type;
5) Place your inner tracker and muon shells in order to satisfy your min. requests on $\delta p/p$ and δz (which you can calculate);
6) Decide what kind of calorimeter you need (study Christian's talk in detail!) and place it;
7) Calculate dose and occupancies and find your closest approach values to the interaction region (compatible with maximum allowed dose and cell size);
8) Go back to point 3) (only once) and re-adjust the values (if needed);
9) You might have learned something;
10) Start your simulations or your R&D (depends on your preference and money)!

References

- *SSC Central Design Group Report*, **SSC-SR-1033** (1988);
- Particle Data Group, *Review of Particle Physics*, Phys. Review, **D66**, (2002);
- S. Tapprogge, High Luminosity Upgrade Steering Group, ATLAS Overview Week, 7 October 2004, Freiburg
- *Supercolliders and Superdetectors*, Proc. of the 19th and 25th Workshop pf the INFN Eloisatron Project, 17 – 22 November 1992, Ed. W.A. Barletta and H. Leutz, World Scientific Pub.;
- A. De Roeck, "SLHC Prospects", FNAL, October 2003;
- CMS and ATLAS TPs and TDRs, CERN, Geneva;
- R. L. Gluckstern, NIM **V.24**, 381 (1963);
- V. Karimäki, NIM **A410**, 284 (1998);
- C. D'Ambrosio et al., "Particle Traking with Scintillating Fibers", IEEE TNS, **V.43**, No.3, (1996).